TECHNISCHE UNIVERSITÄT MÜNCHEN

Lehrstuhl II für Technische Chemie

Acid catalyzed reactions of cyclohexanol in liquid phase

Yuanshuai Liu

Vollständiger Abdruck der von der Fakultät für Chemie der Technischen Universität München zur Erlangung des akademischen Grades eines

Doktors der Naturwissenschaften (Dr. rer. nat.)

genehmigten Dissertation.

Vorsitzender: Univ.-Prof. Dr. Kai-Olaf Hinrichsen

Prüfer der Dissertation:

1. Univ.-Prof. Dr. Johannes A. Lercher
2. Hon.-Prof. Dr. Richard W. Fischer

Die Dissertation wurde am 13.02.2017 bei der Technischen Universität München eingereicht und durch die Fakultät für Chemie am 10.03.2017 angenommen.

To my family

“Measure what is measurable, and make measurable what is not so.”

Galileo Galilei (1564 – 1642)

Acknowledgements

First and foremost, I would like to give my deepest appreciation to my advisor Professor Dr. Johannes A. Lercher. Thank you for offering me this precious opportunity to explore the magic catalysis world together with you in the past four years. Without your professional guidance and your continuously financial support, I could not have completed this thesis. Your profound knowledge in science enlightens me not only in this thesis but also in my future study. Thanks for the trust, inspiration and freedom you have granted to me in the daily research as well as during the thesis writing. In particular, thank you for giving me your impressive patience and kindness in the first two years of my Ph.D. study when we got bogged down in an endless debate over our data distinction between TU München (TUM) and Pacific Northwest National Laboratory (PNNL, USA).

Next, I would like to express my heartfelt gratitude to Dr. Eszter Baráth for her productive discussions and constant encouragement. Prof. Dr. Chen Zhao is gratefully acknowledged for her valuable advice and great help at the beginning of my study. My sincere thanks also go to Dr. Yue Liu for his selfless assistance in and in laboratory work. Particularly, I am utmost grateful to my research partners at PNNL, Dr. Hui Shi and Dr. Donald M. Camaioni, for their excellent instructions, insightful discussions and ceaseless support in experiments, data analysis and paper writing in the past years. And also, I am indebted to Dr. Donghai Mei for the DFT calculations. With his theoretical support, we ultimately achieved a more in-depth understanding of the chemistry in our dehydration work. I appreciate and enjoy the fruitful collaborations, the innumerable teleconferences with all of you. My doctoral study has been made much easier with the help of you guys.

Furthermore, I would like to thank all of our senior scientists in TCII at TUM, Prof. Dr. Andreas Jentys, Dr. Erika E. Ember, Dr. Oliver Y. Gutiérrez, Dr. Maricruz Sanchez-Sanchez and Dr. Ricardo Bermejo-Deval. Thank all of you for your kind help in science as well as in consultation and Praktikum teaching. My sincere appreciation also goes to Prof. Dr. Gary Haller for his valuable comments in my work. The technical and administrative staffs in our group have been very kind and helpful, and I would like to acknowledge all of them here. Franz-Xaver Hecht, Martin Neukamm and Andreas Marx

are acknowledged for their technical supports. Bettina Federmann, Steffi Maier, Karen Schulz and Ulrike Sanwald are acknowledged for their administrative helps. Thank all of you for your supports and inputs in my work.

Special thanks go to my friend and former co-worker Dr. Wenji Song. I deeply appreciate the wonderful experience with you during our collaborations. Thanks a lot for your consistently unconditional assistant over the years. I extend my thanks to my friends, Dr. Xianyong Sun and Dr. Navneet Gupta for the joy and companion at a lot of late nights and weekends in the lab. I also must express great thanks to my former and current colleagues, Dr. Bo Peng, Dr. Yuchun Zhi, Dr. Jiayue He, Dr. Wenhao Luo, Dr. Luis Francisco Gonzalez Peña, Dr. Sebastian Grundner, Dr. Maximilian Hahn, Dr. Stanislav Kasakov, Dr. Jeongnam Kim, Dr. John Ahn, Dr. Tobias Berto, Dr. Udishnu Sanyal, Dr. Sebastian Müller, Yu Lou, Sebastian Foraita, Sebastian Eckestein, Peter Hintermeier, Manuel Wagenhofer. Thank you for your supportive helps during my study in TCII.

Moreover, I would like to thank all following colleagues in TCII. Dr. Linus Schulz, Dr. Christian Gärtner, Moritz Schreiber, Edith Berger, Guoju Yang, Yang Song, Wanqiu Luo, Yang Zhang, Ruixue Zhao, Xi Chen, Guanhua Cheng, Sylvia Albersberger, Matthias Steib, Daniel Melzer, Andreas Ehrmaier, Takaaki Ikuno, Ferdinand Vogelgsang, Martina Braun, Kai Sanwald, Felix M. Kirchberger, Christoph Denk, and all the members of TC II and my friends I do not mention here for their friendship and support during the completion of the work. Great thanks also go to Pro. Dr. Tao Dou, Pro. Dr. Yanjun Gong and Dr. Pengyu Wen, for their ceaseless encouragements and supports during the past couple of years.

Last but not least, I am deeply indebted to my beloved family for their consistent love, understanding, encouragement and support throughout my Ph.D. study.

Yuanshuai Liu

Feb. 2017

Abbreviations

Abbreviation	Elongation
s	Second
min	Minute
h	Hour
Å	Angstrom
nm	Nanometer
g	Gram
mol	Mole
M	Mole per liter
(m)L	(Milli) liter
°C	Celsius degree
K	Kelvin
(k)J	(Kilo) joule
(k)Pa	(Kilo) pascal
wt.%	Weight percent
AAS	Atomic absorption spectroscopy
BET	Brunauer-Emmett-Teller
FT-IR	Fourier transformed infrared spectroscopy
TEM	Transmission electron microscopy
NMR	Nuclear magnetic resonance
TPD	Temperature programmed desorption
XRD	X-ray diffraction
DFT	Density Functional theory
GC	Gas chromatography
MS	Mass spectrometry
TGA	Thermogravimetry analysis
DSC	Differential scanning calorimetry

(continued)

BAS	Brønsted acid site
LAS	Lewis acid site
r	rate
TOF	Turn over frequency
HDO	Hydrodeoxygenation
L-H	Langmuir-Hinshelwood
E-R	Eley-Rideal
RDS	Rate determining step
TST	Transition state theory
TS	Transition state
PhOH	Phenol
DCHE	Dicyclohexyl ether
CHP	Cyclohexylphenol
CHPE	Cyclohexyl phenyl ether
CC	Cyclohexylcyclohexene
DCHP	Dicyclohexylphenol
AG	Aktiengesellschaft
HPLC	High-performance liquid chromatography
Eq.	Equation
i.e.	*id est*
e.g.	*exempli gratia*
ca.	*circa*
vs.	*versus*
NIST	National Institute of Standards and Technology

Abstract

Hydronium ions in aqueous phase catalyze the dehydration of cyclohexanol via monomolecular precursors. In confines such as zeolite pores they are more active than in water, which is caused by an enhanced association between the hydronium ion and alcohol, as well as a greater activation entropy. Alcohol dimers, forming in apolar solvents, reduce the rate of reaction by stabilizing the ground state. Alkylation of arene rings with cyclohexanol requires the formation of a cyclohexyl carbenium ion, which is more difficult to generate in water than in apolar organic solvents.

Kurzzusammenfassung

Oxoniumionen in wässriger Phase katalysieren die monomolekulare Dehydratisierung von Cyclohexanol. Räumlich beschränkte Oxoniumionen in Zeolithporen zeigen eine erhöhte Aktivität aufgrund einer stärkeren Assoziation mit dem Alkohol sowie einer höheren Aktivierungsentropie. In aprotischen Lösungsmitteln bilden sich Dimere, die die Raten durch Stabilisierung des Grundzustands verringern. Die Alkylierung an aromatischen Ringen durch Cyclohexanol erfolgt über die Bildung von Cyclohexylkationen, die in aprotischen Lösungen leichter zu bilden sind als in Wasser.

Table of contents

Chapter 1

Introduction

1.1 General background

Current production of fuels and chemicals relies heavily on the use of nonrenewable fossil resources, *i.e.*, petroleum, coal, and natural gas. Nowadays, the reserves of these fossil resources are diminishing, whereas the global demands for the fossil-based energies are rising continuously. In response to the growing energy consumption and the increasing depletion of fossil-based feedstocks, the use of alterative 'renewable and sustainable' resources such as biomass, carbon dioxide and solar energy for the production of raw materials and energy vectors, has been therefore subjected to intensive attention during the past decade.[1-3]

In this context, biomass, the only sustainable organic carbon resource in nature,[4,5] is becoming one of the most attractive and promising alternatives for the development of new solutions to produce energy and chemicals due to its abundance and net zero carbon emission. For example, today biomass has contributed about 10% of the total energy consumption in the world.[6] And it is expected that 30% of the direct fuel production would be met by renewable biomass resources by 2025.[7] Likewise, as forecast by Shell,[8] the worldwide consumption of energy will double in size by 2050 (see **Figure 1-1 a**). Although fossil resources still remain the dominated energy suppliers, the energy derived from biomass will dramatically increase in this half century. In addition, biomass will in particular diversify the supply of transportation fuels. Liquid biofuels production from the corn-based (1^{st} generation) and lignocellulosic (2^{nd} generation) materials will be a significant part of biomass utilization from 2020 to 2050, as shown in **Figure 1-1 b**.

As a result, one may thus predict that the future fuels and chemicals production will progressively move from use of high-cost and environmental damaging fossil-based feedstocks to the sustainable and low-carbon energy carriers. In this evolution, biomass together with its derivates is projected to change the global energy matrix as well as the industrial objectives in the foreseeable future.[3,9] Moreover, the use of sustainable energy is also driven in part geopolitical benefits.[3] Indeed, countries or regions with lack of fossil resources but possess large reserves of biomass, have established the relevant polices in the development of biomass utilization. The U.S. Department of Energy has set ambitious goals to generate 20% of transportation fuels and 25% of chemicals production

from biomass by 2030.[10,11] The European Union has also set a mandatory target to derive 20% of energy and a minimum target of 10% for biofuels form biomass by 2020.[11] Similarly, the consumption of biofuels (mainly ethanol and biodiesel) in China will reach 12 million metric tons by 2020.[12]

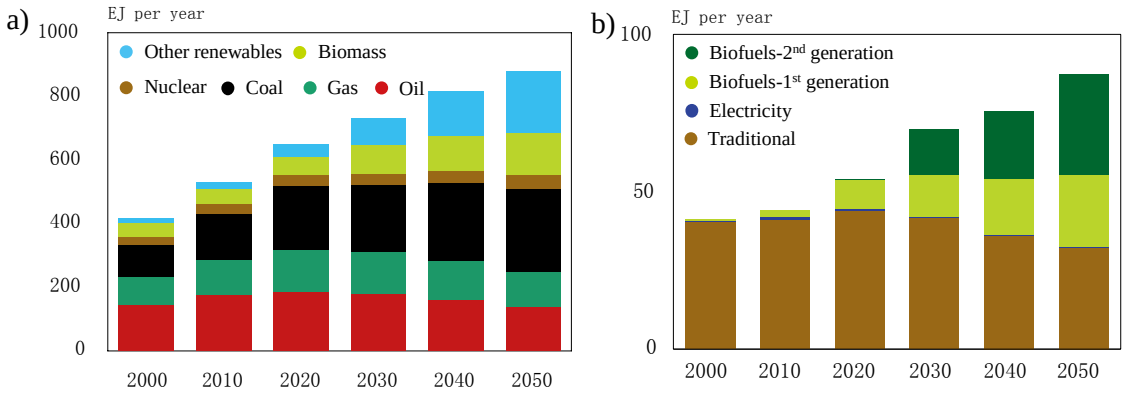

Figure 1-1. The global energy consumption outlook to 2050: Primary energy by source (a) and final energy consumption from biomass (b). Adapt form ref. [8].

In order to convert biomass into high-value energy forms, identifying the suitable raw materials and developing the effective refinery processes are of paramount importance. To our best knowledge, the first generation biomass feedstocks derived from the edible plant materials (*e.g.*, sugars and starches) have received much criticism over its remarkable competition with food supplies. In addition, the replacement of classical forest lands for fuel-crops will simultaneously bring about severe deforestation, further accelerate the global warming.[13] Consequently, the sustainable production of fuels and chemicals without affecting food supplies and land usage encourages researchers to develop effective technologies to transform more abundant and non-edible lignocellulosic biomass.

Many of the current petrochemical processes are generally constructed from a few simple molecules. Following a similar approach, biorefinery could be achieved by employing the representative platform molecules.[13] Due to a high content of oxygen-containing functional groups in biomass-derived bio-oils, most of the platform molecules are water-soluble. In particular, the ubiquitous presence of water in these bio-oils makes

it a promising reaction medium in upgrading processes under mild conditions.[14] In this thesis, cyclohexanol is selected as a platform molecule and the related reactions including dehydration and alkylation will be comprehensively investigated in liquid phase over acid catalysts.

1.2 Biomass and bio-oils

Biomass, originally generated from biological photosynthesis using atmospheric carbon dioxide, water and sunlight, refers to organic materials such as wood, grass, algae, agriculture crops and their residues and wastes.[15,16] As the fourth largest energy carriers in the world (following oil, coal and natural gas), biomass is primarily used to supply heat and power through combustion, a low-level utilization strategy. In the concept of exploring sustainable energy, significant efforts have been devoted in the field of transformation of biomass to high-value products. Take woody biomass for example, it has already been widely used in biorefinery processes benefited to its low ash content and high-quality bio-oil production.[17] Lignocellulose in raw materials such as wood, grass and agricultural residues, represents the most abundant form of terrestrial biomass and offers great potential as the alternative feedstock because (i) lignocellulose is the most abundant component of biomass with about 170 billon metric tons of annual production[18], but is only limited used (< 5%) for diverse purposes until now[19]; (ii) the use of lignocellulose will not bring about strong competition between chemical production and food supplies. In terms of both aspects, lignocellulosic biomass is thus considered as a more practicable and sustainable material for the replacement of fossil resources to produce fuels and chemicals. In general, most of the lignocellulosic biomass compose of 35-50% of cellulose, 20-35% of hemicellulose, and 10-25% of lignin.[16] The structures of three fractions are shown in **Figure 1-2**. As to the carbohydrate-based components in lignocellulose, cellulose is biopolymer composed of glucose monomer and exists in crystalline, while hemicellulose has an amorphous structure and consists of many different sugar monomers. Different from above two components, lignin is a three dimensional biopolymers consisting of abundant aromatic/phenolic functionalities. The detailed structure is described in **Section 1.3**. Among three primary components,

hemicellulose and cellulose have been studied for a long time, and some related biorefinery technologies have been applied in industry for producing biofuels and fine chemicals.[20-22] In recent years, lignin is also recognized as a promising candidate for the production of high-value chemicals. The major technologies for lignin transformation are discussed in **Section 1.3**.

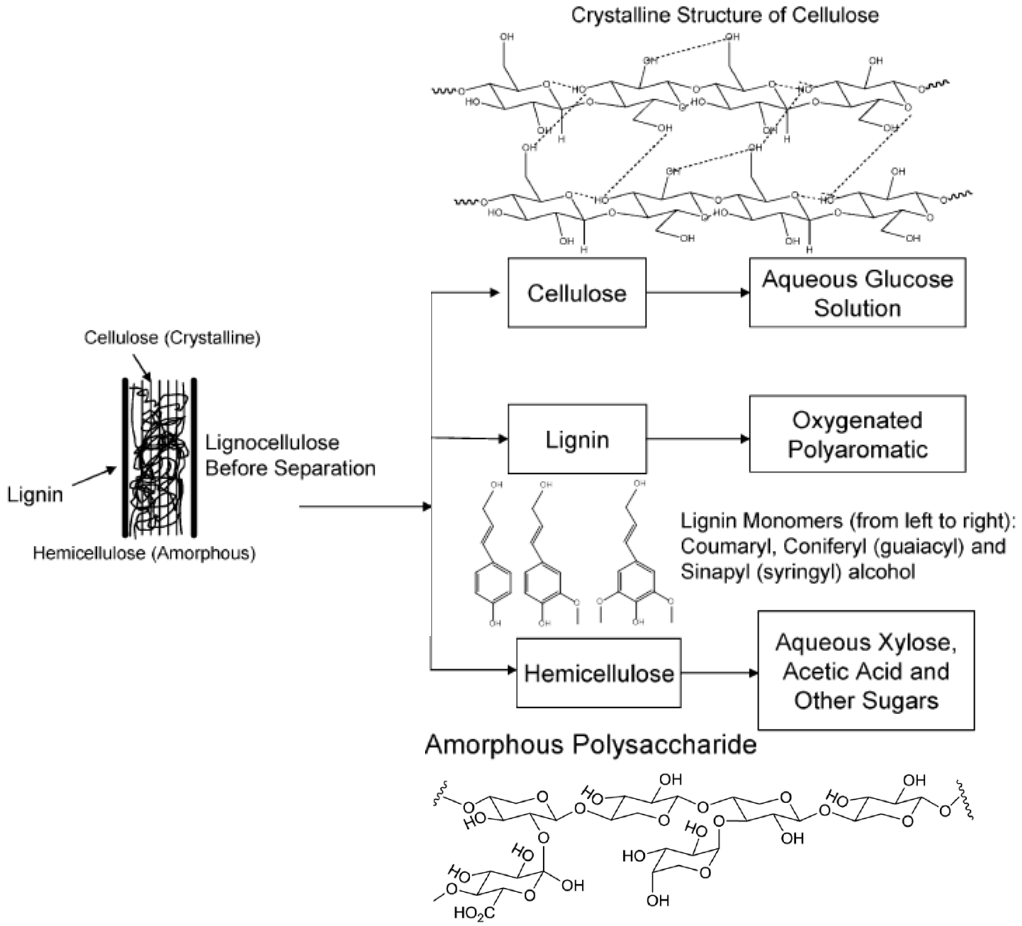

Figure 1-2. Structures of different biomass fractions (cellulose, hemicellulose and lignin). Adapt form ref. [23].

The primary liquid mixture form the degradation (*e.g.*, liquefaction or pyrolysis) of lignocellulosic biomass is generally called bio-oil, which contains a large variety of oxygenated compounds.[25,26] The composition of bio-oil obtained from the depolymerization or fragmentation of lignocellulosic biomass is shown in **Figure 1-3**. Lignin-derived compounds are principally constituted by the aromatic molecules such as phenols and guaiacols, whereas the sugars, miscellaneous oxygenates, furan/pyran ring-

containing compounds are primarily produced from the cellulose and hemicellulose. The other components such as acids, alcohols, ethers and ketones are also included in such bio-oil. Many studies indicate that the components distribution depends mainly on the nature of the biomass raw materials and the degradation processes.[25,27,28]

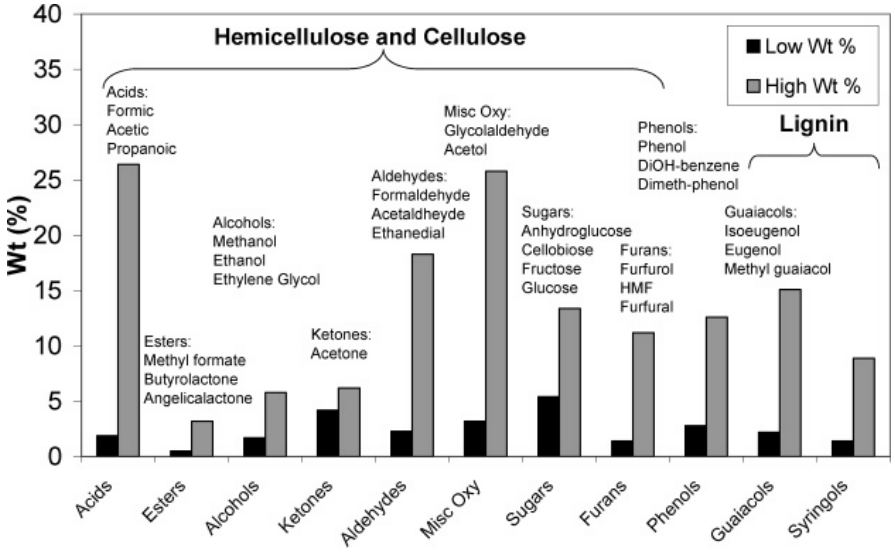

Figure 1-3. Chemical composition of bio-oil from depolymerization and fragmentation of lignocellulosic biomass.[24]

1.3 Lignin as a renewable energy carrier

Lignin accounts for 10-25% weight of lignocellulose and contains approximately 40% of the possible energy of the biomass due to its high content of organic carbon.[16,29] Nevertheless, lignin is often treated as a waste stream in most current biorefinery technologies and combusted to produce heat and power for biorefinery processes, rather than used as a feedstock for the production of value-added chemicals.[30] In this sense, the effective use of lignin to produce valuable fuels and chemicals is expected to have great potential of development in the future.

Lignin is a class of amorphous tridimensional biopolymer built of three cinnamyl alcohol monomers: p-coumaryl alcohol, coniferyl alcohol, and sinapyl alcohol, linked via C-C and C-O bonds.[11,31] The content of each unit in lignin differs on the basis of plants. The representative structure of lignin is given in **Figure 1-4**. Compared with cellulose

and hemicellulose, the decomposition of lignin is generally easier.[32] Furthermore, much less oxygen content in lignin than cellulose/hemicellulose makes it a more promising feedstock for transformation.[14,33,34] Depolymerization is an effective process which can decompose the complex lignin into small pieces for further production of high-value chemicals via catalytic methods. Through a variety of depolymerization/degradation treatments, *e.g.*, the process of pyrolysis, gasification, hydrogenolysis, chemical oxidation, and hydrolysis, the compounds rich in aromatics/phenolics could be obtained from lignin. [32,33,35]

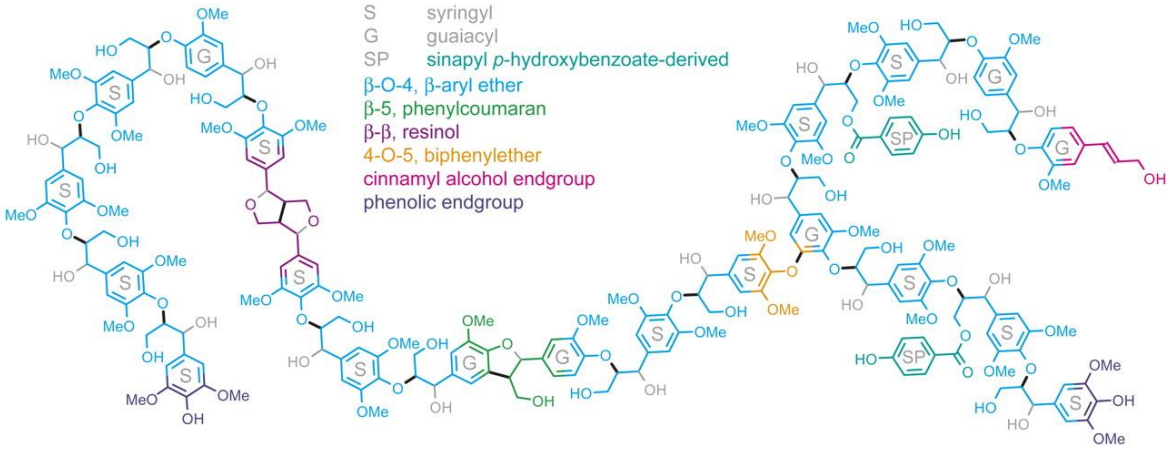

Figure 1-4. Representative structure of a lignin polymer.[36]

The major technologies for lignin transformation are summarized in **Figure 1-5**. These processes are achieved by thermochemical treatments under different conditions, *e.g.*, in an oxidizing environment (with O_2, H_2O_2, etc.), in a reducing environment (with H_2 or a hydrogen donor solvent as a reductant), or in a neutral environment.[30] For example, pyrolysis of lignin, usually in the absence of oxygen and at the temperature between 300 and 600 °C,[37] generates liquid oil, solid char, and gases. The products distribution is affected by the feedstock types as well as the treatment conditions including heating rates and reaction temperatures.[38] Gasification converts lignin into gaseous products like H_2, CO_2 and CO at the temperature between 700 and 1000 °C.[37] The valuable bio-syngas generated from depolymerization of lignin can also be used for producing liquid fuels through Fischer–Tropsch synthesis techniques.[39] Oxidation represents thermal treatment in the presence of oxygen at lower temperatures of

0−250 °C,[30] and it favors the conversion of lignin into aromatic alcohols, aldehydes, and acids that are target fine chemicals or platform molecules.

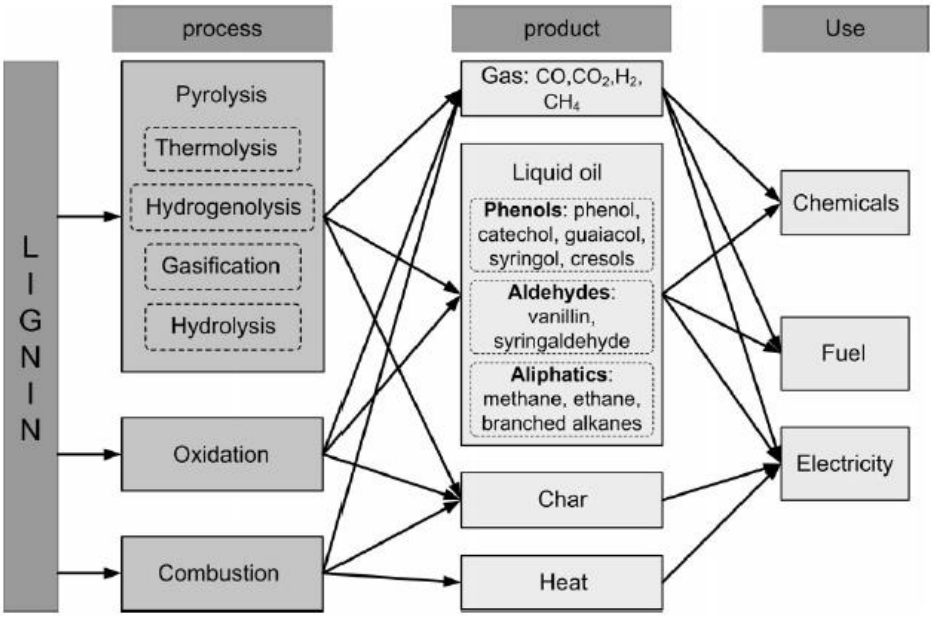

Figure 1-5. Thermochemical processes of lignin conversion.[32]

1.4 Catalytic upgrading of lignin-derived bio-oils

The hydrodeoxygenation (HDO) of lignin-derived phenolics into fuels and chemicals in the presence of hydrogen, primarily, either via direct hydrogenolytic C−O bond cleavage over metal surfaces, or via sequential hydrogenation-dehydration reactions catalyzed by admixtures or nano-domains composed of metal and acid functions often referred to as dual-functional catalysts, has been intensively investigated, using model compounds representative of lignin-derived bio-oils such as phenol, guaiacol, anisole, etc.[20,40-45,35,36] Phenol is the simplest phenolic monomer and it has been preferentially studied in recent studies.[14,44,46,47] A typical hydrogenation-dehydration reaction sequence in aqueous-phase HDO of phenol over dual-functional catalysts is shown in **Scheme 1-1**, in which phenol is first converted to cyclohexanol by hydrogenation over metal sites, and subsequent dehydration of cyclohexanol on acid domains leads to the formation of cyclohexene which is in turn hydrogenated to produce saturated cyclohexane.

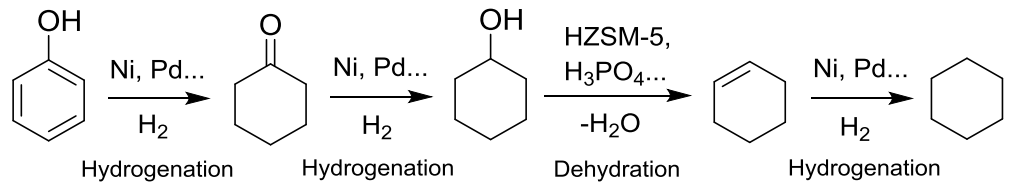

Scheme 1-1. Reaction pathway for phenol hydrodeoxygenation over Ni/HZSM-5 in aqueous phase. Adapt form ref. [47] and ref. [48].

In this typical phenol HDO sequence over a dual-functional catalyst, the dehydration reaction, which occurs on the acid sites, is the only step that ejects O-atoms. Depending on the catalyst formulation, the acid-catalyzed dehydration step can be rate-limiting in the overall reaction cascade, *e.g.*, with a highly active hydrogenation component (Pd) and a weak acid (H_3PO_4).[36] During the HDO of phenol, acid-catalyzed C-C bond coupling reactions simultaneously take place, producing heavier hydrocarbons from phenol reacting with its potential products such as cyclohexanol and cyclohexene. The integration of O-removal and C-C bond formation provides a feasible scheme for converting the phenolic bio-oil into transportation fuels ranged hydrocarbons without adding of additional alkylating reagents.

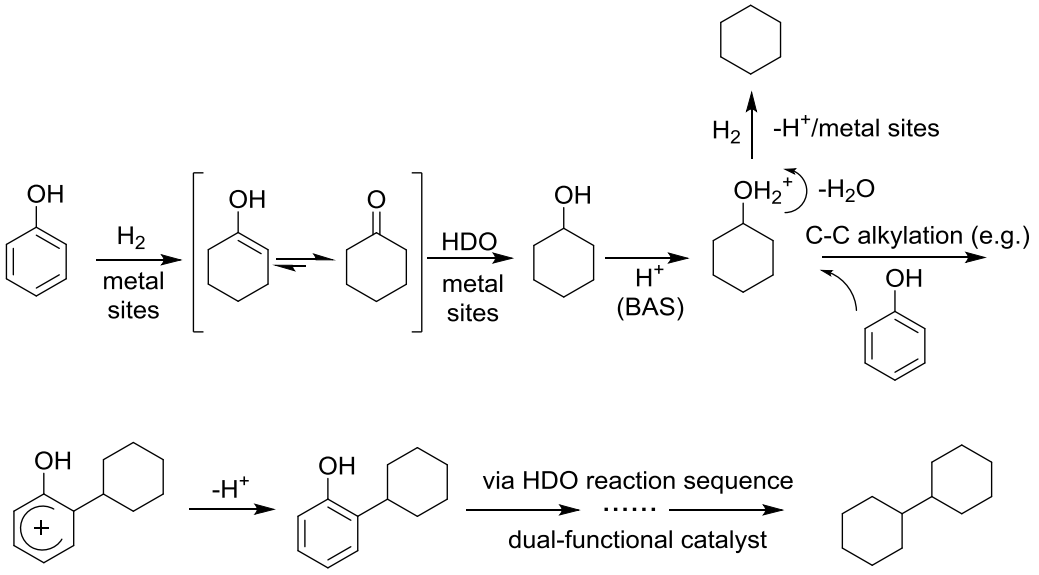

Scheme 1-2. Proposed reaction pathways for the catalytic phenol hydrodeoxygenation and hydroalkylation in aqueous phase. Adapt form ref. [46].

Lercher group reported the hydrodeoxygenation[45,49,50] and hydroalkylation[40,46] of phenol over the dual-functional catalysts operated in aqueous phase. The phenol or substituted phenolic compounds have been abundantly used in aqueous-phase hydroalkylation in the presence of metal sites (Pd, Ni) and solid or liquid acid catalysts. The proposed reaction pathway is illustrated in **Scheme 1-2**, where phenol simultaneously reacts with the in situ formed cyclohexanol or cyclohexene to produce the alkylphenols which can be further hydrodeoxygenated to the gasoline or diesel ranged hydrocarbons. The produced bi- or tri-cycloalkanes which are free of sulfur, oxygen, or polyaromatics can be applied as high-grade bio-fuels.

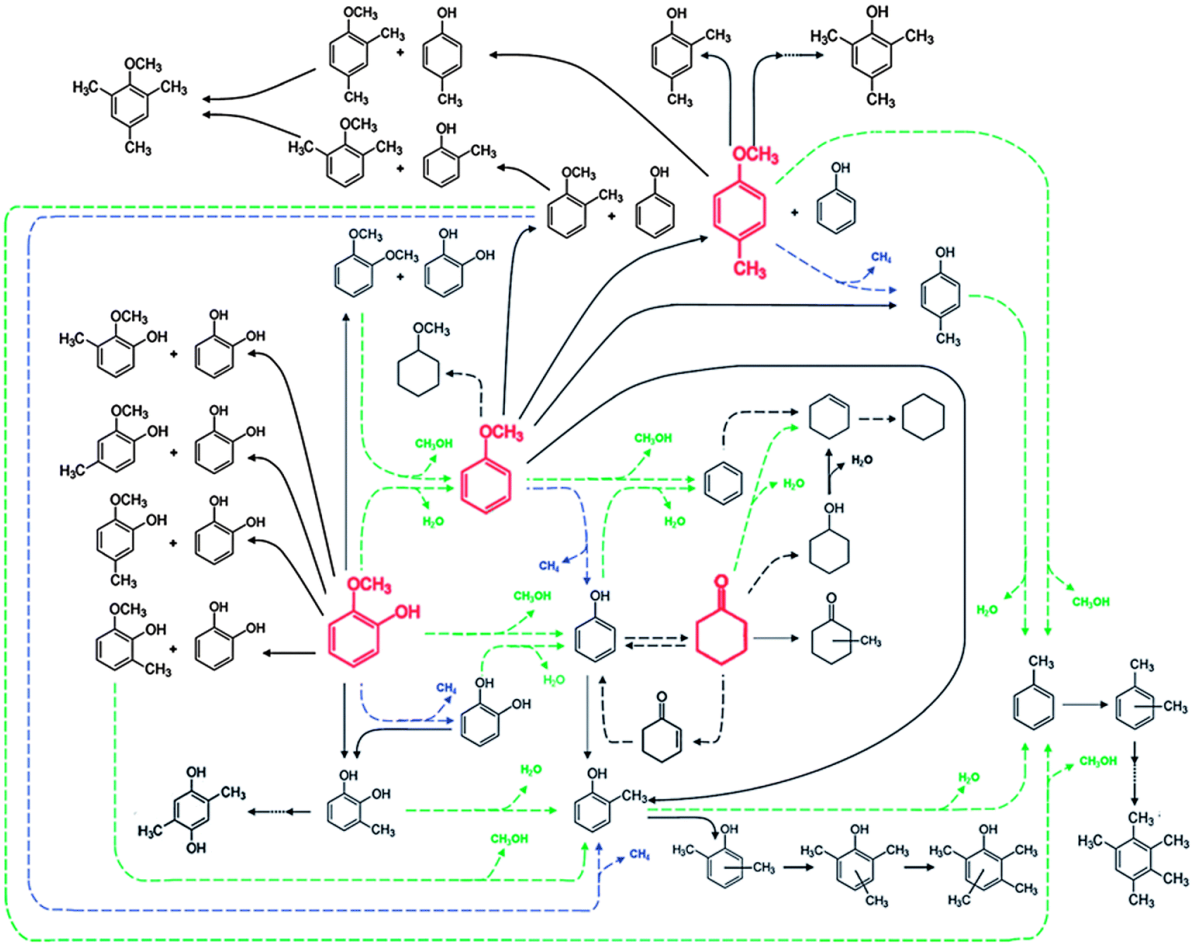

Scheme 1-3. Proposed reaction network for the conversion of lignin-derived compounds (each compound shown in red was used as a reactant).[51] HDO, hydrogenolysis, and hydrogenation (or dehydrogenation) reactions are represented by dashed green, blue, and black arrows, respectively. Alkylation reactions are represented by solid black arrows.

A more comprehensive reaction network using the compounds representative of lignin-derived bio-oils such as guaiacol, anisole, and other reaction intermediates over Pt/γ-Al_2O_3 at 300 °C in the presence of 1.40 bar H_2 has been proposed in **Scheme 1-3**.[51]

A variety of solid acid catalysts such as zeolites, oxides, sulfonated carbon and heteropolyacids, have served as important functional materials for the production of fuels and chemicals in current chemical industry.[52] The main advantages of the solid acids in comparison to traditional mineral acids (*e.g.*, H_2SO_4, HCl and H_3PO_4) are that they are non-corrosive and easy to separate from the reaction mixture for recycle. Among these solid acid catalysts, much attention has been focused on zeolites attributed to their high surface area, high adsorption capacity, adjustable acidity, shape selectivity, high thermal and hydrothermal stability.[53] Benefited from these unique properties, zeolites have been widely used as catalysts in the conventional petrochemical industry,[53,54] as well as in the transformation of biomass.[55,56] Regarding biorefinery processes, the robust zeolites that are active and stable in hot liquid water are required due to the omnipresence of water in biomass feedstocks. Zeolite catalysts and their stability under hydrothermal conditions will be discussed in later sections.

1.5 Zeolite catalysts and their application in biomass conversion

Zeolites are a class of relatively well-defined porous materials built of SiO_4 and AlO_4 tetrahedral units.[57] Adjacent tetrahedra are linked at their corners through an oxygen atom forming channels, cages and different frameworks. Since aluminum is at +3 oxidation state, the AlO_4 tetrahedra have a net negative charge associated with Al that requires an equivalent charge-balancing cation, *e.g.*, Na^+, K^+ and H^+, to ensure the electroneutrality of the framework.[58] If a proton is the charge-balancing cation, a Brønsted acid site (BAS) is generated. In addition, the migration of Al centers from lattice produces octahedrally coordinated aluminum species that are generally denoted as extra framework aluminum (EFAL), which is believed to be responsible for the Lewis acidity in zeolites.[59] Due to the divers and adjustable acidity, together with the unique structures, zeolites have been abundantly used as catalysts, ion-exchange reagents,

adsorbents, etc. Currently, more than 200 different zeolite structures are known, and among these, MFI, FAU and BEA-type zeolites are three most popular zeolites used in traditional chemical industry, as well as in biomass conversion. **Figure1-6** shows the different framework of these three zeolites.

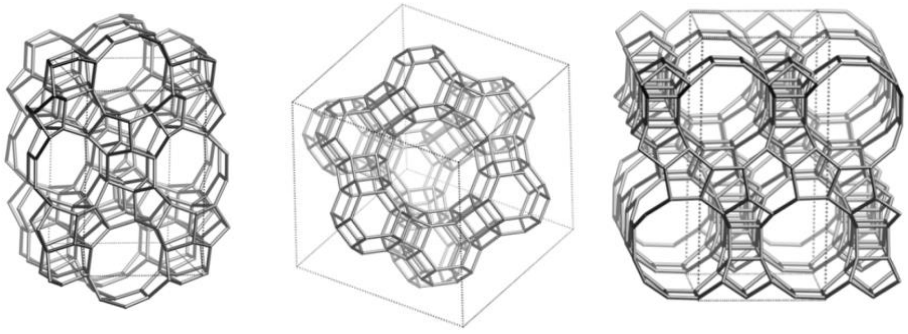

[010] **[111]** **[010]**

MFI **FAU** **BEA**

Figure 1-6. The framework structures of MFI, FAU and BEA-type zeolite. All information obtained from IZA website.

In the transformation of biomass, zeolites are commonly used in catalytic degradation of lignocellulosic raw materials to bio-oils, as well as in the subsequently catalytic upgrading of bio-oils to desired hydrocarbons. The products distribution remarkably relies on the acidity and shape selectivity of the applied zeolite catalysts.[55,60-62] The Si/Al ratio leads to the different concentrations and strength of acid sites, while the pore size controls the access of reactants to these active centers. Here, three zeolites (**Figure 1-6**) with different topology structures are described. Zeolite ZSM-5 (MFI-type) has a tridimensional pore structure consisting of two perpendicular 10-membered ring (MR) channels (sinusoidal: 5.3Å×5.6Å; straight: 5.1Å×5.5Å). Zeolite Y exhibits the FAU structure and it has a tridimensional pore structure with channels running perpendicular to each other in the x, y, and z planes. The pore opening of HY is 7.4Å and it contains a larger cavity with diameter of 12Å. Zeolite BEA is a highly disordered structure formed by the random intergrowth of two polymorphs namely A and B. BEA possesses an interconnected tridimensional pore network delimited by 12MR channels with an approximate diameter of 7.5–8 Å and cavities of 12–13 Å at the intersections.

In zeolite-catalyzed biomass conversion, the products distribution is affected by the acidity and framework structure of the selected zeolites. For a given platform molecule such as glucose, the correlation among the biomass feedstock, the pyrolysis products and the zeolite pore size is shown in **Figure 1-7**.[62] In general, the catalysts with small pore size (< 5 Å, 8MR ring zeolite such as SAPO-34) will not be able to produce any aromatics but only CO, CO_2 and water, because the reactant molecules cannot diffuse into the zeolite channels and the reactions predominately take place on external surface of zeolite. Medium-pore zeolites (5.2-5.9 Å, 10MR ring zeolite such as ZSM-5) can generate aromatics with high yields. As previously reported, HZSM-5 is a selective catalyst for the production of aromatic hydrocarbons from bio-oil vapors,[63] attributed to its moderately internal voids for the formation of transition states and the appropriate size of pore-openings for the diffusion of aromatic molecules. Larger-pore zeolites with pore diameter > 7.2 Å (12 MR ring zeolite such as HBEA and HY) allow the reactions inside of channels, showing a high yield for coke formation but a low yield for aromatics.

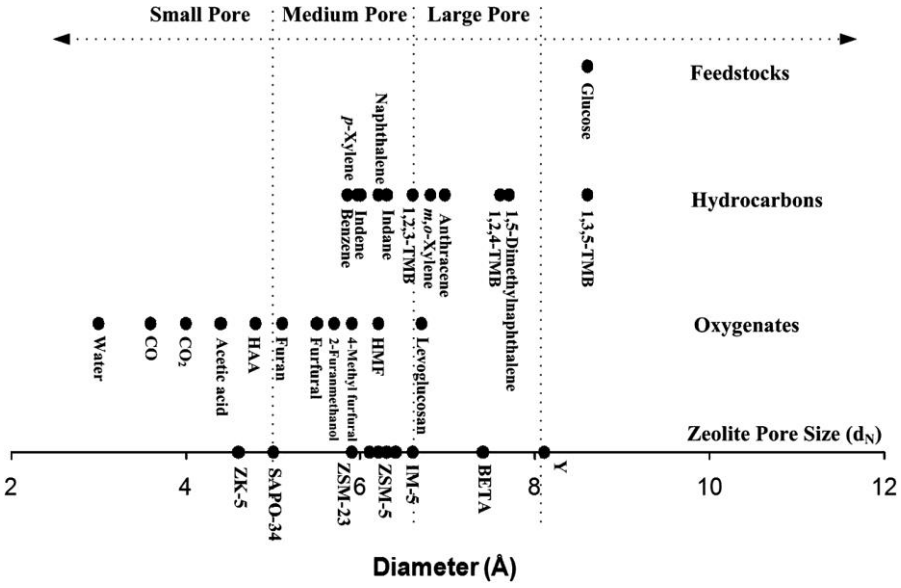

Figure 1-7. Schematic of zeolite pore diameter compared to the kinetic diameter of feedstocks and products in the catalytic pyrolysis of glucose.[62]

1.6 The state of BAS and zeolites stability in aqueous phase

Regardless of the impact of water on the relevant reactions, the highly hydrothermal stability of zeolites in hot liquid water is one important concern from the practical point of view when they are used in upgrading of bio-oil in the presence of abundant water. Unlike their highly hydrothermal stability in vapor phase, the zeolites suffer much server degradation in hot liquid water.[64-66] As previously reported, delamination of zeolites occurs with relatively small structure damage after a long-time treatment at 500°C in vapor-phase water, whereas a dramatic structure collapse and crystallinity loss happens in aqueous phase at 200°C.[67]

Specific interactions between water molecules and acid sites on zeolites have been studied by numerous researchers. Lercher *et al.*[68] reported that water initially interacted with LAS or defects of HZSM-5 at its very low equilibrium pressures, and then the interaction with strong BAS became significant at higher pressures of water. Upon these BAS, water adsorbed initially with a stoichiometry ratio of 1:1 at lower pressures, whereas larger water clusters (H_2O/strong BAS ratio > 1) formed at higher pressures. Similarly, four water molecules were observed to adsorb on each BAS, forming a $H_9O_4^+$ in HMOR with Si/Al ratios > 5.[69] The water cluster formation was also observed on zeolite HBEA[70], HSSZ-13 and HSAPO-34[71]. Interestingly, as observed on HZSM-5 and HMOR, the clustering of water already starts before the complete coverage of BAS. When exposing zeolites to water vapor, two adsorption forms of water on BAS have been suggested: a hydrogen-bonded model (neutral complex) and a protonated model (ion pair structure), as shown in **Figure 1-8**. [72] The adsorption model primarily depends on the size of formed water cluster. For instance, hydronium ions are not formed in a few amounts of H_2O adsorption on zeolites at a low coverage of BAS. With increasing the uptake of H_2O, proton transfer form bridging hydroxyl groups (BAS) to water clusters becomes favorable because lager water clusters possess a proton affinity sufficiently high to abstract protons from the zeolite framework.[71] Water adsorption on BAS of zeolites has been intensively investigated by means of IR spectroscopy. The characteristic band at 2885 and 2463 cm^{-1} were assigned to the formation of hydronium ions.[68] The monomeric hydrogen-bonded water, the protonated dimeric $H_5O_2^+$ and lager water

clusters were inferred based on IR spectroscopy.[73,74] The IR bands associated with the adsorbed water on HZSM-5 are compiled in **Table 1-1**.

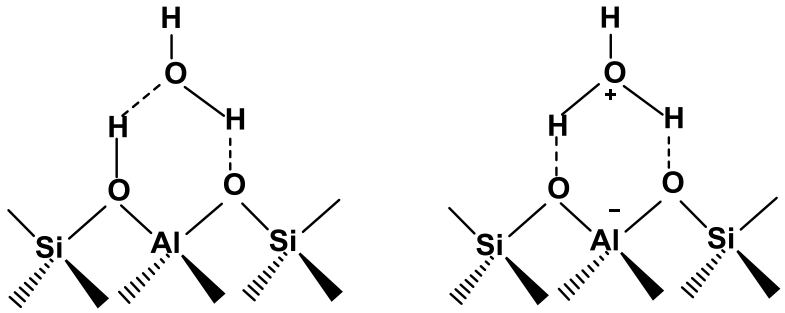

(a) Hydrogen-bonded model **(b) protonated model**

Figure 1-8. Proposed structures of water adsorbed on BAS.[72]

Figure 1-1. IR bands assignment for water adsorption on HZSM-5.[74]

Assignment	Monomer	Dimer	Polymer
ν(OH)	3701	3600	3429
	~3550	~3366	
	2872[a]	3213	
	2460[a]		
	~1700[a]	~1700	
δ(HOH)			1659
δ(OH)	1350		
γ(OH)	875		

[a] (A, B, C) triplet.

Thus, regarding specific biomass conversion in aqueous phase, the state of BAS cannot be considered as a proton attached to the zeolite lattice anymore. Both strong and weak Brønsted acid sites on zeolites generate hydronium ions in aqueous phase, revealed by the in-depth characterizations of zeolite HBEA using extended X-ray absorption fine structure (EXAFS) and ^{27}Al MAS NMR spectroscopy.[68,69] In addition, these hydronium ions are found to have equal activity in the aqueous-phase dehydration of cyclohexanol.[75] Previous work suggests that framework defects, *e.g.*, silanol-nests, are the primary centers causing the decomposition of zeolite lattice in hot liquid water,[65] and that the degradation of zeolite HBEA proceeds via selective hydrolysis of framework T−O−T bond.[76] The proposed degradation routes for zeolites in hot liquid water are

shown in **Figure 1-9**. Resasco *et al.*[67] have shown that the density of silanol-terminated defects plays the most crucial role in determining the zeolite hydrothermal stability in hot liquid water, compared to the other parameters such as the number of BAS, Si-O-Si groups, topology structures and EFAL species. Therefore, repairing the Si−OH defects via postsynthetic modification of the zeolite with organosilanes is expected to increase the hydrophobicity of the defective sties that leads to stabilization of the zeolite in hot liquid water. Recently, Lercher *et al.*[77] have reported an effective modification strategy to improve the zeolite HBEA stability in aqueous phase by silyation treatment using trimethylchlorosilane as silyating agent. The Si-OH bonds in HBEA are eventually removed by reaction with trimethylchlorosilane to form the Si-O-Si bonds which are more hydrophobic. The microporosity is only retained in the silylated HBEA, in spite of the mesopores generation in both treated and untreated samples.

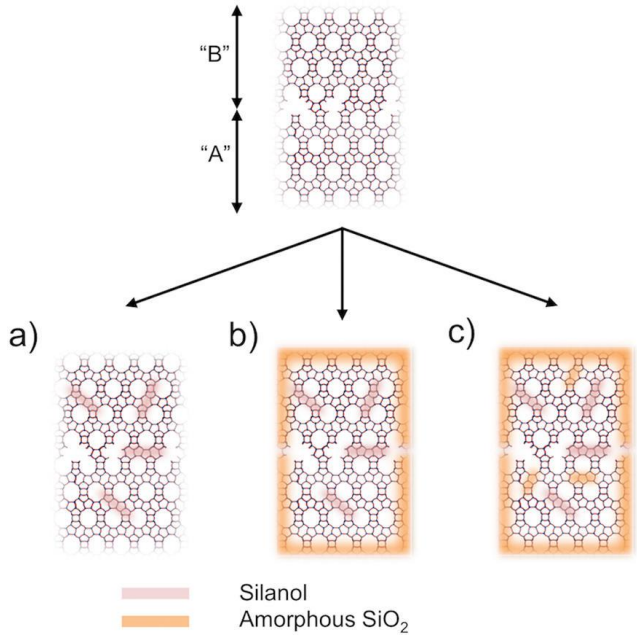

Figure 1-9. Suggested pathways for zeolite degradation in hot liquid water.[76] (a) Si−OH group formation from the selective hydrolysis of framework T−O−T, (b) the formation of amorphous silica cap on the surface, and (c) collapse of the zeolite framework and degradation to an amorphous material.

1.7 Zeolite-catalyzed dehydration of alcohol

The oxygen removal step is crucial to control the reactivity of intermediates and a variety of reactions including hydrogenolysis, dehydration, decarbonylation and decarboxylation have been used to reduce the oxygen content in biomass feedstocks.[13] Cycloalcohols are the reaction intermediates in the process of hydrogenation/HDO of lignin-derived phenolic compounds. Accordingly, the acid-catalyzed alcohol dehydration becomes one of the promising strategies for elimination of oxygenated functionalities during the upgrading of bio-oils. In hydrogenation-dehydration reaction sequence, as previously shown in **Scheme 1-1**, the dehydration reaction is typically two orders of magnitude slower than the hydrogenation step and thus limits the whole reaction rate,[44] which is in accordance with the kinetic assessment that the C-O bond cleavage is more costly in activation barrier than the hydrogen addition step.[48] Therefore, finding highly active and stable catalysts for the dehydration of cycloalcohols is a crucial task for HDO of phenolic compounds to saturated hydrocarbons, especially in the presence of hot liquid water. The acidity and microporosity in zeolites enable them to be good candidates for selective dehydration of biomass-derived intermediates, *e.g.*, zeolites HBEA shows a high performance in deoxygenation of the lignin-derived platform molecules.[46,47]

The dehydration of alcohol can go through either an E1 or an E2 elimination mechanism, generally referring to the unimolecular and bimolecular reaction routes, respectively. A given alcohol can undergo dehydration by any one of two mechanisms, depending predominately on the reaction conditions, *e.g.*, the applied catalyst, the alcohol structures (*i.e.*, primary, secondary and tertiary), the reaction temperatures and the reaction media. In the presence of a strong acid and a weak base, alcohol dehydration occurs primarily via E1 elimination. A carbocation intermediate is formed by the loss of the protonated hydroxyl group ($-OH_2^+$) as water. In an E1 mechanism, the formation of the carbocation is the rate-limiting step, and the subsequent formation of the alkene is facile followed by removal of a proton from the carbocation. During E1 elimination, some carbocations can undergo the carbon skeletons rearrangements to form more stable intermediates. In an E2 mechanism, alcohol dehydration occurs via β elimination, in

which the proton on the β carbon and the hydroxyl group are eliminated in a concerted manner.

In gas-phase dehydration in the absence of water, BAS-catalyzed alcohol dehydration was proposed to undergo E1 mechanism,[78,79] in which the formation of surface-bonded alkoxide and water was suggested as the rate-limiting step.[72] On γ-Al_2O_3, however, E2-type mechanism for the unimolecular dehydration of alcohol, involving concurrent cleavage of C_α–O and C_β–H bonds, was proposed based on the observed kinetic isotope effect (KIE).[80] In aqueous phase, while the dehydration of primary alcohols in supercritical water was suggested to undergo E2 elimination pathway,[81] the dehydration of secondary alcohols catalyzed by mineral acids was suggested to proceed via the E1 mechanism.[82] Previously, Lercher *et al.*[83] used in-situ magic angle spinning (MAS) ^{13}C nuclear magnetic resonance (NMR) spectroscopy to investigate the reaction mechanism of cyclohexanol dehydration on a high-silica HBEA in aqueous phase. It was demonstrated that the E1 elimination mechanism most favorably explains the scrambling rates of the ^{13}C-label, in accord with conclusions reached for gas phase dehydration over zeolites. The in-situ ^{13}C MAS NMR results together with the proposed reaction mechanism are shown in **Figure 1-10**.

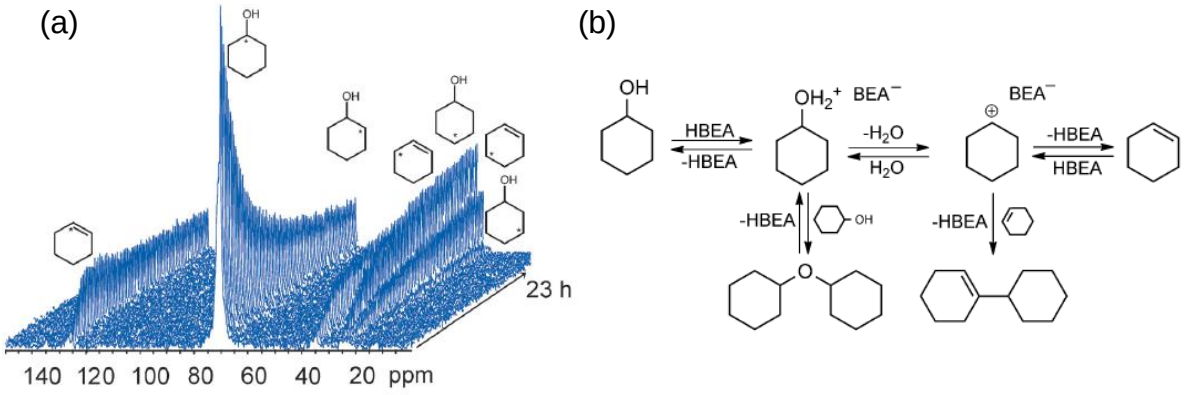

Figure 1-10. Dehydration of cyclohexanol on HBEA in aquoue phase monitored by in-situ NMR.[83] (a) Stacked plot of MAS-NMR spectra as a function of time, (b) proposed reaction parthway for cyclohexanol dehydration in water over HBEA zeolite.

Gas-phase dehydration of alcohols, from primary to tertiary, acyclic and cyclic, has been extensively studied on solid acids. The negative effects of the alcohol partial pressure on the olefin formation rates have been commonly observed on zeolites[84-86] and POM clusters[87-89]. The decrease in rates with increasing the alcohol pressures was ascribed to the formation of the unreactive (protonated) alcohol dimer occupying the acid sites, thus inhibiting the overall dehydration reaction. In contrast, far less is known about the kinetics and mechanism of dehydration catalyzed by acids in liquid media. Therefore, in this thesis, the detailed kinetics and mechanisms for the liquid-phase dehydration of alcohol are investigated.

1.8 Zeolite-catalyzed alkylation of phenol

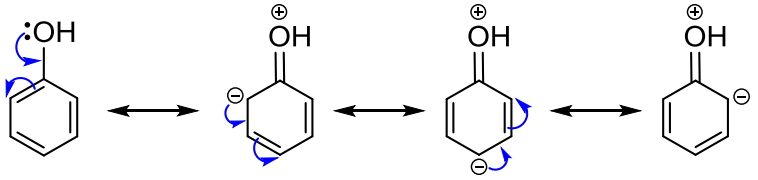

Scheme 1-4. The negative charge delocalized by resonance to three different carbons on phenol.

Alkylation is a common method for C–C bond formation that can build desirable objectives from small organic molecules. The hydrodeoxygenation (HDO) reaction sequence is often combined with C–C bond formation via related processes, *e.g.*, aldol-condensation, ketonization and oligomerization. Since lignin-derived bio-oils are typically phenolic molecules with carbon atoms of C_6-C_9, these C–C coupling steps can produce larger fuel ranged hydrocarbons, as those currently used in diesel engines (C_{10}–C_{20}) and jets (C_9–C_{16}).[13]

Phenol, the simplest platform molecule in lignin-derived bio-oils, is usually taken as an example for the alkylation study. The reactivity of the hydroxyl group of phenol strongly activates the ring substituents, especially at the *ortho* (*o*-C-alkylation) and *para* (*p*-C-alkylation) positions.[90] Moreover, the cation can be localized at the oxygen of the hydroxyl group leading to the formation of ethers (C-O-alkylation).[91,92] For alkylation of phenol, O-alkylation (ether formation) generally occurs at low temperatures, short

residence time and on weaker acid sites.[93-95] C-alkylation is favored in the presence of olefins and the ratios of *ortho*/*para* selectivity is related to the nature of the employed olefins[96] as well as the catalyst applied[93]. The electrophilic substitution toward *ortho* positon of phenol is favored when the secondary carbocation is the electrophile.[96] Compared to the mineral acids traditionally used in the Friedel-Crafts type reactions,[97] heterogeneously acidic zeolites are more attractive for C-C bond formation in the field of biomass conversion.[98,99] In addition, unlike the homogeneous acids, the local increase of reactant concentrations in zeolite pores can lead to the enhancement of the reaction rates.[100]

Previous studies devoted to the alkylation of phenol use the straight or branched alcohols or alkenes as alkylating agents over solid catalysts in vapor- or liquid-phase.[91-93] However, phenol alkylation with its potential products, cyclohexanol and cyclohexene, especially in liquid phase, has not been sufficiently investigated. Lercher *et al.*[36] studied aqueous-phase phenol alkylation with cyclohexanol over a variety of solid catalysts including zeolites, Amberlyst®15, Nafion/SiO_2 (SAC-13), $Cs_{2.5}H_{0.5}PW_{12}O_{40}$ and H_2SO_4-ZrO_2. Only zeolite-type acids (HBEA and HY) with relatively larger pore size performed higher selectivity in alkylation, while the non-zeolitic solid acids solely catalyzed the alcohol dehydration, not C-C bond formation. Therefore, the combination of spacious zeolite constrains and BAS is an essential criteria for C-C bond formation. With non-zeolitic solid acids, the reason for their inactivity in alkylation was attributed to the limited adsorption capacity of reactants.

1.9 Scope of this thesis

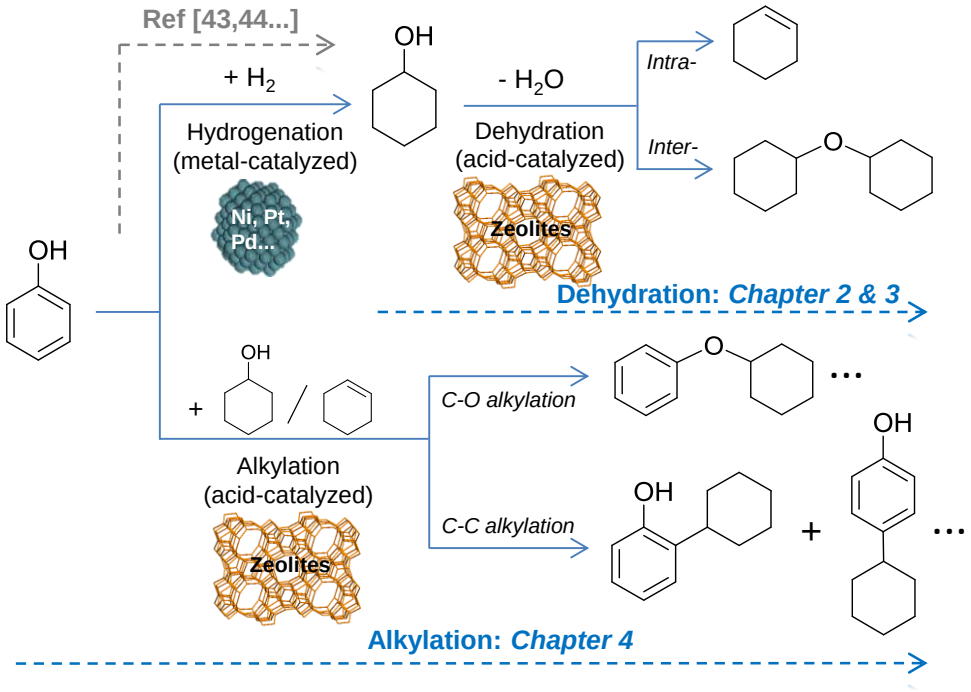

Figure 1-11. Schematic illustration of cyclohexanol-related reactions during the HDO of phenol in liquid phase.

The catalytic upgrading of lignin-derived phenolic compounds for the production of transportation fuels and high-value chemicals offers a promising strategy to reduce the dependence of the chemical industry on conventional fossil resources. Phenol, the simplest molecule representative of lignin-derived bio-oils, has been abundantly employed as a platform molecule to investigate the chemistry involved in the lignin-to-fuels upgrading processes such as aqueous-phase hydrodeoxygenation (HOD). The catalytic hydrogenation-dehydration sequence of phenol over a dual-functional catalyst in aqueous phase (as shown in **Scheme 1-1**) contains the hydrogenation of phenol, ketone and alkene over the metal function and the dehydration of alcohol on acid domains, and in which the O-removal step limits the whole reaction rate. In addition, the acid-catalyzed C-C bond formation (C-alkylation) coupled with these O-removal steps can produce fuel ranged hydrocarbons, offering an alternative upgrading approach. Thus, understanding the fundamental chemistry in both cylohexanol-related dehydration and alkylation reactions, together with identifying the effective catalysts for two elementary processes

will be of vital importance. In this context, the focus of this thesis will be laid on two major parts: 1) the acid-catalyzed dehydration of cyclohexanol, and 2) the acid-catalyzed alkylation of phenol with cyclohexanol. The detailed study items in each chapter of this thesis are illustrated in **Figure 1-11**.

Increasing the rates of alcohol dehydration is one of the key tasks in the utilization of biomass and is especially challenging in the presence of bulk water. Previously, we found acidic zeolite HBEA showed a higher activity for the aqueous-phase dehydration of cyclohexanol than the mineral acids, *e.g.*, H_3PO_4. Moreover, it is already clear that the Brønsted acid sites confined in zeolite pores exist as the hydronium ions in the presence of water, which have the same nature as those dissociated from the liquid acids. This allows us to study the catalytic consequence of constrains around the hydronium ions in aqueous phase. Therefore, in the second chapter of this thesis, we investigated the aqueous-phase cyclohexanol dehydration using homogeneous H_3PO_4 and heterogeneous zeolite HBEA to determine the effect of the microenvironments on catalysis. We reported how confines of zeolitic nanopores enhance the catalytic rates of hydronium ions for alcohol dehydration, using thermochemical and kinetic measurements in conjunction with density functional theory (DFT) and isotope labelling experiments.

After the in-depth study of the consequence of microenvironments on aqueous-phase cyclohexanol dehydration, in the third chapter, we reported the detailed kinetic evaluation of cyclohexanol dehydration in aqueous phase and in its neat liquid form without the presence of intentionally added water. Tow high-silica HBEA (Si/Al = 75 and 71) zeolites with well-defined Al T-site distributions, minimum extra-framework Al moieties, as well as decent hydrothermal stability at moderate temperatures relevant to dehydration catalysis (160−200 °C) were employed as catalysts and were characterized in detail, aiming to establish a reliable and unequivocal structure-property relation in the liquid-phase dehydration, as well as the impact of reaction medium (*e.g.*, water as solvent or solvent-free). Experimental kinetics, characterizations, together with DFT calculations collectively supplied insights into the most probable reactive intermediates and activation barriers for kinetically relevant elementary steps of cyclohexanol dehydration occurring in HBEA pores.

In the fourth chapter of this thesis, the solid-acid-catalyzed alkylation of phenol with cyclohexanol or cyclohexene in liquid hydrocarbons (decalin) and aqueous phase were comprehensively studied. We have previously reported (hydro)alkylation reactions of phenol and substituted phenols with cyclohexanol using heterogeneous catalysts in aqueous phase, however, the reaction mechanism has not been sufficiently explored. Furthermore, in liquid phase, as we have already shown in the third chapter that solvents can also play an important role in determining the status of active sites as well as the relevant reaction intermediates. Accordingly, in this chapter, a variety of solid acids, including the microporous zeolites (HBEA, HY and HZSM-5), macroporous resin (Nafion/SiO_2) and γ-Al_2O_3 were first used to investigate the structure-reactivity relation in the phenol alkylation in decalin. After testing the different solid acids, we focused on one of the representative and most active large-pore zeolites, HBEA (Si/Al = 75), to further explore the kinetic and mechanistic aspects of phenol alkylation in decalin and compare those with aqueous phase phenol alkylation on the same catalyst.

The final chapter summarizes the integrated conclusions of this thesis and generalizes some insights into the catalyst design for the liquid-phase upgrading of bio-oils into desired fuels and chemicals.

1.10 References

[1] Nel, W. P.; Cooper, C. J. *Energy Pol.* **2009**, *37*, 166.

[2] Shafiee, S.; Topal, E. *Energy Pol.* **2009**, *37*, 181.

[3] Lanzafame, P.; Centi, G.; Perathoner, S. *Chem. Soc. Rev.* **2014**, *43*, 7562.

[4] Gallezot, P. *Chem. Soc. Rev.* **2012**, *41*, 1538.

[5] Melero, J. A.; Iglesias, J.; Garcia, A. *Energ. Environ. Sci.* **2012**, *5*, 7393.

[6] Balat, M.; Ayar, G. *Energ. Source.* **2005**, *27*, 931.

[7] Koh, M. P.; Hoi, W. K. *Biomass Bioenergy* **2003**, *25*, 517.

[8] In *Shell energy scenarios to 2050*, **2008**. http://www.shell.com/global/future-energy/scenarios/2050.html

[9] Centi, G.; Perathoner, S. In *Sustainable Industrial Chemistry*; Wiley-VCH Verlag GmbH & Co. KGaA: 2009, p 1.

[10] Author, N. G. *Biomass as Feedstock for a Bioenergy and Bioproducts Industry: The Technical Feasibility of a Billion-Ton Annual Supply, April 2005*, Office of Scientific and Technical Information (OSTI), **2005**.

[11] Zakzeski, J.; Bruijnincx, P. C. A.; Jongerius, A. L.; Weckhuysen, B. M. *Chem. Rev.* **2010**, *110*, 3552.

[12] Li, J.; Wang, X. *Energy Pol.* **2012**, *41*, 519.

[13] Serrano-Ruiz, J. C.; Luque, R.; Sepúlveda-Escribano, A. *Chem. Soc. Rev.* **2011**, *40*, 5266.

[14] Zhao, C.; Lercher, J. A. *Angew. Chem. Int. Ed.* **2012**, *51*, 5935.

[15] In *Biomass Gasification Design Handbook*; Elsevier BV: 2010, p 325.

[16] Zhou, C.-H.; Xia, X.; Lin, C.-X.; Tong, D.-S.; Beltramini, J. *Chem. Soc. Rev.* **2011**, *40*, 5588.

[17] Carpenter, D.; Westover, T. L.; Czernik, S.; Jablonski, W. *Green Chem.* **2014**, *16*, 384.

[18] Amidon, T. E.; Liu, S. *Biotechnol. Adv.* **2009**, *27*, 542.

[19] Corma, A.; Iborra, S.; Velty, A. *Chem. Rev.***2007**, *107*, 2411.

[20] Ruppert, A. M.; Weinberg, K.; Palkovits, R. *Angew. Chem. Int. Ed.* **2012**, *51*, 2564.

[21] Dutta, S.; De, S.; Saha, B.; Alam, M. I. *Catal. Sci. Technol.* **2012**, *2*, 2025.

[22] Akhtari, S.; Sowlati, T.; Day, K. *Renew. Sust. Energ. Rev.* **2014**, *33*, 117. RENEW SUST ENERG REV

[23] Huber, G. W.; Iborra, S.; Corma, A. *Chem. Rev.* **2006**, *106*, 4044.

[24] T. A. Milne, F. Agblevor, M. Davis, S. Deutch, D. Johnson, in *Developments in Thermal Biomass Conversion* (Eds.: A. V. Bridgwater, D. G. B. Boocock), Blackie Academic and Professional, London, **1997**.

[25] Venderbosch, R. H.; Prins, W. *Biofuels, Biofuels, Bioprod. Biorefin.* **2010**, *4*, 178.

[26] Zhang, J.; Toghiani, H.; Mohan, D.; Pittman, C. U.; Toghiani, R. K. *Energy & Fuels* **2007**, *21*, 2373.

[27] Dickerson, T.; Soria, J. *Energies* **2013**, *6*, 514.

[28] Mohan, D.; Pittman, C. U.; Steele, P. H. *Energy & Fuels* **2006**, *20*, 848.

[29] Perlack, R. D.; Wright, L. L.; Turhollow, A. F.; Graham, R. L.; Stokes, B. J.; Erbach, D. C. *Biomass as feedstock for a bioenergy and bioproducts industry: The technical feasibility of a billion-ton annual supply*, Office of Scientific and Technical Information (OSTI), 2005.

[30] Li, C.; Zhao, X.; Wang, A.; Huber, G. W.; Zhang, T. *Chem. Rev.* **2015**, *115*, 11559.

[31] Chakar, F. S.; Ragauskas, A. J. *Ind Crops Prod* **2004**, *20*, 131.

[32] Pandey, M. P.; Kim, C. S. *Chem. Eng. Technol.* **2011**, *34*, 29.

[33] Roberts, V. M.; Stein, V.; Reiner, T.; Lemonidou , A.; Li, X.; Lercher, J. A. *Chem. Eur. J.* **2011**, *17*, 5939.

[34] Huber, G. W.; Corma, A. *Angew. Chem. Int. Ed.* **2007**, *46*, 7184.

[35] Stärk, K.; Taccardi, N.; Bösmann, A.; Wasserscheid, P. *ChemSusChem* **2010**, *3*, 719.

[36] Vanholme, R.; Demedts, B.; Morreel, K.; Ralph, J.; Boerjan, W. *Plant Physiol.* **2010**, *153*, 895.

[37] Huber, G. W.; Iborra, S.; Corma, A. *Chem. Rev.* **2006**, *106*, 4044.

[38] Ferdous, D.; Dalai, A. K.; Bej, S. K.; Thring, R. W. *Energy & Fuels* **2002**, *16*, 1405.

[39] Lappas, A. A.; Iatridis, D. K.; Vasalos, I. A. *Ind. Eng. Chem. Res.* **2011**, *50*, 531.

[40] Zhao, C.; Song, W.; Lercher, J. A. *ACS Catal.* **2012**, *2*, 2714.

[41] Yan, N.; Yuan, Y.; Dykeman, R.; Kou, Y.; Dyson, P. J. *Angew. Chem. Int. Ed.* **2010**, *49*, 5549.

[42] Hong, D.-Y.; Miller, S. J.; Agrawal, P. K.; Jones, C. W. *Chem. Commun.* **2010**, *46*, 1038.

[43] Zhao, C.; Lercher, J. A. *ChemCatChem* **2011**, *4*, 64.

[44] Zhao, C.; He, J.; Lemonidou, A. A.; Li, X.; Lercher, J. A. *J. Catal.* **2011**, *280*, 8.

[45] Zhao, C.; Kasakov, S.; He, J.; Lercher, J. A. *J. Catal.* **2012**, *296*, 12.

[46] Zhao, C.; Camaioni, D. M.; Lercher, J. A. *J. Catal.* **2012**, *288*, 92.

[47] Song, W.; Liu, Y.; Baráth, E.; Wang, L. L.; Zhao, C.; Mei, D.; Lercher, J. A. *ACS Catal.* **2016**, *6*, 878.

[48] He, J.; Zhao, C.; Lercher, J. A. *J. Catal.* **2014**, *309*, 362.

[49] Zhao, C.; Kou, Y.; Lemonidou, A. A.; Li, X.; Lercher, J. A. *Chem. Commun.* **2010**, *46*, 412.

[50] Zhao, C.; Lercher, J. A. *ChemCatChem* **2012**, *4*, 64.

[51] Saidi, M.; Samimi, F.; Karimipourfard, D.; Nimmanwudipong, T.; Gates, B. C.; Rahimpour, M. R. *Energy Environ. Sci.* **2014**, *7*, 103.

[52] Corma, A. *Chem. Rev.* **1995**, *95*, 559.

[53] Corma, A. *Chem. Rev.* **1997**, *97*, 2373.

[54] Primo, A.; Garcia, H. *Chem. Soc. Rev.* **2014**, *43*, 7548.

[55] Ennaert, T.; Van Aelst, J.; Dijkmans, J.; De Clercq, R.; Schutyser, W.; Dusselier, M.; Verboekend, D.; Sels, B. F. *Chem. Soc. Rev.* **2016**, *45*, 584.

[56] Resasco, D. E.; Wang, B.; Crossley, S. *Catal. Sci. Technol.* **2016**, *6*, 2543.

[57] Weitkamp, J. *Solid State Ion.* **2000**, *131*, 175.

[58] Davis, M. E. *Acc. Chem. Res.* **1993**, *26*, 111.

[59] Guisnet, M.; Wang, Q. L.; Giannetto, G. *Catal. Lett.* **1990**, *4*, 299.

[60] Carlson, T. R.; Tompsett, G. A.; Conner, W. C.; Huber, G. W. *Top. Catal.* **2009**, *52*, 241.

[61] Aho, A.; Kumar, N.; Eränen, K.; Salmi, T.; Hupa, M.; Murzin, D. Y. *Fuel* **2008**, *87*, 2493.

[62] Jae, J.; Tompsett, G. A.; Foster, A. J.; Hammond, K. D.; Auerbach, S. M.; Lobo, R. F.; Huber, G. W. *J. Catal.* **2011**, *279*, 257.

[63] Adjaye, J. D.; Sharma, R. K.; Bakhshi, N. N. In *Progress in Catalysis, Proceedings of the 12th Canadian Symposium on Catalysis*; Elsevier BV: 1992, p 301.

[64] Zapata, P. A.; Huang, Y.; Gonzalez-Borja, M. A.; Resasco, D. E. *J. Catal.* **2013**, *308*, 82.

[65] Ravenelle, R. M.; Schüβler, F.; D'Amico, A.; Danilina, N.; van Bokhoven, J. A.; Lercher, J. A.; Jones, C. W.; Sievers, C. *J. Phys. Chem. C* **2010**, *114*, 19582.

[66] Zapata, P. A.; Faria, J.; Ruiz, M. P.; Jentoft, R. E.; Resasco, D. E. *J. Am. Chem. Soc.* **2012**, *134*, 8570.

[67] Zhang, L.; Chen, K.; Chen, B.; White, J. L.; Resasco, D. E. *J. Am. Chem. Soc.* **2015**, *137*, 11810.

[68] Jentys, A.; Warecka, G.; Derewinski, M.; Lercher, J. A. *J. Phys. Chem.* **1989**, *93*, 4837.

[69] Chen, N. Y. *J. Phys. Chem.* **1976**, *80*, 60.

[70] Pazé, C.; Bordiga, S.; Lamberti, C.; Salvalaggio, M.; Zecchina, A.; Bellussi, G. *J. Phys. Chem. B* **1997**, *101*, 4740.

[71] Bordiga, S.; Regli, L.; Lamberti, C.; Zecchina, A.; Bjørgen, M.; Lillerud, K. P. *J. Phys. Chem. B* **2005**, *109*, 7724.

[72] Sauer, J. *Science* **1996**, *271*, 774.

[73] Buzzoni, R.; Bordiga, S.; Ricchiardi, G.; Spoto, G.; Zecchina, A. *J. Phys. Chem.* **1995**, *99*, 11937.

[74] Kondo, J. N.; Iizuka, M.; Domen, K.; Wakabayashi, F. *Langmuir* **1997**, *13*, 747.

[75] Vjunov, A.; Derewinski, M. A.; Fulton, J. L.; Camaioni, D. M.; Lercher, J. A. *J. Am. Chem. Soc.* **2015**, *137*, 10374.

[76] Vjunov, A.; Fulton, J. L.; Camaioni, D. M.; Hu, J. Z.; Burton, S. D.; Arslan, I.; Lercher, J. A. *Chem. Mater*.**2015**, *27*, 3533.

[77] Prodinger, S.; Derewinski, M. A.; Vjunov, A.; Burton, S. D.; Arslan, I.; Lercher, J. A. *J. Am. Chem. Soc.* **2016**, *138*, 4408.

[78] Gentry, S. J.; Rudham, R. *J. Chem. Soc., Faraday Trans. 1: Physical Chemistry in Condensed Phases* **1974**, *70*, 1685.

[79] Jacobs, P. *J. Catal.* **1977**, *50*, 98.

[80] Knözinger, H. *Angew. Chem. Int. Ed.* **1968**, *7*, 791.

[81] Akiya, N.; Savage, P. E. *Ind. Eng. Chem. Res.* **2001**, *40*, 1822.

[82] Carey, F. A.; Sundberg, R. J. In *Advanced Organic Chemistry*; Springer Nature, p 473.

[83] Vjunov, A.; Hu, M. Y.; Feng, J.; Camaioni, D. M.; Mei, D.; Hu, J. Z.; Zhao, C.; Lercher, J. A. *Angew. Chem. Int. Ed.* **2013**, *53*, 479.

[84] Chiang, H.; Bhan, A. *J. Catal.* **2010**, *271*, 251.

[85] Zhi, Y.; Shi, H.; Mu, L.; Liu, Y.; Mei, D.; Camaioni, D. M.; Lercher, J. A. *J. Am. Chem. Soc.* **2015**, *137*, 15781.

[86] Knaeble, W.; Iglesia, E. *J. Phys. Chem. C* **2016**, *120*, 3371.

[87] Lee, K. Y.; Arai, T.; Nakata, S.; Asaoka, S.; Okuhara, T.; Misono, M. *J. Am. Chem. Soc.* **1992**, *114*, 2836.

[88] Macht, J.; Janik, M. J.; Neurock, M.; Iglesia, E. *J. Am. Chem. Soc.* **2008**, *130*, 10369.

[89] Macht, J.; Janik, M. J.; Neurock, M.; Iglesia, E. *Angew. Chem. Int. Ed.* **2007**, *46*, 7864.

[90] Ma, Q.; Chakraborty, D.; Faglioni, F.; Muller, R. P.; Goddard, W. A.; Harris, T.; Campbell, C.; Tang, Y. *J. Phys. Chem. A* **2006**, *110*, 2246.

[91] Sarish, S.; Devassy, B.; Bohringer, W.; Fletcher, J.; Halligudi, S. *J. Mol. Catal. A* **2005**.

[92] Anand, R.; Gore, K. U.; Rao, B. S. *Catal. Lett.* **2002**, *81*, 33.

[93] Yadav, G. D.; Kumar, P. *Appl. Catal. A* **2005**, *286*, 61.

[94] Gagea, B. C.; Parvulescu, A. N.; Parvulescu, V. I.; Auroux, A.; Grange, P.; Poncelet, G. *Catal. Lett.* **2003**, *91*, 141.

[95] Karthik, M.; Tripathi, A. K.; Gupta, N. M.; Vinu, A.; Hartmann, M.; Palanichamy, M.; Murugesan, V. *Appl. Catal. A* **2004**, *268*, 139.

[96] Chaudhuri, B.; Sharma, M. M. *Ind. Eng. Chem. Res.* **1991**, *30*, 227.

[97] Rueping, M.; Nachtsheim, B. J. *Beilstein J. Org. Chem.* **2010**, *6*, 6.

[98] Kubička, D.; Kubičková, I.; Čejka, J. *Catal. Rev.* **2013**, *55*, 1.

[99] Resasco, D. E.; Wang, B.; Crossley, S. *Catal. Sci. Technol.* **2016**, *6*, 2543.

[100] Liu, Y.; Vjunov A.; Shi, H.; Eckstein, S.; Camaioni, D. M.; Mei, D.; Baráth, E.; Lercher, J. A. *Nat. Commun.* **2017**, 8, 14113.

Chapter 2

Enhancing the catalytic activity of hydronium ions through constrained environments

The dehydration of alcohols is involved in many organic conversions but has to overcome high free energy barriers in water. Here we demonstrate that hydronium ions confined in the nano-pores of zeolite HBEA catalyze aqueous phase dehydration of cyclohexanol at a rate significantly higher than hydronium ions in water. This rate enhancement is not related to a shift in mechanism; for both cases, the dehydration of cyclohexanol occurs via an E1 mechanism with the cleavage of C_β–H bond being rate-determining. The higher activity of hydronium ions in zeolites is caused by the enhanced association between the hydronium ion and the alcohol, as well as a higher intrinsic rate constant in the constrained environments compared to water. The higher rate constant is caused by a greater entropy of activation, rather than a lower enthalpy of activation. These insights should allow us to understand and predict similar processes in confined spaces, as well as to design new acid catalysts.

---

1. This chapter is based on the article: Liu, Y. *et al.* Enhancing the catalytic activity of hydronium ions through constrained environments. *Nat. Commun.* 8, 14113 doi: 10.1038/ncomms14113 (2017).

2. DFT (density functional theory) calculations in this chapter were provided by Dr. Donghai Mei (PNNL, USA); Experiments using isotope-labeled chemicals were performed by Dr. Hui Shi (PNNL); Aqueous-phase adsorption experiments were carried out by Sebastian Eckstein (TUM).

2.1 Introduction

Despite the seemingly ubiquitous use in organic conversion sequences, the dehydration of alcohols by hydronium ions in aqueous phase is surprisingly challenging, requiring reaction temperatures above 100 °C to occur at industrially acceptable rates.[1] The reasons for this lie in significant enthalpic and entropic barriers for the formation of carbocationic intermediates as well as for their decomposition to form the olefin and water. Enzymes, in contrast, are able to catalyze dehydration of alcohols with high rates at temperatures close to ambient,[2] which is attributed to the unique microenvironment of the catalytically active centers in the three-dimensional enzyme structures and the nearly concerted acid base interactions. In translating this concept to inorganic catalysts we have shown in recent preliminary experiments that zeolite pores are able to substantially increase the rate at which hydronium ions catalyze reactions.[3]

In order to delineate the thermodynamic and kinetic impact of the sub-nanometer sized confines on the catalytic chemistry of hydronium ions, the kinetics and elementary steps of the dehydration of a secondary alcohol, cyclohexanol, in water, as well as in pores of zeolite Beta (BEA) are explored. In-depth characterizations of this zeolite by extended X-ray absorption fine structure (EXAFS) and ^{27}Al MAS NMR spectroscopy showed that in the presence of adsorbed water the charge-balancing protons form hydronium ions, $H_3O^+(H_2O)_n$, that reside locally near the zeolite Al_3^+ T-site bearing the charge-balancing protons in the absence of water.[4-6] Previous studies also provided infrared spectroscopic evidence for the formation of H-bonded and protonated polar molecules (*e.g.*, alcohol and water) at acid sites on HBEA and HZSM-5 zeolites.[7,8] More importantly, the principal reaction network of the zeolite BEA-catalyzed dehydration established by in situ magic angle spinning (MAS) ^{13}C nuclear magnetic resonance (NMR) spectroscopy[9] in aqueous phase enables us to analyze in this contribution the role of the confines on the catalytic properties of hydronium ions.

Here, thermochemical and kinetic measurements are used in conjunction with density functional theory (DFT) and isotope labelling to elucidate quantitatively the reaction pathway in the aqueous phase dehydration of alcohols in constrained environment and

analyze the benefits of such a sterically tailored environment based on transition state theory (TST).

2.2 Experimental section

2.2.1 Zeolite catalysts

Zeolite HBEA150 (SiO_2/Al_2O_3 = 150) was obtained from Clariant in H-form. HBEA150 was calcined at 500 °C in a 100 mL min^{-1} flow of dry air for 6 h prior to the reaction. Detailed descriptions of characterization methods are provided in the Supplementary Methods.

2.2.2 Catalyst characterization

The Si and Al contents in the zeolite samples were measured by atomic absorption spectroscopy (AAS) on a UNICAM 939 AA-Spectrometer.

The BET specific surface area and pore volume (BJH method) were determined after activation in vacuum at 200 °C for 2 h followed by nitrogen adsorption on a PMI automatic Sorptometer.

The scanning electron microscopy (SEM) images were recorded on a JEOL 500 scanning electron microscope (accelerating voltage 25 kV). The samples were prepared by depositing a drop of an ultrasonicated methanol suspension of the solid material onto a carbon-coated Cu grid. The dry samples were gold-coated prior to imaging.

XRD patterns were collected using a Philips X'Pert Pro System, with Cu-Kα radiation source operating at 45 kV and 40 mA. The sample was measured with a scanning rate of 0.02º s^{-1} in the 5-70º 2θ-range.

The infrared (IR) spectra of adsorbed pyridine were recorded with a Perkin–Elmer 2000 spectrometer at a resolution of 4 cm^{-1}. The catalyst samples were prepared as self–supporting wafers and activated in vacuum (p = 10^{-6} mbar) at 450 °C for 1 h at a heating rate of 10 °C min^{-1}. After cooling to 150 °C, the sample was equilibrated with 0.1 mbar pyridine for 0.5 h followed by outgassing for 1 h and the acquisition of the spectrum.

Finally, desorption program (up to 450 °C with 10 °C min^{-1} and 0.5 h at 450 °C) was initiated and the spectra were recorded until equilibrium was achieved. The concentrations of BAS and Lewis acid sites (LAS) are quantified using the integrated areas of peaks at 1540 cm^{-1} and 1450 cm^{-1}, respectively. The number of pyridine molecules retained after evacuation at 150 and 450 °C were used to determine the concentrations of total and strong acid sites, respectively. For calibration of the method, a standard (Zeolite HZSM-5 with Si/Al = 45, acid site concentration = 360 μmol g^{-1}) was used. For quantification, molar integral extinction coefficients of 0.73 cm μmol^{-1} and 0.96 cm μmol^{-1} were used for Brønsted and Lewis acid sites, respectively.

2.2.3 Liquid phase adsorption and calorimetry

Heat of adsorption, *i.e.*, uptake of cyclohexanol (Sigma Aldrich, 99%) from aqueous solutions into zeolite HBEA150, was determined by liquid calorimetry using a Setaram Calvet C80 calorimeter. Reversal mixing cells were used in order to separate the adsorptive from the adsorbent. The lower compartment was loaded with 0.03 g zeolite (m) immersed in 0.8 mL water. The upper compartment was loaded with 0.2 mL of the desired cyclohexanol solution resulting in a total volume (V) of 1 mL with a concentration c_0. Reference cell is loaded with identical compositions, without zeolite. Uptake (q) was determined using liquid NMR, and quantification was accomplished adding an internal standard (1,3,5-trioxane; Sigma Aldrich, ⩾ 99%) to the solution at equilibrium (c_e), assuming $q=V(c_0-c_e)m^{-1}$. Adsorption isotherms were obtained immersing 100, 50 or 20 mg of zeolite in a cyclohexanol solution of a defined concentration for at least 24 h. The solution was separated from the zeolite and the residual concentration was determined via liquid NMR using the internal standard, trioxane.

2.2.4 Kinetic measurements

Kinetic measurements were performed at 160 – 200 °C using a 300 mL Hastelloy PARR reactor. An example of a typical reaction in aqueous phase: 3.3 g cyclohexanol and 100 mL 0.02 M aqueous H_3PO_4 (Sigma Aldrich, ⩾99.999% trace metals basis) solution, or 140 mg HBEA and 80 mL 0.32 M aqueous cyclohexanol solution, are sealed

in the reactor. In all cases, the reactor is then pressurized with 50 bar H_2 at room temperature and heated up while stirred vigorously (~ 700 rpm). Rates do not vary with the stirring speed that is greater than 400 rpm (See details in **Appendix**). The reaction time is reported counting from the point when the set temperature is reached (12–15 min). Upon completion the reactor is cooled using an ice/water mixture. As olefin is formed, which is segregated as another liquid phase, the contents are extracted using dichloromethane (Sigma Aldrich, HPLC grade; 25 mL per extraction, 4 times) or ethyl acetate. It is important that the extraction work-up be completed in a short period of time (20 min) to minimize the loss of the volatile olefin phase; this way, the carbon balance could be maintained typically better than 85% and even better than 95% in favorable cases. The organic phase after being dried over sodium sulfate (Acros Organics, 99%, anhydrous) is analyzed on an Agilent 7890A GC equipped with a HP–5MS 25 m × 0.25 μm (i.d.) column, coupled with Agilent 5975C MS. 1,3-dimethoxybenzene (Sigma Aldrich, 99%) was used as the internal standard for quantification.

Cyclohexanol dehydration reactions catalyzed by the mixture of HBEA150/siliceous BEA and H_3PO_4 were performed at 170 °C using a 300 mL Hastelloy PARR reactor. 140 mg HBEA150 or 500 mg siliceous BEA together with 10.0 g cyclohexanol and 100 mL 0.02 M aqueous H_3PO_4 (Sigma Aldrich, ⩾99.999% trace metals basis) were sealed in the reactor. The experimental protocol was identical to that described above.

2.2.5 H/D kinetic isotope effects and ^{18}O-tracer experiments

Rates of dehydration of perdeuterated cyclohexanol (0.10–0.11 M; present as $C_6D_{11}OH$ in water) were measured in the Parr reactor, using protocols identical to those described for standard reactions using non-labeled alcohol (see above).

Experiments using ^{18}O-labeled water and non-labeled cyclohexanol (0.3 M) were carried out in a ~2 mL stirred batch reactor constructed from a stainless steel "tee" (HiP), while ensuring similar solution-to-headspace ratios (0.3–0.4) as in the Parr reactor. The mixture after reaction was extracted with dichloromethane (0.5 mL per extraction, 4 times), dried over Na_2SO_4 and analyzed with GC–MS. The intensity ratio between two O-containing fragment ions (m/e = 57 and 59) can be used to quantify the extent of ^{18}O-

incorporation into cyclohexanol (the ratio between the single ion areas for m/e = 59 and m/e = 57 is 0.01 for unlabeled alcohol).

2.2.6 In situ liquid phase IR measurements

An in situ time-resolved IR study was conducted in a Parr reactor of a similar head-space-to-liquid volume ratio and feed composition at 200 °C, in order to confirm the validity of the ex-situ GC analyses of reaction kinetics. Measurements were performed using a React IR 1000 spectrometer (Mettler Toledo) connected to a 100 mL PARR Hastelloy autoclave. A diamond window in the autoclave allowed collection of the in situ liquid IR spectra. First, a background is collected for the system containing 50 mL 0.02 M H_3PO_4 solution at 200 °C in the presence of 3.0 MPa H_2. The reactor is then cooled to ambient temperature and 5.0 g cyclohexanol (~0.90 M, fully miscible with water at 200 °C) is added, the autoclave is flushed with H_2 and pressurized 3.0 MPa H_2. IR spectra are collected every 10 min for 240 min at 200 °C with a stirring speed of 900 rpm.

2.2.7 Gas-phase calorimetric and gravimetric measurements

Gas-phase calorimetric and gravimetric measurements were performed at 48 °C on a Setaram TGA-DSC 111 microbalance attached to a UHV system. The catalyst was first pressed into wafers, subsequently crushed in small particles and then charged into a crucible with the mass between 13 to 22 mg. Before measurement, the sample was activated at 450 °C for 1 h with a heating ramp of 10 °C min^{-1} under vacuum ($p < 10^{-6}$ bar). Cyclohexanol vapor was introduced into the closed system in small pressure steps from 10^{-3} to 0.8 mbar, allowing sufficient time to reach adsorption equilibration. The weight increase and heat flux were monitored during pressure equilibration with cyclohexanol. The heats of adsorption were obtained by integration of the recorded heat flux signal observed during stepwise increase of the cyclohexanol pressure.

2.2.8 H_3PO_4 uptake on HBEA and BEA from aqueous phase

1.0 g HBEA150 was added into ~20-25 mL aqueous H_3PO_4 (0.02 M), allowed to equilibrate in the oven at 25 °C for 24-48 h, and centrifuged to retain the solution (Sample A). The same experiment was performed with a purely siliceous BEA (Sample B). The reference was the same H_3PO_4 solution without adding HBEA150. Samples for

^{31}P NMR measurements were prepared by mixing 300 μL of H_3PO_4 solution (Solution A or B, or reference) and 200 μL of D_2O (99.9 atom % D, Sigma-Aldrich), and then 300 μL of 0.02 M NaH_2PO_2 (Sigma Aldrich, ⩾99%; dissolved in water) was added as the internal standard for quantification. 600 μL of such a mixture was placed in an NMR sample tube and the measurement was performed on a Bruker AVHD 300 spectrometer with a deuterium lock resonance. ^{31}P free induction decays (FIDs) were collected at 12149.5 Hz by using 11.25 μs pulses and 36 s relaxation delays (with decoupling). Both sample and reference solutions were prepared and measured for three times.

2.2.9 DFT calculations

All DFT calculations employed a mixed Gaussian and plane wave basis sets and were performed using the CP2K code.[10] The basis set superimposition error (BSSE) derived from Gaussian localized basis set used in our CP2K calculations has been estimated to be ~3 kJ mol^{-1}.[11] The core electrons were represented by norm–conserving Goedecker–Teter–Hutter pseudo-potentials[12-14] and the valence electron wave function was expanded in a double-zeta basis set with polarization functions[15] along with an auxiliary plane wave basis set with an energy cutoff of 360 eV. In all calculations we used the generalized gradient approximation exchange-correlation functional of Perdew, Burke, and Enzerhof (PBE).[16] All configurations were optimized using the Broyden–Fletcher–Goldfarb–Shanno (BGFS) algorithm with SCF convergence criteria of 10^{-8} au. In order to compensate the long-range van der Waals (vdW) interaction between adsorbate molecules and the zeolite, we employed the DFT–D3 scheme[17] with an empirical damped potential term added into the energies obtained from exchange–correlation functional. A periodic three-dimensional all siliceous BEA structure of $Si_{64}O_{128}$ with experimental lattice parameters of 12.6614×12.6614×26.4061 Å^3 was used in this work.[18] The unit cell of the HBEA with Si/Al = 15 ratio then was built by simply replacing four T-site (T3, T4, T5 and T9) Si atoms with four Al atoms. This resulting negative charges were compensated by adding four H atoms at the oxygen atoms which are close neighbors of Al atoms on the zeolite frame, yielding the active Brønsted acidic sites, *i.e.*, Si-O(H)-Al-O of the HBEA zeolite.

The adsorption energy of cyclohexanol into the pore of HBEA zeolite is calculated as follows:

$$E_{ads} = E_{C_6H_{11}OH+HBEA} - E_{HBEA} - E_{C_6H_{11}OH}$$

where $E_{C_6H_{11}OH+HBEA}$ is the total energy of cyclohexanol adsorbed in the pore of HBEA; E_{HBEA} is the total energy of the HBEA; and $E_{C_6H_{11}OH}$ is the total energy of cyclohexanol in vacuum.

The Gibbs free energy changes (ΔG°) along different reaction pathways were calculated using statistical thermodynamics.[19] To account for important entropic contribution, the method for calculating the vibrational entropic term, employed by De Moor *et al.*,[20] was used in this work.

2.3 Results

2.3.1 H_3PO_4-catalyzed aqueous phase cyclohexanol dehydration

Dehydration of cyclohexanol catalyzed by dilute hydronium ions (dissociated from H_3PO_4) leads solely to the formation of cyclohexene. Possible alkylation products, cyclohexyl cyclohexene and dicyclohexyl ether, were not observed. The absence of bimolecular reactions is concluded to be caused by the unfavorable conditions for bimolecular reactions at the low reactant concentrations. The low solubility of cyclohexene in the aqueous phase also disfavors bimolecular reactions with reactive intermediates such as cyclohexyloxonium and cyclohexyl cations.

The concentration of the hydronium ions, upon proper corrections (**Table 2A-1** and the details in **Appendix**), has been used to calculate the turnover frequencies (TOFs) reported in **Table 2-1** for the H_3PO_4-catalyzed dehydration (**Figure 2A-1**, in **Appendix**). The rate of the cyclohexanol dehydration was proportional to the concentration of hydronium ions, rather than the total H_3PO_4 concentrations, consistent with specific acid catalysis in the studied range of dilute H_3PO_4 concentrations (0.02−0.09 M; **Fig. 2A-2**). The turnover rate of cyclohexanol dehydration is roughly first order in alcohol at low concentrations (~0.1–0.3 M), but

deviates from first order behavior at higher concentrations (0.90 M; **Fig. 2A-3**). The measured activation barrier was ~158 kJ mol^{-1} at two alcohol concentrations (0.32 and 0.90 M; see **Table 2-1** and **Fig. 2A-4**).

2.3.2 Zeolite-catalyzed aqueous phase cyclohexanol dehydration

The detailed physicochemical properties of zeolite HBEA150 (SiO_2/Al_2O_3 = 150) are given in the **Appendix** (**Figs. 2A-5** and **2A-6**, **Tables 2A-2** and **2A-3**). As with H_3PO_4, cyclohexene was the main product of cyclohexanol dehydration on zeolite HBEA in dilute aqueous solutions (0.32−1.1 M). The nearly 100% selectivity to cyclohexene at short reaction times (*e.g.*, < 1 h at 200 °C) indicates that water elimination proceeds preferentially via an intramolecular rather than an intermolecular pathway. In contrast to H_3PO_4, HBEA catalyzed also ether formation and C–C alkylation reactions at higher conversions,[9] suggesting that the large intracrystalline voids of zeolite BEA allow bimolecular reactions.[21]

The rates and TOFs for the dehydration of cyclohexanol on HBEA (**Fig. 2A-8**) are also reported in **Table 2-1**. The dehydration TOFs on HBEA were an order of magnitude higher than those catalyzed by aqueous phase hydronium ions at 0.32 M alcohol concentration (**Table 2-1**). Note that TOFs were obtained by normalizing the rates to the concentration of total Brønsted acidic sites (BAS) in HBEA150 (**Fig. 2A-2**), as we have shown earlier that all the BAS are present in the form of solvated hydronium ions,[4] which are equally active in aqueous phase dehydration.[22] Surprisingly, the activation energies (162-164 kJ mol^{-1}, see **Fig. 2A-9**) measured on HBEA in aqueous phase were similar to those (158 kJ mol^{-1}) measured in aqueous H_3PO_4. However, the rate was zero-order in cyclohexanol (measured: 0.1 ± 0.1; see **Fig. 2A-10**), much lower than the first-order dependence observed in H_3PO_4 solution. The zero-order kinetics for cyclohexanol suggests that nearly all hydronium ions are interacting with the alcohol or maintain – at least – a fully occupied precursor state to the alcohol–hydronium ion complex. Another interesting observation is that the dehydration of cyclohexanol catalyzed by a mixture of H_3PO_4 (0.02 M) and HBEA150 (140 mg) showed a significantly higher reaction rate than the sum of the individual rates on each acid (**Table 2A-4**).

Table 2-1. Rates and activation energies for dehydration of cyclohexanol

Reaction conditions [a]	Kinetic measurement [b]	Reaction temperature [°C]					E_a [c]
		160	170	180	190	200	(kJ mol^{-1})
Cyclohexanol (~0.32 M), 0.02 M H_3PO_4	Rate (mol L^{-1} s^{-1})	5.5×10^{-6}	1.3×10^{-5}	2.9×10^{-5}	6.4×10^{-5}	1.5×10^{-4}	157 ± 3
	TOF ($mol_{alcohol}$ $mol_{acid\ sites}^{-1}$ s^{-1})	1.4×10^{-3}	3.5×10^{-3}	8.6×10^{-3}	2.1×10^{-2}	5.6×10^{-2}	
Cyclohexanol (~0.90 M), 0.02 M H_3PO_4	Rate (mol L^{-1} s^{-1})	1.3×10^{-5}	3.1×10^{-5}	6.9×10^{-5}	1.5×10^{-4}	3.7×10^{-4}	158 ± 4
	TOF ($mol_{alcohol}$ $mol_{acid\ sites}^{-1}$ s^{-1})	2.9×10^{-3}	7.6×10^{-3}	1.9×10^{-2}	4.4×10^{-2}	1.2×10^{-1}	
Cyclohexanol (~0.32 M), 140 mg HBEA150	Rate (mol g_{HBEA}^{-1} s^{-1})	3.7×10^{-6}	1.0×10^{-5}	2.6×10^{-5}	6.4×10^{-5}	1.8×10^{-4}	164 ± 3
	TOF ($mol_{alcohol}$ $mol_{acid\ sites}^{-1}$ s^{-1})	1.9×10^{-2}	5.2×10^{-2}	1.4×10^{-1}	3.3×10^{-1}	9.3×10^{-1}	
Cyclohexanol (~0.90 M), 140 mg HBEA150	Rate (mol g_{HBEA}^{-1} s^{-1})	4.2×10^{-6}	1.2×10^{-5}	3.4×10^{-5}	7.2×10^{-5}	2.0×10^{-4}	162 ± 4
	TOF ($mol_{alcohol}$ $mol_{acid\ sites}^{-1}$ s^{-1})	2.2×10^{-2}	6.2×10^{-2}	1.8×10^{-1}	3.8×10^{-1}	1.03	

[a] Reactor was pressurized with 50 bar H_2 at ambient temperature and stirred vigorously at 700 rpm. The rates were determined from the formation of cyclohexene after the set temperature was reached. The concentrations denoted are based on the density of water at room temperature. [b] TOF is determined as olefin formation rate (mol L^{-1} s^{-1}) normalized to the concentration of hydronium ions (H_3PO_4) or total BAS (HBEA). The concentration of hydronium ions in the H_3PO_4–catalyzed experiments depends on temperature and cyclohexanol concentration; [c] Activation barriers are determined from the Arrhenius plots for TOFs (a directly measured property).

2.3.3 Adsorption of cyclohexanol on zeolite HBEA

The adsorption isotherm of cyclohexanol and the associated heats of adsorption are shown in **Fig. 2-1**. Microgravimetric analyses of gas-phase cyclohexanol adsorption on the zeolite provide an estimate of the maximum alcohol uptake in the absence of water (see **Fig. 2A-12**).

Langmuir-type isotherms satisfactorily describe the uptake of cyclohexanol from both gas (without water) and aqueous phase on zeolite HBEA150. The saturation uptakes of cyclohexanol and water (**Table 2A-5**) correspond to 8 cyclohexanol and 10 water molecules per unit cell (u.c) at the saturation limit (room temperature). In good agreement, a maximum of 8 cyclohexanol molecules or 20−30 water molecules in one unit cell are allowable at the highest pore filling degree, according to DFT calculations.

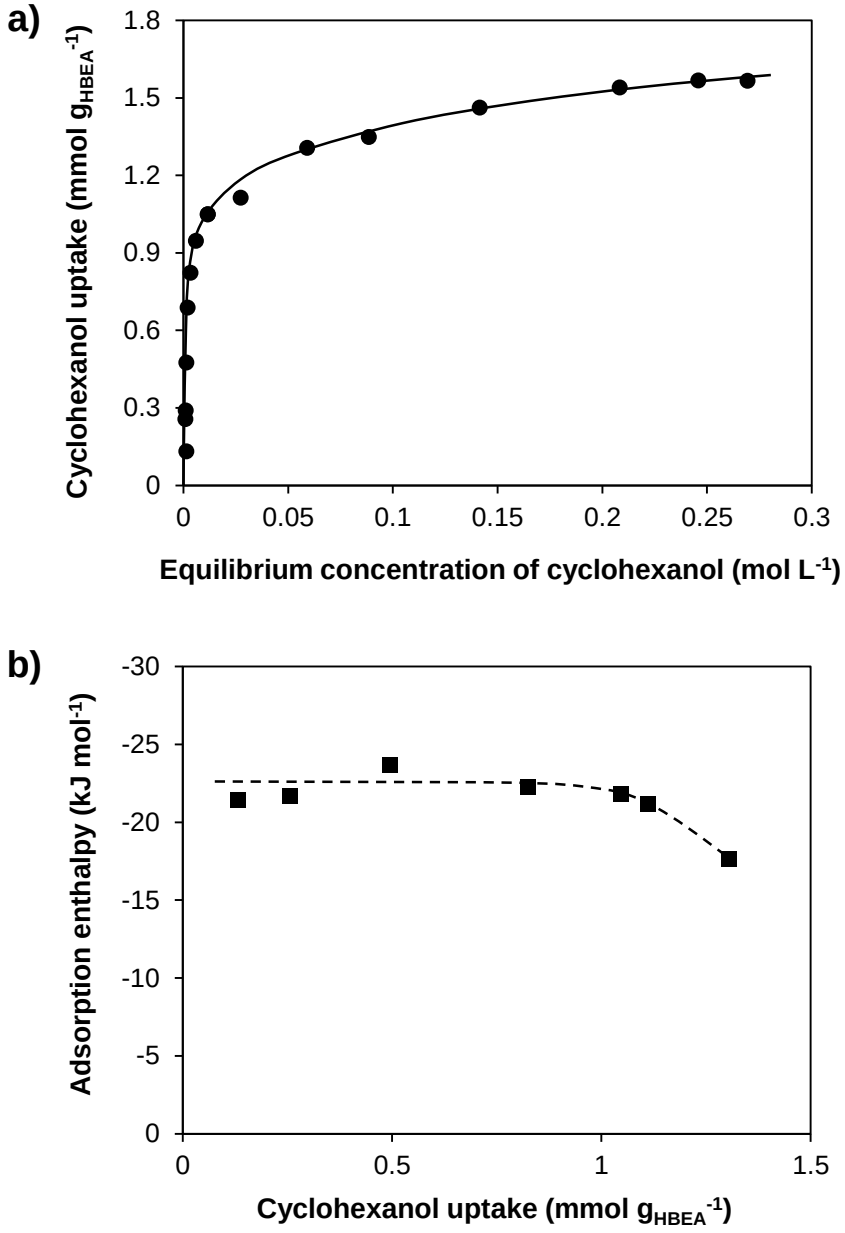

Figure 2-1. Adsorption of cyclohexanol from aqueous solutions onto HBEA. (a) Cyclohexanol adsorption isotherm measured by ^{1}H NMR and (b) heat of adsorption measured by calorimetry, both determined for aqueous solutions and HBEA150 at 25 °C.

Adsorption equilibrium constants (K_{ads}) for cyclohexanol uptake, along with the measured enthalpies and entropies were determined (**Table 2A-7**). The molar adsorption enthalpy of cyclohexanol adsorbed from aqueous phase is −22 kJ mol^{-1} (**Fig. 2-1**). This enthalpy is the result of transferring cyclohexanol from the aqueous medium (breaking H-

bonding between cyclohexanol and water) and the displacement of water by cyclohexanol in the zeolite pores, the magnitude depending on the strengths of interactions between cyclohexanol/water and the pores as well as the BAS.

With increasing temperatures (7−80 °C), saturation uptakes decreased from 1.75 to 1.31 mmol g_{HBEA}^{-1} (**Table 2A-6**). This decrease is caused by the density change of the adsorbed phase in the micropore with temperature.[13] By extrapolating saturation uptakes to 160−200 °C it is estimated that ~5 cyclohexanol molecules are present per unit cell at saturation limit under reaction conditions (see **Section A6** in **Appendix**). Assuming that the remaining micropore volume is filled by water, the concentration of water molecules in the pore would increase to ~20/u.c. at reaction temperatures. Note that the initial alcohol-to-water ratio in the zeolite pore is, thus, a factor of 50 higher than in solution (*e.g.*, 5.3–5.6×10^{-3} for 0.32 M solution at 160–200 °C). Extrapolation of K_{ads} to reaction temperatures suggests that K_{ads} decreased from 20 to 12 as the reaction temperature increased from 160 to 200 °C. This suggests an almost complete pore filling under reaction conditions, in line with the zero-order kinetic regime for the main dehydration pathway.

2.3.4 Mechanism of dehydration of cyclohexanol in aqueous phase

Having established the principal kinetic features of the elimination of water from cyclohexanol catalyzed by hydronium ions, we use the H/D kinetic isotope effect and ^{18}O-tracer experiments to investigate whether the elimination occurs via an E1 or E2 mechanism.

The TOFs for dehydration using $C_6H_{11}OH$ and $C_6D_{11}OD$ (forming $C_6D_{11}OH$ upon exchange with H_2O) are shown in **Table 2-2**. H/D kinetic isotope effects (KIEs) of ~3 were observed for olefin formation catalyzed by hydronium ions in open water and in the nano-pores of HBEA. A KIE of such a magnitude indicates that C–H(D) bond cleavage is involved in the kinetically relevant step (*i.e.*, its rate constant appears in the kinetic expression). The primary KIE is inconsistent with the formation of the carbocation or the C–O bond cleavage being rate-determining. Both steps would have secondary KIEs for rehybridization of α-C from sp^3 to sp^2, estimated to be <1.3 at 150–190 °C. In turn, this indicates that either an E1 mechanism with a kinetically relevant C–H bond cleavage or

an E2 mechanism in which the C–O and the C–H bonds are cleaved in a concerted step is in agreement with the observed KIE.

Table 2-2. H/D isotope effects. [a]

Reactant	Turnover frequency	
	H_3PO_4 (10^{-3} s^{-1}) [c]	HBEA (10^{-2} s^{-1}) [d]
$C_6H_{11}OH$	3.5 ± 0.2	5.5 ± 0.3
$C_6D_{11}OD$ [b]	1.2 ± 0.1	1.9 ± 0.1
KIE	3.0 ± 0.4	2.9 ± 0.3

[a] Reactant conversions were kept at 5–10% and dicyclohexyl ether selectivities at 0–2%; Cyclohexanol and perdeuterated cyclohexanol were dissolved in unlabeled water (~ 0.1 M); 98 atom% isotopic purity for $C_6D_{11}OD$. [b] Forming $C_6D_{11}OH$ upon exchange with H_2O. [c] At 180 °C; [d] At 170 °C.

Table 2-3. ^{18}O-exchange during cyclohexanol dehydration.[a]

Catalyst	^{18}O in the recovered alcohol (%)	Conversion (%)
HBEA	9	19
H_3PO_4	17	18

[a] Extent of ^{18}O-exchange from $H_2{}^{18}O$ (97% isotopic purity) into cyclohexanol during dehydration of unlabeled cyclohexanol (0.30 M in $H_2{}^{18}O$) over HBEA and H_3PO_4 in aqueous phase at 180 °C.

To discriminate between the two mechanistic possibilities, ^{18}O-labeled water was used as the solvent (**Table 2-3**). The reverse rate at 20% conversion, *i.e.*, the hydration of cyclohexene, would lead to ~2% ^{18}O-incorporation, based on the analysis of the effective equilibrium constant (**Table 2A-9**) obtained by fitting the derived rate expression (details shown in **Section A8**, **Appendix**) to the in situ time-resolved IR data collected during cyclohexanol dehydration (**Fig. 2A-13**). As olefin hydration hardly occurred under the applied conditions on HBEA and H_3PO_4, the E2-like pathways alone, with concerted C–O and C–H bond scissions, cannot explain the significant ^{18}O-incorporation (9–17%) into cyclohexanol. With the S_N2 path for oxygen exchange between water and secondary/tertiary alcohols also ruled out,[24-27] the only possible pathway for this level of ^{18}O-incorporation would be recombination between ^{18}O-water and an intermediate, which

is formed upon C–O bond cleavage and which precedes the C_β–H bond cleavage TS. This, in turn, makes the E1-type path the dominating mechanism for dehydration of cyclohexanol, regardless of whether the hydronium ion exists in homogeneous solution or localized in a pore.

2.3.5 DFT calculations of hydronium ion catalyzed pathways in HBEA

The DFT calculations only address the kinetically relevant intermediates for protonation and H_2O-elimination. Other steps, such as desorption of water and olefins, will be discussed elsewhere, because they are irrelevant for the rates of dehydration. The calculated energy profiles for the reaction at 170 °C are shown in **Fig. 2-2**. The BEA unit cell may contain 3–10 H_2O molecules in proximity to the hydronium ion. For the theoretical evaluation of the interaction of the alcohol with the hydronium ion, we chose an example hydronium ion cluster with a $H_3O^+(H_2O)_7$ structure, the presence of which was identified by *ab initio* molecular dynamics (AIMD) simulations (a total of 26 water molecules in the unit cell; see **Fig. 2A-14**). This structure includes extended hydration shells beyond the first shell.

Up to 4 cyclohexanol molecules were considered in addition to the hydronium ion in one BEA unit cell. The alcohol is seen to interact with the hydronium ion, forming an H-bond, while also interacting with the pore walls. The calculated enthalpy and free energy for cyclohexanol (gas) adsorption and subsequent interaction with the zeolitic hydronium ion (A, **Fig. 2-2**) were -108 and -50 kJ mol^{-1}, respectively. These values are in reasonable agreement with gas phase adsorption and calorimetric measurements (**Fig. 2A-12**). The H-bonded cyclohexanol is protonated and forms an alkoxonium ion (B, **Fig. 2-2**). The activation barrier for this step is 69 kJ mol^{-1} (from A to TS1, Fig. 2-2). This protonation step is endothermic ($\Delta H° = +$ 36 kJ mol^{-1}) and endergonic ($\Delta G° = +$ 55 kJ mol^{-1}). Thus, the protonated alcohol is expected to be a minority species at typical reaction temperatures.

For comparison DFT calculations were performed for both E1- and E2-type elimination paths. On the E1-type path, the C−O bond cleavage has an activation barrier of 95 kJ mol^{-1}, with an entropy gain of 34 J mol^{-1} K^{-1}. In TS2, the leaving OH_2 is almost neutral, and the positive charge remains largely on the $[C_6H_{11}]$ moiety. Next, the $C_6H_{11}^+$

carbenium ion deprotonates to the hydronium ion cluster forming cyclohexene. In TS3, a H_2O molecule nearby acts as the base to abstract the β-H; the C_β–H bond is almost fully broken (2.46 Å; see **Fig. 2A-15**). This deprotonation has a small barrier (43 kJ mol^{-1}) in the forward direction and a higher barrier (92 kJ mol^{-1}) in the reverse direction. The higher free energy barrier for deprotonation (from C to TS3) than for C–O bond recombination (from C to TS2) is in line with the kinetic relevance of C–H bond cleavage concluded from the measured primary H/D isotope effects.

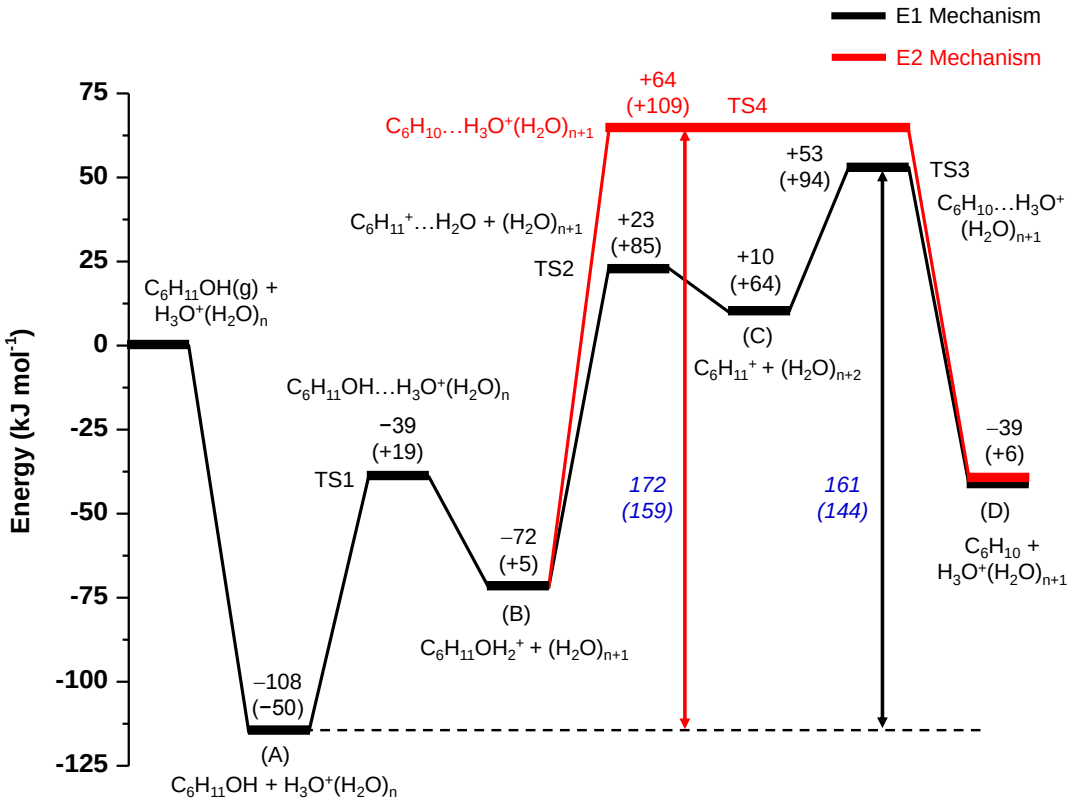

Figure 2-2. DFT calculations of cyclohexanol dehydration on HBEA. The energy diagram is shown for the aqueous phase dehydration of cyclohexanol over a periodic HBEA ($Al_4H_4Si_{60}O_{128}$) model. The active site in zeolite equilibrated with aqueous phase is modeled by $H_3O^+(H_2O)_7$, with the configurations and energies optimized. All species, except for those denoted with (g), are in the unit cell. The detailed structures and configurations of the adsorbed intermediates, transition states and the $H_3O^+(H_2O)_7$ hydronium ion cluster are shown in the **Fig. 2A-15**. Enthalpy and free energy values (at 170 °C) are shown outside and inside the brackets, respectively.

In comparison, on the E2-type path, the enthalpy of activation and entropy of activation calculated at 170 °C were 137 kJ mol^{-1} and 74 J mol^{-1} K^{-1}, respectively (from B to TS4). These activation energies and entropies are larger than the corresponding values for the E1-type path (Fig. 2-2), making the latter also more plausible from the point of DFT modeling.

2.3.6 Causes for the rate increase by pore constraint

Let us analyze in the next step the reasons for the markedly higher (*e.g.*, ~16 times at 180 °C and 0.32 M cyclohexanol) rates catalyzed by hydronium ions present in the pore of zeolite BEA compared to that in open water.

For brevity, in aqueous H_3PO_4, we represent the hydrated hydronium ion as an Eigen-type[28,29] structure, $H_3O^+(H_2O)_3$(aq), in which only the numbers of first-shell waters are shown. Without steric constraints, the reaction starts with the association of the hydronium ion with cyclohexanol, presumably replacing a H_2O molecule by cyclohexanol in the first solvation shell of the hydronium ion[30] (Equation (2-1)).

$$ROH(aq) + H_3O^+(H_2O)_3(aq) \rightleftharpoons H_3O^+(H_2O)_2(ROH)(aq) + H_2O(l) \qquad (2\text{-}1)$$

Under reaction conditions, this step is quasi-equilibrated, with an association constant $K_{L,a}$ (where the subscript "L" stands for the liquid phase, and "a" stands for association).

The steps following the association of the proton with the alcohol are all unimolecular, as we demonstrate later. Together, they can be written as equation (2-2), with a collective forward rate constant $k_{L,d}$ (where "d" stands for dehydration)

$$H_3O^+(H_2O)_2(ROH)(aq) \rightarrow H_3O^+(H_2O)_3(aq) + R(-H) \qquad (2\text{-}2)$$

where R(-H) represents the olefin product (cyclohexene) having one less hydrogen than the alkyl group R (cyclohexyl).

The rate of dehydration normalized to the concentration of total hydronium ions $[H_3O^+]_0$ ($[H_3O^+]_0 = [H_3O^+(H_2O)_3] + [H_3O^+(H_2O)_2ROH]$) is TOF (**Table 2-1**) and defined as the product of the rate constant $k_{L,d}$ and the fraction of hydronium ions associated with the alcohol, $\theta_{L,a}$. (Equation (2-3) and (2-4); details of derivation and calculation shown in **Sections A10**, **A11** and **A12**, **Appendix**)

$$\frac{r}{[H_3O^+]_0} = TOF_L = k_{L,d}\theta_{L,a} \qquad (2\text{-}3)$$

$$\theta_{L,a} = \frac{K_{L,a}\frac{[ROH]_{aq}}{[H_2O]_l}}{1+K_{L,a}\frac{[ROH]_{aq}}{[H_2O]_l}} \qquad (2\text{-}4)$$

The association constant $K_{L,a}$ was derived from initial reaction rates, r, measured at two different alcohol concentrations (0.32 and 0.90 M). The values of $K_{L,a}$, the alcohol-hydronium ion association equilibrium constant, decreased modestly from 40 to 37 with increasing temperature from 160 to 200 °C (**Table 2A-13**). A similar weak temperature dependence had been reported for the protonation of C_2–C_4 aliphatic alcohols by aqueous sulfuric acids (exothermicity of –2 kJ mol^{-1}).[31] At 0.32 M and 160–200 °C, the fraction of hydronium ions associated with cyclohexanol ($\theta_{L,a}$) was approximately 0.17 (**Table 2A-13**). With the regressed $K_{L,a}$ and $k_{L,d}$, the changes in enthalpy and entropy for association equilibrium between hydronium ion and cyclohexanol in H_3PO_4, as well as the intrinsic activation barriers for H_3PO_4-catalyzed dehydration were determined (**Tables 2A-16** and **2A-17**).

In analogy to the plain aqueous phase dehydration, the rate normalized to the hydronium ion concentration in zeolite HBEA (TOF) is

$$TOF_z = k_{z,d}\theta_{z,a} \qquad (2\text{-}5)$$

$\theta_{z,a}$ is the fractional coverage or association of the hydronium ions with cyclohexanol. In zeolite HBEA, ~5 cyclohexanol and ~20 water molecules occupy a unit cell, while in a 0.32 M solution, one cyclohexanol molecule shares the volume with 180 water molecules. Consequently, $\theta_{z,a}$ has a value at least close to 1, in comparison to a $\theta_{L,a}$ value of 0.17 in a solution containing 0.02 M H_3PO_4 and 0.32 M cyclohexanol. In turn, the rate constant in zeolite HBEA ($k_{z,d}$) is at least ~2.7 times higher than that in the homogeneous acid solution ($k_{L,d}$) (see **Section A12** in **Appendix**). Altogether, the analysis shows that the HBEA pore provides an environment that not only increases the fraction of hydronium ions associated with alcohol, but also increases the intrinsic dehydration rate constant, collectively contributing to more than one order of magnitude enhancement in rate compared to the homogeneously catalyzed dehydration (**Table 2-1**).

Interestingly, the observed rates with a mixture of H_3PO_4 and HBEA were higher than the sum of rates obtained with the individual acids (**Table 2A-4**), presumably due to phosphoric acid being adsorbed in the pore.[32,33] We speculate that additional hydronium ions generated by dissociation of phosphoric acid in the pore partly account for this rate enhancement, while alternative elimination pathways (*e.g.*, cyclohexyl phosphate ester-mediated[34]) may be available in the unique confines of the zeolite (see extended discussion in the **Section A5** in **Appendix**). However, the concentration of H_3PO_4 and the extent of its dissociation in the zeolite pore at reaction temperature are presently not known, preventing a quantitative analysis of the potential causes.

2.4 Discussion

In the catalytic sequence of the zeolite-catalyzed dehydration, cyclohexanol is first adsorbed from aqueous solution into intracrystalline voids. From aqueous phase, this step is accompanied with a change of −22 kJ mol^{-1} in enthalpy and −25 J mol^{-1} K^{-1} in entropy (**Table 2A-7**). In the presence of water, the zeolite BAS form confined hydronium ions.[4-8] The hydronium ion protonates the alcohol, to which it is H-bonded. DFT calculations suggest that the alcohol protonation equilibrium constant in zeolites depends critically on the number of water molecules in the hydronium-ion cluster (**Table 2A-10**). While water has a smaller proton affinity than cyclohexanol, a cluster of water molecules ($n \geq 3$) may have a higher proton affinity than cyclohexanol. As a consequence, proton transfer from a hydronium ion-water cluster to cyclohexanol will become progressively more favorable as the cluster decreases in size. In aqueous solution, the prevalent hydronium ion in zeolite HBEA was simulated as $H_3O^+(H_2O)_7$. With this cluster, protonation of cyclohexanol is thermodynamically unfavorable (DFT: $\Delta G° = +55$ kJ mol^{-1}). Accordingly, a majority of the BAS interacts with the alcohol without a significant extent of proton transfer. In turn, the measured enthalpy of activation (159 kJ mol^{-1}) and corresponding entropy change (87 J mol^{-1} K^{-1}) reflect the difference between the kinetically relevant TS (*i.e.*, C_β–H bond cleavage TS) and the H-bonded alcohol state (A in **Fig. 2-2**).

Because of the weak temperature dependence of $K_{L,a}$ and $[ROH]_{aq}/[H_2O]_l$ ratio (equation (2-3)), the intrinsic activation barrier (Table 2-4) is anticipated to be close to the measured energy of activation (**Table 2-1**). As discussed, the intrinsic rate constants for H_3PO_4-catalyzed dehydration were determined at 160–200 °C, yielding the activation enthalpy (157 kJ mol^{-1}) and the activation entropy (73 J mol^{-1} K^{-1}). Thus, the dehydration of aqueous cyclohexanol occurs in HBEA with a similar activation enthalpy, yet a greater entropy gain than in aqueous acidic solution (**Table 2-4**).

Table 2-4. Intrinsic activation parameters for aqueous phase dehydration of cyclohexanol. [a]

Kinetic parameter	H_3PO_4	HBEA
$\Delta H°^{\ddagger}$ /kJ mol^{-1}	157 ± 3	159 ± 4
$\Delta S°^{\ddagger}$/J mol^{-1} K^{-1}	73 ± 7	87 ± 9
$\Delta G°^{\ddagger}_{180}$ /kJ mol^{-1}	124 ± 1	120 ± 1

[a] Intrinsic standard activation enthalpies, entropies and Gibbs free energies are determined according to transition state theory, see **Section A13** in **Appendix**. The error bars for $\Delta H°^{\ddagger}$ and $\Delta S°^{\ddagger}$ represent the 1-σ standard deviations, while the error bar for $\Delta G°^{\ddagger}$ represents the maximum error rounded up to the nearest integer.

Thus, cyclohexanol dehydration was catalyzed with markedly higher rates when the hydronium ions were confined in zeolite pores. This rate enhancement is partly explained by the intrinsic rate constant for dehydration, which was at least 2–3 times higher in HBEA than in water. Noteworthily, the intrinsic enthalpies of activation were similar for catalysis in BEA pores as in water, while the associated entropy of activation was greater for hydronium ion catalysis in the zeolite pores than in water. The largest effect arising from a constrained environment is, however, related to the higher association extent of cyclohexanol with the hydronium ion. We attribute this to the lower entropy loss when forming an association complex in the zeolite pore. In contrast to plain aqueous phase, the lower entropy of molecules mobile in pores of molecular sieves will lead to a much smaller loss in forming the reactant-catalyst adduct. Such enhanced association between substrate and active site, as well as the entropically favored intrinsic kinetics within sterically constrained environments bears a strong resemblance to enzyme catalysis.[35,36]

2.5 Conclusions

The hydronium ion-catalyzed cyclohexanol dehydration in aqueous phase was explored using H_3PO_4 and HBEA zeolites, at mild temperatures (160−200 °C). Isotopic experiments reveal that the aqueous-phase dehydration of cyclohexanol, whether catalyzed by hydronium ion in HBEA or aqueous H_3PO_4, occurs predominantly via an E1-type mechanism with the cleavage of C_β–H being the kinetically relevant elementary step. Adsorption of cyclohexanol molecules in the HBEA zeolites is favorable and leads to pore saturation with approximately 5 cyclohexanol and 20 water molecules per unit cell at reaction temperatures of 160−200 °C. The concentration ratios of cyclohexanol relative to water being 50 times higher than those in homogeneous solution under reaction conditions. After making proper corrections for the differences in the association probability of cyclohexanol and the hydronium ion active site, the intrinsic rate constants for dehydration are found to be higher by a factor of 2–3 in HBEA than in water. Intrinsic enthalpies of activation are similar, while the concomitant entropy gain is greater for HBEA- than for H_3PO_4-catalyzed dehydration in water. This work suggests a new approach to designing reaction environments that could lead to enzyme-like activities and selectivities.

This analysis now sets the stage for evaluating other zeolites, making HBEA the standard to which others zeolites may be compared. By measuring the thermodynamics for adsorption and the thermochemical kinetic parameters for catalysis by other zeolites, quantitative comparisons may be made of the effects of confinement on the factors which control catalytic activity.

2.6 Appendix

A1. Dissociation equilibrium constant for the first proton of H_3PO_4

Table 2A-1. Dissociation equilibrium constants for the first proton of H_3PO_4 at reaction temperature.[a]

Temperature (°C)	$K_{a,1}$ (10^{-4})
160	9.43
170	7.76
180	6.36
190	5.20
200	4.23

[a] The equilibrium constant $K_{a,1}$ for aqueous H_3PO_4 solutions at elevated temperatures is given by $pK_{a,1}=756.276/T-4.0886+0.012396T$.[1] The corrective concentrations of hydronium ions are calculated in **Section A11**.

A2. Dehydration of cyclohexanol catalyzed by aqueous H_3PO_4

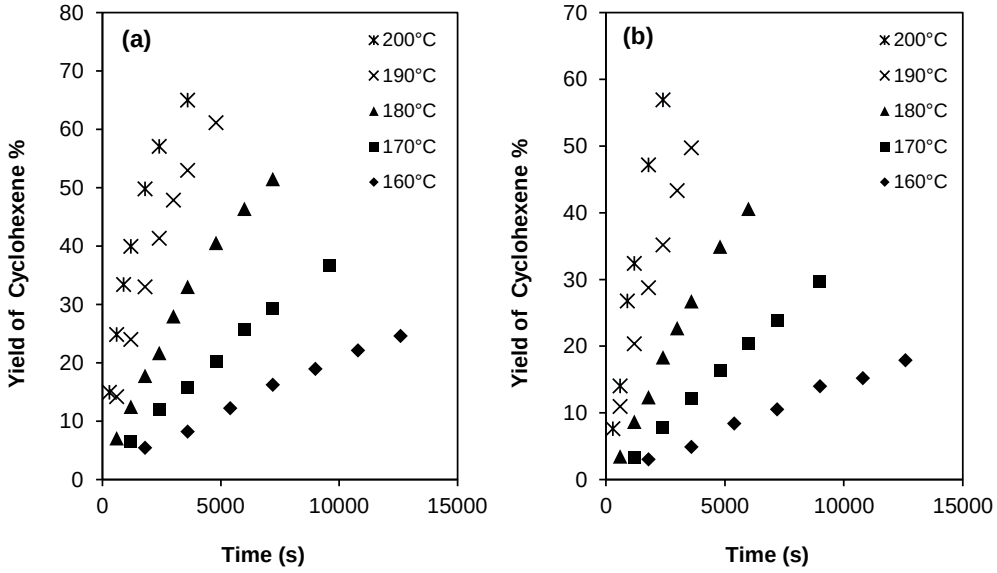

Figure 2A-1. Olefin yield-time plots for H_3PO_4-catalyzed dehydration of cyclohexanol in aqueous phase. (a) 0.32 M cyclohexanol (room temperature, r.t.), (b) 0.90 M cyclohexanol (r.t.). Reaction conditions: cyclohexanol (3.3 or 10.0 g), H_3PO_4 solution (100 mL, 0.02 M at r.t.), 50 bar H_2 (r.t.), stirred at 700 rpm, 160−200 °C.

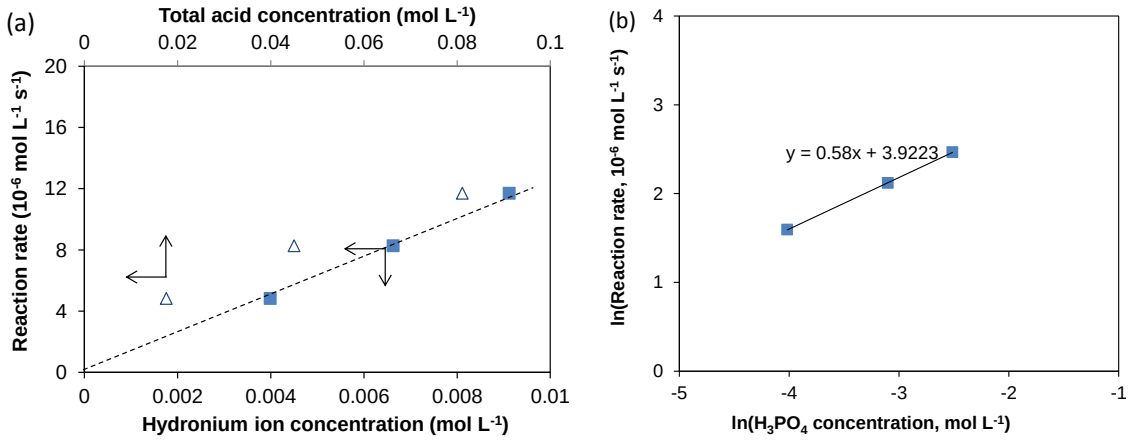

Figure 2A-2. (a) Proportionality of reaction rate to the concentration of hydronium ion and total acid and (b) the reaction order with respect to the concentration of H_3PO_4. The dehydration of cyclohexanol to cyclohexene was carried out at 160 °C in aqueous solutions containing 0.32 M (at r.t.) cyclohexanol and various concentrations of H_3PO_4 (0.02−0.09 M at r.t.). Rates and concentrations in the plots are corrected for solution density at 160 °C. Reaction order with respect to total acid concentration is approximately 0.6 (b). This supports the claim that hydronium ions dissociated from the H_3PO_4 are responsible for the catalytic reaction.

The dissociation constant of the first proton is much greater than the next two, leading to the hydronium ion concentration of H_3PO_4 solutions dependent almost exclusively on the equilibrium constant ($K_{a,1}$) for the first deprotonation step at reaction temperatures. The $pK_{a,1}$ values at elevated temperatures for H_3PO_4 in water could be found in literature.[1] At 160 °C, for instance, the $K_{a,1}$ is 9.43×10^{-4}. The concentration of hydronium ions can be determined as:

$$[H_3O^+] = \frac{-K_{a,1} + \sqrt{K_{a,1}{}^2 + 4K_{a,1}[H_3PO_4]}}{2}$$

There is a small correction due to the slightly enhanced ionization of H_3PO_4 in the presence of alcohol (see **Section A11**). **Fig. 2A-2(a)** shows that the reaction rate is proportional to the concentration of hydronium ions, rather than the concentration of total acid. This suggests that under such dilute concentrations of H_3PO_4, only hydronium ions act as the catalyst.

For a small $K_{a,1}$ as is the case here, the hydronium ion concentration can be approximated using the following equation:

$$[H_3O^+] = \sqrt{K_{a,1}[H_3PO_4]}$$

In line with this, **Fig. 2A-2(b)** shows that the reaction order with respect to total acid concentration is approximately 0.6. Again, this supports the claim that hydronium ions dissociated from the H_3PO_4 are responsible for the catalytic reaction.

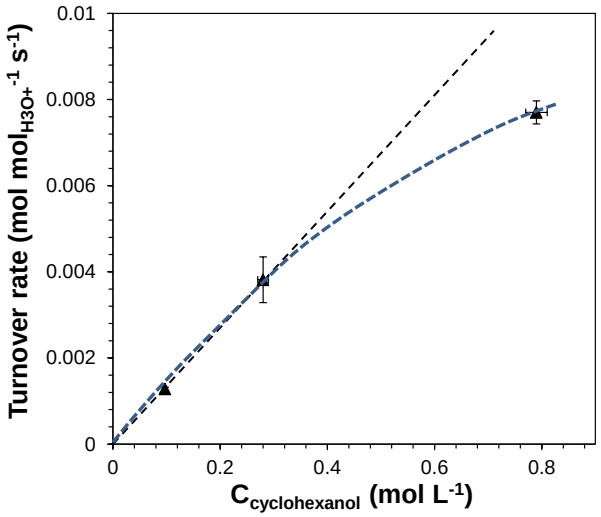

Figure 2A-3. Measurement of the reaction order with respect to cyclohexanol concentration in dilute aqueous H_3PO_4 solutions. Turnover rates (normalized to hydronium ion concentrations) of cyclohexanol dehydration to cyclohexene were measured in aqueous solutions containing 0.02 M (r.t.) H_3PO_4 and various concentrations of cyclohexanol (0.10−0.90 M at r.t.). The uncertainties in the measured rates are < ± 5%. Concentrations of cyclohexanol in the plot have been corrected for vapor phase loss and solution density change at 170 °C. TOFs are based on the corrected concentrations of cyclohexanol and hydronium ions at reaction temperatures (**Table 2A-13**). At low alcohol concentrations (< 0.32 M, r.t.), the dehydration TOF was observed to be first order with respect to the concentration of cyclohexanol. At higher alcohol concentrations (0.90 M, r.t.), the increase in TOF is less than proportional to the increase in the concentration of cyclohexanol.

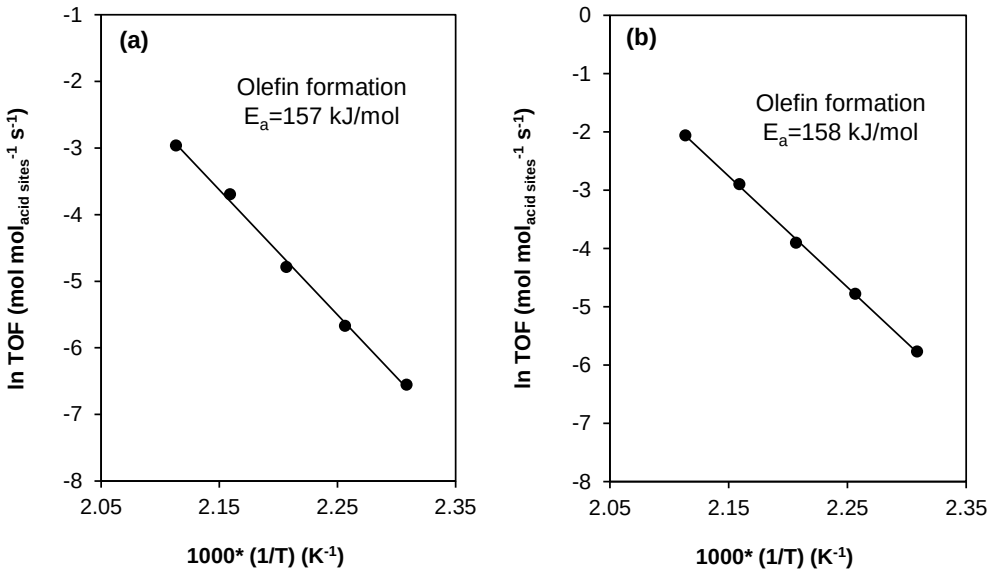

Figure 2A-4. Arrhenius plots for H_3PO_4-catalyzed dehydration of cyclohexanol in aqueous phase. (a) 0.32 M cyclohexanol (r.t.), (b) 0.90 M cyclohexanol (r.t.). Reaction conditions: cyclohexanol (3.3 or 10.0 g), H_3PO_4 solution (100 mL, 0.02 M at r.t.), 50 bar H_2 (r.t.), stirred at 700 rpm, 160−200 °C. TOFs are based on the corrected concentrations of cyclohexanol and hydronium ions at reaction temperatures (**Table 2A-13**).

A3. Physicochemical properties of HBEA150

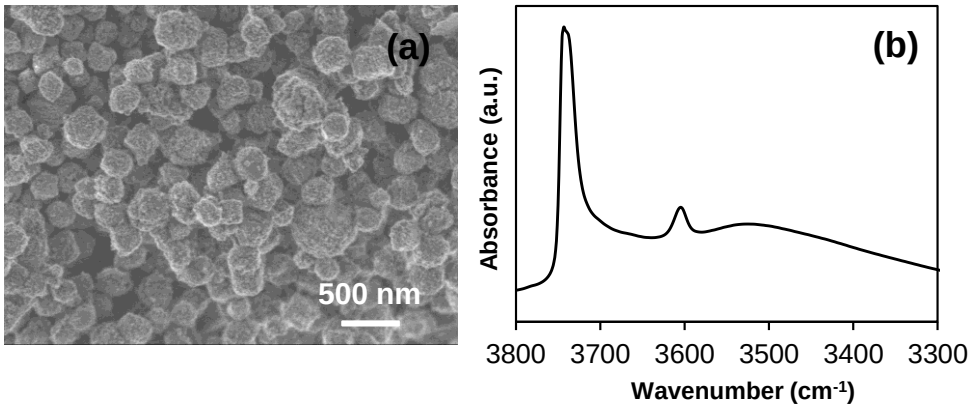

Figure 2A-5. (a) Scanning electron microscopy (SEM) image and (b) the OH-stretching vibration region of the infrared (IR) spectrum of HBEA150. SEM image shows that HBEA150 has particles with rounded corners and average diameters of ~200−300 nm. Two distinct bands of free OH groups were detected; the band at 3740 cm^{-1} is attributed to terminal and internal Si–OH groups (non-acidic), while the band at 3605 cm^{-1} is attributed to the Brønsted-acidic bridging hydroxyl groups associated with Al T sites.

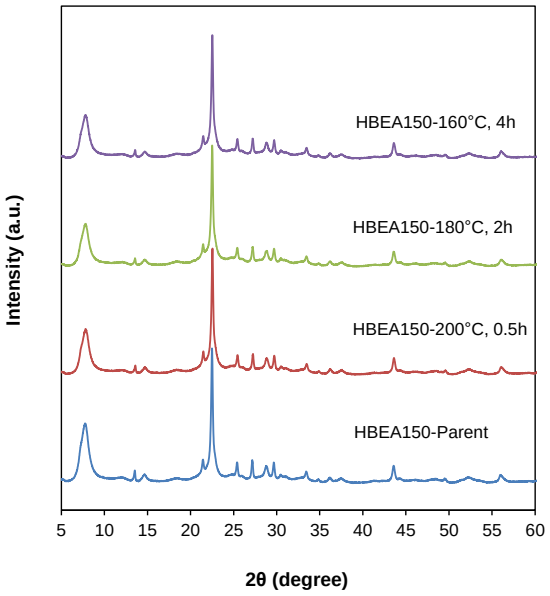

Figure 2A-6. X-ray diffractograms of parent and water treated HBEA150 samples. Sample-specific treatment conditions are reported in the plot. No appreciable changes in XRD patterns were observed after hydrothermal treatment for 0.5−4 h at 160 °C and 0.5−2 h at 180 °C, implying the HBEA150 sample retains structural integrity under conditions typical for catalysis. This was also confirmed by the BET results of these four samples by N_2 adsorption and desorption shown in **Table 2A-3.**

Table 2A-2. The textural and acid properties of the studied HBEA zeolite characterized by N_2 adsorption/desorption and IR adsorbed pyridine.

Zeolite	Si/Al ratio[a]	Pore surface area (m^2/g)	Mesopores (m^2/g)	Micropores (m^2/g)	Pore volume (cm^3/g)	Mesopores (cm^3/g)	Micropores (cm^3/g)
HBEA150	71	624	122	502	0.37	0.17	0.20
Zeolite	Acid site concentration [µmol/g]						
	Brønsted	Lewis	Total[b]	Strong Brønsted	Strong Lewis	Strong total	
HBEA150	192	41	233	181	24	205	

[a] Si/Al ratios are determined from element analysis. [b] Total acid sites are defined as those that retain pyridine after outgassing at 150 °C for 1 h following saturation of the surface by pyridine. [c] Strong acid sites are defined as those that retain pyridine after outgassing at 450 °C for 1 h following saturation of all sites by pyridine.

Table 2A-3. Textural properties of the HBEA150 (parent and hydrothermally treated) samples measured by N_2 adsorption and desorption.

Sample	BET surface area (m^2 g^{-1})			Pore volume (cm^3 g^{-1})		
	Micro	Meso	Total	Micro	Meso	Total
HBEA150 parent	502	122	624	0.20	0.17	0.37
HBEA150 200 °C 0.5 h	373	241	614	0.16	0.34	0.50
HBEA150 180 °C 2 h	376	204	580	0.16	0.29	0.45
HBEA150 160 °C 4 h	406	196	602	0.17	0.28	0.45

A4. Dehydration of cyclohexanol catalyzed by HBEA150 in aqueous phase

In contrast to the reaction catalyzed by a mineral acid (H_3PO_4) in aqueous phase, the solid HBEA zeolite catalyst together with water, the organic reactant and products, and the high pressure H_2 gas, constitute a more complicated heterogeneous reaction system. The reaction rates may be limited by the mass transport phenomena between liquid-solid, liquid-liquid, or liquid-gas phases. For kinetic measurements, all experiments must be performed in the kinetic regime without mass transport limitations. To gain insights into possible mass transfer effects, the experiments with varying agitating speeds were performed (**Table 2A-7**). Mass transfer limitations do exist when the stirring speed is less than ~ 500 rpm. To exclude mass transfer effects, all further systematic studies have been performed with a stirring speed of 700 rpm.

Our previous study employed a series of HBEA zeolites with different Si/Al ratios in this reaction.[2] Turnover frequencies (TOFs) were found to be similar among these samples, indicating the absence of intracrystalline diffusion limitation. Earlier, we also estimated the Weisz-Prater number, Thiele modulus and Damkoehler numbers that support the absence of diffusion limitations in these kinetic measurements.[3]

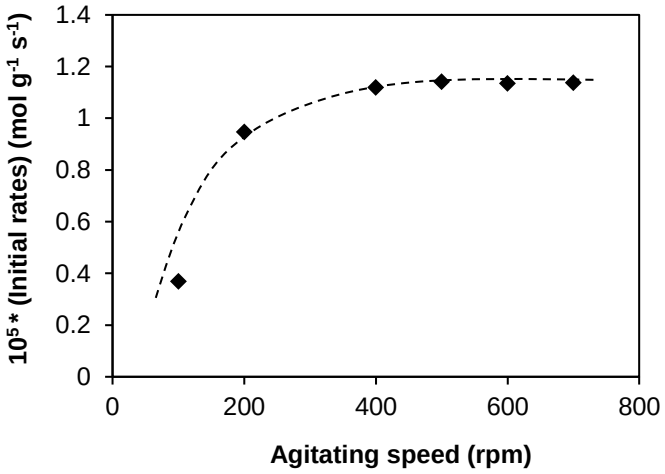

Figure 2A-7. Mass transfer limitation analysis for zeolite-catalyzed dehydration in aqueous phase. Test conditions: 140 mg of HBEA150, 3.3 g of cyclohexanol and 100 g of H_2O, 50 bar H_2 (charged at room temperature), reaction T = 200 °C. Mass transfer limitations do exist when the stirring speed is less than ~ 400 rpm. To exclude mass transfer effects, all kinetic measurements have been performed with a stirring speed of 700 rpm.

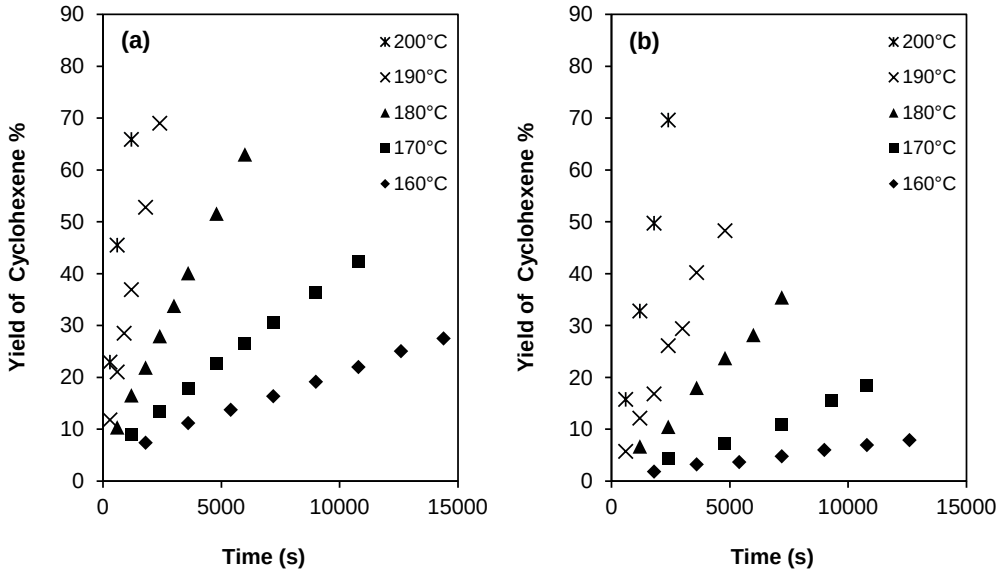

Figure 2A-8. Olefin yield-time plots for HBEA-catalyzed dehydration of cyclohexanol in aqueous phase. (a) 0.32 M cyclohexanol (r.t.), (b) 0.90 M cyclohexanol (r.t.). Reaction conditions: cyclohexanol (3.3 or 10.0 g), HBEA150 (140 mg), water (100 g), 50 bar H_2 (r.t.), stirred at 700 rpm, 160−200 °C.

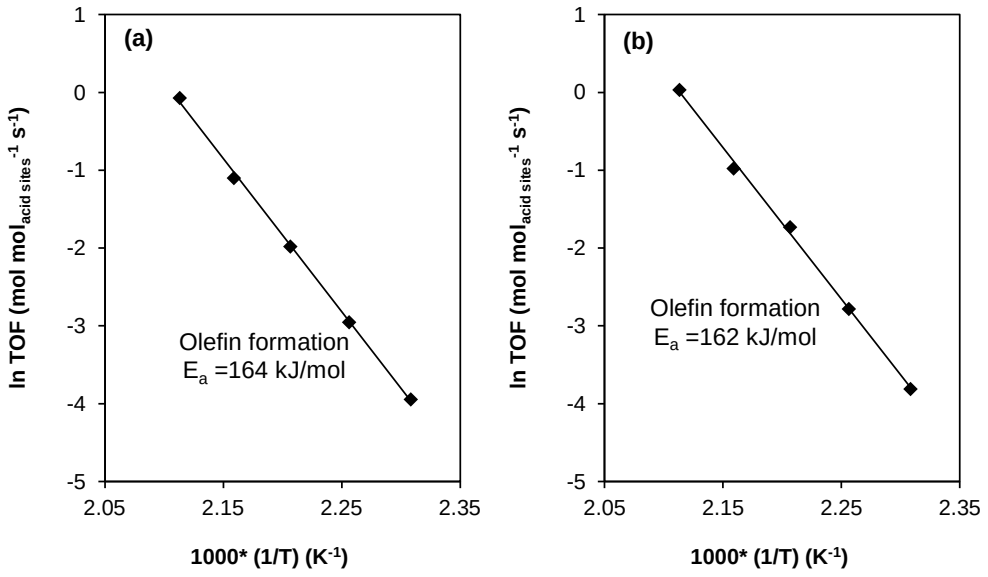

Figure 2A-9. Arrhenius plots for HBEA-catalyzed dehydration of cyclohexanol to cyclohexene in aqueous phase. (a) 0.32 M cyclohexanol (r.t.), (b) 0.90 M cyclohexanol (r.t.). Reaction conditions: cyclohexanol (3.3 or 10.0 g), water (100 g), HBEA150 (140 mg), 50 bar H_2 (r.t.), stirred at 700 rpm, 160−200 °C. TOFs are based on the BAS concentration on HBEA-150, see **Table 2-1**.

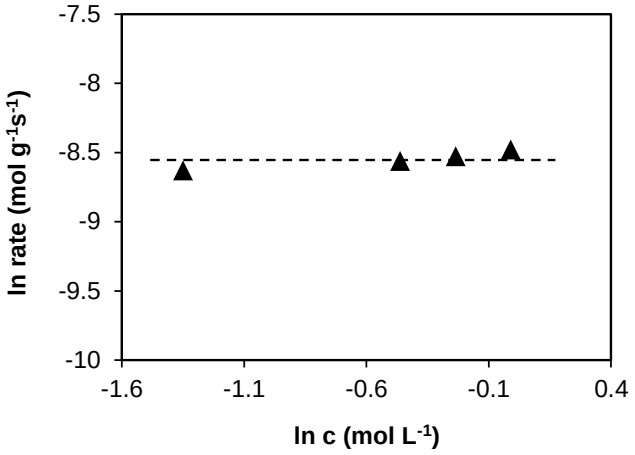

Figure 2A-10. The dependence of the mass-specific reaction rate on the concentration of cyclohexanol for dehydration over HBEA150 in aqueous phase. Reaction conditions: cyclohexanol (3.3 g, 8.0 g, 10.0 g and 12.5 g), HBEA-150 (140 mg), water (100 g), stirred at 700 rpm, 200°C. Aqueous concentrations of cyclohexanol higher than 0.32 M are not possible at room temperature due to the solubility of cyclohexanol in water; at 200 °C, the solutions are monophasic for all of these concentrations (0.32−1.1 M at r.t.). All concentrations in graph have been corrected to 200 °C.

Note that the approach of model-fitting the kinetic evolution of cyclohexanol (concentration or IR absorbance, as described below in **Section A7** for H_3PO_4-catalyzed dehydration kinetics) is not applicable to the evaluation of the relative contributions of forward and reverse reactions to the measured rates in zeolite-catalyzed dehydration. The reasons are two-fold. First, at sufficiently high conversions, bimolecular reactions take place to significant extents in zeolites. These reactions would shift the intramolecular dehydration equilibrium. Second, the reaction is zero-order in cyclohexanol for zeolites at the start of the reaction and up to relatively high conversions; however, when approaching equilibrium, the reaction order transitions from zero order to fractional orders, and eventually to first order, as conversion of cyclohexanol continues to increase and its concentration in the pores continues to drop. These complications altogether lead to remarkably more complex kinetic models, the solutions to which would require more precise knowledge about adsorption of reactants and products in zeolite at reaction temperatures, phase distribution of all volatile compounds, as well as thermodynamics and kinetics of side reactions.

To gain insights into the extent of reverse reactions in zeolites, an alternative experimental approach was used. By adding ~ 10 mg of a reduced 10%Pd/Al_2O_3 catalyst (Pd dispersion: 11 %; immeasurable activity when used alone for dehydration at 160−200 °C) to catalyze hydrogenation of cyclohexene produced, the reverse olefin hydration reaction was essentially removed, as evidenced by the predominant fraction (> 95 %) of cyclohexane in the products. The turnover rates determined this way for cyclohexane formation are 7.0×10^{-2} and 4.0×10^{-1} mol mol_{BAS}^{-1} s^{-1} at 170 and 190 °C, respectively, over HBEA150. The differences compared with the reported values in **Table 2-1** in the main text (~6.0×10^{-2} and ~3.5×10^{-1} mol mol_{BAS}^{-1} s^{-1}; based on cyclohexene formation) are considered to be slightly beyond experimental uncertainties, possibly indicating a small extent of back reaction. Nevertheless, the barriers are largely unaffected.

A5. Cyclohexanol dehydration catalyzed by mixture of H_3PO_4 and HBEA in aqueous pahse

Table 2A-4. Reaction rates comparison in the dehydration of cyclohexanol to cyclohexene catalyzed by H_3PO_4, HBEA and their mixture (H_3PO_4+HBEA) at 170°C.[a]

Reaction	Catalyst	Rate ($mol_{cyclohexene}$ s^{-1})	Reaction conditions [b]
1	H_3PO_4	3.48×10^{-6} [c]	0.02 M H_3PO_4 (100 mL), 10.0g cyclohexanol, 50bar H_2, 700rpm, 170°C.
2	HBEA150	1.66×10^{-6} [c]	140 mg HBEA-150, 100 mL H_2O, 10.0g cyclohexanol, 50bar H_2, 700rpm, 170°C.
3	H_3PO_4 + HBEA150	6.85×10^{-6}	140 mg HBEA-150, 0.02 M H_3PO_4 (100 mL), 10.0g cyclohexanol, 50bar H_2, 700rpm, 170°C.
4	H_3PO_4 + Si-BEA[d]	3.59×10^{-6}	500 mg Si-BEA, 0.02 M H_3PO_4 (100 mL), 10.0g cyclohexanol, 50bar H_2, 700rpm, 170°C.

[a] The purely siliceous BEA zeolite (Si-BEA) is used as a reference. [b] The concentrations and volumes denoted are based on the density of water at room temperature. [c] Normalizing the rates to the number of hydronium ions will lead to the same TOFs shown in Table 1 in main text. [d] Zeolite Si-BEA is homemade with the physicochemical properties: BAS (0), LAS (0.027 mmol g^{-1}), BET surface area (469 m^2 g^{-1}), total pore volume (0.22 cm^3 g^{-1}).

The observed rate with a mixture of H_3PO_4 and HBEA was higher than the sum of rates obtained with the individual acids (see **Table 2A-4**), presumably as a result of phosphoric acid being adsorbed in the pore. On the contrary, no increase in dehydration rate was observed using the mixture of siliceous BEA (Si-BEA) and H_3PO_4. We attribute this to the well-known high hydrophobicity of the all-siliceous BEA that prevents an appreciable amount of water and H_3PO_4 from entering the pore.

To confirm our speculations, H_3PO_4 uptake on HBEA150 and siliceous BEA (Si-BEA) was measured at 25 °C by ^{31}P NMR spectroscopy. We observed significant H_3PO_4 adsorption on zeolite HBEA150 (56 μmol g^{-1}) but found no measurable uptake by Si-BEA (see **Table 2A-5** and **Fig. 2A-11**). This proves that H_3PO_4 could diffuse into the pores of HBEA150, but could not get into Si-BEA. However, because the NMR measurement was not performed under the reaction conditions (170 °C, in the presence of cyclohexanol), and because the extent of H_3PO_4 dissociation in the zeolite pore is not known, it is currently not possible to establish a quantitative relation between the increase in the number of acidic species in the pore and the activity enhancement with the combination of H_3PO_4 and HBEA150.

Table 2A-5. Concentration measured at 25 °C by ^{31}P NMR of H_3PO_4 solutions before and after adding HBEA150 and siliceous BEA.

	Concentration of H_3PO_4 in solutions (M)
Reference (0.02 M H_3PO_4)	0.020
Sample A (20-25 mL 0.02 M H_3PO_4 + 1.0 g HBEA150)	~0.0176
Sample B (20-25 mL 0.02 M H_3PO_4 + 1.0 g purely siliceous BEA)	~0.020

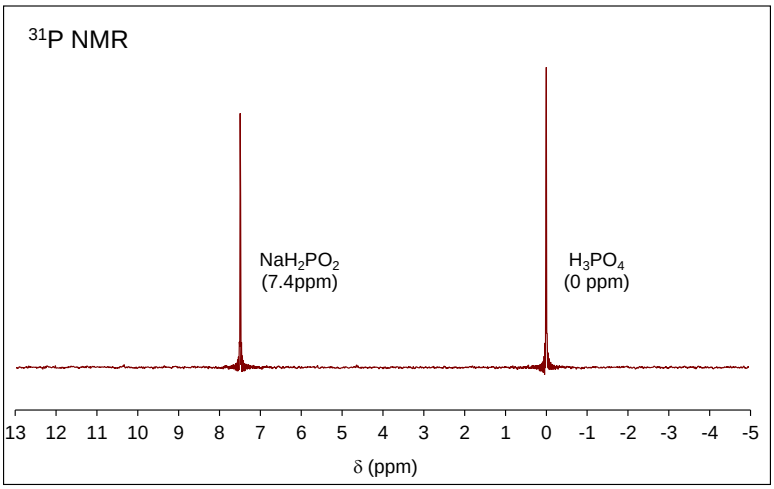

Figure 2A-11. A representative ^{31}P NMR spectrum of a H_3PO_4 solution with NaH_2PO_2 as the internal standard.

A6. Calorimetric and gravimetric measurements of cyclohexanol adsorption on HBEA150 in gas and liquid phase

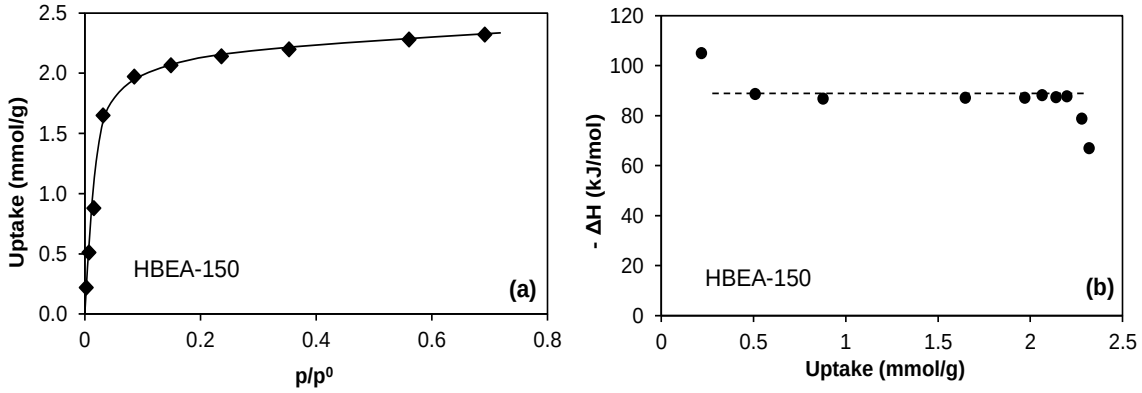

Figure 2A-12. Calorimetric measurements of cyclohexanol adsorption on HBEA150 and siliceous BEA in gas phase. The measurements were performed at 48 °C (p^0 is the saturated vapor pressure of cyclohexanol at 20 °C; p^0 = 1.2 mbar). (a): adsorption isotherms of cyclohexanol on HBEA150; (b): heat of adsorption as function of cyclohexanol uptake on HBEA150. The adsorption isotherm was fitted with a Langmuir adsorption model to derive the adsorption equilibrium constant for HBEA150, which was estimated to be 3.4×10^4 bar^{-1} (note: if referenced to the standard state of 1 bar pressure for gas, this constant becomes unitless at the same value).

Table 2A-6. Saturation uptake measured from adsorption isotherms of cyclohexanol from aqueous solutions to zeolite HBEA150.

Adsorption temperature (°C)	Saturation uptake (mmol g^{-1})
7	1.75
25	1.57
50	1.54
60	1.47
80	1.31

At room temperature, the saturation uptake of cyclohexanol was determined to be 1.6 ± 0.1 mmol g_{HBEA}^{-1} (**Fig. 2-1**). For gas phase adsorption of cyclohexanol, of 2.2 ± 0.2 mmol g_{HBEA}^{-1} was determined (**Fig. 2A-12(a)**). Assuming a liquid density (0.962 g cm^{-3}) for the adsorbed cyclohexanol, an uptake of 2.2 mmol g_{HBEA}^{-1} in the absence of water

corresponds to 0.23 $cm^3\ g_{HBEA}^{-1}$, comparable to the micropore volume of the sample (**Table 2A-2**). In the presence of water, the saturation uptake of cyclohexanol corresponds to an occupied volume of 0.16 $cm^3\ g_{HBEA}^{-1}$. Subtracting this value from the micropore volume, and if solely attributing this difference (0.04 $cm^3\ g_{HBEA}^{-1}$) to water in the pores, the adsorbed amount of water would be ~2 mmol g_{HBEA}^{-1}.

The adsorption isotherms of cyclohexanol from aqueous solutions onto zeolite HBEA150 have been measured at various temperatures (7–80 °C). Langmuir-type adsorption model, as discussed in the main text, has been applied to fit these measured isotherms to obtain adsorption constant (K_{ads}) and saturation uptake (q_{max}) at each temperature. Detailed results will be reported in a subsequent publication. Important to this work is what we show below regarding the estimation of adsorption capacity under reaction conditions.

It was found that the saturation uptake decreased as adsorption temperature increased (**Table 2A-6**). This decrease in the saturation uptake with increasing adsorption temperature stems from the decrease in density of the adsorbate phase in the micropore (like thermal expansion of a liquid) as a function of temperature. The temperature dependence takes the form:

$$\frac{1}{q_{max}}\frac{dq_{max}}{dT} = -\delta \qquad \text{(2A-1)}$$

where δ is the temperature coefficient of expansion.

Plotting measured/regressed saturation adsorption capacity at different temperatures as a function of temperature yielded a slope ($-\delta$) of –0.0037 K^{-1}. Having extrapolating these experimentally determined q_{max} and K_{ads} to reaction temperatures using the same temperature dependence as determined between 7 and 80 °C, we found that the saturation uptake of cyclohexanol would decrease from 1.05 to 0.92 mmol g_{HBEA}^{-1} at 160–200 °C. Assuming that the remaining micropore volume (total V_{micro} = 0.20 $cm^3\ g^{-1}$) is filled by adsorbed water, the uptake of water in the pore would increase from 3.9 to 4.2 mmol g_{HBEA}^{-1} (compared with 1.8 mmol g_{HBEA}^{-1} at room temperature) with temperature increasing from 160 to 200 °C.

Table 2A-7. Equilibrium constants, heats of adsorption, and entropy changes for cyclohexanol uptake on HBEA150 zeolite.[a]

Parameter	Gas phase	Aqueous phase
K_{ads}	3.4×10^{4} [b]	3.2×10^{2} [c]
$\Delta H°_{ads}$ (kJ mol^{-1})	–88	–22
$\Delta S°_{ads}$ (J mol^{-1} K^{-1})	–186	–25

[a] Adsorption constants were derived from the slope of the linearized Langmuir isotherm, standard molar enthalpy changes of cyclohexanol adsorption were determined by microcalorimetry and separate isotherm measurements, and standard molar entropy changes were obtained from transition state theory formalism that relates all thermodynamic quantities. Standard states for gas phase molecules, aqueous phase molecules and adsorbed molecules are 1 bar, 1 M, and pore-filling fraction or surface site coverage = 1, respectively; [b] At 48 °C; [c] At 25 °C.

A7. In situ cyclohexanol dehydration in dilute H_3PO_4 solutions monitored with IR

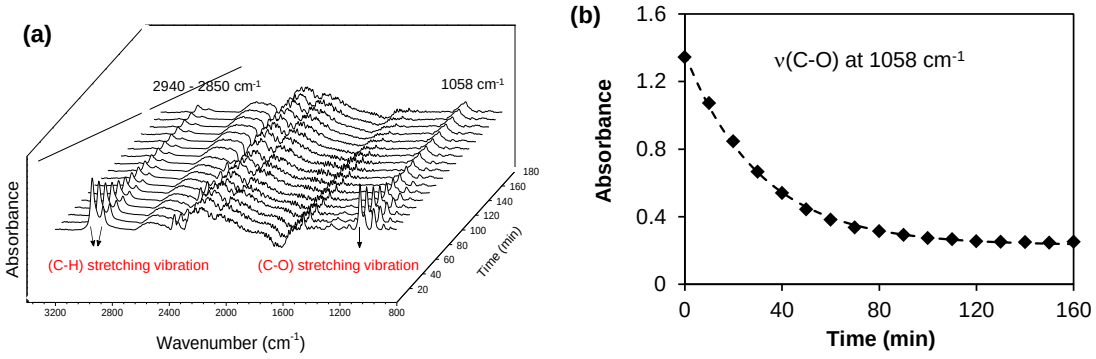

Figure 2A-13. In situ cyclohexanol dehydration in dilute H_3PO_4 solutions monitored with IR. (a) IR spectra acquired during aqueous phase cyclohexanol dehydration catalyzed by H_3PO_4; (b) The measured (markers) and fitted (curve) IR absorbance at 1058 cm^{-1} as a function of residence time. Reaction conditions: 5.0 g cyclohexanol (~0.90 M at r.t.), 50 mL 0.02 M (r.t.) H_3PO_4 in water, 200 ºC. 2850–2940 cm^{-1} and 1058 cm^{-1} are attributed to C–H and C–O stretching vibrations from aquesou-phase cyclohexanol, respectively. A reversible first-order equation was used for fitting in (b).

Figure 2A-13 shows both the stacked data plot over 180 min and the temporal evolution of the IR absorbance at a single wavenumber unique to cyclohexanol (1058 cm^{-1}), which shows an exponential decay over time. Since the measured alcohol absorbance is proportional to its concentration in solution, the time-resolved evolution of this absorbance can be used to follow the reaction kinetics.

The IR spectra in **Fig. 2A-13(a)** exhibit absorption bands characteristic of cyclohexanol: C–H and C–O stretching vibrations (2850–2940 cm^{-1} and 1058 cm^{-1}, respectively). Because the diamond window used to monitor transformations is installed at the bottom of the reactor, the fractions lighter than water, *i.e.*, cyclohexene (liquid and vapor) in this case, were not monitored during the experiment. However, the rate of cyclohexanol disappearance must be equal to that of cyclohexene formation, as the alcohol dehydrates exclusively to the olefin in H_3PO_4-catalyzed reactions.

Although the measured reaction order was less than 1 (**Figure 2A-3**), a satisfactory best-fit to the experimental data (**Fig. 2A-13(b)**) could be obtained using the kinetic equation derived based on the assumption of reversible first-order kinetics with respect to cyclohexanol concentration. This fit yields an initial cyclohexanol decay rate of 4.0×10^{-4} mol L^{-1} s^{-1} at 200 °C, which is nearly identical to the result obtained in the batch autoclave (3.7×10^{-4} mol L^{-1} s^{-1}, **Table 2-1** in the main text).

More importantly, by following the reaction to equilibrium, pseudo-first-order rate constants for forward and reverse reactions were also roughly estimated; the forward rate constant is much higher than the effective reverse pseudo-first-order rate constant (including water concentration and taking into account the partitioning of cyclohexene between gas and solution phases), by a factor of 8.5 ± 1.7, at 200 °C (**Table 2A-9**). These results suggest that the net reaction rate measured at conversions lower than 10 % can be considered to represent nearly exclusively the forward reaction rate.

Next, we give the derivation of reversible first-order equation for in situ cyclohexanol dehydration in dilute H_3PO_4 solutions monitored with IR.

A8. Derivation of reversible first-order equation for in situ cyclohexanol dehydration in dilute H_3PO_4 solutions monitored with IR

An illustration of a reversible first-order dehydration reaction in aqueous phase is shown in Supplementary **Scheme 2A-1**.

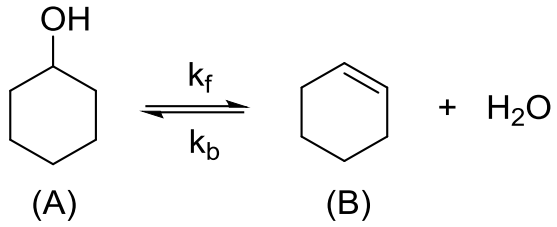

Scheme 2A-1. A reversible first-order dehydration reaction in aqueous phase.

At reaction temperature, however, a significant amount of cyclohexene (B) is distributed into the gas phase. The distribution of B between gas and aqueous phases is defined by Henry's law. It is reasonable to neglect the portion of A that is in the gas phase due to its high boiling point relative to the reaction temperature. The reaction is assumed to occur only in the aqueous solution which contains the catalyst (hydronium ions).

Definitions:

K_H = Henry's law constant in the unit of M/bar

$[A]_{aq}$ = concentration of cyclohexanol in aqueous solution

$[B]_{aq}$ = concentration of cyclohexene in aqueous solution

V_g = volume of reactor headspace

V_{aq} = volume of aqueous solution in the reactor

The total moles ($n_A + n_B$) of A and B is constant in the reactor at different times. Therefore,

$$n_{A,aq,t=0} + n_{B,g,t=0} + n_{B,aq,t=0} = n_{A,aq,t} + n_{B,g,t} + n_{B,aq,t} \quad (2A\text{-}2)$$

$$n_{A,aq,t=0} - n_{A,aq,t} = n_{B,g,t} - n_{B,g,t=0} + n_{B,aq,t} - n_{B,aq,t=0} \quad (2A\text{-}3)$$

Using Henry's law that applies to the phase distribution for B between gas and solution, we obtain:

$$n_{B,g} = \frac{n_{B,aq}}{V_{aq} K_H} \frac{V_g}{RT} = \frac{n_{B,aq}}{K_H RT} \frac{V_g}{V_{aq}} \quad (2A\text{-}4)$$

Substitute into (2A-3) and rearrange

$$n_{A,aq,t=0} - n_{A,aq,t} = (n_{B,aq,t} - n_{B,aq,t=0})\left(1 + \frac{1}{K_H RT}\frac{V_g}{V_{aq}}\right) \quad (2A\text{-}5)$$

In the same solution, both sides in (2A-5) can be divided by V_{aq}, which gives

$$[A]_{aq,t=0} - [A]_{aq,t} = ([B]_{aq,t} - [B]_{aq,t=0})\left(1 + \frac{1}{K_H RT}\frac{V_g}{V_{aq}}\right) \quad (2A\text{-}6)$$

$$[B]_{aq,t} = \frac{[A]_{aq,t=0} - [A]_{aq,t}}{1 + \frac{1}{K_H RT}\frac{V_g}{V_{aq}}} + [B]_{aq,t=0} \quad (2A\text{-}7)$$

The reaction occurs in the aqueous phase, such that the rate of cyclohexanol consumption is

$$-r = \frac{\partial[A]}{\partial t} = k_f[A]_{aq,t} - k_b[B]_{aq,t}[H_2O] = k_f[A]_{aq,t} - k_b'[B]_{aq,t} \quad (2A\text{-}8)$$

where $k_b' = k_b[H_2O]$ as a result of the almost constant molar concentration of water. Substituting (2A-7) into (2A-8) and rearrange

$$-r = \frac{\partial[A]}{\partial t} = \left(k_f + \frac{k_b'}{1 + \frac{1}{K_H RT}\frac{V_g}{V_{aq}}}\right)[A]_{aq,t} - k_b'\left(\frac{[A]_{aq,t=0}}{1 + \frac{1}{K_H RT}\frac{V_g}{V_{aq}}} + [B]_{aq,t=0}\right) \quad (2A\text{-}9)$$

At $t = \infty$, the reaction reaches equilibrium and the net rate drops to zero

$$-r = \frac{\partial[A]}{\partial t} = \left(k_f + \frac{k_b'}{1 + \frac{1}{K_H RT}\frac{V_g}{V_{aq}}}\right)[A]_{aq,t=\infty} - k_b'\left(\frac{[A]_{aq,t=0}}{1 + \frac{1}{K_H RT}\frac{V_g}{V_{aq}}} + [B]_{aq,t=0}\right) \quad (2A\text{-}10)$$

Combining (2A-9) and (2A-10)

$$-r = \frac{\partial[A]}{\partial t} = \left(k_f + \frac{k_b'}{1 + \frac{1}{K_H RT}\frac{V_g}{V_{aq}}}\right)([A]_{aq,t} - [A]_{aq,t=\infty}) \quad (2A\text{-}11)$$

The integration of the above differential equation gives:

$$\int_{[A]_{aq,t=0}}^{[A]_{aq}} \frac{d[A]_{aq}}{[A]_{aq} - [A]_{aq,t=\infty}} = -\left(k_f + \frac{k_b'}{1 + \frac{1}{K_H RT}\frac{V_g}{V_{aq}}}\right)\int_0^t dt \quad (2A\text{-}12)$$

$$\ln\frac{[A]_{aq}-[A]_{aq,t=\infty}}{[A]_{aq,t=0}-[A]_{aq,t=\infty}}=-(k_f+\frac{k_b'}{1+\frac{1}{K_H RT}\frac{V_g}{V_{aq}}})t \quad \text{(2A-13)}$$

$$([A]_{aq}-[A]_{aq,t=\infty})=([A]_{aq,t=0}-[A]_{aq,t=\infty})\exp[-(k_f+\frac{k_b'}{1+\frac{1}{K_H RT}\frac{V_g}{V_{aq}}})t] \quad \text{(2A-14)}$$

Let $[A]_{aq}$ be y (t) and t be x, rearrange (2A-14) into

$$y=([A]_{aq,t=0}-[A]_{aq,t=\infty})\exp[-(k_f+\frac{k_b'}{1+\frac{1}{K_H RT}\frac{V_g}{V_{aq}}})x]+[A]_{aq,t=\infty} \quad \text{(2A-15)}$$

Eq. (2A-15) can be used to fit the disappearance of cyclohexanol (IR absorbance or equivalent concentration) in aqueous solution as a function of time.

The React IR results were fitted by this equation and the results are shown in **Table 2A-8**. Note that here, the absorbance at 1058 cm^{-1} (C−O stretches of cyclohexanol, reported in **Fig. 2A-13**), instead of the concentration of cyclohexanol, is fitted. The physical meanings of other parameters can be referred to in Eq. (2A-15). Equivalent concentrations of cyclohexanol can be obtained by assuming proportionality between absorbance and concentration in dilute solutions.

Table 2A-8. The fitted parameters from React IR using an equation derived on basis of first-order reversible kinetics. Reaction conditions: cyclohexanol (0.9 M) in H_3PO_4 solution (0.02 mol L^{-1}, 50 mL), 200 °C, 30 bar H_2 (charged at ambient temperature), stirred at 900 rpm. The physical meanings of the parameters can be referred to in Eq. (2A-15). Note that the y-axis corresponds to IR absorbance, so not in concentration units (see **Fig. 2A-13**).

Model Equation	$y = a*\exp(-x/\tau) + y_0$	
Reduced Chi-Sqr	1.48×10^{-4}	
Adj. R-Square	0.9986	
Fitted Parameters	Value	Standard Error
y_0	0.2313	0.0054
a	1.1334	0.0107
τ	31.0495	0.6781

The moles of A in the aqueous solution at equilibrium, $n_{A,aq,t=\infty}$, almost equals to the total moles of B ($n_{B,total,t=\infty}$) in both gas ($n_{B,g,t=\infty}$) and solution ($n_{B,aq,t=\infty}$) subtracted from the initial moles of A (no reaction, $n_{A,aq,ini}$). Based on (2A-4), together with the above consideration:

$$n_{A,aq,t=\infty} = n_{A,aq,ini} - n_{B,total,t=\infty} = n_{A,aq,ini} - (1 + \frac{1}{K_H RT}\frac{V_g}{V_{aq}})n_{B,aq,t=\infty} \quad (2A\text{-}16)$$

$$[A]_{aq,t=\infty} = [A]_{aq,ini} - (1 + \frac{1}{K_H RT}\frac{V_g}{V_{aq}})[B]_{aq,t=\infty} \quad (2A\text{-}17)$$

The starting concentration of [A] in aqueous phase is *ca.* 0.88 M. At equilibrium, the concentration of A ($[A]_{aq,t=\infty}$) is 0.075 M. According to (2A-17), the term of

$$(1 + \frac{1}{K_H RT}\frac{V_g}{V_{aq}})[B]_{aq,t=\infty} \text{ is 0.805 M.}$$

At equilibrium, according to (2A-8),

$$K_{eq} = \frac{k_f}{\frac{k_b'}{1 + \frac{1}{K_H RT}\frac{V_g}{V_{aq}}}} = 0.805 / 0.075 = 10.2$$

Table 2A-9. Fitted parameters from the least-squares regression of *in situ* kinetics obtained by IR. Reaction conditions: cyclohexanol in H_3PO_4 solution (50 mL, 0.02 M at r.t.), 200 °C, 30 bar H_2 (charged at r.t.), stirred at 900 rpm.

Parameters	Cyclohexanol concentration	
	0.90 M (r.t.)	0.32 M (r.t.)
k_f (s^{-1})	4.43×10^{-4}	5.77×10^{-4}
$k_{b,eff}$ (s^{-1})[a]	4.34×10^{-5}	8.54×10^{-5}
K_{eq} (dimensionless)[b]	10.2	6.76

[a] Effective first-order reverse reaction constant, $k_{b,eff} = \frac{k_b'}{1 + \frac{1}{K_H RT}\frac{V_g}{V_{aq}}}$, as defined in the text.

[b] $$K_{eq} = \frac{k_f}{\frac{k_b'}{1 + \frac{1}{K_H RT}\frac{V_g}{V_{aq}}}}$$

Table 2A-9 lists the fitted parameters from the least-square regression of *in situ* kinetics based on the time-evolution of IR absorbance for H_3PO_4-catalyzed aqueous phase dehydration of cyclohexanol at 200 °C. The fitting of kinetic results into a reversible first-order kinetics model at two concentrations yields somewhat different forward and reverse rate constants. Overall, the reverse reaction occurs at a much slower rate at conversions < 10 % than the forward reaction. Thus the measured initial rate should primarily reflect the forward dehydration reaction.

A9. Density functional theory (DFT)

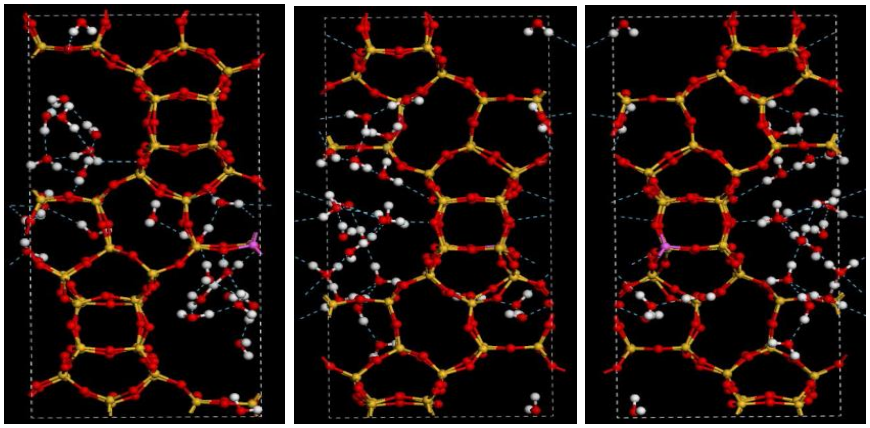

Figure 2A-14. Water Structure inside the pores of HBEA (1 Al per unit cell). Typical hydronium ion cluster containing 8-10 water molecules with a total of 26 water molecules. T = 500 K, AIMD 10 ps.

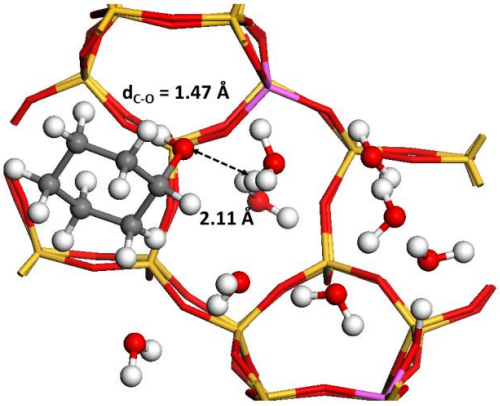

(A)

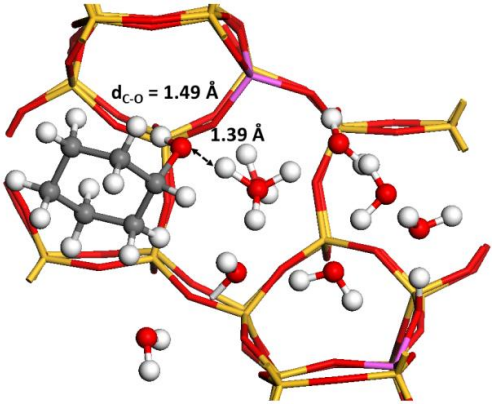

(TS1)

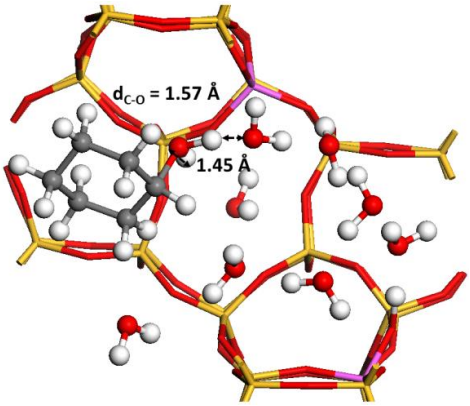

(B)

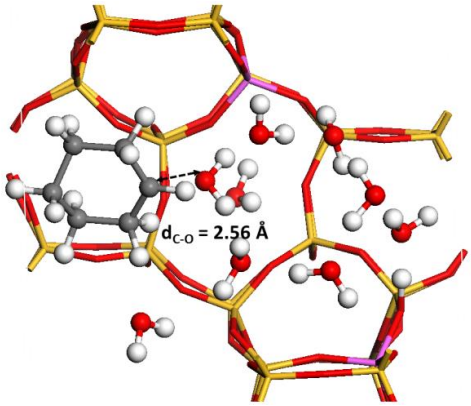

(TS2)

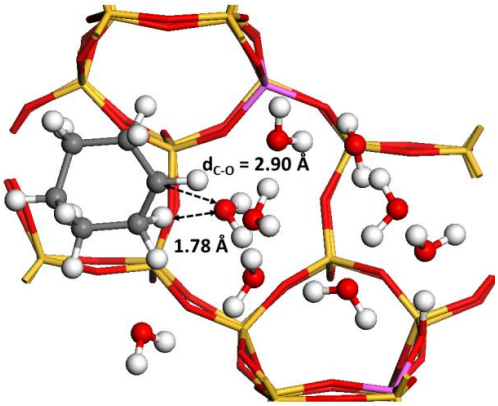

(C)

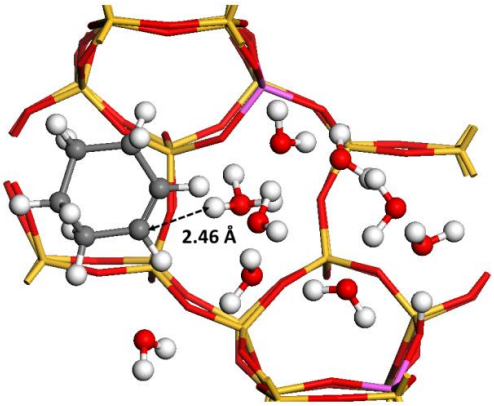

(TS3)

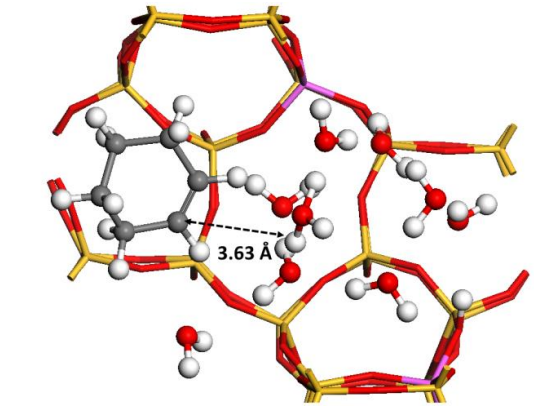

(D)

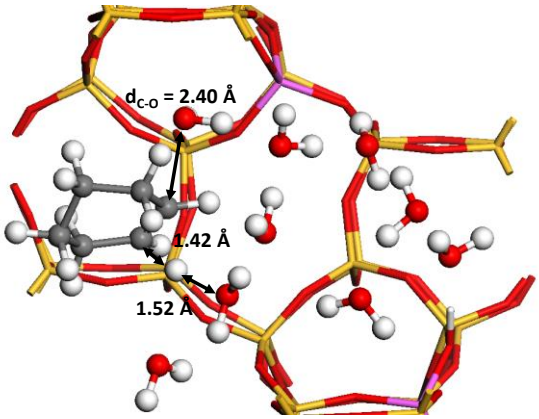

(TS4)

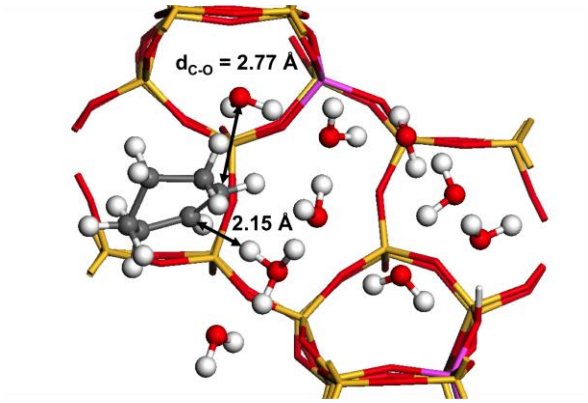

(D')

Figure 2A-15. DFT-optimized structures of reaction intermediates (A–D') and transition states (TS1–TS4) in the aqueous phase cyclohexanol dehydration to cyclohexene in HBEA pore via E1 and E2-like elimination pathways.

Table 2A-10. Proton affinities (ΔH_{PA}, for the process $A + H^+ \rightarrow AH^+$) of a single water molecule, water clusters and cyclohexanol in vacuum and HBEA.

Species (A)	ΔH_{PA} (kJ mol^{-1})	
	Vacuum	HBEA
H_2O	-702	NA
$(H_2O)_2$	-837	+45
$(H_2O)_3$	-918	-12
$(H_2O)_4$	-930	-31
$(H_2O)_5$	-966	-32
$C_6H_{11}OH$	-787	-25

A10. Derivation of rate expression for cyclohexanol dehydration in aqueous phase

A proposed sequence of steps within an E1-type mechanistic framework (with the C–H bond cleavage being kinetically relevant) for aqueous phase dehydration of cyclohexanol catalyzed by H_3PO_4 is shown below:

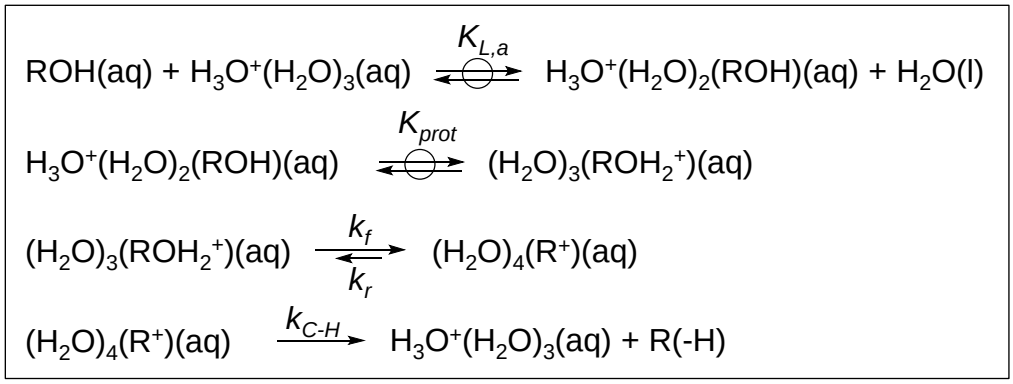

Scheme 2A-2. A proposed sequence of steps within an E1-type mechanistic framework (with the C–H bond cleavage being kinetically relevant) for aqueous phase dehydration of cyclohexanol catalyzed by H_3PO_4. Association of the alcohol with hydronium ion and the subsequent protonation is proposed to be sufficiently fast and quasi-equilibrated (a circle on top of a two-way arrow). The hydronium ion is represented as $H_3O^+(H_2O)_3$(aq), the association complex as $H_3O^+(H_2O)_2$(ROH)(aq), the olefin product as R(-H).

It has been demonstrated from isotope experiments (see main text) that the prevalent dehydration mechanism is of E1-type with the C_β–H bond cleavage as the kinetically relevant step, for aqueous phase dehydration of cyclohexanol both in dilute H_3PO_4 and in HBEA. A classical sequence of steps for homogeneous acid catalyzed dehydration is proposed above. A similar sequence should apply to HBEA-catalyzed dehydration in aqueous phase, yet with additional adsorption (from aqueous phase to intrazeolite voids where active sites reside) and desorption steps (from intrazeolite sites to aqueous/gas phases).

Next, we derive the kinetic expression for this mechanistic sequence. We use concentration terms instead of activities for solution species in dilute systems, assuming activity coefficients for the solution species are unity.

For the first step shown above, *i.e.*, association of cyclohexanol with hydronium ion, letting the initial proton concentration be $[H_3O^+]_0$, we have:

$$\frac{[H_2O(l)][H_3O^+(H_2O)_2(ROH)(aq)]}{[ROH(aq)]([H_3O^+]_0 - [H_3O^+(H_2O)_2(ROH)(aq)])} = K_{L,a} \tag{2A-18}$$

Solving the Eq. (2A-18) gives:

$$\frac{[H_3O^+(H_2O)_2(ROH)(aq)]}{[H_3O^+]_0} = \frac{K_{L,a}\frac{[ROH(aq)]}{[H_2O(l)]}}{1 + K_{L,a}\frac{[ROH(aq)]}{[H_2O(l)]}} \tag{2A-19}$$

For the second step, proton transfer from water cluster to ROH, we have:

$$\frac{[H_3O^+(H_2O)_2(ROH)(aq)]}{[(H_2O)_3(ROH_2^+)(aq)]} = K_{prot} \tag{2A-20}$$

Thus, we have:

$$\frac{[(H_2O)_3(ROH_2^+)(aq)]}{[H_3O^+]_0} = \frac{K_{prot}}{1 + K_{prot}} \frac{K_{L,a}\frac{[ROH(aq)]}{[H_2O(l)]}}{1 + K_{L,a}\frac{[ROH(aq)]}{[H_2O(l)]}} \tag{2A-21}$$

For the third step, C–O bond cleavage, applying steady-state assumption to the solvated carbenium-ion intermediate, $(H_2O)_4(R^+)(aq)$, we have:

$$\begin{aligned} k_f[(H_2O)_3(ROH_2^+)(aq)] - k_r[(H_2O)_4(R^+)(aq)] \\ = k_{C-H}[(H_2O)_4(R^+)(aq)] \end{aligned} \tag{2A-22}$$

$$[(H_2O)_4(R^+)(aq)] = \frac{k_f[(H_2O)_3(ROH_2^+)(aq)]}{k_r + k_{C-H}} \tag{2A-23}$$

The expression for TOF is (equal to that of the fourth step):

$$TOF_L = \frac{k_{C-H}[(H_2O)_4(R^+)(aq)]}{[H_3O^+]_0} \tag{2A-24}$$

Replacing the terms for $[(H_2O)_4(R^+)(aq)]$, we have:

$$TOF_L = \frac{k_f k_{C-H}}{k_r + k_{C-H}} \frac{K_{prot}}{1 + K_{prot}} \frac{K_{L,a} \frac{[ROH(aq)]}{[H_2O(l)]}}{1 + K_{L,a} \frac{[ROH(aq)]}{[H_2O(l)]}} \quad \text{(2A-25)}$$

Let $\frac{k_f k_{C-H}}{k_r + k_{C-H}} \frac{K_{prot}}{1+K_{prot}} = k_{L,d}$, we arrive at the Eq. (2-3) shown in the main text:

$$TOF_L = k_{L,d} \frac{K_{L,a} \frac{[ROH(aq)]}{[H_2O(l)]}}{1 + K_{L,a} \frac{[ROH(aq)]}{[H_2O(l)]}}$$

The temperature dependence for $k_{L,d}$, in its current functional form ($\frac{k_f k_{C-H}}{k_r + k_{C-H}} \frac{K_{prot}}{1+K_{prot}}$), is complex. However, considering the DFT estimates for protonation in zeolite, K_{prot} is likely much smaller than 1 such that $\frac{K_{prot}}{1+K_{prot}} \approx K_{prot}$. Moreover, the more rapid microscopic reverse of C–O bond cleavage (k_r) than the C–H bond cleavage (k_{C-H}) would allow $\frac{k_f k_{C-H}}{k_r + k_{C-H}}$ to be approximated as $\frac{k_f k_{C-H}}{k_r} = K_{C-O} k_{C-H}$. Therefore, we have: $k_{L,d} = k_{C-H} K_{C-O} K_{prot}$.

Scheme 2A-3 shows an illustrative energy diagram of aqueous phase cyclohexanol dehydration catalyzed by H_3PO_4, starting with the associated complex formed between cyclohexanol and protonated water cluster (hydronium ion). For $k_{L,d} = k_{C-H} K_{C-O} K_{prot}$, the corresponding changes of enthalpy, entropy and free energy reflect the differences in these parameters between the association complex and the TS for the C_β–H bond cleavage (red broken arrows in **Scheme 2A-3**). The analysis above applies analogously to zeolite HBEA, with the additional adsorption step.

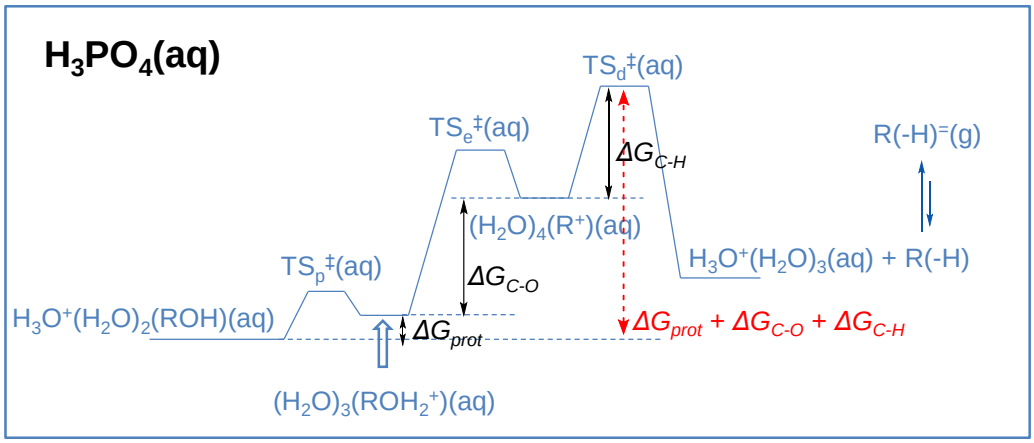

Scheme 2A-3. An illustrative free-energy diagram of alcohol (ROH) dehydration in aqueous phase catalyzed by H_3PO_4, via an E1-type mechanism with kinetically relevant C–H bond cleavage. All intermediates and TSs (TS_p, protonation of alcohol; TS_e, C–O bond cleavage leading to elimination of water; TS_d, deprotonation of carbenium ion) are solvated. The schemes do not rigorously reflect the actual relative energy levels of the different states.

A11. Mathematical approach for the determination of hydronium ion concentration, association equilibrium constant and intrinsic rate constant for H_3PO_4-catalyzed dehydration

Since H_3PO_4 is a weak acid with incomplete dissociation of even its first proton (the other two hardly dissociated without high concentrations of bases) in water at all practical temperatures, the extent of H_3PO_4 dissociation is affected by temperature, total acid concentration, as well as additional equilibria that involve (*i.e.*, consume or produce) any of the species (*e.g.*, H_3PO_4, hydronium ion, anions) that is present in the acid dissociation equilibrium:

$$H_3PO_4 + H_2O = H_2PO_4^- + H_3O^+ \qquad K_{a,1} = \frac{[H_3O^+][H_2PO_4^-]}{[H_3PO_4]}$$

The equilibrium constant $K_{a,1}$ is documented for aqueous H_3PO_4 solutions at elevated temperatures, with a functional relation of $pK_{a,1}$=756.276/T-4.0886+0.012396T.[18] The $K_{a,1}$ values are calculated for reaction temperatures (**Table 2A-1**).

The produced hydronium ion is partly associated with cyclohexanol, the reactant (**Scheme 2A-2**). Potentially, this additional step with equilibrium constant $K_{L,a}$ would shift the acid dissociation equilibrium as it converts H_3O^+, or $[H_3O^+(H_2O)_3]$, into $[H_3O^+(H_2O)_2(ROH)]$, as represented earlier. Consequently, $K_{L,a}$ is the key parameter to be solved or regressed; it links the acid dissociation step with a known equilibrium constant with the alcohol-hydronium ion association step.

If the concentration of dissociated proton is $[a]$, then $[H^+(H_2O)_3ROH] = [a]*\theta_{L,a}$, $[H_2PO_4^-] = [a]$, $[H_3O^+(H_2O)_3] = [a](1-\theta_{L,a})$, and $[H_3PO_4] = [H_3PO_4]_0 - [a]$ when the two steps reach their respective equilibrium. Thus, we have:

$$K_{a,1} = \frac{[a](1-\theta_{L,a})[a]}{[H_3PO_4]_0 - [a]}$$

where $K_{a,1}$ is known (**Table 2A-1**), $[a] = [H_3O^+(H_2O)_2(ROH)] + [H_3O^+(H_2O)_3]$, and the extent of alcohol-hydronium ion association, $\theta_{L,a} = \frac{K_{L,a}\frac{[ROH(aq)]}{[H_2O(l)]}}{1+K_{L,a}\frac{[ROH(aq)]}{[H_2O(l)]}}$, is a single-valued function of $K_{L,a}$. The following quadratic equation can be derived:

$$[a] = \frac{-K_{a,1} + \sqrt{(K_{a,1})^2 + 4 \times K_{a,1} \times (1-\theta_{L,a})[H_3PO_4]_0}}{2 \times (1-\theta_{L,a})}$$

From Eq. (2-3) in the main text, we find that TOF ratios at two concentrations (0.32 and 0.90 M at which extensive rate data were measured) are equal to the ratios of $\theta_{L,a}$, and would provide another independent functional relation to $K_{L,a}$. TOF is normalized to the summed concentration of $[H_3O^+(H_2O)_2(ROH)]$ and $[H_3O^+(H_2O)_3]$, that is, $[a]$.

$$\frac{TOF_{L,1}}{TOF_{L,2}} = \frac{\theta_{L,a,1}}{\theta_{L,a,2}} = \frac{\frac{K_{L,a}\frac{[ROH(aq)]_1}{[H_2O(l)]_1}}{1+K_{L,a}\frac{[ROH(aq)]_1}{[H_2O(l)]_1}}}{\frac{K_{L,a}\frac{[ROH(aq)]_2}{[H_2O(l)]_2}}{1+K_{L,a}\frac{[ROH(aq)]_2}{[H_2O(l)]_2}}}$$

While solving $K_{L,a}$ directly from the above functional relations seems quite challenging, an alternative approach is: 1) give initial guess for $K_{L,a}$ and obtain $\theta_{L,a}$ (recall that $\theta_{L,a} = \frac{K_{L,a}\frac{[ROH(aq)]}{[H_2O(l)]}}{1+K_{L,a}\frac{[ROH(aq)]}{[H_2O(l)]}}$), at each [ROH]/[$H_2O$] ratio; 2) solve for [$a$] at each [ROH]/[$H_2O$] ratio from the quadratic equation; 3) use measured volumetric reaction rates and [a] to calculate TOF ratios at the two concentrations; 4) calculate TOF ratios in another way that uses the relation that the ratios of TOF are equal to the ratios of $\theta_{L,a}$; 5) regress $K_{L,a}$ to obtain absolute agreement between the TOF ratios determined via steps 1-3 and steps 1,4. The so determined $K_{L,a}$ and $\theta_{L,a}$ are listed in **Table 2A-13** and discussed in **Section A12**.

Table 2A-11. Henry's law constants of cyclohexanol at 160 and 200 °C (determined in this work), at 170-190 °C (interpolated) and at room temperature (NIST data[4]). Here, $K_H = C_{aq}/P_{gas}$

Temperature (°C)	K_H (mol L^{-1} bar^{-1})
160	1.45
170	1.06
180	0.79
190	0.59
200	0.45
25	170

Finally, we note that corrections for volume expansion and vaporization (water and cyclohexanol) have been made to obtain more accurate estimates for the actual [ROH]/[H_2O] ratio under reaction conditions. The extent of volume expansion is calculated based on the decrease of density of water at 160–200 °C. For the estimation of cyclohexanol vapor in the headspace, Henry's law constants (K_H) were first determined at 160 and 200 °C; K_H at 170–190 °C were obtained from interpolation using room temperature value (NIST) and the two measured values (see **Table 2A-11** for K_H at 160–200 °C). After these corrections, the actual [ROH]/[H_2O] ratios at 160–200 °C for the 3.1 wt% and 9.1 wt% cyclohexanol solutions are 5.3–5.6×10^{-3} (*vs.* 5.8×10^{-3} at r.t.) and 1.5–1.6×10^{-2} (*vs.* 1.6×10^{-3} at r.t.), respectively. So these corrections turn out to be very small.

Table 2A-12. Concentrations of cyclohexanol, hydronium ion and [ROH]/[H_2O] ratio in the starting reaction mixture at reaction temperatures. I: 3.1 wt% solution; II: 9.1 wt% solution. The densities of both solutions are assumed to change with the temperature as pure water does (d = 0.90, 0.89, 0.88, 0.87 and 0.86 at 160, 170, 180, 190 and 200 °C, respectively).

Temperature (°C)	[ROH] (M)	[ROH]/[H_2O] (10^{-2} M)	[H_3O^+] (10^{-3} M)
160	I: 0.28	I: 0.56	I: 4.0
	II: 0.80	II: 1.59	II: 4.55
170	I: 0.27	I: 0.55	I: 3.6
	II: 0.77	II: 1.57	II: 4.1
180	I: 0.27	I: 0.55	I: 3.3
	II: 0.76	II: 1.55	II: 3.7
190	I: 0.26	I: 0.54	I: 3.0
	II: 0.74	II: 1.54	II: 3.5
200	I: 0.25	I: 0.53	I: 2.7
	II: 0.72	II: 1.51	II: 3.0

A12. Comparison of association equilibrium constants and intrinsic rate constants for H_3PO_4- and HBEA-catalyzed dehydration

Using measured rate data (H_3PO_4-catalyzed reactions) at the two alcohol concentrations and correcting for solution volume and extent of acid dissociation under reaction conditions, the $K_{L,a}$ and $k_{L,d}$ were determined (**Section A10**) and compiled in **Table 2A-13**. Because of the high sensitivity of $K_{L,a}$ to measured rate ratios, the errors in the kinetic measurements eventually lead to significant uncertainties in the value of $K_{L,a}$. The enthalpy and entropy changes determined from the Van't Hoff plot of the determined $K_{L,a}$ were found to be -3kJ mol^{-1} and 24 J mol^{-1} K^{-1}, respectively (**Figure 2A-16**).

Table 2A-13. Equilibrium constants ($K_{L,a}$) for association between hydronium ion and cyclohexanol, the extent of association $\theta_{L,a}$ for two aqueous solutions of cyclohexanol and rate constants ($k_{L,d}$) for H_3PO_4-catalyzed cyclohexanol dehydration at different temperatures. The corrected mole concentrations at high temperatures are compiled in **Table 2A-12**.

Temperature (°C)	$K_{L,a}$ [a] (dimensionless)	$\theta_{L,a}$		$k_{L,d}$ (s^{-1})
		0.32 M (r.t.)	0.90 M (r.t.)	
160	39.5	1.79×10^{-1}	3.81×10^{-1}	7.61×10^{-3}
170	38.9	1.75×10^{-1}	3.75×10^{-1}	2.02×10^{-2}
180	38.3	1.72×10^{-1}	3.70×10^{-1}	5.01×10^{-2}
190	37.8	1.68×10^{-1}	3.64×10^{-1}	1.25×10^{-1}
200	37.3	1.64×10^{-1}	3.57×10^{-1}	3.42×10^{-1}

[a] Calculated from the Van't Hoff equation.

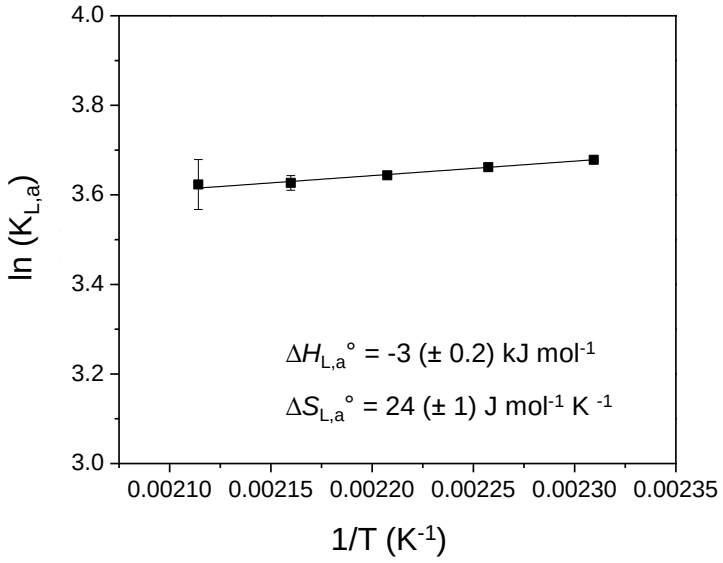

Figure 2A-16. Van't Hoff plot ($\ln(K_{L,a})$–(1/T)) to determine the changes in enthalpy ($\Delta H_{L,a}°$) and entropy ($\Delta S_{L,a}°$) for association equilibrium between hydronium ion and cyclohexanol. The detailed calculations of $K_{L,a}$ are shown in **Section A10**, and the values are compiled in **Table 2A-13**.

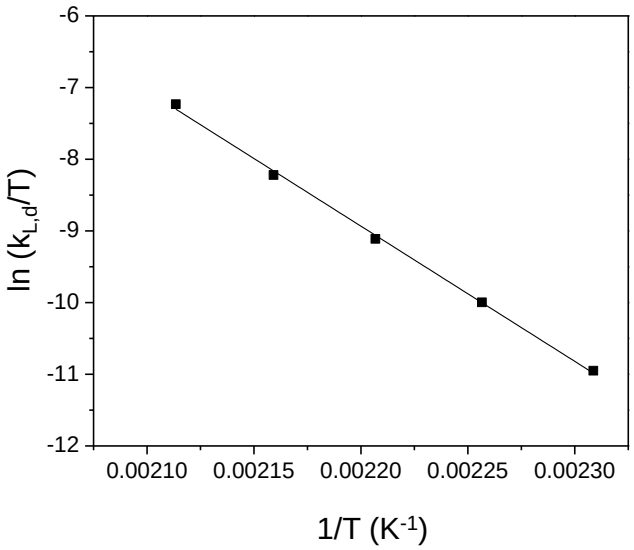

Figure 2A-17. Eyring plot ($\ln(k_{L,d}/T)$–$(1/T)$) to determine the enthalpy ($\Delta H^{\circ\ddagger}$) and entropy gained/lost ($\Delta S^{\circ\ddagger}$) required to reach the transition state complex. The detailed method is given in **Section A13.** The values of $k_{L,d}$ are compiled in **Table 2A-13**.

From equation (3) in the main text, the rate constants ($k_{L,d}$) were determined from TOF ratios (**Table 2-1** in the main text) and $\theta_{L,a}$ (**Table 2A-13**). Then, the intrinsic activation enthalpy and entropy (reported in **Table 2-4** in the main text) were determined from the Eyring plot of $\ln(k_{L,d}/T)$ as a function of 1/T (**Fig. 2A-17**).

$\theta_{z,a}$ is likely close to 1, as a result of the [ROH]/[H_2O] in the pore being 0.25 (5 and 20/u.c. for cyclohexanol and water, respectively, at reaction conditions); almost every hydronium ion in the pore is associated with cyclohexanol. In this case, $TOF_z \approx k_{z,d}$, and the ratio of $k_{z,d}/k_{L,d}$ was determined to be 2.7 ± 0.2, indicating that the intrinsic rate constants for cyclohexanol dehydration in HBEA are substantially higher than in aqueous solution.

A13. Calculation of activation enthalpies and entropies based on transition state theory formalism

Transition state theory (TST) assumes that a hypothetical transition state (activated complex) exists between reactants and products during a chemical reaction and that a quasi-equilibrium is established between the reactant and the TS. According to the Erying equation, if the rate constant has been experimentally determined, the theory can be used to calculate the Gibbs free energy, activation enthalpy and entropy. The results are compiled in Table 4 of the main text. The approach is briefly summarized below:

$$k_{rxn} = \frac{k_B T}{h} e^{\Delta S^{\ddagger}/R} e^{-\Delta H^{\ddagger}/RT} \tag{2A-26}$$

Rearrange the Eq. (2A-26) into the logarithmic form:

$$\ln\left(\frac{k_{rxn}}{T}\right) = \left(\ln\frac{k_B}{h} + \frac{\Delta S^{\ddagger}}{R}\right) - \frac{\Delta H^{\ddagger}}{R}\left(\frac{1}{T}\right) \tag{2A-27}$$

Thus, the enthalpy required ($\Delta H^{\ddagger}$) and entropy gained/lost ($\Delta S^{\ddagger}$) to reach the transition state complex can be determined using Eyring plots (ln(k/T)–(1/T)), see Eq. (2A-27).

A14. Error analysis for kinetic parameters

The standard error in $\Delta G^{\circ\ddagger}$ was estimated from the quantities obtained from the sum of squares of residuals that is determined by the regression analysis of the intrinsic rate constant. Specifically, for zeolite, $TOF_z = k_z$, according to the Eyring equation,

$$\Delta G^{\circ\ddagger} = RT\ln(k_B/h) - RT\ln(TOF_z/T)$$

Here, $RT\ln(k_B/h)$ is a constant, so for $\Delta G^{\circ\ddagger}$, the only error source is $\Delta\ln(TOF_z/T)$. Then, we have $\Delta\Delta G^{\circ\ddagger} = RT*\Delta\ln(TOF_Z/T)$. $\Delta H^{\circ\ddagger}$ and $\Delta S^{\circ\ddagger}$ as they are derived from the slope and intercept of the Eyring plot shown in Eq. (2A-27). For $\Delta H^{\circ\ddagger}$ and $\Delta S^{\circ\ddagger}$, the probability density of the normal distribution is given by the equation:

$$f(x) = \frac{1}{\sqrt{2\sigma^2\pi}} \exp[-\frac{(x-\mu)^2}{2\sigma^2}] \tag{2A-28}$$

μ is the mean or expectation of the distribution for values of $\Delta H^{\circ\ddagger}$ and $\Delta S^{\circ\ddagger}$, while σ is the standard deviation. Then we have the normal distribution for $\Delta H^{\circ\ddagger}$ and $\Delta S^{\circ\ddagger}$.

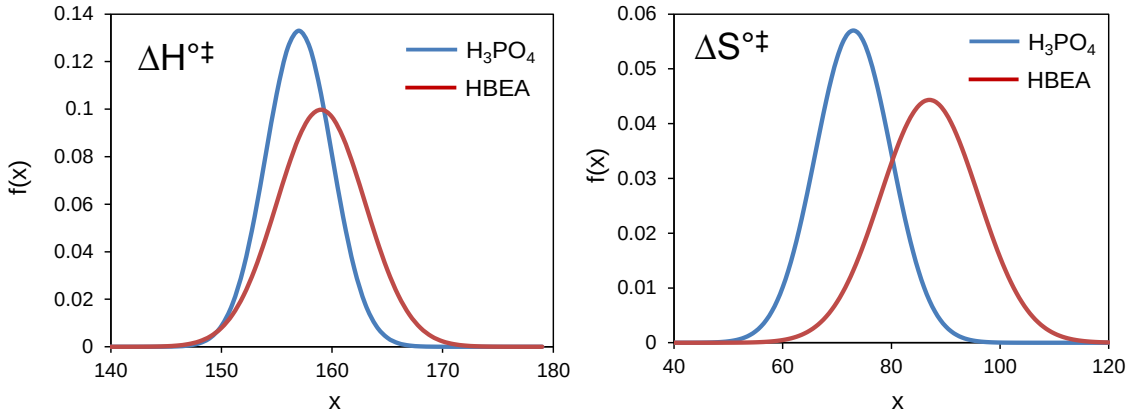

According to the probability density function, we can compare the $\Delta H^{\circ\ddagger}$ and $\Delta S^{\circ\ddagger}$ in H_3PO_4- and HBEA-catalyzed cyclohexanol dehydration, as shown below:

Probability	$\Delta H^{\circ\ddagger}$	$\Delta S^{\circ\ddagger}$
HBEA>H_3PO_4	0.69	0.90
HBEA=H_3PO_4	0.07	0.02
HBEA<H_3PO_4	0.24	0.08

It can be seen that in terms of $\Delta H^{\circ\ddagger}$, 157 (± 3) kJ mol^{-1} for H_3PO_4-catalyzed dehydration is nearly the same as 159 (± 4) kJ mol^{-1} for HBEA-catalyzed dehydration, while for $\Delta S^{\circ\ddagger}$, the difference is statistically significant, *i.e.*, the $\Delta S^{\circ\ddagger}$ in HBEA-catalyzed reaction is larger than that in H_3PO_4-catalyzed reaction with a 90% probability.

A14. References for Appendix

1. Rudolph, W. W. *J Solution Chem* **2012**, 41, 630.
2. Vjunov, A.; Fulton, J. L.; Huthwelker, T.; Pin, S.; Mei, D.; Schenter, G. K.; Govind, N.; Camaioni, D. M.; Hu, J. Z.; Lercher, J. A. *J. Am. Chem. Soc.* **2015**, *137*, 2409.
3. Vjunov, A.; Hu, M. Y.; Feng, J.; Camaioni, D. M.; Mei, D.; Hu, J. Z.; Zhao, C.; Lercher, J. A. *Angew. Chem. Int. Ed.* **2013**, *53*, 479
4. Http://webbook.nist.gov/cgi/cbook.cgi?ID=C108930&Mask=10#Solubility

2.7 References

[1] Zhao, C.; Lercher, J. A. *Angew. Chem. Int. Ed*. **2012**, 51, 5935.

[2] Marlière, P. Method for producing an alkene comprising step of converting an alcohol by an enzymatic dehydration step. EP2336341, June 30, 2011.

[3] Zhao, C.; Lercher, J. A. *ChemCatChem* **2011**, *4*, 64.

[4] Vjunov, A.; Fulton, J. L.; Huthwelker, T.; Pin, S.; Mei, D.; Schenter, G. K.; Govind, N.; Camaioni, D. M.; Hu, J. Z.; Lercher, J. A. *J. Am. Chem. Soc.* **2014**, *136*, 8296.

[5] Corma, A.; Moliner, M.; Cantín, Á.; Díaz-Cabañas, M. J.; Jordá, J. L.; Zhang, D.; Sun, J.; Jansson, K.; Hovmöller, S.; Zou, X. *Chem. Mater.* **2008**, *20*, 3218.

[6] Vjunov, A.; Fulton, J. L.; Camaioni, D. M.; Hu, J. Z.; Burton, S. D.; Arslan, I.; Lercher, J. A. *Chem. Mater.* **2015**, *27*, 3533.

[7] Pazé, C.; Bordiga, S.; Lamberti, C.; Salvalaggio, M.; Zecchina, A.; Bellussi, G. *J. Phys. Chem. B* **1997**, *101*, 4740.

[8] Bordiga, S.; Lamberti, C.; Bonino, F.; Travert, A.; Thibault-Starzyk, F. *Chem. Soc. Rev.* **2015**, *44*, 7262.

[9] Vjunov, A.; Hu, M. Y.; Feng, J.; Camaioni, D. M.; Mei, D.; Hu, J. Z.; Zhao, C.; Lercher, J. A. *Angew. Chem. Int. Ed.* **2014**, *53*, 479. **53**, 479-482, (2013).

[10] Bandow, S.; Maruyama, Y.; Bi, X. X.; Ochoa, R.; Holden, J. M.; Lee, W. T.; Eklund, P. C. *Mater. Sci. Eng.* **1995**, *204*, 222.

[11] VandeVondele, J.; Hutter, J. *J. Chem. Phys.* **2007**, *127*, 114105.

[12] Goedecker, S.; Teter, M.; Hutter, J. *Phys. Rev. B* **1996**, *54*, 1703.

[13] Hartwigsen, C.; Goedecker, S.; Hutter, J. *Phys. Rev. B* **1998**, *58*, 3641.

[14] Krack, M. *Theor Chem Acc* **2005**, *114*, 145.

[15] Van Houteghem, M.; Verstraelen, T.; Ghysels, A.; Vanduyfhuys, L.; Waroquier, M.; Van Speybroeck, V. *J. Chem. Phys.* **2012**, *137*, 104506.

[16] Perdew, J. P.; Burke, K.; Ernzerhof, M. *Phys. Rev. Lett.* **1996**, *77*, 3865.

[17] Grimme, S.; Antony, J.; Ehrlich, S.; Krieg, H. *J. Chem. Phys.* **2010**, *132*, 154104.

[18] Newsam, J. M.; Treacy, M. M. J.; Koetsier, W. T.; Gruyter, C. B. D. *Proc. R. Soc. A* **1988**, *420*, 375.

[19] Psofogiannakis, G.; St-Amant, A.; Ternan, M. *J. Phys. Chem. B* **2006**, *110*, 24593.

[20] De Moor, B. A.; Ghysels, A.; Reyniers, M.-F. o.; Van Speybroeck, V.; Waroquier, M.; Marin, G. B. *J. Chem. Theory Comput.* **2011**, *7*, 1090.

[21] Chiang, H.; Bhan, A. *J. Catal.* **2010**, *271*, 251.

[22] Vjunov, A.; Fulton, J. L.; Huthwelker, T.; Pin, S.; Mei, D.; Schenter, G. K.; Govind, N.; Camaioni, D. M.; Hu, J. Z.; Lercher, J. A. *J. Am. Chem. Soc.* **2015**, *137*, 2409.

[23] Do, D. D. Pure Component Adsorption in Microporous Solids. In Adsorption Analysis: Equilibria and Kinetics; Imperial College Press: London, 1998; Vol. 2, pp 149-190.

[24] Bunton, C. A.; Konasiewicz, A.; Llewellyn, D. R. *J. Chem. Soc (Resumed)* **1955**, 604.

[25] Bunton, C. A.; Llewellyn, D. R. *J. Chem. Soc. (Resumed)* **1957**, 3402.

[26] Merritt, M. V.; Bell, S. J.; Cheon, H. J.; Darlington, J. A.; Dugger, T. L.; Elliott, N. B.; Fairbrother, G. L.; Melendez, C. S.; Smith, E. V.; Schwartz, P. L. *J. Am. Chem. Soc.* **1990**, *112*, 3560.

[27] Merritt, M. V.; Anderson, D. B.; Basu, K. A.; Chang, I. W.; Cheon, H.-J.; Mukundan, N. E.; Flannery, C. A.; Kim, A. Y.; Vaishampayan, A.; Yens, D. A. *J. Am. Chem. Soc.* **1994**, *116*, 5551.

[28] Eigen, M. *Angew. Chem. Int. Ed.* **1964**, *3*, 1.

[29] Markovitch, O.; Agmon, N. *J. Phys. Chem. A* **2007**, *111*, 2253.

[30] Wells, C. F. *Trans. Faraday Soc.* **1965**, *61*, 2194.

[31] Michelsen, R. R. *et al*. In *Protonation of Alcohols in Sulfuric Acid Solutions at UT/LS Conditions*. Eos Trans. AGU, 88(52), Fall Meeting Suppl., Abstract A21E-0798, 2007.

[32] van der Bij, H. E.; Weckhuysen, B. M. *Chem. Soc. Rev.* **2015**, *44*, 7406.

[33] Uzunova, E. L.; Mikosch, H. *Micropor. Mesopor. Mater.* **2016**, *232*, 119.

[34] Roberts, J. D. & Caserio, M. C. Basic Principles of Organic Chemistry, second edition; W. A.

[35] Bruice, T. C.; Lightstone, F. C. *Acc. Chem. Res.* **1999**, *32*, 127.

[36] Fischer, M.; Haase, I.; Kis, K.; Meining, W.; Ladenstein, R.; Cushman, M.; Schramek, N.; Huber, R.; Bacher, A. *J. Mol. Biol.* **2003**, *326*, 783.

Chapter 3

The impact of water on the liquid-phase dehydration of cyclohexanol

The acid-catalyzed dehydration of cyclohexanol is investigated using two HBEA zeolites (Si/Al = 71 and 75) with different Al T-site distributions. The distribution of BAS among different crystallographic positions of the BEA framework is inconsequential to cyclohexanol dehydration in liquid phase, both in water and in neat cyclohexanol. The density functional theory (DFT) calculations show that cyclohexanol molecules are primarily hydrogen-bonded to the hydronium-ions in zeolites at reaction temperatures of 160−200 °C in aqueous phase. Proton transfer from the hydronium ion cluster to cyclohexanol is thermodynamically unfavorable for HBEA in aqueous medium, rendering protonated alcohol as the minority species. The reaction proceeds with enthalpic barriers of ~160 kJ mol^{-1} and entropy gains of 85 J mol^{-1} K^{-1} for aqueous-phase HBEA catalyzed dehydration of cyclohexanol. The number of intraporous water molecules in aqueous phase or solvent-free conditions significantly changes the solvation environments of the BAS and alters its acid strength. In consequence, proton transfer from the $H_3O^+(H_2O)_n$ cluster to cyclohexanol becomes favorable as fewer water molecules are associated with the proton. This change in the nature of the active site results in a significantly lower activation barrier (by ~40 kJ mol^{-1}) and less entropy gain (by ~60 J mol^{-1} K^{-1}) for dehydration of neat-alcohol than in aqueous medium. DFT calculations show that, in neat alcohol, cyclohexanol dehydration occurs mainly via dimer-mediated routes.

---

1. DFT calculations in this chapter were provided by Dr. Donghai Mei at PNNL (USA); ^{27}Al MAS NMR was provided by Dr. Alekesei Vjunov and Dr. Jianzhi Hu at PNNL (USA).

3.1 Introduction

The conversion of renewable biomass resources to fuels and fine chemicals not only mitigates greenhouse-gas emissions, but also reduces the dependence of the chemical industry on traditional fossil resources.[1,2] The abundance of lignocellulosic biomass, in particular lignins which contain less oxygen than cellulose, makes it a promising feedstock for producing gasoline- or diesel-range fuel components.[3-5] Among the various catalytic routes to upgrade lignin, liquid phase hydrodeoxygenation (HDO) of lignin-derived molecules can be performed efficiently over a vast variety of heterogeneous catalysts at moderate temperatures (100−250 °C). Heterogeneously catalyzed HDO catalysis proceeds, primarily, either via direct hydrogenolytic C−O bond cleavage over metal (or functional analogs such as metal carbides and sulfides) surfaces,[6-9] or via sequential hydrogenation-dehydration reactions catalyzed by admixtures or nano-domains composed of metal and acid functions often referred to as bifunctional catalysts.[8-14] Different extents of hydrogen addition, C−C bond formation (via alkylation or aldol-type reactions) and ring/chain isomerization can be coupled with these O-removal steps to produce aromatics[15] or saturated hydrocarbons with different carbon numbers,[13,16] offering substantial process flexibility in these lignin-to-fuels upgrading approaches.

The building units of lignin are primarily phenolics. Because phenol is the simplest phenolic monomer, its catalytic HDO reaction has been subject to a great number of investigations.[10,13,14,16−20] In a typical phenol HDO sequence over a bifunctional catalyst, the dehydration reaction, which occurs on the acid function, is the only step that ejects O-atoms. Depending on the catalyst formulation, the acid-catalyzed dehydration step can be rate-limiting in the overall reaction cascade, *e.g.*, with a highly active hydrogenation component (Pd) and a mineral acid (H_3PO_4). [14]

While homogeneous acids can catalyze alcohol dehydration, the use of solid acids is advantageous, as it circumvents the problems of corrosiveness and neutralization of highly acidic waste streams. In addition, solid acid catalysts can be easily separated, regenerated and recycled. Gas-phase dehydration of mono-alcohols, from primary to tertiary, acyclic and cyclic, has been extensively studied on solid acids, such as γ-

Al_2O_3,[21-26] poloyoxometallates,[27-31] supported metal oxides[32,33] and zeolites.[29-31,34-36] In contrast, far less is known about the kinetics and mechanism of dehydration catalyzed by solid acids in liquid media. In particular, the conversion of biomass-derived feedstocks to liquid fuels is most beneficial in aqueous medium, because of the ubiquitous presence of water in the biomass-derived bio-oils.

Among porous solid acids, aluminosilicate zeolites are a class of relatively well-defined materials that contain Brønsted acid sites (BAS) in confined spaces of molecular dimensions that solvate all states along the reaction coordinate.[37-42] Previously, we used in situ magic angle spinning (MAS) ^{13}C nuclear magnetic resonance (NMR) spectroscopy to investigate the reaction mechanism of cyclohexanol dehydration on a high-silica HBEA (Si/Al = 75) in aqueous phase.[43] Remarkably, the presence of a surface-bound alkoxide was not supported by NMR, contrary to spectroscopic measurements and theoretical predictions that identify the surface alkoxide as the stable species in gas phase reactions mediated by carbenium-ion-like transition states.[44-47] In-depth ex situ characterizations of this zeolite (HBEA150, 150 being the SiO_2/Al_2O_3 ratio) by extended X-ray absorption fine structure (EXAFS) and ^{27}Al MAS NMR spectroscopies, before and after treatment in hot liquid water, reveal that this material contains limited amounts (6−9%) of extra-framework Al species,[48] and that the local structure in the vicinity of the BAS site remains unaltered even as the framework begins to undergo degradation in hot liquid water (*e.g.*, 48 h at 160 °C).[49]

On zeolites, the charge-balancing proton (BAS) in the presence of adsorbed water exists as a hydronium ion (*e.g.*, $(H_2O)_n \cdot H_3O^+$) that resides locally near to the zeolite T-site.[48,50] To determine the effect of the microenvironments on catalysis, we recently investigated the aqueous-phase cyclohexanol dehydration using H_3PO_4 and zeolite HBEA,[51] and reported how confines of, *e.g.*, zeolitic nano-pores, enhance the catalytic rates of hydronium ions for alcohol dehydration by more than an order of magnitude relative to hydronium ions in an unconstrained aqueous solution. We showed that the hydronium ion within steric structures bears a strong resemblance to enzyme catalysis. The rate enhancement is driven by an increased association between the hydronium ion and alcohol, as well as a greater entropy of activation. These details of hydronium-ion-catalyzed dehydration of cyclohexanol in aqueous phase have been explored; however,

the nature of the active sites in different solvation environments in liquid phase, *e.g.*, in the presence and absence of water, is still not clearly studied.

In the present work, we report the detailed kinetic evaluation of cyclohexanol dehydration in aqueous phase and in its neat liquid form (solvent-free), using high-silica HBEA catalysts with well-defined Al T-site distributions, minimum extra-framework Al moieties, as well as good hydrothermal stability at the chosen reaction temperatures for dehydration catalysis (160−200 °C). We interpret these kinetic data based on a proposed sequence of steps and use transition state theory (TST) formalisms to evaluate the enthalpy–entropy trade-offs in liquid-phase dehydration catalysis over HBEA. Density functional theory (DFT) calculations have been employed to provide insights into the most probable reactive intermediates for kinetically relevant elementary steps of cyclohexanol dehydration occurring in HBEA pores, specifically adsorption and protonation equilibria. The combination of experimental and theoretical results leads to a complete energetics landscape in zeolite HBEA in liquid phase.

3.2 Experimental section

3.2.1 Chemicals

Cyclohexanol (Sigma–Aldrich, 99%), cyclohexene (Sigma–Aldrich, 99%, GC grade), 1,3–dimethoxybenzene (Sigma–Aldrich, 99%), dichloromethane (Sigma–Aldrich, HPLC grade), 2-cyclohexen-1-one (Sigma-Aldrich, ≥ 95%), ethyl acetate (Sigma-Aldrich, > 99.9% HPLC assay), hydrogen (Westfalen AG, 99.999 vol%), sodium sulfate (Acros Organics, 99%, anhydrous) are used as-received without further purification.

3.2.2 Zeolite catalysts

Two different batches of HBEA150, Si/Al = 71(a) and 75(b), respectively, were obtained from Clariant in H-form. HBEA150-a (an older batch) was calcined at 500 °C in a 100 cm^3 min^{-1} flow of dry air for 6 h prior to the reaction. Preliminary tests show that such thermal treatment is unnecessary for HBEA150-b (a newer batch and better sealed), which was hence used as received.

3.2.3 Catalyst characterization

XRD patterns were collected using a Philips X'Pert Pro System, with Cu-Kα radiation source operating at 45 kV and 40 mA. The sample was measured with a scanning rate of 0.02º s^{-1} in the 5–70º 2θ-range. Atomic absorption spectroscopy (AAS), measured on a UNICAM 939 AA–Spectrometer, was used to determine the Si and Al contents in two HBEA-150 zeolites. The scanning electron microscopy (SEM) images were recorded on a JEOL 500 scanning electron microscope (accelerating voltage 25 kV). The samples were prepared by depositing a drop of an ultrasonicated methanol suspension of the solid material onto a carbon-coated Cu grid. The dry samples were gold–coated prior to imaging.

The infrared (IR) spectra of adsorbed pyridine were recorded with a Perkin–Elmer 2000 spectrometer at a resolution of 4 cm^{-1}. The catalyst samples were prepared as self–supporting wafers and activated in vacuum (p = 10^{-6} mbar) at 450 °C for 1 h at a heating rate of 10 °C min^{-1}. After cooling to 150 °C, the sample was equilibrated with 0.1 mbar pyridine for 0.5 h followed by outgassing for 1 h and the acquisition of the spectrum. Finally, desorption program (up to 450 °C with 10 °C min^{-1} and 0.5 h at 450 °C) was initiated and the spectra were recorded until equilibrium was achieved. The concentrations of BAS and Lewis acid sites (LAS) are quantified using the integrated areas of peaks at 1540 cm^{-1} and 1450 cm^{-1}, respectively. The number of pyridine molecules retained after evacuation at 150 and 450 °C were used to determine the concentrations of total and strong acid sites, respectively.

3.2.4 Al distribution analysis

The Al distribution in HBEA150-a and HBEA150-b was determined using the procedure reported in literature.[48,49] The ultra–high field ^{27}Al MAS NMR experiments were performed on a Varian–Agilent Inova 63–mm wide–bore 850 MHz NMR spectrometer. The main magnetic field was 19.97 T and the corresponding ^{27}Al Larmor–frequency was 221.4 MHz. Experiments were performed using a commercial 3.2 mm pencil type MAS probe. In a typical experiment about 15 mg of sample powder were loaded in the rotor and measured at ambient temperature. The HBEA samples were stored for 48 h in a desiccator over a saturated $Ca(NO_3)_2$ aqueous solution leading to a hydrated

state that is expected to contain Al tetrahedral that have minimal distortions and that have the maximum ^{27}Al MAS NMR spectral resolution.[79] A single pulse sequence with a pulse length of 2.0 ms, corresponding to a pulse angle of 45°, was selected for acquiring each ^{27}Al MAS NMR spectrum with a recycle time of 1 s and total accumulation of 5000 scans. The spectra were acquired at a sample spinning rate of 20 kHz ± 2 Hz and were referenced to 1.5 M $Al(NO_3)_3$ in H_2O (0 ppm) using the center of the octahedral peak of solid γ–Al_2O_3 (at 13.8 ppm) as a secondary reference. For quantitative measurements, the weights of samples loaded into the MAS rotor were recorded and four spectra were acquired to check the stability of the spectrometer. The matching and tuning conditions of the RF circuit of the NMR probe were set using a network analyzer. All other experimental conditions were kept identical for all analyzed samples. In this way, the absolute peak areas normalized to the spectrometer standard were proportional to the Al in the sample. The spectra were analyzed using the MestreNova 8.1 software package.

3.2.5 Kinetic measurements

Kinetic measurements were performed at 160 – 200 °C using a 300 mL Hastelloy PARR reactor. An example of a typical reaction in aqueous phase: 3.3-10.0 g cyclohexanol, 140-170 mg HBEA zeolites, 80-100 mL H_2O, are sealed in the reactor. In solvent-free cases, 200 mg HBEA and 100 g cyclohexanol are sealed in the reactor (The detailed reaction conditions were compiled in **Table 3A-1, Appendix**). In all cases, the reactor is then pressurized with 50 bar H_2 at room temperature and heated up while stirred vigorously (~ 700 rpm). Rates do not vary with the stirring speed that is greater than 400 rpm (See details in **Chapter 2**). The reaction time is reported counting from the point when the set temperature is reached (12–15 min). Upon completion the reactor is cooled using an ice/water mixture and the organic compounds are extracted using ethyl acetate or dichloromethane. The organic phase after being dried over sodium sulfate is analyzed on an Agilent 7890A GC equipped with a HP–5MS 25 m × 0.25 μm (i.d.) column, coupled with Agilent 5975C MS. 1,3-dimethoxybenzene or 2-cyclohexen-1-one were used as the internal standard for quantification. The carbon balance in all cases was maintained typically at 90 ± 5%.

3.2.6 Gas-phase IR of adsorbed cyclohexanol and gravimetric measurements

IR spectra of adsorbed cyclohexanol were recorded on a Bruker VERTEX 70 spectrometer at a resolution of 4 cm^{-1} with 150 scans. The zeolite wafers were activated at 450 °C for 1 h under vacuum ($p < 10^{-6}$ bar), and then cooled down to 40 °C. The cylohexanol was stepwise introduced into the vacuum system with increasing the partial pressure of cyclohexanol from 0.0005 to 0.0015 mbar. The spectra were recorded until equilibrium was achieved. Finally, the system was evacuated at 40 °C for 10 h to remove the physically adsorbed cyclohexanol.

Gravimetric (TGA) experiments were carried out using a microbalance mounted within a high vacuum chamber at 40 °C. The HBEA150 was pressed into wafers and subsequently crushed in small particles and then charged into a crucible. The sample mass could be continuously monitored using a Setaram 111 microbalance. Before measurement, the sample was activated at 450 °C for 1 h with a heating ramp of 10 °C min^{-1} under vacuum ($p < 10^{-6}$ bar). Cyclohexanol was adsorbed by exposing HBEA150 to 0.003 mbar of vapor until reaching the equilibrium. Following exposure, HBEA150 was then evacuated under pressure of 10^{-6} mbar at 40°C until no further decline of uptake could be measured by the microbalance.

3.2.7 DFT calculations

All DFT calculations employed a mixed Gaussian and plane wave basis sets and were performed using the CP2K code. The detailed protocol was described in **Chapter 2**.

3.3 Results

3.3.1 Characterization of HBEA150 zeolites

Two batches of HBEA150 zeolite with nearly identical chemical composition used in this work were obtained from Clariant (HBEA150-a, HBEA150-b). Extensive characterizations of HBEA150-b has been reported previously.[48,49] The physicochemical properties of the two HBEA are compiled in **Table 3-1**. Si/Al ratios of 71 and 75 correspond to, on average, *ca.* 0.8 Al-atom per unit cell, suggesting a low statistical

probability of Al pairs (*i.e.*, Al atoms having Al atoms in next-nearest-neighbor T sites).[52] This was confirmed by single pulse ^{29}Si NMR showing little intensity at -98 ppm indicating negligible fractions of Si in Q^2 sites as well as in paired Al sites (Al–O–Si–O–Al).[53] As shown later by ^{27}Al NMR, the two HBEA150 exhibit somewhat different Al T-site distributions.

Table 3-1. The physicochemical properties of the studied HBEA zeolite samples.[a]

	HBEA150-a	HBEA150-b
Si/Al ratio (mol mol^{-1})	71	75
Average particle size (nm)	~200-500	~200-300
Mespore surface area (m^2 g^{-1})	122	91
Micropore surface area (m^2 g^{-1})	502	506
Mespore volume (cm^3 g^{-1})	0.17	0.29
Micropore volume (cm^3 g^{-1})	0.20	0.18
BAS concentration (μmol g^{-1})	192	167
BAS (S) concentration (μmol g^{-1}) [b]	181	146
LAS concentration (μmol g^{-1})	41	36
LAS (S) concentration (μmol g^{-1}) [b]	24	33

[a] Si/Al ratios are determined by element analysis (by AAS); The Particle size are determined by SEM; Surface area and pore volume are determined by N_2 adsorption and desorption. [b] BAS (S) and LAS (S) denote the strong acid sites defined as those that retain pyridine after outgassing at 450 ℃ for 1 h following saturation of all sites by pyridine.

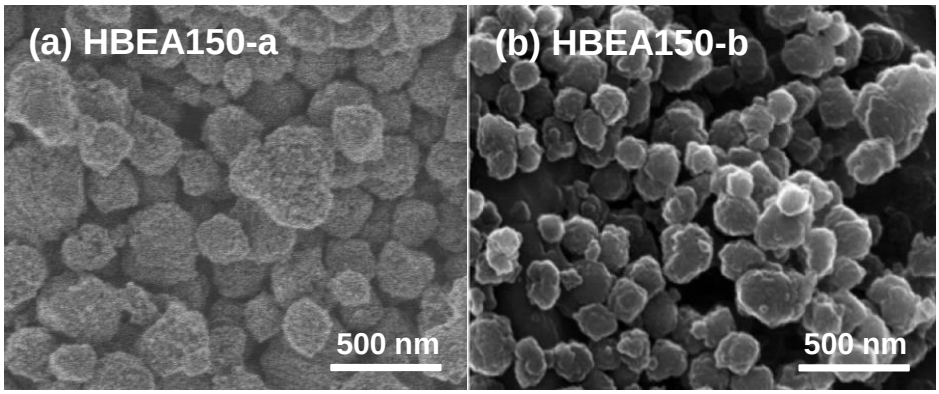

Figure 3-1. The SEM characterization for the studied zeolite HBEA150-a (a) and HBEA150-b (b).

The SEM images of two HBEA150 are shown in **Figure 3-1**. Two zeolites exhibit almost identical particle morphology, feature more or less cubic particles with rounded

corners. HBEA150-a shows a relatively larger particle size with range of ~200-500 nm, compared with HBEA150-b, ~200-300 nm. Analysis of the powder X-ray diffraction (XRD) patterns (**Figure 3A-1**, **Appendix**) revealed that HBEA150 is highly crystalline without amorphous domains of detectable dimensions, and that they are composed of polymorphs A and B in a 1:1 ratio.[48]

In the absorbance FTIR spectrum (OH stretching vibration region) of HBEA150-a acquired after activation (**Figure 3-2**), two distinct bands for the hydroxyl groups were detected: the band at ~3740 cm^{-1} is attributed to terminal and internal Si–OH groups (non-acidic), while the band at ~3605 cm^{-1} is attributed to the Brønsted-acidic bridging hydroxyl groups connected to strictly tetrahedral framework Al. They are superimposed on a broad absorption due to H-bonded hydroxyl groups. Hydroxyls associated with extraframework Al (EFAL), which would appear at ~3665 and ~3780 cm^{-1},[54-56] were not observed, in line with their low LAS concentrations determined by IR of adsorbed pyridine (**Table 3-1**). HBEA150-a showed a broader band at ~3740 cm^{-1} with a slightly shift to the low-wavenumber direction, which was attributed to the relatively higher concentration of hydroxyls situated inside the zeolite channels (~3680-3730 cm^{-1}).[57,58]

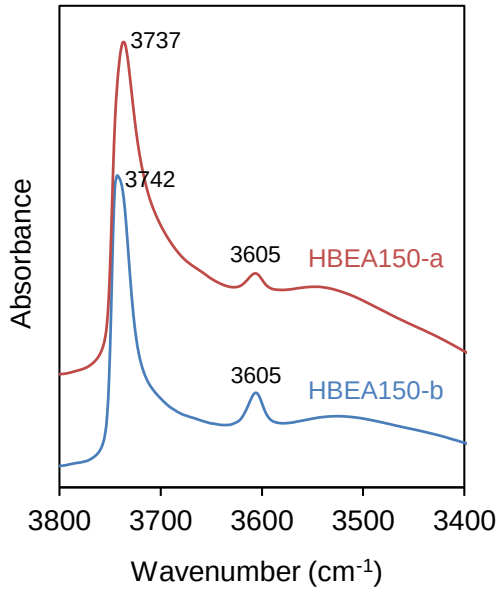

Figure 3-2. The OH-stretching vibration region of the infrared (IR) spectrum (acquired after sample activation in vacuum for 1 h at 450 °C) of HBEA150-a and HBEA150-b.

Importantly, both HBEA150 samples retain structural integrity under catalytically relevant conditions. For instance, no appreciable changes in XRD patterns were observed after hydrothermal treatment for 0.5-4 h at 160 °C and 0.5-2 h at 180 °C.[51] While zeolite framework long-range order decreases over time in hot liquid water, [59] Vjunov *et al.*[49] previously demonstrated that, even at 300 °C in liquid water, little modification of the Al coordination occurs prior to complete framework decomposition. Interestingly, we find that the presence of cyclohexanol molecules in aqueous phase even slows down the degradation (**Figure 3A-2**, see extended discussion in Appendix). We surmise that the abovementioned phenomenon is due to the displacement of water from the zeolite pores by the alcohol, which adsorbs more strongly, thus lowering the rate of Si-O-Si hydrolysis. The hydrothermal stability of two HBEA150 is of importance to the present work, because it guarantees that the kinetic data obtained on similar time scales at 160−200 °C is not impacted by transport phenomena (*e.g.*, pore restrictions) and/or altered void dimensions (leading to different solvation strengths) induced by modifications in long-range order of the zeolite. In addition, the good hydrothermal stability of the selected zeolite was also revealed by the constant retention of active sites (BAS) after the water treatment at rigorous conditions, see details in next paragraph.

The acid properties of the two HBEA150 were characterized by IR spectra after pyridine adsorption (quantitative results shown in **Table 3-1**). The concentrations of BAS and Lewis acid sites (LAS) are quantified using the integrated areas of peaks at ~1540 cm^{-1} and ~1450 cm^{-1}, respectively (**Figure 3-3**). The number of pyridine molecules retained after evacuation at 150 and 450 °C were used to determine the concentrations of total and strong acid sites, respectively. Both HBEA150 materials contain predominantly strong BAS, a common observation for zeolites with low Al concentrations.[60] Heterogeneously catalyzed aqueous-phase biomass conversion requires robust acidic catalysts that are active and stable in hot liquid water. Total and strong BAS concentrations, as measured by pyridine adsorption, decrease by ~ 4 % after hot liquid water treatment at 200 °C for 40 min (**Figure 3-4**), which is in agreement with the Al-EXAFS and ^{27}Al MAS NMR characterizations reported previously.[49] In present study, XRD and IR adsorbed pyridine collectively demonstrate that HBEA150 zeolite suffered

minor degradation during the dehydration reaction under the applied conditions in aqueous phase.

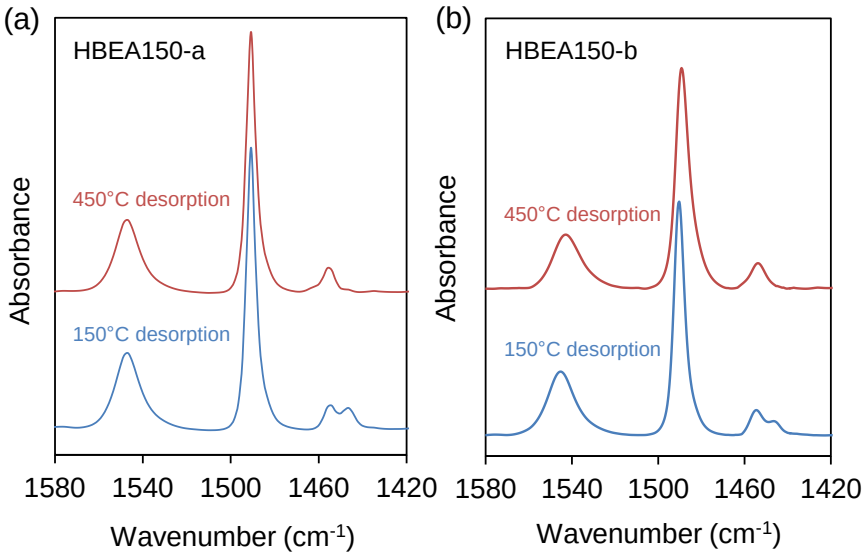

Figure 3-3. IR spectra of adsorbed pyridine on two HBEA150 zeolites. The amount of pyridine molecules retained after evacuation at 150 and 450 °C were used to determine the concentrations of total and strong acid sites, respectively.

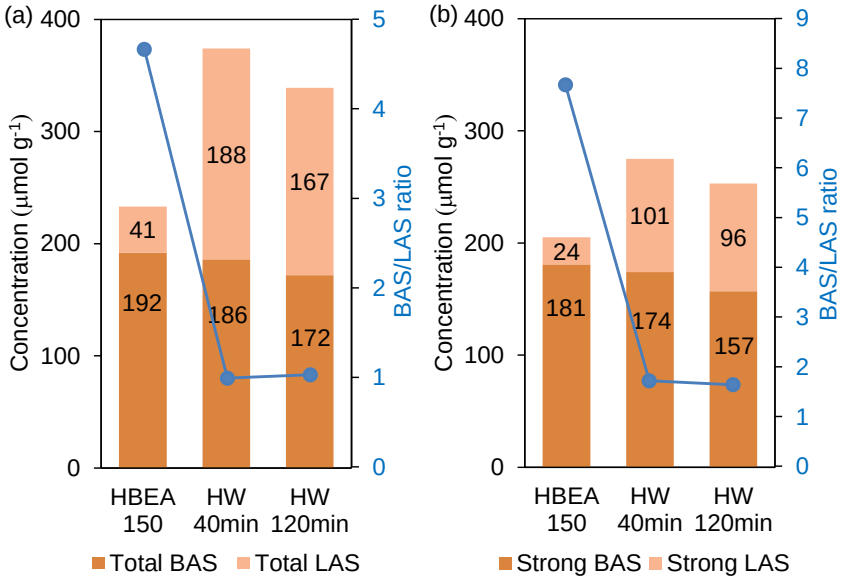

Figure 3-4. The acidity change of HBEA150-a treated in the hot liquid water (HW) at different time. The concentration of the total acid sites (a) and strong acid sites (b) are differentiated by the desorption of pyridine at 150 and 450 °C, respectively.

3.3.2 Al T-site distributions in HBEA150 samples

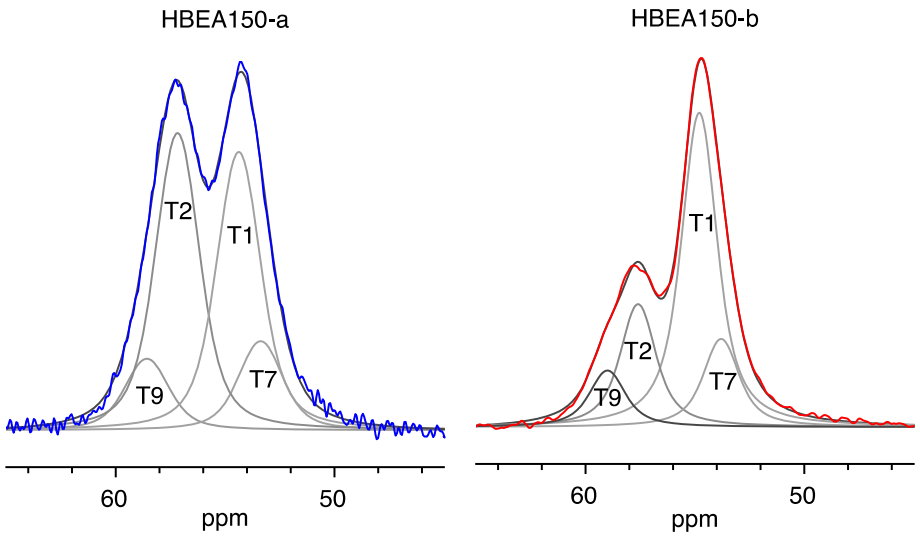

Figure 3-5. ^{27}Al MAS NMR spectra showing the tetrahedral Al species of the HBEA150-a (left) and HBEA150-b (right) zeolites used in this work. The fitted NMR peaks as well as the T-Site assigned are also shown.

Tetrahedral regions of the ^{27}Al MAS NMR spectra of the studied HBEA as well as the fitted peaks, discussed in the next paragraph, are shown in **Figure 3-5**. The measured chemical shifts are in agreement with values previously reported for other HBEA materials.[61] Both samples exhibit low concentrations of octahedral Al (**Figure 3A-3, Appendix**) typically observed in the ~ 0 ppm region.[62] While the tetrahedral Al results in NMR peaks at chemical shifts of ~ 50 – 62 ppm, the two zeolites appear to have different Al T-site distributions based on peak positions and their relative intensity. In the case of HBEA150-a, there are two peaks of almost equal intensities at 54.3 and 57.3 ppm, respectively. In contrast, the HBEA150-b sample exhibits two peaks at 54.7 and 57.8 ppm with relative intensities of the two peaks equal to 7:3, respectively. Penta-coordinated or extra-framework tetrahedral (distorted) Al moieties that appear in the 30–40 ppm[63,64] and 40–45 ppm[65] regions, respectively, were not observed, in agreement with the absence of extra-framework Al-OH bands in the IR spectra (**Figure 3-1**). Extra-framework Al species would form additional sites for adsorption and catalysis, occlude

pores, and impact the neighboring framework sites to extents that are hard to quantify.[66] Thus, the minimal amounts of extra-framework Al species in the two HBEA150 zeolites, evidenced by IR and ^{27}Al MAS NMR spectroscopies, remove the complications and uncertainties potentially caused by either space-occluding or acidity-enhancing effects on catalysis. This also simplifies calculation studies of the catalytic system allowing the use of theoretical models with standard BEA framework cell parameters to determine the strengths of and solvation environments around the framework BAS.

The distribution of Al in HBEA is determined using the DFT-calculated NMR chemical shifts for the nine different T–sites of the BEA framework. The chemical shifts were calculated using the Al–$(OSi)_4(OH)_{12}^-$ cluster derived from the DFT optimized unit cell of BEA that was reported previously.[48a] The NMR fits to the measured spectra are shown in **Figure 3-5**. For HBEA150-a, the NMR fitting using the DFT calculated chemical shifts suggests that the majority of Al occupies T1 and T2 sites with ~ 40% total Al in each site, which are part of 4- and 5-member rings in the zeolite framework. The Al concentration in the T7 and T9 is determined at 12 and 10%, respectively. In the case of HBEA150-b, Al preferentially (54%) populates T1 sites. Like in HBEA150-a, the T2, T7 and T9 sites are also populated with Al, which is distributed as 21, 15 and 10 % of the total Al in the sample, respectively. We note that for both zeolites there is no indication of substantial tetrahedral Al concentration in the T3, T4, T5, T6 and T8 sites of HBEA150.

3.3.3 The impact of catalyst amount on cyclohexanol dehydration

For kinetic measurements, the obtained turnover frequencies (TOFs) or the specific reaction rates should remain changeless along with the variation of catalyst amount, especially considering the degradation of zeolites in hot liquid water. To gain insights into the probable effects of it, the dehydration experiments with varying catalysts amount were performed in both aqueous phase and neat cyclohexanol. The results are shown in **Figure 3-6**. In aqueous phase, the mass-specific dehydration rates deviated from the average value when using fewer amounts of zeolite, *e.g.*, 0.04 g HBEA150. On the contrary, the dehydration rates were unchanged in solvent-free conditions (neat alcohol in the absence of water). The decrease in dehydration rates over too little HBEA150 in

aqueous phase is probably caused by the degradation of zeolites,[49,59,67,68] while using a considerable amount of catalyst (*e.g.*, ≥ 0.14 g) would diminish the effect of zeolite collapse in hot liquid water. The detailed reaction conditions are compiled in **Table 3A-1**.

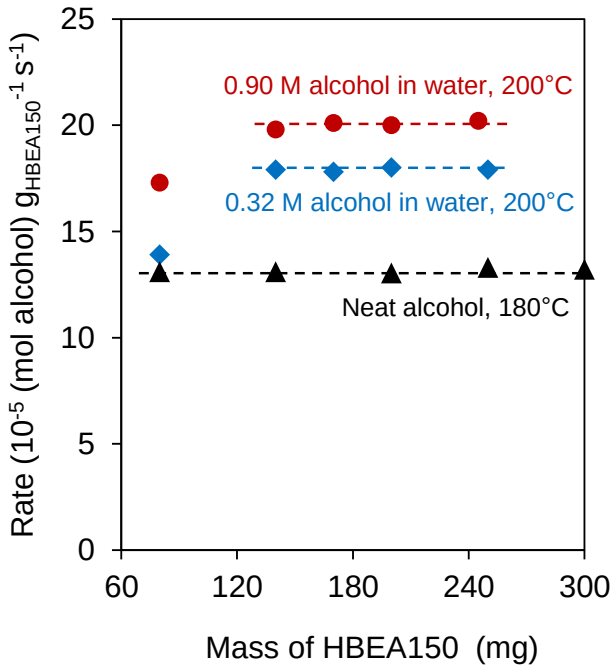

Figure 3-6. The dependence of the mass-specific reaction rates on the catalyst amount for cyclohexanol dehydration over HBEA-150-a (0.04-0.3 g) in aqueous phase and neat alcohol.

3.3.4 HBEA-catalyzed dehydration of aqueous cyclohexanol

The measured reaction rates and turnover frequencies (TOFs) for the HBEA–catalyzed cyclohexanol dehydration are reported in **Figure 3-7** (also see the values in **Table 3A-1**). Based on the saturation uptake (~ 0.92-1.05 mmol $g_{HBEA150}^{-1}$ at 160–200 °C in aqueous phase) reported in our recent work,[51] we conclude that this amount of zeolite (≤ 0.2 g) does not appreciably (at most by 1%) decrease the concentration of cyclohexanol in the bulk solution from its initial value.

Over zeolite HBEA, cyclohexene is the main product from cyclohexanol dehydration in dilute aqueous solutions (0.33−1.1 M). The high (99−100%) selectivity to the olefin at short residence times (*e.g.*, <1 h at 200 °C) indicates that water elimination proceeds

preferentially via the intramolecular rather than intermolecular pathways. This is in agreement with previous work on liquid phase alcohol dehydration (200 °C) suggesting that while primary alcohol dehydration favors high ether yields, secondary alcohols preferentially undergo intramolecular dehydration leading to the olefin.[69] In contrast to H_3PO_4,[51] HBEA can catalyze ether formation and C–C alkylation reactions to greater extents at higher conversions,[43] suggesting that the large intracrystalline voids of BEA zeolites allow the formation of dimeric species and exert a specific influence stabilizing the TS of the bimolecular reactions.[34]

Note that TOFs were obtained by normalizing the rates to the concentration of total BAS, as we surmised in an earlier study that all the BAS are present in the form of solvated hydronium ions,[48a] which are equally active in aqueous phase dehydration.[52] Both hydronium ions and H-bonded water clusters were proposed in earlier studies for various microporous solid acids in contact with water vapor, such as HSAPO-34,[70] NaHZSM-5,[71] and HNaY.[72]

Remarkably, the two HBEA zeolites, with different Al T-site distributions, afforded similar TOFs, within ± 10%, and similar activation energies, within ± 5%, in aqueous phase dehydration. Therefore, the hydronium ions, irrespective of their locations in the BEA framework, catalyze aqueous phase dehydration with almost identical kinetic constants.

Two scenarios could account for the very small fractional order with respect to the bulk concentration of cyclohexanol measured over HBEA (**Figure 3-8**). One possibility is a full coverage of active sites by protonated alcohol species. Alternatively, as we have suggest in our recent work,[51] that the apparent zero-order in aqueous phase is due to a high occupancy of pore volume by cyclohexanol molecules at the chosen alcohol/catalyst ratios (n_{ROH}:n_{H+} = 1200−3500) and temperatures (160−200 °C). Under the conditions applied, the hydronium ions confined in zeolites nano-pores are proposed to be completely associated with cyclohexanol via H-boding. Note, however, that the reaction conditions used in this work, temperature and substrate/catalyst ratio in particular, differ from those reported in our previous NMR study,[43] leading to different pore occupancies and, thus, different kinetic regimes.

3.3.5 HBEA-catalyzed dehydration of neat cyclohexanol

Dehydration of neat cyclohexanol, without water intentionally added, was also performed on both HBEA150 zeolites. In principle, the concentration of water in liquid phase could influence the amount of water adsorbed in the internal voids of zeolites and, in turn, affect the number of associated water in the vicinity of framework BAS. Adventitious water initially present in zeolites and/or in the alcohol feed did not lead to appreciable experimental variability (not shown here), implying that such low concentrations of water do not influence the performance of the catalytic sites.

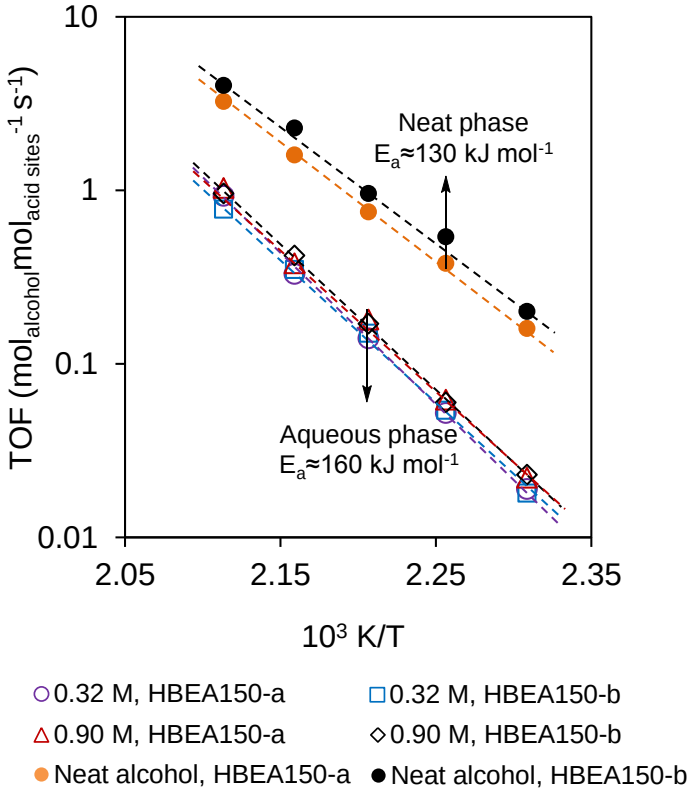

Figure 3-7. Arrhenius plots for the dehydration of cyclohexanol over two HBEA-150 zeolites in aqueous phase and neat alcohol.

As shown in **Figure 3-7** and **Table 3A-1**, similar TOFs (within ±20%) and energies of activation (within ±3%) for olefin formation were measured for the two HBEA150. Different Al T-sites associated with protons have slightly different intrinsic acid strengths;[73] for example, a distribution of the deprotonation energies (DPE, a type of

theoretical descriptor for acid strength in gas phase) of the BAS of 25−27 kJ mol^{-1} was estimated for HZSM-5[74] and HBEA zeolite.[48] Therefore, it is concluded that such subtle differences in acid strength, or differences in spatial constraints at T-sites,[75] is inconsequential to cyclohexanol dehydration in both water and neat liquid phase.

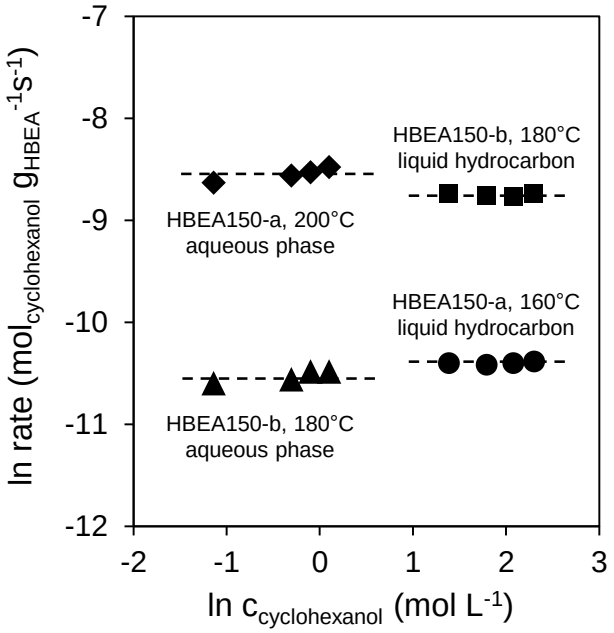

Figure 3-8. The dependence of the mass-specific reaction rates on the concentration of cyclohexanol for dehydration over zeolite HBEA150 in aqueous phase and in organic phase (decalin or pure alcohol). In all cases, the reaction orders are near 0 (± 0.1) with respect to the concentration of cyclohexanol.

In stark contrast to aqueous phase dehydration, intermolecular water elimination also took place in neat alcohol experiments yielding dicyclohexyl ether with molar selectivities of 4−6% (**Figure 3A-4**). Such bimolecular reactions are expected to become favorable both kinetically and thermodynamically in neat alcohol because of the much higher alcohol concentration (*ca.* 10 M) and little initial concentrations of water. A general trend is found that the selectivity to ether decreases at higher temperatures, indicating lower activation energies for ether formation.

The energy of activation for olefin formation in neat alcohol was determined to be ~ 130 kJ mol^{-1} on both HBEA150 zeolites, which is ~ 30 kJ mol^{-1} lower than that observed in dilute aqueous solutions (**Figure 3-7**). In both cases, dehydration occurs in the same

kinetic regime corresponding to (near) pore saturation, revealed by the zeroth reaction order as shown in **Figure 3-8**. The turnover rates observed for pure cyclohexanol dehydration on HBEA150 were 4−10 times higher than those observed for the aqueous phase dehydration. This is only a modest enhancement considering the greatly lowered barrier, caused by a smaller entropy gain (**Table 3-2**).

$$k = \frac{k_B T}{h} e^{\Delta S^{\ddagger}/R} e^{-\Delta H^{\ddagger}/RT} \qquad (3\text{-}1)$$

The enthalpy and entropy of activation in both aqueous phase and neat alcohol were calculated using transition state theory (Eq. (3-1)), also see **Figure 3A-5**. The results are compiled in **Table 3-2**. In later sections, DFT calculations are employed to shed light on the transition state enthalpy and entropy in the two scenarios

Table 3-2. Kinetic parameters determined for HBEA-catalyzed dehydration of aqueous and neat cyclohexanol.[a]

	$\Delta H^{\circ\ddagger}$ (kJ·mol^{-1})	$\Delta S^{\circ\ddagger}$ (J·mol^{-1}·K^{-1})	$\Delta G^{\circ\ddagger}_{170^{\circ}C}$ (kJ·mol^{-1})
Aqueous, HBEA150-a	158 ± 4	85 ± 8	120 ± 8
Aqueous, HBEA150-b	157 ± 4	82 ± 5	121 ± 6
Neat cyclohexanol, HBEA150-a	125 ± 1	22 ± 2	115 ± 2
Neat cyclohexanol, HBEA150-b	128 ± 7	25 ± 4	117 ± 9

[a] In all cases, the formation of cyclohexene showed (near) zeroth order in cyclohexanol.

3.3.6 DFT calculations of the dehydration reaction over HBEA

In order to better understand the disparate TOFs and activation energies (**Figure 3-7** and **Table 3A-1**) determined in aqueous phase and under solventless conditions, we performed DFT calculations for two scenarios, which mimic the reaction environment at the active site in HBEA under high-water (aqueous) and low-water (neat alcohol) conditions. The main goal was to define the kinetically relevant states in the protonation

and H_2O-elimination steps that occur inside the zeolite pore, and to enable comparison with the measured barriers in the corresponding kinetic regime. Other steps (*e.g.*, desorption of water and olefin, hydride shifts) are not discussed here, because they are irrelevant to the kinetics of dehydration catalysis. The calculated energy profiles for the 170 °C reaction (an example temperature) are shown in **Figures 3-9 a** and **3-9 b** for the aqueous and neat alcohol phase, respectively.

DFT calculations were performed to evaluate the relative enthalpies and free energies of having different numbers of H_2O molecules in the BEA unit cell, in the absence of cyclohexanol. Although considering all details of calculations goes beyond our goal here, the results show unequivocally that in a BEA unit cell containing 3−10 H_2O molecules in proximity to the Brønsted acidic Si−OH−Al, the proton is not associated with the framework bridging hydroxyl, but is transferred to the adjacent water cluster. The DFT calculations also suggest that a single or even two H_2O molecules are insufficient to stabilize the protons. Hence, for the theoretical evaluation of the aqueous phase dehydration pathways reported in this work we chose an example hydronium ion cluster with a $H_3O^+(H_2O)_7$ structure, the presence of which was identified by *ab initio* molecular dynamics (AIMD) simulations.[51] DFT calculations for the aqueous phase dehydration of cyclohexanol has been discussed in details in **Chapter 2**, and in this chapter we will recall these details and compare them with the dehydration in neat alcohol.

Next, calculations were performed with up to 8 cyclohexanol molecules in addition to a protonated water cluster loaded in one BEA unit cell. This roughly corresponds to the actual reaction conditions, where several cyclohexanol molecules are present in the pores. Following adsorption in the zeolite pore, the alcohol interacts with the BAS, forming a H-bond to the hydronium ion residing there, while also interacting with the pore walls. The calculated enthalpy and free energy (at 170 °C) for cyclohexanol adsorption and subsequent interaction with the hydronium ion (A, **Figure 3-9 a**) are -108 and -50 kJ mol^{-1}, respectively. The H-bonded cyclohexanol then undergoes protonation by the hydronium ion to form an alkoxonium ion. The calculated activation barrier for alcohol protonation is 69 kJ mol^{-1} (TS1, **Figure 3-9 a**). This protonation step is endothermic ($\Delta H° = +$ 36 kJ mol^{-1}) and endergonic ($\Delta G° = +$ 55 kJ mol^{-1}). Thus, the protonated alcohol (B, **Figure 3-9 a**) is expected to be a minority species at typical reaction temperatures.

Subsequently, dehydration to cyclohexene may occur by E1- and E2-type elimination paths. On the E1-type path, the slightly elongated C−O bond (1.57 Å) in the protonated cyclohexanol continues to stretch along the reaction coordinate (the distance between the alcohol C-atom and O-atom of the leaving OH_2 is ~ 2.56 Å at the TS2). The C−O bond cleavage has an activation barrier of 95 kJ mol^{-1}, with an entropy gain of 34 J mol^{-1} K^{-1}. In TS2, the leaving OH_2 is almost neutral, and the positive charge (+ 1.01 |e|) remains largely on the [C_6H_{11}] moiety. Next, the $C_6H_{11}^+$ carbenium ion deprotonates to form cyclohexene, the proton returning to the hydronium ion cluster. In TS3, a H_2O molecule nearby acts as the base that pulls off the β-H and C_β–H bond is almost fully broken (2.46 Å). This deprotonation step has a small barrier (43 kJ mol^{-1}) in the forward direction and a higher barrier (92 kJ mol^{-1}) in the reverse direction. The detailed structures and configurations of the adsorbed intermediates, transition states and the $H_3O^+(H_2O)_7$ hydronium ion cluster are shown in **Figure 2A-15**, **Chapter 2**.

An E2-type TS (TS4, **Figure 3-9 a**) was located in which both C–O and C_β–H bonds are partially broken at 2.40 Å and 2.15 Å, respectively. The enthalpy of activation and entropy of activation calculated at 170 °C are 137 kJ mol^{-1} and 74 J mol^{-1} K^{-1}, respectively (from B to TS4). This corresponding free energy of activation is 104 kJ mol^{-1}. These activation parameters are somewhat larger than the corresponding values given above for the E1-type path, *i.e.*, $\Delta\Delta H^‡$ = 11 kJ mol^{-1} and $\Delta\Delta G^‡$ = 15 kJ mol^{-1} from B to TS4 (**Figure 3-9 a**). Such differences at this level of theory are not significant and therefore, both mechanisms are deemed viable. We note in passing that in-situ ^{13}C NMR measurements have shown significant migration of the hydroxyl group during dehydration of 1-^{13}C-cyclohexanol in aqueous phase over the same HBEA150-b catalyst. This migration is consistent with facile 1,2-hydride shifts from the cyclohexyl cation.

The calculated barriers may also be compared to experiment. Because the protonated cyclohexanol (B, **Figure 3-9 a**) is so much less stable than the hydrogen bonded alcohol (A, **Figure 3-9 a**), the measured barrier should be compared to the change in energies between states A and TS3, i.e., $\Delta H^‡_{A,TS3}$ = 161 kJ mol^{-1} and $\Delta G^‡_{A,TS3}$ = 144 kJ mol^{-1}. In comparison, the experimentally-determined barriers for aqueous phase dehydration over HBEA150 (**Table 3-2**) are $\Delta H^‡$ = 158 ± 4 kJ mol^{-1} and $\Delta G^‡_{170°C}$ = 120 ± 8 kJ mol^{-1}. While the calculated enthalpic barrier agrees with experiment, the free energy barrier is

different from ex periment by ~24 kJ mol^{-1}. This difference in free energy is not significant considering that protocol used to estimate zero point and thermal corrections introduces more error in the entropy than the enthalpy.

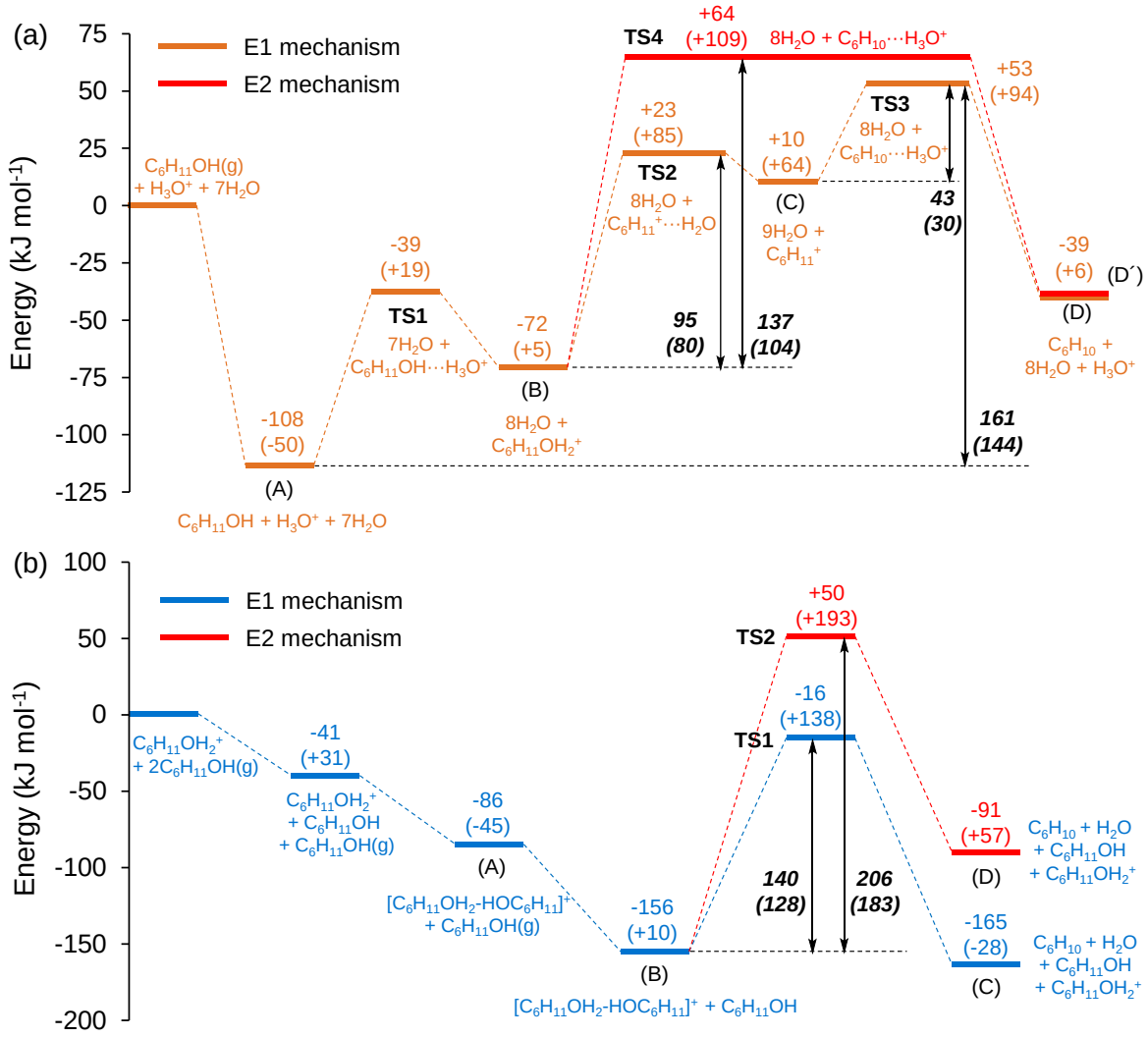

Figure 3-9. The DFT-based energy diagram (170 °C) for the aqueous (a) and pure alcohol (b) phase dehydration of cyclohexanol over a periodic HBEA ($Al_4H_4Si_{60}O_{128}$) model is shown. Aqueous phase and neat phase are modeled respectively by having eight and no water molecules in the vicinity of the framework proton in the unit cell, and optimizing the configurations and energies. All species except for those denoted with (g) are in the unit cell. The detailed structures and configurations of the adsorbed intermediates, transition states and the $H_3O^+(H_2O)_7$ hydronium ion cluster are shown in **Figure 2A-15** (**Chapter 2**) and **Figure 3A-6** (**Chapter 3**). Enthalpy and free energy values are shown outside and inside the brackets, respectively.

Protonated alcohol-alcohol, water-alcohol and water-water dimers have been proposed to form in gas-phase alcohol dehydration on solid acids.[27,29,31,34] The contribution of dimer-mediated routes for alcohol dehydration, however, has never been examined in liquid media. Bearing this in mind, DFT calculations were used to investigate whether dimer-mediated routes can contribute to olefin formation in aqueous phase. In water, the formation of a protonated dimer from two cyclohexanol and $H_3O^+(H_2O)_7$ is highly unfavorable, with free-energy changes of > 80 kJ mol^{-1} uphill (not shown). Thus, we suggest further reactions via the protonated dimer intermediate are highly improbable and irrelevant to aqueous phase dehydration to form olefin.

Next, we turn attention to DFT calculations performed to model the dehydration of neat cyclohexanol over HBEA. The potential energy diagrams for E1- and E2-type paths are shown in **Figure 3-9 b** (structures of the key intermediates and TSs are shown in **Figure 3A-6**). Since relatively less water is expected to be adsorbed under these conditions, three cyclohexanol molecules were used to model the reactions. In contrast to aqueous phase, protonation of even just one cyclohexanol molecule is thermodynamically favorable and nearly barrierless. Interaction of this protonated alcohol with a second alcohol to form a protonated dimer is even more favorable. As a consequence of the much greater stability of the protonated dimer, dehydration of neat liquid cyclohexanol should occur mainly via the dimer intermediate, and the measured barrier (125–128 kJ mol^{-1}) and entropy (22–25 J mol^{-1} K^{-1}) should reflect the corresponding changes when going from the adsorbed dimer to the TS. The E1-type path has a carbenium-ion-like TS (TS1, **Figure 3-9 b**), with the C_α–O bond almost completely broken (2.76 Å) and the C_β–H bond slightly elongated (1.18 Å) due to interaction with the alcohol molecule that is hydrogen-bonded to the water molecule which is formed as the C_α–O bond elongates. Thus, the path is characteristic of a concerted pericyclic reaction. An E2-type path (**Figure 3A-6**) that involves a third cyclohexanol molecule pulling off a β-H (anti-periplanar configuration) from the protonated dimer, appears much less favorable than the E1-type path, as a result of the much higher enthalpic (206 kJ mol^{-1}) and free energy barrier (183 kJ mol^{-1}) for the rate-limiting step. Note that the successor state (D) on the E2 path is much less stable than the successor state (C) on the E1 path. Inspection of the structures C and D shows the protonated alcohol in structure D is further from the site of

negative charge (framework AlO_4^-) in structure C. This separation of charge is a significant factor in the E2 path being more unfavorable.

Overall, the experimental trends in activation enthalpies and entropies (towards formation of the kinetically relevant TSs) are reproduced by the DFT calculations: the enthalpic barrier for aqueous phase dehydration is significantly higher than that for solvent-free dehydration (161 *vs.* 140 kJ mol^{-1} from DFT; 157 *vs*. 125 kJ mol^{-1} from experiments), while the corresponding entropy gain is smaller for dehydration of neat alcohol than for aqueous alcohol (27 *vs*. 38 J mol^{-1} K^{-1} from DFT, 25 *vs*. 85 J mol^{-1} K^{-1} from experiments).

3.3.7 Evidence for the formation of cyclohexanol dimers on HBEA150

The formation of cyclohexanol dimer was experimentally confirmed by the combination of IR (**Figure 3-10**) and microbalance measurements (**Figure 3-11**). The absorbance IR spectra with varied partial pressures of cyclohexanol, as shown in **Figure 3A-7**, reveal that the alcohol molecules primarily interact with BAS of HBEA150. BAS are completely covered at the alcohol partial pressure of 0.0015 mbar at 40 °C. Moreover, the spectra subtracted by the spectrum of parent HBEA150, together with the relations between the coverage of BAS determined by the decrease in the intensity of the free OH stretching vibration at 3610 cm^{-1} and the uptake of alcohol calculated by the increase in intensity of the C-H stretching vibrations for cyclohexanol at 2800-3000 cm^{-1} are shown in **Figure 3-10.** As shown in **Figure 3-10 b**, the nonlinearity of BAS coverage versus cyclohexanol uptake implies the formation of different surface species followed by increasing the alcohol partial pressures or prolonging the adsorption time till the full coverage of BAS. The increasing slop of curve indicates the generation of larger alcohol clusters on HBEA150 surface, such as dimeric or even larger alcohol species.

The rigorous measurement for determining the stable surface species was carried out on a microbalance, see results in **Figure 3-11**. Cyclohexanol was first adsorbed by exposing the activated HBEA150 to cyclohexanol at the vapor pressure of 0.003 mbar at 40 °C, and the uptake of cyclohexanol reached to the equilibria with the coverage of 9.20 ((mol cyclohexanol) (mol BAS)$^{-1}$). Following exposure, HBEA150 was then evacuated under the vacuum of 10^{-6} mbar at 40 °C, and the BAS coverage decreased to 1.95 and

remained constant at evacuation even for longer time (48 h). Combining the IR and microbalance results, it is safe for us to conclude that the cyclohexanol dimers are the stably surface species on HBEA150 at high concentrations of alcohol in the absence of water.

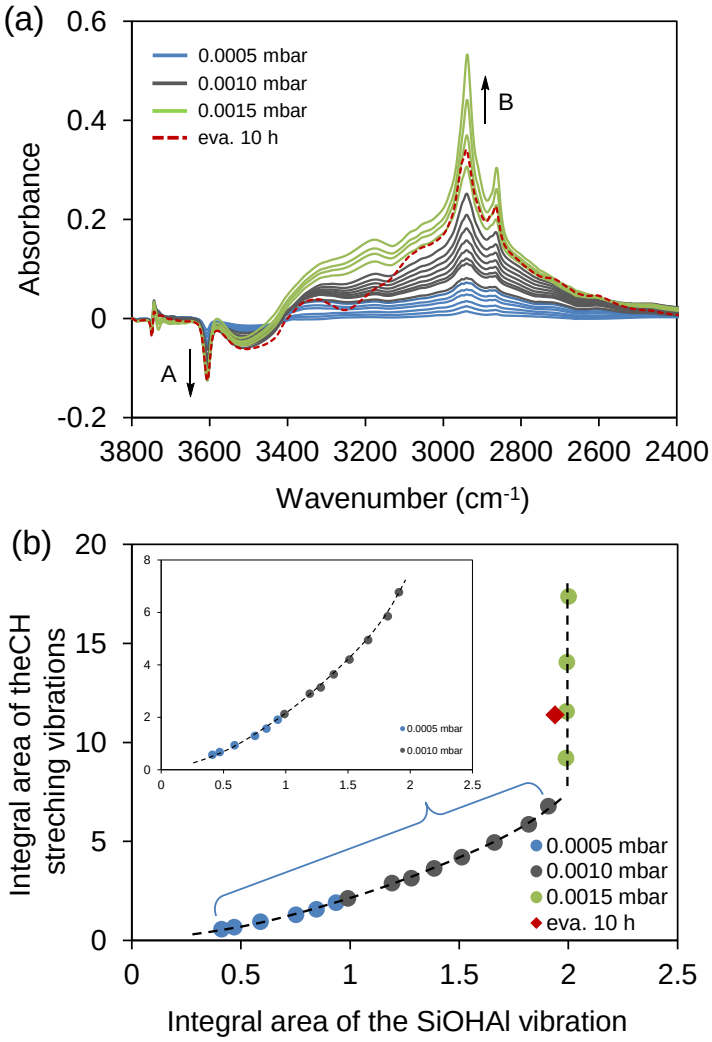

Figure 3-10. Difference in the IR spectra after adsorption of cyclohexanol at partial pressures between 0.0005 to 0.0015 mbar at 40°C. In figure (a), the arrows indicate the changes with increasing adsorption time at a defined pressure. (A) Decreasing intensity caused by the interactions of cyclohexanol with the acidic SiOHAl (3610cm^{-1}) groups. (B) Increasing intensity at 2800-3000 cm^{-1} attributed to the C-H stretches of cyclohexanol. Figure (b) shows the relation between the decrease in the intensity of the free OH stretching vibration(3610 cm^{-1}) and the increase in intensity of the C-H stretching vibrations for

cyclohexanol (2800-3000 cm^{-1}). The red dotted line and point in (a) and (b) are the results come from the 10 hours evacuation followed by the adsorption equilibrium at 0.0015 mbar at 40°C.

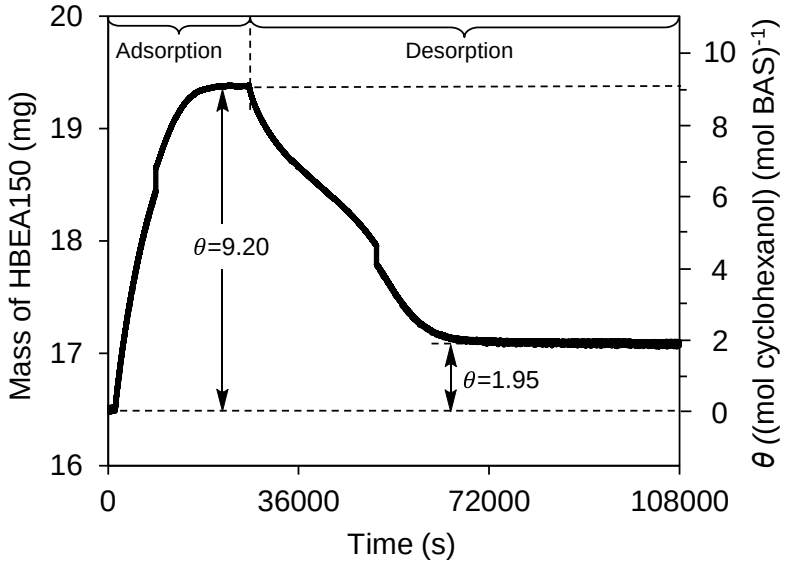

Figure 3-11. TGA measurement of cyclohexanol adsorption with partial pressure of 0.003 mbar over HBEA150 at 40 °C. Coverage of BAS (θ) is defined as the uptake of cyclohexanol per BAS (mol mol^{-1}).

According to the IR and TGA measurements of adsorbed cyclohexanol, there exists a stable adsorption state corresponding to two alcohol molecules per BAS in HBEA150 zeolite. The same results have also been reported on HZSM-5 adsorbing 1-butanol.[76] The alcohol dimers which are unreactive or much less reactive than its monomeric form, has been observed in the gas-phase alcohol dehydration over zeolite catalysts.[34,77,78] Similarly, the contribution of dimer-mediated routes for cyclohexanol dehydration in apolar liquid media is also kinetically examined, as shown in **Figure 3-12**. The decrease in TOFs with increasing the alcohol concentration was ascribed to the formation of the much less reactive (protonated) alcohol dimer occupying the acid sites, further inhibiting the overall dehydration reaction. The experimental data was well fitted by the model of monomer and dimer species with different reactivities, see details in **Chapter 2**. Thus, combining the kinetic, theoretical and characteristic examinations, we conclude that the alcohol dimers forming in organic solvents (hydrocarbon solvents or neat cyclohexanol) reduce the rate of reaction by stabilizing the ground state of reacting substrate. Unlike in

the presence of bulk water, BAS in the form of hydronium ions catalyze the dehydration of cyclohexanol via monomolecular (monomeric cyclohexanol) precursors.

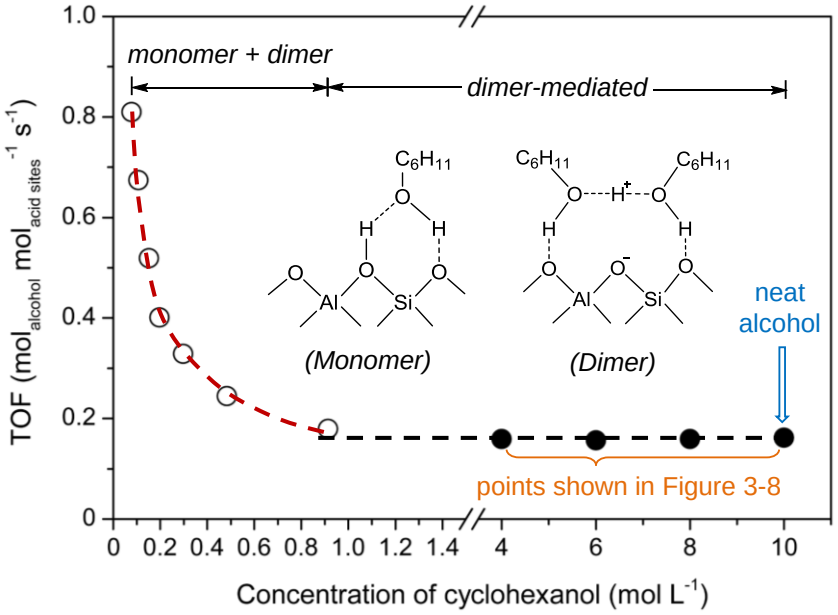

Figure 3-12. The contribution of alcohol dimers in liquid-phase cyclohexanol dehydration to cyclohexene (in decalin and neat alcohol) proved by the kinetic assessment.

3.3.8 Towards a complete energy landscape in HBEA-catalyzed dehydration of cyclohexanol

Characterizations, kinetic evaluations, and DFT calculations have jointly yielded details of unprecedented depths on common mechanistic features and enthalpy-entropy trade-offs in the Brønsted-acid-catalyzed dehydration of cyclohexanol in condensed phases. The active BAS structure in a zeolite equilibrated with an aqueous phase can no longer be considered as a proton attached to the framework O-atoms; instead, it is a protonated water cluster. Effectively, this confined "hydronium ion", which is likely of a less extended structure than aqueous phase hydronium ions, protonates the H-bonded alcohol in the pores. DFT calculations suggest that the protonation equilibrium constant in zeolites critically depends on the number of water molecules in the hydronium-ion-like cluster (**Table 3A-2**). Water has a smaller proton affinity than cyclohexanol, but a cluster

of multiple water molecules ($n \geq 3$) can have a greater proton affinity than cyclohexanol. As a consequence, proton transfer from a hydronium ion-water cluster to cyclohexanol will become progressively more favorable as the bulk liquid phase changes from aqueous to neat alcohol. When protonation favors the alkoxonium ion, the measured activation energy and entropy mainly reflect the differences between the kinetically relevant TS (TS1 in **Figure 3-9 b**) and the protonated alcohol state (B in **Figure 3-9 b**). When protonation of the alcohol is unfavorable, the measured activation energy and entropy mainly reflect the differences between the TS (TS3 in **Figure 3-9 a**) and the state in which the alcohol is H-bonded to the hydronium ion (A in **Figure 3-9 a**).

In aqueous solution, the prevalent hydronium ion in zeolite HBEA was simulated as $H_3O^+(H_2O)_7$. With this cluster, protonation of cyclohexanol is thermodynamically unfavorable (DFT: $\Delta G° = +55$ kJ mol^{-1}). Accordingly, a majority of the BAS (hydronium ions) interacts with the alcohol without a significant extent of proton transfer, as reported in H_3PO_4-catalyzed cyclohexanol dehydration.[51] In turn, the measured energy of activation (~158 kJ mol^{-1}) and corresponding entropy change (~85 J mol^{-1} K^{-1}) mainly reflect the difference between the kinetically relevant TS and the H-bonded alcohol state.

In neat alcohol phase, the concentration of water in the pores, especially during steady-state catalysis, is unknown. It is speculated that protonation of cyclohexanol is favorable, according to DFT estimates using H^+ or smaller $H_3O^+(H_2O)_n$ ($n \leq 3$) clusters. Accordingly, the measured energy of activation (125-127 kJ mol^{-1}) and entropy change (22-25 J mol^{-1} K^{-1}) should primarily reflect the difference between the TS for elimination and the protonated alcohol-dimer state (**Figure 3-9 b**). Remarkably, this difference is smaller than dehydration of aqueous cyclohexanol.

Our DFT models of the HBEA-catalyzed dehydration of cyclohexanol in aqueous and neat phases capture this trend and show (**Figure 3-9**) that the difference is due to the environments of the proton, *i.e.*, hydronium ion-water cluster for dehydration of aqueous cyclohexanol and a protonated alcohol dimer for dehydration of neat cyclohexanol. The hydronium ion-water cluster is relatively more stable than the protonated alcohol. This stabilization of the proton by water, thus accounts for the larger barrier when water is present.

3.4 Conclusions

The catalytic cyclohexanol dehydration has been explored over HBEA zeolites, in aqueous and neat alcohol phases at mild temperatures (160−200 °C). Measured rate constants and activation barriers, in conjunction with DFT calculations yielded an energy landscape for cyclohexanol dehydration over both acids. The catalytic performance of HBEA zeolite is found to be independent of the Al distribution among different crystallographic sites (primarily T1, T2, T7 and T9) of HBEA, in the presence of low and high water concentrations. The dehydration of cyclohexanol catalyzed by HBEA in neat alcohol has lower activation enthalpy and entropy compared to the dehydration in aqueous phase. The dimer-mediated reaction routes contribute to the dehydration of cyclohexanol in organic liquid media in the absence of water, while in aqueous phase the dehydration of cyclohexanol only happens via monomeric pathways. The intrazeolite water concentration modulates the size of the catalytically active hydronium ions, which in turn affects both the protonation equilibrium of cyclohexanol and the rate-limiting C−O bond cleavage. DFT calculations predicts a lower transition state energy and entropy for dehydration on small hydronium-ion clusters that mimics the active-site structure in low-water environment than on big hydronium-ion cluster that mimics the active-site structure equilibrated with aqueous medium, in line with experiments. Work in progress will address the effects of zeolite pore topology and alcohol structure on Brønsted acid catalysis (*e.g.*, dehydration and alkylation) in aqueous and organic liquid phases.

3.5 Appendix

A1. Characterization of parent and water-treated HBEA150 samples

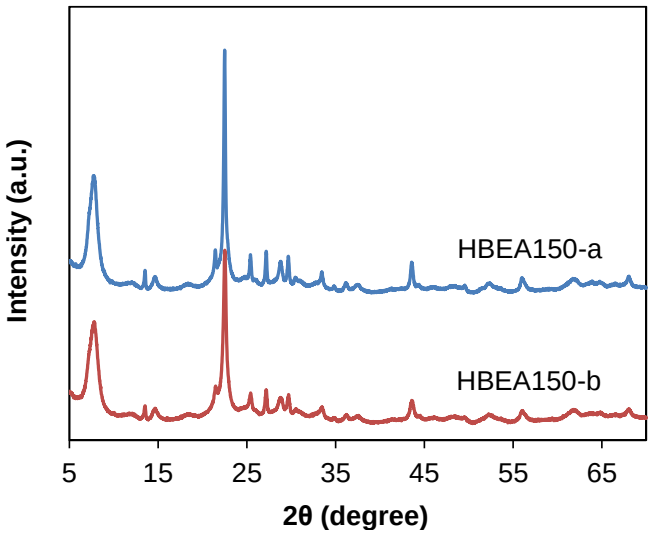

Figure 3A-1. X-ray diffractograms of two parent HBEA150 zeolites.

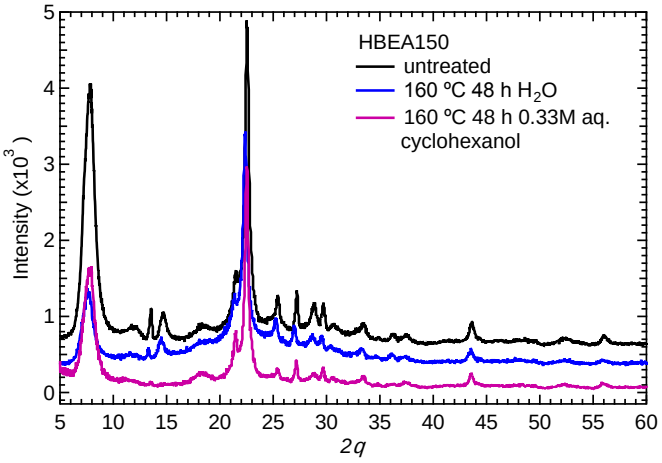

Figure 3A-2. X-ray diffractograms of HBEA150-b untreated (black), HBEA150-b treated with 80 mL water at 160 °C for 48 h (blue) and HBEA150-b treated at 160 °C for 48 h with 80 mL 0.33 M aqueous cyclohexanol (magenta).

The potential structural changes of zeolites have to be considered in aqueous phase at high temperature in the past.[1] Hot liquid water treatment under similar conditions to the reactions was performed to investigate the stability of HBEA150 in the course of catalytic dehydration. According to **Figure 3A-2**, it is safe to say that the HBEA150 zeolite framework suffered minor degradation during hot liquid water treatment at short time (<2 h). Early studies on the stability of zeolites or Al_2O_3 in aqueous-phase catalysis revealed that carbonaceous deposits from the reaction protect the materials against

dissolution, thus improving their hydrothermal stability.[2,3] Thus, during the dehydration reaction, the frameworks of the HBEA zeolites should undergo much less degradation compared with that in pure water. This is clearly evidenced for prolonged treatment (48 h) at 160 °C in water with or without cyclohexanol (**Figure 3A-2**). For instance, the 2θ = 7.7° reflection was the most affected by hot liquid water; its intensity decreased by ca. 75 % compared with the parent zeolite after pure water treatment for 48 h at 160 °C. With 0.33 M cyclohexanol present, the loss of intensity (*ca.* 15 %) was substantially smaller, suggesting less long-range structural change (retention of a larger fraction of coherent lattice planes).

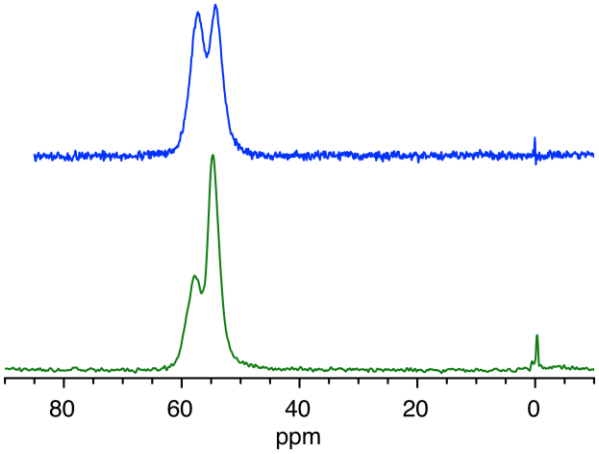

Figure 3A-3. ^{27}Al MAS NMR spectra of the studied HBEA150-a (blue) and HBEA150-b (green) zeolites (both recorded on a 850 MHz spectrometer).

A2. Reaction rates and activation energies of cyclohexanol dehydration over HBEA150 in aqueous phase

Table 3A-1. Reaction rates, turnover frequencies and activation energies for HBEA-catalyzed dehydration of cyclohexanol to cyclohexene.

Reaction conditions [a]	Kinetic measurement [b]	Reaction temperature [°C]					E_a [c]
		160	170	180	190	200	
3.3 g cyclohexanol (~0.32 M) + 100 cm^3 H_2O + 140 mg HBEA150-a	Rate (mol g_{HBEA}^{-1} s^{-1})	3.7×10^{-6}	1.0×10^{-5}	2.6×10^{-5}	6.4×10^{-5}	1.8×10^{-4}	164 ± 3
	TOF (mol$_{alcohol}$ mol$_{acid\ sites}^{-1}$ s^{-1})	0.019	0.052	0.14	0.33	0.93	
2.6 g cyclohexanol (~0.32 M) + 80 cm^3 H_2O + 170 mg HBEA150-b	Rate (mol g_{HBEA}^{-1} s^{-1})	3.0×10^{-6}	9.1×10^{-6}	2.5×10^{-5}	5.8×10^{-5}	1.3×10^{-4}	159 ± 12
	TOF (mol$_{alcohol}$ mol$_{acid\ sites}^{-1}$ s^{-1})	0.018	0.054	0.15	0.35	0.78	
10 g cyclohexanol (~0.90 M) + 100 cm^3 H_2O + 140 mg HBEA150-a	Rate (mol g_{HBEA}^{-1} s^{-1})	4.2×10^{-6}	1.2×10^{-5}	3.4×10^{-5}	7.2×10^{-5}	2.0×10^{-4}	162 ± 4
	TOF (mol$_{alcohol}$ mol$_{acid\ sites}^{-1}$ s^{-1})	0.022	0.062	0.18	0.38	1.03	
8 g cyclohexanol (~0.90 M) + 80 cm3 H_2O + 170 mg HBEA150-b	Rate (mol g_{HBEA}^{-1} s^{-1})	3.8×10^{-6}	1.0×10^{-5}	2.8×10^{-5}	7.0×10^{-5}	1.6×10^{-4}	161 ± 4
	TOF (mol$_{alcohol}$ mol$_{acid\ sites}^{-1}$ s^{-1})	0.023	0.060	0.17	0.42	0.96	
100 g cyclohexanol + 200 mg HBEA150-a	Rate (mol g_{HBEA}^{-1} s^{-1})	3.1×10^{-5}	7.3×10^{-5}	1.4×10^{-4}	3.1×10^{-4}	6.2×10^{-4}	129 ± 6
	TOF (mol$_{alcohol}$ mol$_{acid\ sites}^{-1}$ s^{-1})	0.16	0.38	0.75	1.60	3.25	
100 g cyclohexanol + 200 mg HBEA150-b	Rate (mol g_{HBEA}^{-1} s^{-1})	3.3×10^{-5}	9.0×10^{-5}	1.6×10^{-4}	3.8×10^{-4}	6.7×10^{-4}	128 ± 7
	TOF (mol$_{alcohol}$ mol$_{acid\ sites}^{-1}$ s^{-1})	0.20	0.54	0.96	2.28	4.02	

[a] Reactor was pressurized with 50 bar H_2 at ambient temperature and stirred vigorously. Reaction time is counted as zero when the set temperature is reached. The concentrations denoted are based on the density of water at room temperature. [b] TOF is determined as olefin formation rate (mol L^{-1} s^{-1}) normalized to the concentration of total BAS. [c] Activation barriers are determined from the Arrhenius plots for TOFs (a directly measured property).

A3. Dehydration of cyclohexanol over HBEA zeolites in neat alcohol

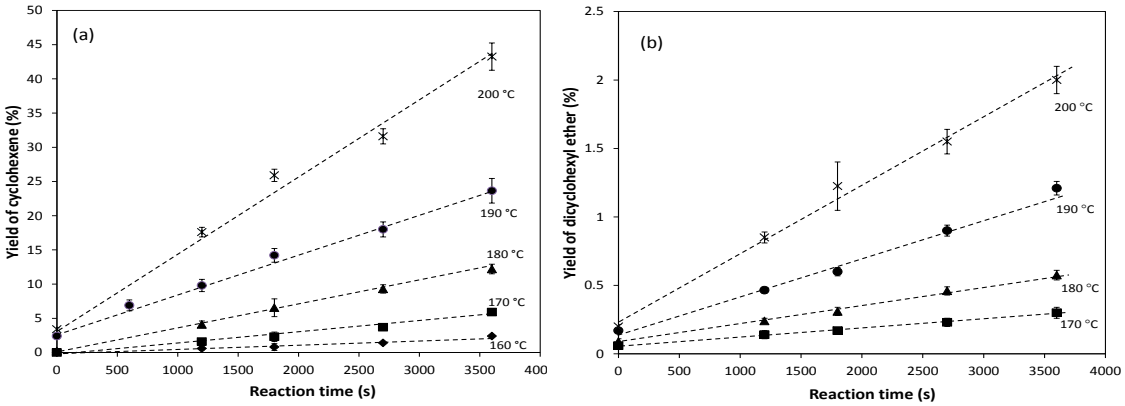

Figure 3A-4. The yields (in mole %) of (a) cyclohexene and (b) dicyclohexyl ether as a function of reaction time in HBEA-catalyzed dehydration of neat cyclohexanol are shown. Error bars represent the standard deviations from both analysis and experiments (repetitions). Reaction conditions: cyclohexanol (100 g), HBEA150-b (200 mg), 50 bar H_2 (room temperature), stirred at 700 rpm.

The neat cyclohexanol dehydration experiment was not designed rigorously anhydrous because both the HBEA and cyclohexanol (liquid) adsorb/absorb moisture

during ambient storage. However, the small quantities of water in the reaction system do not lead to significant variability (< ± 20 %) in rate measurements.

In the case of the neat cyclohexanol dehydration, both cyclohexene and dicyclohexyl ether were observed. The yield-time plots are shown in **Figure 3A-4**. The selectivity to ether is less than 10 % at all temperatures. Rates and activation barriers are reported in **Table 3A-1** and **Figure 3**-7. The extent of reverse reaction was verified by addition of ~ 10 mg of a pre-reduced 10%Pd/Al_2O_3 catalyst (Pd dispersion: 11 %; no measurable activity in the dehydration reaction at 160−200 °C in the absence of an acid co-catalyst) to remove the reverse olefin hydration reaction. Having removed the back reaction, the turnover rates over HBEA150-b (based on cyclohexane formation) are 0.24 and 2.0 mol mol_{BAS}^{-1} s^{-1} at 160 (at conversions below 10 %) and 190 °C (at conversions below 20 %), respectively. The differences compared with the reported values in **Table 3A-1** (0.2 and 2.3 mol mol_{BAS}^{-1} s^{-1}; based on cyclohexene formation) are considered to be within experimental uncertainties (at most ± 20 %). Therefore, in neat alcohol dehydration, the back reaction hardly affects the measurement of initial forward rate, even if water is being produced as reaction progresses.

A4. Calculation of activation enthalpies and entropies based on transition state theory formalism for the HBEA-catalyzed dehydration of cyclohexanol in liquid phase

Eyring equation (Eq. 3-1, see main text) was used to calculate the standard Gibbs free energy, activation enthalpy and entropy. The results are compiled in **Table 3-2** in the main text. Eyring plots were shown in **Figure 3A-5** according to the rearranged equation given as below.

$$\ln\left(\frac{k}{T}\right) = \left(\ln\frac{k_B}{h} + \frac{\Delta S^{\ddagger}}{R}\right) - \frac{\Delta H^{\ddagger}}{R}\left(\frac{1}{T}\right)$$

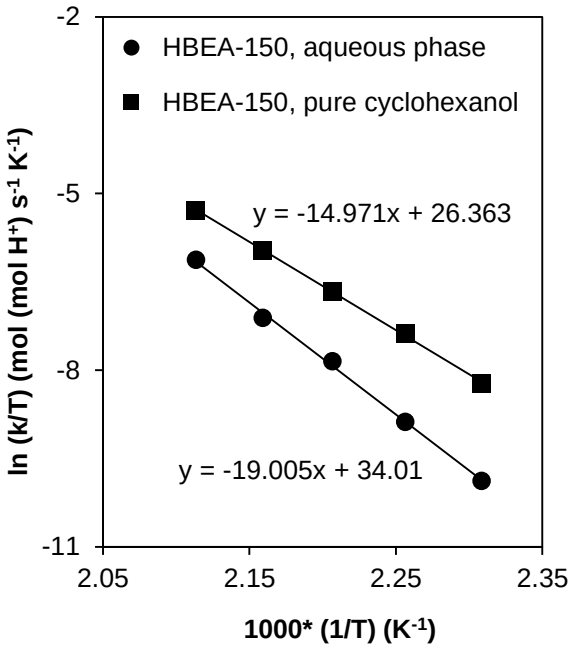

Figure 3A-5. Eyring plots (ln(k/T)–(1/T)) to determine the enthalpy required ($\Delta H^{\ddagger}$) and entropy gained/lost ($\Delta S^{\ddagger}$) to reach the transition state complex.

A5. DFT calculations for the cyclohexanol dehydration in neat alcohol

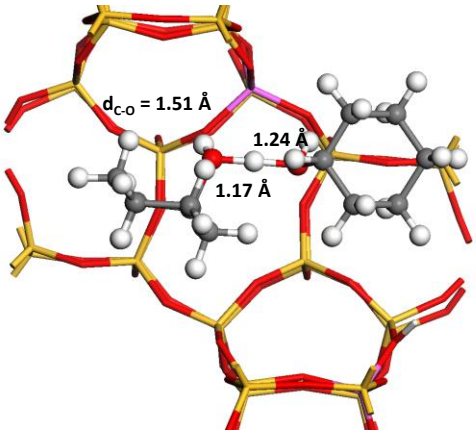

(A)

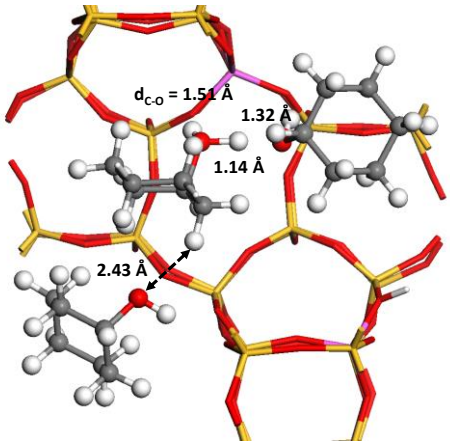

(B)

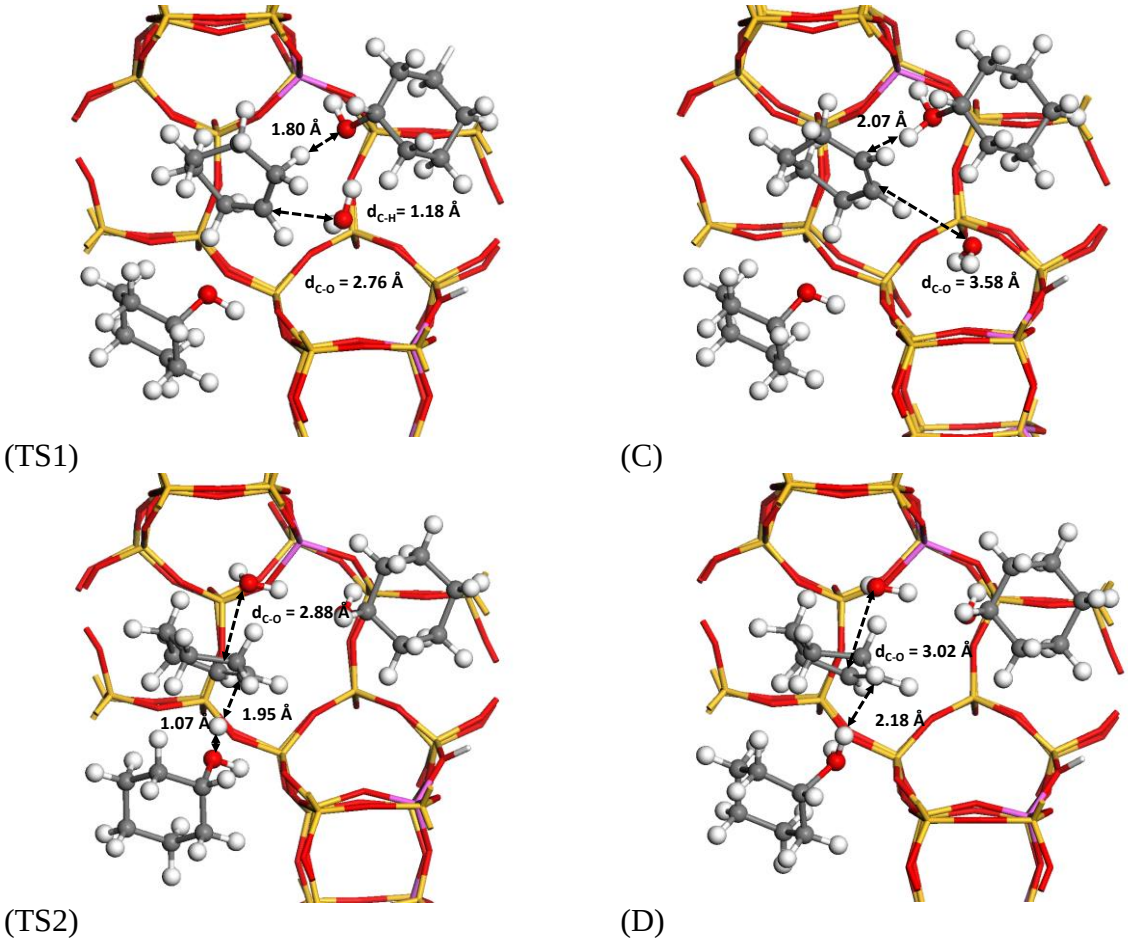

Figure 3A-6. DFT-optimized structures of reaction intermediates (A–D) and transition states (TS1, TS2) in the neat liquid phase cyclohexanol dehydration to cyclohexene via E1 (unimolecular) and E2-type (bimolecular) elimination pathways. The readers are referred to **Figure 3-9 b** (main text) for the corresponding labels of the states.

Table 3A-2. Proton affinities (ΔH_{PA}, for the process $A + H^+ \rightarrow AH^+$) of a single water molecule, water clusters and cyclohexanol in vacuum and HBEA.

Species (A)	ΔH_{PA} (kJ mol^{-1})	
	Vacuum	HBEA
H_2O	-702	NA
$(H_2O)_2$	-837	+45
$(H_2O)_3$	-918	-12
$(H_2O)_4$	-930	-31
$(H_2O)_5$	-966	-32
$C_6H_{11}OH$	-787	-25

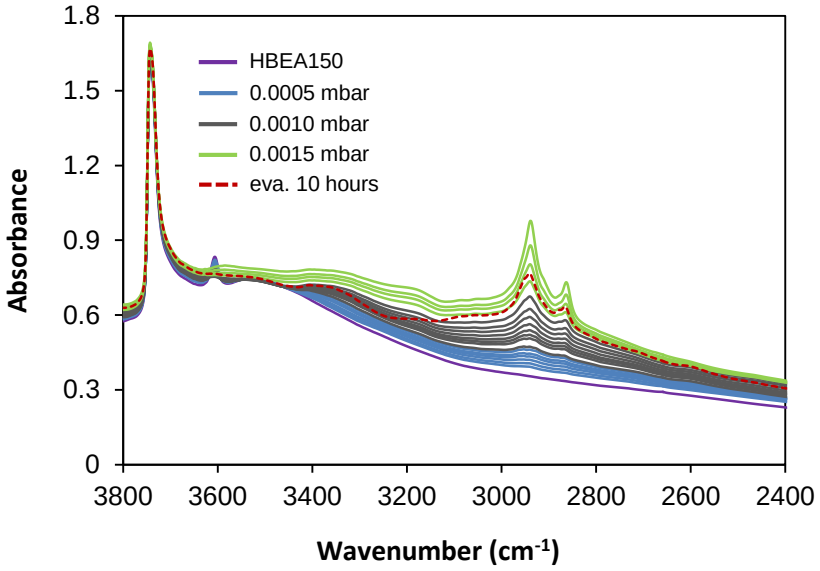

Figure 3A-7. IR spectra after adsorption of cyclohexanol at partial pressures between 0.0005 to 0.0015 mbar at 40 °C.

A6. References for Appendix

1. Ravenelle, R. M.; Schüβler, F.; D'Amico, A.; Danilina, N.; van Bokhoven, J. A.; Lercher, J. A.; Jones, C. W.; Sievers, C. *J. Phys. Chem. C* **2010**, *114*, 19582.

2. Ravenelle, R.; Copeland, J.; Van Pelt, A.; Crittenden, J.; Sievers, C. *Top. Catal.* **2012**, *55*, 162.

3. Pham, H. N.; Anderson, A. E.; Johnson, R. L.; Schmidt-Rohr, K.; Datye, A. K. *Angew. Chem. Int. Ed.* **2012**, *51*, 13163.

3.6 References

[1] Christensen, C. H.; Rass-Hansen, J.; Marsden, C. C.; Taarning, E.; Egeblad, K. *ChemSusChem* **2008**, *1*, 283.

[2] Chheda, J. N.; Huber, G. W.; Dumesic, J. A. *Angew. Chem. Int. Ed.* **2007**, *46*, 7164.

[3] Huber, G. W.; Iborra, S.; Corma, A. *Chem. Rev.* **2006**, *106*, 4044.

[4] Matson, T. D.; Barta, K.; Iretskii, A. V.; Ford, P. C. *J. Am. Chem. Soc.* **2011**, *133*, 14090.

[5] Zakzeski, J.; Bruijnincx, P. C. A.; Jongerius, A. L.; Weckhuysen, B. M. *Chem. Rev.* **2010**, *110*, 3552.

[6] He, J.; Zhao, C.; Lercher, J. A. *J. Am. Chem. Soc.* **2012**, *134*, 20768.

[7] Crossley, S.; Faria, J.; Shen, M.; Resasco, D. E. *Science* **2009**, *327*, 68.

[8] Wang, H.; Male, J.; Wang, Y. *ACS Catal.* **2013**, *3*, 1047.

[9] Saidi, M.; Samimi, F.; Karimipourfard, D.; Nimmanwudipong, T.; Gates, B. C.; Rahimpour, M. R. *Energy Environ. Sci.* **2014**, *7*, 103.

[10] He, J.; Zhao, C.; Lercher, J. A. *J. Catal.* **2014**, *309*, 362.

[11] Li, N.; Huber, G. W. *J. Catal.* **2010**, *270*, 48.

[12] Yan, N.; Yuan, Y.; Dykeman, R.; Kou, Y.; Dyson, P. J. *Angew. Chem. Int. Ed.* **2010**, *49*, 5549.

[13] Hong, D.-Y.; Miller, S. J.; Agrawal, P. K.; Jones, C. W. *Chem. Commun.* **2010**, *46*, 1038.

[14] Zhao, C.; He, J.; Lemonidou, A. A.; Li, X.; Lercher, J. A. *J. Catal.* **2011**, *280*, 8.

[15] Zhu, X.; Lobban, L. L.; Mallinson, R. G.; Resasco, D. E. *J. Catal.* **2011**, *281*, 21.

[16] Zhao, C.; Camaioni, D. M.; Lercher, J. A. *J. Catal.* **2012**, *288*, 92.

[17] Zhao, C.; Kou, Y.; Lemonidou, A. A.; Li, X.; Lercher, J. A. *Angew. Chem. Int. Ed.* **2009**, *48*, 3987.

[18] Zhao, C.; Kou, Y.; Lemonidou, A. A.; Li, X.; Lercher, J. A. *Chem. Commun.* **2010**, *46*, 412.

[19] Shin, E.-J.; Keane, M. A. *J. Catal.* **1998**, *173*, 450.

[20] Zhao, C.; Kasakov, S.; He, J.; Lercher, J. A. *J. Catal.* **2012**, *296*, 12.

[21] DeWilde, J. F.; Chiang, H.; Hickman, D. A.; Ho, C. R.; Bhan, A. *ACS Catal.* **2013**, *3*, 798.

[22] Roy, S.; Mpourmpakis, G.; Hong, D.-Y.; Vlachos, D. G.; Bhan, A.; Gorte, R. J. *ACS Catal.* **2012**, *2*, 1846.

[23] Knözinger, H.; Bühl, H.; Kochloefl, K. *J. Catal.* **1972**, *24*, 57.

[24] Knözinger, H. *Angew. Chem. Int. Ed.* **1968**, *7*, 791.

[25] Knözinger, H.; Köhne, R. *J. Catal.* **1966**, *5*, 264.

[26] Knözinger, H.; Scheglila, A. *J. Catal.* **1970**, *17*, 252.

[27] Macht, J.; Janik, M. J.; Neurock, M.; Iglesia, E. *J. Am. Chem. Soc.* **2008**, *130*, 10369.

[28] Macht, J.; Janik, M. J.; Neurock, M.; Iglesia, E. *Angew. Chem. Int. Ed.* **2007**, *46*, 7864.

[29] Macht, J.; Carr, R. T.; Iglesia, E. *J. Am. Chem. Soc.* **2009**, *131*, 6554.

[30] Macht, J.; Carr, R. T.; Iglesia, E. *J. Catal.* **2009**, *264*, 54.

[31] Carr, R. T.; Neurock, M.; Iglesia, E. *J. Catal.* **2011**, *278*, 78.

[32] Baertsch, C. D.; Komala, K. T.; Chua, Y.-H.; Iglesia, E. *J. Catal.* **2002**, *205*, 44.

[33] Macht, J.; Baertsch, C. D.; May-Lozano, M.; Soled, S. L.; Wang, Y.; Iglesia, E. *J. Catal.* **2004**, *227*, 479.

[34] Chiang, H.; Bhan, A. *J. Catal.* **2010**, *271*, 251.

[35] Jones, A. J.; Carr, R. T.; Zones, S. I.; Iglesia, E. *J. Catal.* **2014**, *312*, 58.

[36] Jones, A. J.; Iglesia, E. *Angew. Chem. Int. Ed.* **2014**, *53*, 12177.

[37] Gounder, R.; Iglesia, E. *Acc. Chem. Res.* **2012**, *45*, 229.

[38] Gounder, R.; Iglesia, E. *Chem. Commun.* **2013**, *49*, 3491.

[39] Corma, A. *Catal. Today* **1997**, *38*, 257.

[40] Davis, M. E. *Acc. Chem. Res.* **1993**, *26*, 111.

[41] Brändle, M.; Sauer, J. *J. Am. Chem. Soc.* **1998**, *120*, 1556.

[42] Bhan, A.; Iglesia, E. *Acc. Chem. Res.* **2008**, *41*, 559.

[43] Vjunov, A.; Hu, M. Y.; Feng, J.; Camaioni, D. M.; Mei, D.; Hu, J. Z.; Zhao, C.; Lercher, J. A. *Angew. Chem. Int. Ed.* **2013**, *53*, 479.

[44] Aronson, M. T.; Gorte, R. J.; Farneth, W. E.; White, D. *J. Am. Chem. Soc.* **1989**, *111*, 840.

[45] Haw, J. F.; Nicholas, J. B.; Xu, T.; Beck, L. W.; Ferguson, D. B. *Acc. Chem. Res.* **1996**, *29*, 259.

[46] Senchenya, I. N.; Kazansky, V. B. *Catal. Lett.* **1991**, *8*, 317.

[47] Sinclair, P. E.; de Vries, A.; Sherwood, P.; Richard A. Catlow, C.; van Santen, R. A. *J. Am. Chem. Soc. Faraday. Trans.* **1998**, *94*, 3401.

[48] (a) Vjunov, A.; Fulton, J. L.; Huthwelker, T.; Pin, S.; Mei, D.; Schenter, G. K.; Govind, N.; Camaioni, D. M.; Hu, J. Z.; Lercher, J. A. *J. Am. Chem. Soc.* **2014**, *136*, 8296; (b) Corma, A.; Moliner, M.; Cantin, Á.; Díaz-Cabañas, M.J.; Jordá, J.L.; Zhang, D.; Sun, J.; Jansson, K.; Hovmöller, S.; Zou, X. *Chem. Mater.* **2008**, *20*, 3218.

[49] Vjunov, A.; Fulton, J. L.; Camaioni, D. M.; Hu, J. Z.; Burton, S. D.; Arslan, I.; Lercher, J. A. *Chem. Mater.* **2015**, *27*, 3533.

[50] Bordiga, S.; Lamberti, C.; Bonino, F.; Travert, A.; Thibault-Starzyk, F. *Chem. Soc. Rev.* **2015**, *44*, 7262.

[51] Liu, Y.; Vjunov A.; Shi, H.; Eckstein, S.; Camaioni, D. M.; Mei, D.; Baráth, E.; Lercher, J. A. *Nat. Commun.* 8, 14113 doi: 10.1038/ncomms14113, **2017**.

[52] Rice, M. J.; Chakraborty, A. K.; Bell, A. T. *J. Catal.* **1999**, *186*, 222.

[53] Vjunov, A.; Derewinski, M. A.; Fulton, J. L.; Camaioni, D. M.; Lercher, J. A. *J. Am. Chem. Soc*. **2015**, 137, 10374.

[54] Kiricsi, I.; Flego, C.; Pazzuconi, G.; Parker, W. O., Jr.; Millini, R.; Perego, C.; Bellussi, G. *J. Phys. Chem.* **1994**, *98*, 4627.

[55] S. Schallmoser, T. Ikuno, M.F. Wagenhofer, R. Kolvenbach, G.L. Haller, M. Sanchez-Sanchez, J.A. Lercher, *J Catal.* **2014**, *316* 93.

[56] A. Janda, A.T. Bell, *J. Am. Chem. Soc.* **2013**, *135* 19193.

[57] Datka, J.; Abramowicz, T. *J. Am. Chem. Soc. Faraday. Trans.* **1994**, *90*, 2417.

[58] Nawrocki, J. *J. Chromatogr. A* **1997**, *779*, 29.

[59] Ravenelle, R.M.; Schüβler, F.; D'Amico, A.; Danilina, N.; van Bokhoven, J.A.; Lercher, J.A.; Jones, C.W.; Sievers, C. *J. Phys. Chem. C* **2010**, *114*, 19582.

[60] Primo, A.; Garcia, H. *Chem. Soc. Rev.* **2014**, *43*, 7548.

[61] (a) van Bokhoven, J. A.; van der Eerden, A. M. J.; Koningsberger, D. C. *J. Am. Chem. Soc.* **2003**, *125*, 7435; (b) Maier, S. M.; Jentys, A.; Lercher, J. A. *J. Phys. Chem. C* **2011**, *115*, 8005.

[62] van Bokhoven, J. A.; Koningsberger, D. C.; Kunkeler, P.; van Bekkum, H.; Kentgens, A. P. M. *J. Am. Chem. Soc.* **2000**, *122*, 12842.

[63] Deng, F.; Yue, Y.; Ye, C. *J. Phys. Chem. B* **1998**, *102*, 5252.

[64] Hunger, M.; Engelhardt, G.; Weitkamp, J. *Microporous Mater.* **1995**, *3*, 497.

[65] Pérez-Pariente, J.; Sanz, J.; Fornés, V.; Corma, A. *J. Catal.* **1990**, *124*, 217.

[66] Schallmoser, S.; Ikuno, T.; Wagenhofer, M. F.; Kolvenbach, R.; Haller, G. L.; Sanchez-Sanchez, M.; Lercher, J. A. *J. Catal.* **2014**, *316*, 93.

[67] Lutz, W.; Toufar, H.; Kurzhals, R.; Suckow, M. *Adsorption* **2005**, *11*, 405.

[68] Zhang, L.; Chen, K.; Chen, B.; White, J. L.; Resasco, D. E. *J. Am. Chem. Soc.* **2015**, *137*, 11810.

[69] Ballantine, J. A.; Davies, M.; Patel, I.; Purnell, J. H.; Rayanakorn, M.; Williams, K. J.; Thomas, J. M. *J. Mol. Catal.* **1984**, *26*, 37.

[70] Smith, L.; Cheetham, A. K.; Morris, R. E.; Marchese, L.; Thomas, J. M.; Wright, P. A.; Chen, J. *Science* **1996**, *271*, 799.

[71] Sárkány, J. *Appl. Catal. A* **1999**, *188*, 369.

[72] Corma, A.; Agudo, A. L. p.; Fornés, V. *J. Am. Chem. Soc., Chem. Commun.* **1983**, 942.

[73] Jones, A.; Iglesia, E. *ACS Catal.* **2015**, *5*, 5741.

[74] Hunger, M. *Catal. Rev.-Sci. Eng.* **1997**, *39*, 345.

[75] Dědeček, J.; Sobalík, Z.; Wichterlová, B. *Catal. Rev.* **2012**, *54*, 135.

[76] Aronson, M. T.; Gorte, R. J.; Farneth, W. E. *J. Catal.* **1986**, *98*, 434.

[77] Zhi, Y.; Shi, H.; Mu, L.; Liu, Y.; Mei, D.; Camaioni, D. M.; Lercher, J. A. *J. Am. Chem. Soc.* **2015**, *137*, 15781.

[78] Knaeble, W.; Iglesia, E. *J. Phys. Chem. C* **2016**, *120*, 3371.

Chapter 4

Solid acid catalyzed alkylation of phenol with cyclohexanol and cyclohexene in liquid phase

Liquid-phase alkylation of phenol with cyclohexanol/cyclohexene in decalin has been investigated over a range of solid acids under mild conditions (≤ 160 °C). Phenol alkylation with cyclohexanol and cyclohexene is catalyzed primarily by Brønsted acid sites (BAS) on solid surfaces. Moderately strong BAS and spacious microporous environments (*e.g.*, large-pore acidic zeolites HBEA and HY) are important criteria for effective phenol alkylation to C-C coupling products, while very strong BAS is responsible for rapid catalyst deactivation in decalin. O-alkylation is kinetically favored and reversible, while C-alkylation occurs preferentially at *ortho*/*para* positions in an irreversible manner. For reactions carried out in decalin, carbenium ion is the direct electrophile for phenol alkylation with either cyclohexanol or cyclohexene. A dominant fraction of cyclohexanol in HBEA pore takes on a protonated dimer form. Carbenium ion can be produced from the alcohol monomer, but not from the protonated dimer species. Adsorption and protonation of olefin at the BAS also produces carbenium ion, and exhibits a relatively low apparent activation barrier (< 50 kJ mol^{-1}). Olefin re-adsorption, however, is greatly suppressed by the presence of alcohol dimer, leading to low alkylation rates at the initial stage of phenol-cyclohexanol alkylation on HBEA zeolites. Reducing the concentration of cyclohexanol leads to exponential increases in initial dehydration and alkylation rates. Adsorption and kinetic measurements show that phenol alkylation with cyclohexene occurs via an Eley-Rideal type mechanism on HBEA in decalin. Phenol alkylation with cyclohexanol is much slower in water than in decalin, due to the much higher barriers for the formation of carbenium ion at the hydronium ion, *i.e.*, the active site in aqueous phase.

4.1 Introduction

Alkylated phenols have been widely used as antioxidant, lubricant oil additives and as hosts of consumer products.[1,2] Biomass-derived phenolic oils, obtained from pyrolysis or hydrolysis of lignin, is becoming a promising feedstock to replace fossil resources for the production of fuels and chemicals via catalytic upgrading.[3-5] Liquid-phase bifunctional hydrodeoxygenation (HDO) offers a feasible scheme for upgrading the biomass-derived phenolics into cycloalkanes via a cascade of steps including hydrogenation (on metal) and dehydration (on acid) under relatively mild conditions.[6] In addition to oxygen removal, acid-catalyzed C–C bond coupling can also take place in the bifunctional HDO process, producing alkylated phenols in the desirable carbon-number range of fuels from reactions of phenolic compounds with small alcohols[7] (from hydrogenation of small carboxylic acids and ketones) or with hydrogenated/hydrodeoxygenated intermediates of phenolics (cycloalcohols or cycloalkenes).[8]

Phenol, the simplest phenolic monomer unit constituting lignin, has been extensively studied as a model compound for bio-oil.[5,6,8] The hydroxyl group of phenol strongly activates the aromatic ring toward electrophilic substitution at the *ortho*- (*o*-C-alkylation) and *para*- (*p*-C-alkylation) positions.[9] Moreover, nucleophilic attack of the phenolic -OH on the alkylating agent (*e.g.*, carbocation) can lead to the formation of ethers (O-alkylation).[10,11] Both Brønsted and Lewis acids are found to catalyze gas- and liquid-phase alkylation of phenol, and heterogeneous acid catalysts are preferred to homogeneous acids for reasons such as easier product separation and catalyst reuse, environmental benignity and, sometimes, a higher degree of selectivity control.

As is true for alkylation of other aromatics, the catalytic activity and preferred reaction pathway of solid-acid-catalyzed phenol alkylation generally depend on the type and strength of acid sites, the alkylating agent (electrophile), reaction temperature, as well as solvent when the reaction is performed in the liquid phase.[7,12-22] For instance, it was first suggested by Tanabe and later by others that *ortho*-substitution is preferred at Lewis acid sites (LAS) on oxides because of a vertical adsorption geometry of phenol on such surfaces.[17,18] In addition, it was often claimed that weak acid sites favor O-

alkylation of phenol with alcohols while strong acid sites preferentially catalyze C-alkylation and di-alkylation.[19] Ether (O-alkylation) is the predominant product when the reactions are performed at low temperature,[20] and the ratios of *ortho*/*para*-substitution products is related to the nature of the olefin employed[21] as well as the type of catalyst.[20] For phenol alkylation with olefin, carbenium ion is considered as the direct alkylating agent.[23-26] The electrophilic substitution at *ortho* positons in phenol alkylation is favored when a secondary carbocation is the electrophile.[21] Carbocation generated from dehydration of cyclohexanol is also suggested as the reactive intermediate in the solvent-less alkylation of phenol with cyclohexanol on solid catalysts.[27] Alternatively, alkyl phenols have also been reported to be produced form intramolecular rearrangement of alkyl aryl ethers.[9,20,22,28]

In the literature, conflicting opinions exist regarding the kinetic mechanism (*i.e.*, Langmuir-Hinshelwood and Eley-Rideal, abbreviated as L-H and E-R) for the alkylation of aromatics. It was suggested by Smirniotis and Ruckenstein that both the pore size of the zeolite and the size of the alkylating agent can determine the kinetic mechanism for alkylation.[29] An E-R type mechanism is favored over a L-H type mechanism for alkylation of benzene on large-pore zeolites such as HY, HBEA and MCM-22[29,30], while both L-H and E-R models have been found to describe alkylation of aromatics with olefin or alcohol on medium-pore zeolites such as HZSM-5[29]. Adsorbed phenol molecules are considered as less reactive species since the electronic density on the aromatic ring is decreased upon interaction with an acid site, rendering an electrophilic attack more difficult. Thus, an E-R type mechanism, with phenol reacting from the liquid phase and cyclohexene reacting as adsorbed species on the surface of the catalyst, is considered by some to be more favorable.[31]

Previous studies on the alkylation of phenol used straight-chain or branched alcohols or alkenes as the alkylating agent over solid catalysts in vapor- or liquid-phase.[10,11,20] However, alkylation of phenol with intermediate products derived from itself during the bifunctional HDO, *i.e.*, cyclohexanol (hydrogenation of phenol) and cyclohexene (dehydration of cyclohexanol), has not been sufficiently explored in the liquid phase. For liquid phase alkylation, solvent can also play an important role in determining the prevalent alkylation mechanism, especially when there are multiple types of potential

alkylating agents (*e.g.*, alkoxonium ion and carbenium ion for alcohol as the co-reactant). We previously reported (hydro)alkylation reactions of phenol and substituted phenols with cyclohexanol using heterogeneous catalysts in aqueous phase.[8,32] Hydroalkylation using substituted phenols in aqueous phase was studied in the presence of Pd/C and varied solid acids.[8] Only large-pore zeolites (*e.g.*, HBEA) exhibited a significant alkylation activity, while other solid acids, such as Amberlyst®15, Nafion/SiO_2 (SAC-13), $Cs_{2.5}H_{0.5}PW_{12}O_{40}$ and H_2SO_4-ZrO_2, catalyzed only alcohol dehydration. With non-zeolitic solid acids, the reason for their inactivity in alkylation was attributed to the limited adsorption of phenol and cyclohexanol, as evidenced by the gas-phase infrared spectroscopy. It was concluded that Brønsted acidic sites (effectively, hydronium ions) confined in a spacious micropore environment deliver efficient phenol alkylation in aqueous phase.

Herein, we report a comprehensive study of solid-acid catalyzed alkylation of phenol, with cyclohexanol or cyclohexene as the co-reactant, in a non-polar liquid phase. Decalin was used as the solvent due to the high solubilities of cyclic and aromatic compounds in it, which makes it more convenient to investigate the reaction kinetics in a single phase. After testing a variety of solid acids, we focused on one of the representative and most active large-pore zeolites, HBEA, to further explore the kinetic and mechanistic aspects of phenol alkylation in decalin and compare those with earlier reports on aqueous phase phenol alkylation on the same catalyst. We show that solvent can dramatically alter the catalytic activity by changing the nature of the most abundant surface species and the pathway via which the electrophile is produced.

4.2 Experimental section

4.2.1 Chemicals

All chemicals were obtained from commercial suppliers: phenol (Sigma-Aldrich, > 99% GC assay), cyclohexanol (Sigma-Aldrich, > 99% GC assay), cyclohexene (Sigma-Aldrich, > 99% GC assay), decalin (Sigma-Aldrich, > 99%, anhydrous mixture of cis +

trans), 2-cyclohexen-1-one (Sigma-Aldrich, ≥ 95%), ethyl acetate (Sigma-Aldrich, > 99.9% HPLC assay), hydrogen (Westfalen AG, 99.999 vol%).

4.2.2 Catalysts

HBEA-150 (Süd Chemie, Si/Al = 75), HBEA-38 (Zeolyst, Si/Al = 19), HY-80 (Zeolyst, Si/Al = 40), HY-30 (Zeolyst, Si/Al = 15), HZSM-5-90 (Süd Chemie, Si/Al = 45), SAC-13 (13 wt. % Nafion on silica, Sigma–Aldrich), γ-Al_2O_3 (Evonik). All zeolite catalysts were obtained in H-form and activated at 500 °C in air for 6 h before use. γ-Al_2O_3 was calcined at 500 °C 4 h prior to use. SAC-13 was dried at 180 °C for 2 h in N_2 atmosphere before being used in the reaction.

4.2.3 Catalysts characterizations

The BET specific surface area and pore volume were determined by nitrogen adsorption-desorption isotherms measured at -196 °C using a PMI automatic Sorptometer. The samples were activated in vacuum at 200 °C for 2 h before measurement. Apparent surface area was calculated by applying the Brunauer-Emmett-Teller (BET) theory, and the t-plot method was used to determine the pore volumes.

The scanning electron microscopy (SEM) was recorded on a JEOL 500 SEM-microscopy (accelerating voltage 25 kV). The samples were prepared by depositing a drop of an ultrasonicated methanol suspension of the solid material onto a carbon-coated Cu grid. The dry samples were gold-coated prior to scanning.

The crystal structures of the zeolites were analyzed by X-ray powder diffraction (XRD) using a Philips X'Pert Pro System, with the Cu-Kα radiation source operating at 45 kV and 40 mA. The samples were measured with a scanning rate of 0.017 °/s in the range of 5–70 ° (2θ).

The infrared (IR) spectra of adsorbed pyridine were recorded on a Perkin-Elmer 2000 spectrometer at a resolution of 4 cm^{-1}. For zeolites and γ-Al_2O_3, the sample was loaded as a self-supporting wafer and activated in vacuum (p = 10^{-6} mbar) at 450 °C for 1 h (heating rate = 10 K min^{-1}). After cooing to 150 °C, the sample was equilibrated with 0.1 mbar of pyridine for 30 min followed by outgassing for 1 h, after which a spectrum with the chemisorbed pyridine was recorded. Finally, a desorption program (up to 450 °C

with 10 K min^{-1} and 0.5 h at 450 °C) was employed and the spectra were recorded until adsorption equilibrium was achieved. For SAC-13, the sample was activated at 180 °C for 2 h, without performing a high temperature (≥ 180 °C) desorption step, due to the low thermal stability of the sulfonate group. The concentrations of Brønsted and Lewis acid sites were calculated from the integral intensities of the peaks at 1540 and 1450 cm^{-1}, respectively, in the IR spectra of adsorbed pyridine. The amount of pyridine molecules retained after evacuation at 150 and 450 °C were used to determine the concentrations of total and strong acid sites, respectively. For quantification, molar integral extinction coefficients of 0.73 and 0.96 cm μmol^{-1} were used for Brønsted and Lewis acid sites, respectively. The extinction coefficients were determined from a standard sample for which the acid concentrations are known (HZSM–5, Si/Al = 45 from Clariant).

Temperature programmed desorption (TPD) of NH_3 was performed in a 6–fold parallel reactor system. The solid catalysts were activated in He at 500 °C with a heating rate of 5 °C min^{-1} for 1 h. NH_3 was adsorbed with a partial pressure of 1 mbar at 100 °C. Subsequently, the samples were purged with He (30 mL min^{-1}) for 2 h to remove physisorbed molecules. For the TPD measurement, the samples were heated up in flowing He from 100 to 760 °C with a temperature increment of 10 °C min^{-1} to desorb NH_3. The desorbed NH_3 (channel m/z =16) were monitored by mass spectrometry (Balzers QME 200). For acid site quantification, a reference (HZSM-5 with Si/Al = 45 from Clariant) with known acidity was used to calibrate the signal.

IR spectra of adsorbed cyclohexene were recorded on a Bruker VERTEX 70 spectrometer at a resolution of 4 cm^{-1} with 150 scans. The sample wafers were activated at 450 °C for 1 h, and then cooled down to 40 °C. The adsorbates were stepwise introduced into the vacuum system and the equilibration with the adsorbates was performed in small pressure steps. The spectra were recorded after reaching the equilibrium.

Liquid-phase adsorption isotherms of phenol and cyclohexanol onto HBEA-150 were obtained by immersing 20 mg of zeolite in a decalin solution containing phenol or cyclohexanol at a defined concentration at 25 °C for at least 24 h. The solution was

separated from the zeolite and the residual concentration was determined via a gas chromatograph (GC) using 2-cyclohexen-1-one as internal standard.

4.2.4 Catalytic reactions

Phenol alkylation with cyclohexanol over various solid acids in decalin. A typical experiment was carried out in the Parr reactor (Series 4843, 300 mL), phenol (5.0 g), cyclohexanol (5.0 g) and HBEA-150 catalyst (0.2 g) mixed with 100 mL decalin was charged into the autoclave and reacted at 160 °C. After loading the mixture, the reactor was firstly flushed with 3 MPa H_2 three times, charged with 5 MPa H_2, and then heated up. The time at which the temperature reached the set point was counted as time zero. The stirring speed was kept at 700 rpm. In some cases, there were already appreciable extents of reaction during heat-up. The real-time sampling was employed and the chemicals were detected by a gas chromatograph (GC, Shimadzu 2010) with a HP-5 capillary column (30 m × 250 μm) and flame ionization detector (FID). In addition, a gas chromatograph combined with a mass spectrometer (GC-MS, Shimadzu QP 2010S) was used to identify the organic compounds.

The calculations of conversion and yield were based on carbon mole basis. Conversion = (weight of converted reactant/weight of the starting reactant) × 100 %. Yield of liquid products (C %) = (C atoms in liquid products/C atoms in the starting reactant) × 100 %. The carbon balance in the liquid phase for all experiments was better than 90 ± 5 % in this work.

Phenol alkylation with cyclohexene over various solid acids in decalin. For the reaction of phenol-cyclohexene alkylation, phenol (5.0 g), cyclohexene (5.0 g), catalyst (1.0 g) and 100 mL decalin was loaded into the 300 mL Parr reactor. The reaction was carried out at 160 °C under 5 MPa H_2 (charged at ambient temperature) and a stirring speed of 700 rpm. Samples were analyzed through GC and GC-MS.

Kinetic measurements of cyclohexanol dehydration over HBEA-150 in decalin. The dehydration of cyclohexanol was also performed in the same Parr reactor: cyclohexanol (0.05-20 g), HBEA-150 (0.02-0.2 g), and 100 mL decalin were sealed in the reactor. The reactions were carried out at 160 °C. For all cases, the reactor was then pressurized with 5

MPa H_2 and heated up while stirred at 700 rpm. Samples were analyzed through GC and GC-MS. Turnover frequencies (TOFs), defined as the mole of produced cyclohexene per mole of BAS per second, were determined as initial reaction rates with the conversion of cyclohexanol below 10%.

Kinetic measurements of phenol alkylation with cyclohexene over HBEA-150 in decalin. Kinetic measurements for alkylation were performed at 130–160 °C in Parr reactor using HBEA-150 as the catalyst. A typical reaction in decalin: 0.05 mol cyclohexanol, 0.05 mol cyclohexene, 0.1 g HBEA-150 and 100 mL decalin. Reactions were performed under 5 MPa H_2 at ambient temperature and a stirring speed of 700 rpm. Samples were analyzed through GC and GC-MS. The initial rate was calculated by the first derivative at time zero of the function obtained by the regression of product formation data with the function of $y=y_0+Aexp\ (-x/t)$.

Phenol alkylation with cyclohexnaol over HBEA-150 in aqueous phase. For the aqueous phase phenol-cyclohexanol alkylation at 170°C, an example of a typical reaction: phenol (5.0 g), cyclohexanol (5.0 g), HBEA-150 (1.0 g) and 100 mL water was sealed in the reactor. The reactor was then pressurized with 5 MPa H_2 and heated up with a stirring speed of 700 rpm. After the reaction, the reactor was cooled using ice/water mixture. The organic phase was extracted using 60 mL ethyl acetate (mixed with internal standard, 2-cyclohexen-1-none) and analyzed through GC and GC-MS.

Kinetic measurements of phenol alkylation with cyclohexene over HBEA-150 in aqueous phase. Kinetic measurements for aqueous-phase phenol-cyclohexene alkylation were carried out at 140–170 °C. A typical reaction: phenol (0.05 mol), cyclohexene (0.05 mol), HBEA-150 (0.4 g), and 100 mL water were charged in the reactor. The reaction operations, products extraction and analysis were mentioned above.

Dehydration and alkylation reactions operated in glove box. The cyclohexanol, cyclohexene and decalin were died by 3A zeolite in Schlenk flask. The catalyst and phenol was dried at 200°C in Schlenk tube with N_2 gas flow for 2 h. The Schlenk flasks/tubes were sealed and then transferred to the glove box. The Parr autoclave, together with stirrer, was preheated at 100°C before transferred into the glove box. A reaction mixture was charged into the autoclave, sealed in glove box and then transferred

out for the dehydration and alkylation reactions. The operations outside of the glove box were described above.

4.3 Results and discussion

4.3.1 Physicochemical properties of the solid acids

Table 4-1. Acidity measurements of the studied catalysts using TPD of NH_3 and IR spectra of adsorbed pyridine

Entry	Sample	Acid sites determined by Py-IR (mmol g^{-1}) [a]						TPD-NH_3 (mmol g^{-1})
		Brønsted	Lewis	Total	Strong Brønsted	Strong Lewis	Strong total	
1	HBEA-150	0.19	0.04	0.23	0.18	0.03	0.21	0.21
2	HBEA-38	0.54	0.30	0.84	0.50	0.23	0.73	0.68
3	HY-80	0.15	0.01	0.16	0.10	0.01	0.11	0.15
4	HY-30	0.60	0.23	0.83	0.13	0.17	0.30	0.62
5	HZSM-5-90	0.36	0.05	0.41	0.32	0.03	0.35	0.38
6	γ-Al_2O_3	0	0.09	0.09	0	0.03	0.03	0.09
7	SAC-13	0.12	0	0.12	-[b]	-[b]	-[b]	-[b]

[a] The amount of pyridine molecules retained after evacuation at 150 and 450 °C were used to determine the concentrations of total and strong acid sites, respectively. [b] Desulfonation of SAC-13 occurs at temperatures above 210 °C,[33] thus, the temperature programed desorption of pyridine and NH_3 could not be carried out on this material.

The acid site (Brønsted/Lewis) concentrations of the studied catalytic materials were characterized by IR spectroscopy of adsorbed pyridine (**Figure 4A-1**, in **Appendix**) and TPD of NH_3. The quantitative results are compiled in **Table 4-1**. In general, acidities determined by NH_3-TPD are in good agreement with the total acid concentrations measured by IR using pyridine as a probe molecule. Most of the BAS in HBEA and HZSM-5 zeolites qualify as strong sites that are defined as those able to retain pyridine even after a desorption step at 450 °C (see Experimental). In comparison, Y-type zeolites, especially HY-30 (entry 4), exhibited a notably lower fraction of strong BAS. The majority of LAS in all the five zeolites were found to be strong. Silica-supported Nafion (SAC-13) contained exclusively BAS (entry 7) with the intrinsic acid strength similar to concentrated H_2SO_4.[34] The BAS concentration of SAC-13 was determined to be

0.12 mmol g^{-1}, in good agreement with previous reports. [35,36] γ-Al_2O_3 contained only LAS (0.09 mmol g^{-1}), two thirds of which is classified as relatively weak sites (i.e., not able to retain pyridine at 450 °C). Other properties of these solid acids, including pore volume and particle size, are shown in the **Appendix** (**Table 4A-1, Figs. 4A-1, 4A-2, 4A-3**).

4.3.2 Alkylation of phenol with cyclohexanol/cyclohexene

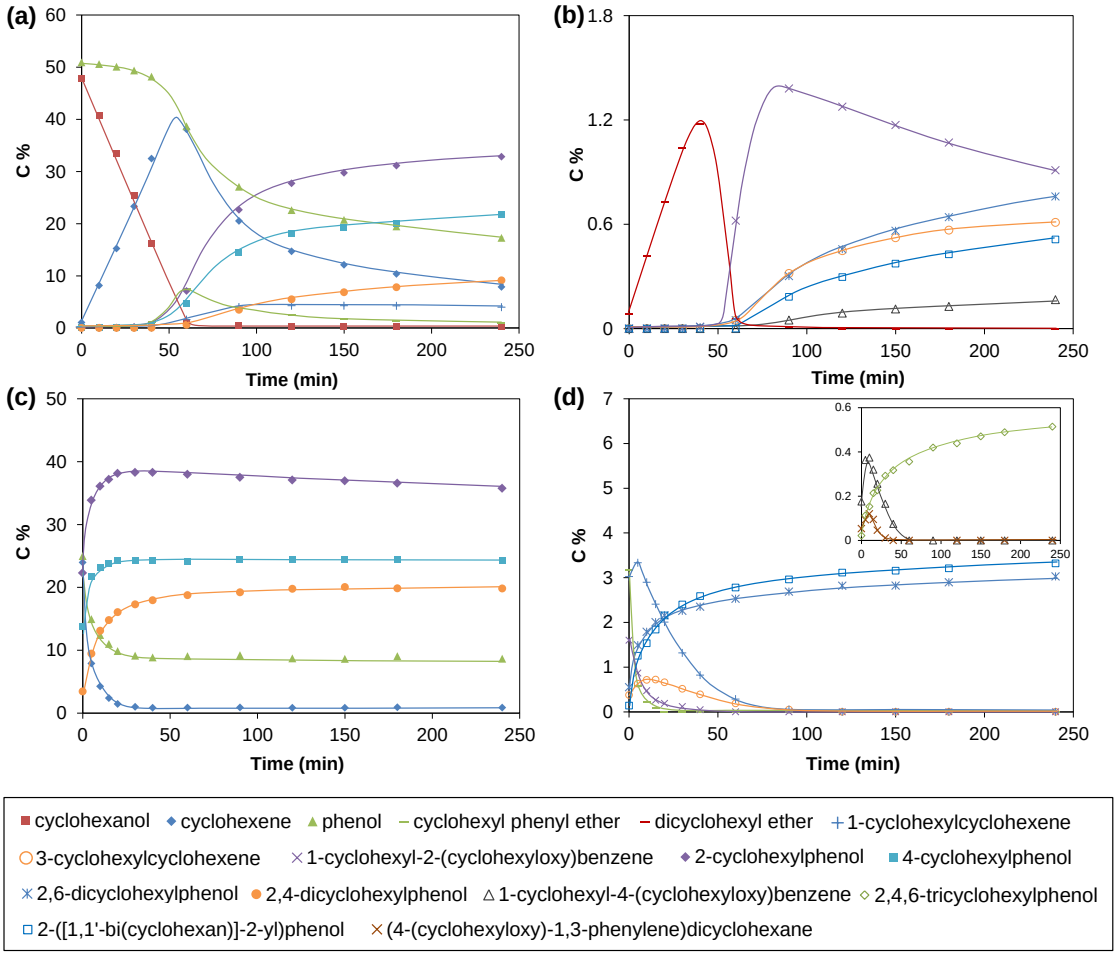

Figure 4-1. Carbon-based concentration-time profiles of phenol alkylation with cyclohexanol (a, b) and cyclohexene (c, d) on HBEA-150 in decalin. Reaction conditions: 5.0 g phenol, 5.0 g cyclohexanol (a, b) or cyclohexene (c, d), 0.2 g (a, b) or 1.0 g (c, d) HBEA-150, 100 mL decalin, 5 MPa H_2 (ambient temperature), stirred at 700 rpm, 160 °C.

Cyclohexanol or cyclohexene was used as the co-reactant for phenol alkylation. The chemical structures of the related compounds (reactants and products) are compiled in **Fig. 4A-4**. The carbon-based concentration-time profiles of these reactions are presented in **Fig. 4-1** for HBEA-150 and in **Appendix** (**Section A2**) for other catalysts. No products were formed from the phenol-cyclohexanol-cyclohexene mixture over α-Al_2O_3 under the studied conditions (**Fig. 4A-5**), indicating the absence of non-catalytic thermal reactions.

Fig. 4-1 (a) and **(b)** show the concentration-time profiles for the reaction of phenol and cyclohexanol in decalin at 160 °C on HBEA-150. Dehydration of cyclohexanol was almost the only reaction for the first 40 min (**Fig. 4-1 (a)**), forming cyclohexene and dicyclohexyl ether (DCHE), while phenol remained largely unreacted (less than 2 % conversion; TOF of $\sim 3.5\times10^{-3}$ s^{-1}). The intermolecular dehydration product of cyclohexanol, DCHE, reached its maximum concentration (<1.2 C%) in 40 min, but quickly disappeared afterwards (**Fig. 4-1 (b)**). The C-C and C-O bond coupling, forming alkylated phenols, cyclohexylcyclohexenes and alkyl phenyl ethers, had been hardly detectable until ~ 70 % of cyclohexanol was dehydrated to cyclohexene, which started to decrease after cyclohexanol was fully converted. In contrast, phenol alkylation occurred in parallel with cyclohexanol dehydration on HBEA-38 and the two HY zeolites (**Figs. 4A-6, 4A-7, 4A-8**). The C-C alkylation products kept increasing with increasing residence time after 40 min, while most of the C-O alkylation products, *e.g.*, cyclohexyl phenyl ether (CHPE), first increased and then decreased. No de-alkylation or cracking of alkylation products was observed during the whole reaction course, suggesting that C-alkylation is virtually irreversible (further discussed at the end of this section).

Ortho- and *para*-substitutions were observed with different selectivities on different catalysts. On HBEA, the ratio of 2-cyclohexylphenol (2-CHP) and 4-cyclohexylphenol (4-CHP) was somewhat larger than 1 but less than 2 (**Fig. 4-1 (a) and 4A-6**). On the two HY zeolites, this ratio was *ca.* 3, larger than the statistical ratio (2:1). Thus, the more spatially demanding *ortho*-substitution product was formed with a higher selectivity inside larger pores (*i.e.*, HY). Meta-substitution, *e.g.*, 3-cylohexylphenol (3-CHP), was not detected on any of the studied catalysts. Di-alkylation was observed on HBEA and HY zeolites, preferably producing 2,4-dicyclohexylphenol (2,4-DCHP). On HY, the 2,6-DCHP was produced at much higher selectivities than on HBEA, apparently also for

steric reasons. Phenol-cyclohexanol alkylation was observed to a much smaller extent on SAC-13, forming only CHPE, 2- and 4-cyclohexylphenol (**Fig. 4A-9**).

Finally, we note that the formation of phenol alkylation and olefin dimerization products became very slow after 240 min (**Fig. 4-1 (a)** and **(b)**). Adding more catalysts (0.4 g) could further increase the yields of C–C coupling products (**Fig. 4A-10**). The increasingly slower conversion at higher residence times was caused by depletion of reactants and catalyst deactivation, which could be due to oligomerization of olefin that results in coke formation, or strong adsorption of phenolic compounds.[37] Alkylation of phenol with cyclohexanol was faster on HBEA-38 than on HBEA-150 in the first 40 min, but became slower on HBEA-38 than on HBEA-150 afterwards (cf. **Figs. 4-1** and **4A-6**). Thus, catalyst deactivation occurred to a greater extent on HBEA-38. Unlike HBEA, the two HY zeolites (SiO_2/Al_2O_3 = 80 and 30) exhibited comparable product evolution patterns from alkylation (cf. **Figs. 4A-7** and **4A-8**). We tentatively attribute the different impacts of the Si/Al ratio on catalyst deactivation to the different distributions of acidity for HBEA and HY zeolites (**Table 4-1**). Specifically, all types of acid sites are present at much higher concentrations in HBEA-38 than in HBEA-150, while the two HY zeolites contain comparable concentrations of strong BAS, 0.10 - 0.13 mmol g^{-1}. Thus, it seems plausible that that catalyst deactivation occurs mainly at these strong BAS.

When cyclohexene was used to alkylate phenol on HBEA-150, alkylation started instantaneously (**Fig. 4-1 (c)** and **(d)**). 2-, 4-CHP and 2,4-DCHP were among the major products, accounting for more than 80 C% in total. The formation rates of these products were much faster than when using cyclohexanol as the co-reactant; the kinetic data are shown in Section 2.4. The selectivity pattern appeared largely similar to those for phenol-cyclohexanol alkylation, except for significantly higher selectivity towards di-alkylation (especially 2,4-DCHP) and lower selectivity to O-alkylation (CHPE). Within the minor products, three-ring products were formed at somewhat higher yields than in phenol-cyclohexanol alkylation, at the expense of some two-ring products such as 1- and 3-cyclohexylcyclohexenes (1- and 3-CC). The plateaus of product concentrations were at different levels when using zeolite HY-80 (**Fig. 4A-11**), indicating that the final composition of the mixture was not set by reaction thermodynamics. Because of the significant amount of di-alkylation products (**Fig. 4-1 (c)**), phenol was in excess and

cyclohexene was almost completely converted, causing the conversion to cease after 50 min. On the medium-pore zeolite HZSM-5, the major product was CHPE, while C-alkylation remained low (< 2%) and limited to mono-alkylation, producing 2- and 4-CHP in an equimolar ratio (**Fig. 4A-12**). The low alkylation activity on HZSM-5 was attributed to the small confining space which limited the formation of transition sates or the diffusion of the products, rather than the inaccessibility of the reactant to acidic OH groups. This is also in line with our previous study, performed in aqueous phase, showing that HZSM-5 only favored the dehydration of cyclohexanol but not alkylation.[8] In contrast to its poor performance in phenol-cyclohexanol alkylation, SAC-13 showed a high activity, comparable to those of HBEA and HY zeolites in phenol-cyclohexene alkylation (**Fig. 4A-13**). The *ortho*- to *para*- ratio for mono-C-alkylation was 3.5:1 on SAC-13. This ratio being higher than those observed for zeolites is indicative of little steric constraints on the transition states for alkylation on SAC-13. With initially added water, much lower activity in dehydration (**Fig. 4A-14**) as well as alkylation (**Table 4A-2**) was observed. This suggests that water produced by the dehydration of cyclohexanol deactivates SAC-13 by competitive adsorption or swelling.

The alkylation of phenol with cyclohexene was also studied over γ-Al_2O_3, which contained only LAS (~ 90 mmol g^{-1}). γ-Al_2O_3 did not detectably catalyze any reactions at 160 °C and showed a low activity even at 200 °C for both dehydration (**Fig. 4A-15**) and alkylation (**Fig. 4A-16**). These results suggest that the similar LAS on zeolite catalysts are also inactive for C-C coupling at 160 °C. Interestingly, LAS-catalyzed alkylation gave a 2-CHP selectivity of ~80 % and the highest ratio of *ortho*/*para* substitution (~110), characteristically different from BAS-catalyzed alkylation. Based on a detailed infrared study of a series of methylated phenols chemisorbed on γ-Al_2O_3,[38] Taylor and Ludlum proposed that phenol forms a phenolate species which has its aromatic ring titled upward such that the *para* position is farther away from the oxide surface than the *ortho* position. This would explain the exceptionally high selectivity to *ortho*-substitution on γ-Al_2O_3 (**Table 4-2**).

Table 4-2 compiles the selectivities to six main C-C and C-O coupling products (1-CC, 2- and 4-CHP, 2,4- and 2,6-DCHP, CHPE) over different catalysts at the reaction time of 240 min, after which only slight changes in the composition of reaction mixture

Table 4-2. Alkylation of phenol with cyclohexanol or cyclohexene on different solid acids[a]

Entry	Catalyst	Reactants	Conv.[b] (%)	Alkylation products selectivity[c] (%)						Sum[d] (%)
				2-CHP	4-CHP	2,4-DCHP	2,6-DCHP	1-CC	CHPE	
1	HBEA-150	Phenol, cyclohexanol	66.1, 99.6	40.9	27.2	11.4	0.9	5.0	1.2	86.6
2	HY-80	Phenol, cyclohexanol	55.1, 99.4	37.1	11.4	15.2	5.6	1.2	3.4	73.9
3	HBEA-38	Phenol, cyclohexanol	48.1, 99.1	31.9	21.2	3.2	0.4	2.7	5.5	64.9
4	HY-30	Phenol, cyclohexanol	51.0, 99.3	38.4	12.0	11.2	4.3	1.0	3.2	70.1
5	SAC-13	Phenol, cyclohexanol	11.2, 98.3	5.8	2.4	0	0	0	12.0	20.2
6	HBEA-150	Phenol, cyclohexene	81.5, 98.4	41.9	28.5	23.2	3.5	0	0	97.1
7	HY-80	Phenol, cyclohexene	79.8, 96.6	30.6	9.9	39.4	16.0	0	0	95.9
8	HZSM-5-90	Phenol, cyclohexene	8.4, 9.9	15.5	14.7	0	0	1.5	67.5	99.2
9	SAC-13	Phenol, cyclohexene	87.3, 97.8	40.2	11.3	26.2	12.9	0	0	90.6
10	γ-Al_2O_3	Phenol, cyclohexene	18.7, 20.0	78.9	0.7	0.2	0.1	0	20	99.9

[a] Reaction conditions: phenol (5.0 g), cyclohexanol (5.0 g), cyclohexene (5.0 g), decalin (100 mL), solid catalyst (0.2-1.0 g, detailed catalyst amounts shown in SI), 5 MPa H_2 (ambient temperature), 240 min, stirred at 700 rpm. [b] The two values correspond to the individual conversions of the two reactants. [c] 2-CHP, 4-CHP, 2,4-DCHP, 2,6-DCHP, 1-CC and CHPE are the abbreviations of 2-cyclohexylphenol, 4-cyclohexylphenol, 2,4-dicyclohexylphenol, 2,6-dicyclohexylphenol, 1-cyclohexylcyclohexene and cyclohexyl phenyl ether respectively. [d] Values represent the sum of six products listed in the table.

could be observed. For phenol-cyclohexanol alkylation, HBEA-150 showed much higher selectivities to C-C coupling compared to HBEA-38, with total C-selectivities to the six products being ~87% and ~65 %, respectively (cf. entry 1 and 3). In comparison, HY zeolites with SiO_2/Al_2O_3 ratios of 80 and 30 yielded similar quantities of alkylation products at the end of reaction (see entry 2 and 4). Higher conversions of reactants and

selectivities to alkylation products were observed when cyclohexene was the co-reactant on large-pore zeolites (HBEA and HY, with effective pore opening of 0.66 and 0.74 nm, respectively) and SAC-13 (see entry 6, 7 and 9). The formation of two-ring products was favored on HBEA-150 (with selectivity of ~70%, entry 6), while HY-80 showed enhanced formation of three-ring products (with selectivity of ~56%, entry 7). The selectivities to two- and three-ring products were ~52 % and ~39 % over SAC-13 under the same conditions (entry 9). On the medium-pore zeolite HZSM-5 with an effective pore opening of 0.56 nm, a low alkylation activity between phenol and cyclohexene was observed (~2.3 C% of C-alkylation and ~5 C% O-alkylation after 240 min of reaction, entry 8).

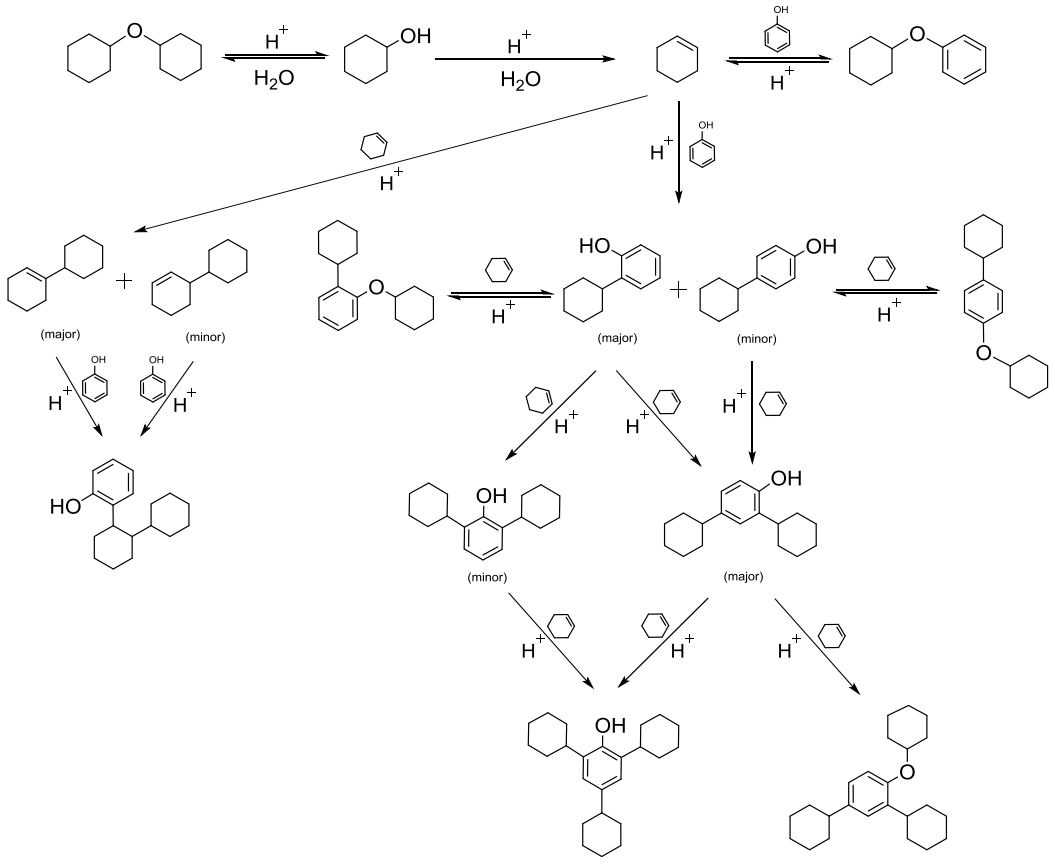

Scheme 4-1. Proposed reaction pathways for alkylation of phenol with cyclohexanol over BAS (H^+) in decalin at 160 °C. Major and minor products are defined based on their relative selectivities. C-alkylation steps are shown as irreversible (one-directional arrows) and O-alkylation steps are drawn as reversible (double arrows).

A reaction network for phenol-cyclohexanol alkylation, consistent with all the experimental observations described above, is shown as **Scheme 4-1**. We only consider BAS-catalyzed pathways hereafter, as LAS are demonstrated to be much less active under the applied conditions (see above). Cyclohexanol dehydration forms cyclohexene and DCHE as the initial products. Phenol alkylation hardly occurs before a majority of cyclohexanol is converted via dehydration. Cyclohexene, or, effectively, the carbenium ion generated from its adsorption at BAS, is a more potent alkylating agent (electrophile) than cyclohexanol (or protonated cyclohexanol). The cyclohexylphenols react with cyclohexene to from the three-ring or even larger C- and O-alkylation products. 1- and 3-CCs formed from cyclohexene dimerization could react with phenol through similar routes as cyclohexene.

Consistent with previous reports, BAS-catalyzed C-alkylation occurs preferentially at *ortho*/*para* positions in a virtually irreversible manner.[11,39] This was suggested from the absence of de-alkylation throughout the reaction, in contrast to the decomposition of ether products (O-alkylation and intermolecular dehydration) after reaching maxima. The different reversibility of C- and O-alkylation was further corroborated by using 4-CHP and CHPE as the reactant, respectively. The de-alkylation of 4-CHP to phenol and cyclohexene occurred at a much lower rate, by at least two orders of magnitude, than C-alkylations (**Fig.4-2**). The formation of other detectable alkylated products (*e.g.*, 2-CHP, 2,4-DCHP, etc.) was depicted in **Fig. 4-2 (b)**. The very low de-alkylation rates could be explained by the much higher activation energies for de-alkylation than for alkylation, as a result of the strong exothermicity of alkylation steps.[31] In contrast, CHPE decomposed to phenol and cyclohexene rapidly, as well as forming various C-alkylation products (**Fig.4-3**). This observation allows us to conclude that phenol and cyclohexene are primary products from the decomposition of CHPE, and that 2-CHP, 2,4- and 2,6-DCHP are secondary products generated from the reaction of phenol with cyclohexene. The formation of cyclohexyl phenols via the intramolecular rearrangement of cyclohexyl phenyl ether is not supported by the present data. The same conclusion was reached for liquid phase decomposition of isopropoxybenzene over HY-30, where isopropyl phenol, phenol and propylene were all observed as primary products.[7]

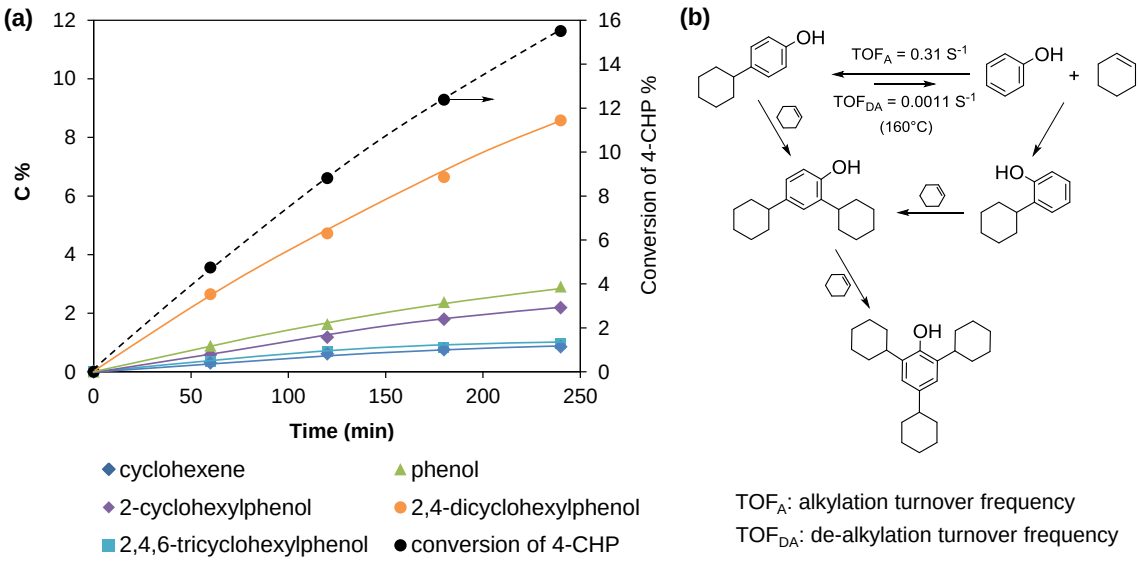

Figure 4-2. Reaction of 4-cyclohexyl phenol (4-CHP) on HBEA-150 in decalin. (a) Carbon-based concentration-time profiles; (b) Proposed reaction network. Reaction conditions: 4-CHP (0.5 g), HBEA-150 (0.2 g), decalin (100 mL), T= 160 °C, 5 MPa H_2 (ambient temperature), stirred at 700 rpm.

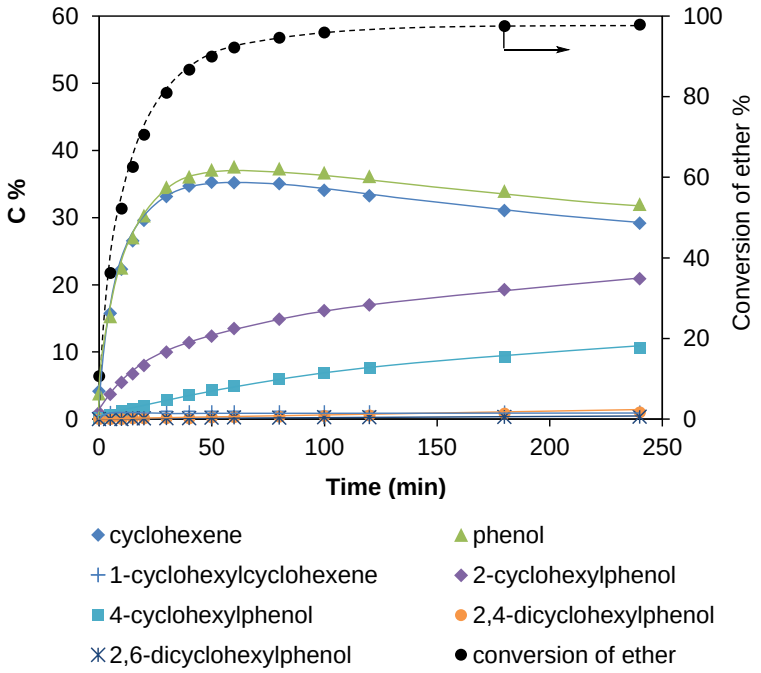

Figure 4-3. Carbon-based concentration-time profiles of the decomposition of cyclohexyl phenyl ether on HBEA-150 in decalin. Reaction conditions: cyclohexyl phenyl ether (2.0 g), HBEA-150 (0.1 g), decalin (100 mL), T= 160 °C, 5 MPa H_2 (ambient temperature), stirred at 700 rpm.

4.3.3 Dehydration of cyclohexanol on HBEA-150 in decalin

We chose HBEA-150 as a representative zeolite catalyst for further investigating the phenol alkylation chemistry. Recall that little phenol alkylation was observed until >70% of cyclohexanol was converted via dehydration (**Fig. 4-1 (a)**). This observation indicates that either phenol, or cyclohexene, or both, hardly competes against cyclohexanol (or its derived surface intermediate) for the BAS. The dehydration of cyclohexanol was then performed over HBEA-150 in the absence of phenol at 160 °C (**Fig. 4-4**). At 0.5 M alcohol concentration, the initial rate of cyclohexene formation (~0.23 s^{-1}) was lower than that (~0.37 s^{-1}) obtained in the presence of phenol (**Fig. 4A-17**). Therefore, phenol has a measurable impact on the adsorption of cyclohexanol and its dehydration. This would mean, in turn, that the initially low activity of phenol alkylation is caused by the inability of cyclohexene, not phenol, to compete with cyclohexanol for the BAS.

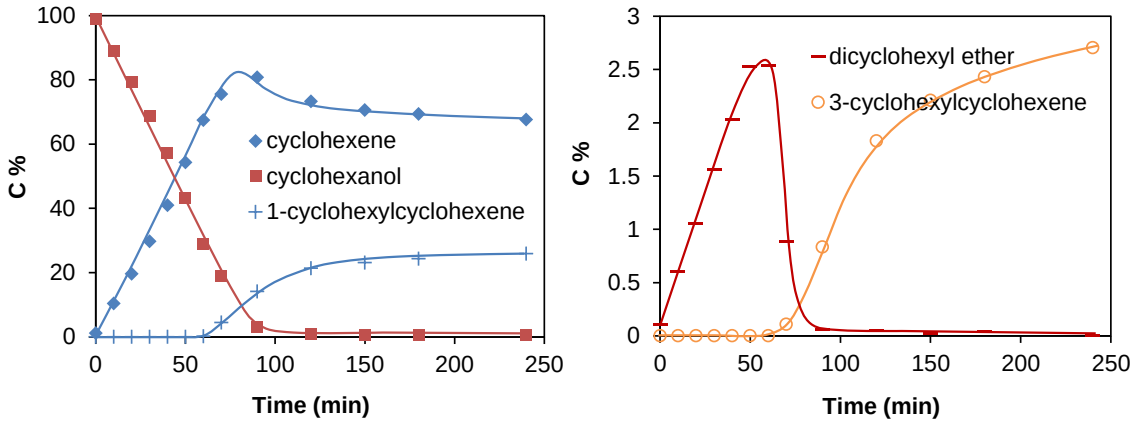

Figure 4-4. Carbon-based concentration-time profiles of cyclohexanol dehydration on HBEA-150 in decalin at 160 °C. Reaction conditions: 5.0 g cyclohexanol, 0.2 g HBEA-150, 100 mL decalin, 5 MPa H_2 (ambient temperature), stirred at 700 rpm.

The rate of cyclohexanol dehydration being higher in the presence of phenol was, however, not expected from the outset, and this observation would suggest that a decrease in the local concentration of cyclohexanol at the BAS actually leads to faster dehydration kinetics. To understand this, the rate of cyclohexanol dehydration was measured as a function of its concentration in decalin (**Fig. 4-5**). The asymptotic decrease in olefin formation rate with increasing alcohol concentration (0.1–1.7 M) is reminiscent

of those observed for gas-phase alcohol dehydration over zeolites[40-42] and POM clusters[43-45], which has been attributed to the formation of the unreactive or much less reactive (protonated) alcohol dimer occupying the acid sites. Similarly, we conclude that for cyclohexanol dehydration on HBEA in decalin, the cyclohexanol dimer was also less active than the monomer. The contribution of monomer- and dimer-mediated routes for olefin formation can be quantitatively derived from the measured dependence of rates on alcohol concentration as shown in **Fig. 4-5**. While a detailed analysis of the dehydration kinetics is outside the scope of this work (to be reported in another contribution), we determined that the cyclohexanol dimer is the most abundant surface species (dimer: monomer ratio > 20) at a cyclohexanol concentration of 0.5 M as was used for alkylation. Thus, cyclohexanol dehydration mainly occurs via the dimeric-mediated route at cyclohexanol concentration of 0.5 M at 160 °C (**Fig. 4-5**). From the above analysis, it can be deduced that a decrease in local alcohol concentration at the BAS, *e.g.*, induced by co-adsorption of phenol, would shift the equilibrium between monomer and dimer, leading to a greater contribution of the high-activity monomer-mediated route. As the concentration of cyclohexanol decreases as it gets converted, there is a gradual shift to monomer-mediated dehydration with a higher rate. This increase in forward rates, however, appeared to be offset by reverse reaction or catalyst deactivation, causing the apparent zero-order kinetics (**Fig. 4- 1 (a)** and **4-4 (a)**).

The dehydration mechanism (**Scheme 4A-1)** is discussed in greater detail in the **Appendix**. According to a comprehensive DFT study on alcohol dehydration on solid Brønsted acids,[46] the monomer-mediated route for olefin formation involves a carbenium ion-type intermediate (step 3, **Scheme 4A-1**), while the dimer-mediated route does not require the intermediacy of carbenium ion (step 5, **Scheme 4A-1**). Since carbenium ion is the most potent electrophile in the reaction system, the absence of carbenium ion-type intermediate along the dimer-mediated dehydration route could explain the low phenol-cyclohexanol alkylation reactivity on HBEA-150 at initial reaction stage (< 40 min, **Fig. 4-1 (a)**). Alternatively, the fact that cyclohexene hardly re-adsorbs on BAS in the presence of cyclohexanol dimers is also able to account for the low alkylation reactivity at the initial stage of phenol-cyclohexanol reaction. More importantly, by using lower concentrations of cyclohexanol, the initial alkylation rate

could be remarkably enhanced (**Figs. 4-6** and **4A-18**). This is because the electrophile, carbenium ion, can be generated more facilely from the alcohol monomer (111 kJ mol^{-1} from monomer *vs.* 140 kJ mol^{-1} from dimer; results not shown), the surface coverage of which becomes significant at low alcohol concentrations. It could also be that initial alkylation rate increased as a result of less difficult olefin adsorption at a lower surface abundance of strongly held dimer species.

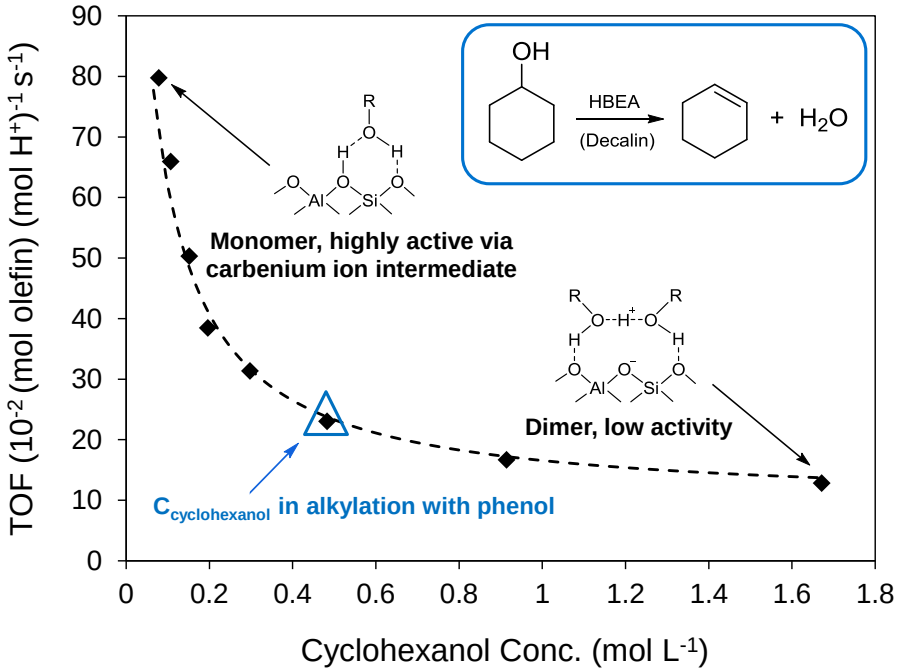

Figure 4-5. Measured turnover frequencies (TOFs) for olefin formation as a function of cyclohexanol concentration in decalin (0.02−2 M) over HBEA-150 at 160 °C (♦). TOFs were determined by normalizing the rates to the concentration of BAS. The dashed curves represent the fitting of experimental data points to **Eq. (S-1), SI.**

Note that the dehydration rate in decalin (0.23 s^{-1} at 0.5 M alcohol concentration, **Fig.4-5**) was an order of magnitude higher than that (~0.02 s^{-1}) for cyclohexanol dehydration on the same catalyst in water. (see details in **Chapter 2**) The activation energy was determined to be 140 kJ mol^{-1} (**Table 4A-3**), 20 kJ mol^{-1} lower than that for cyclohexanol dehydration on HBEA-150 in water.

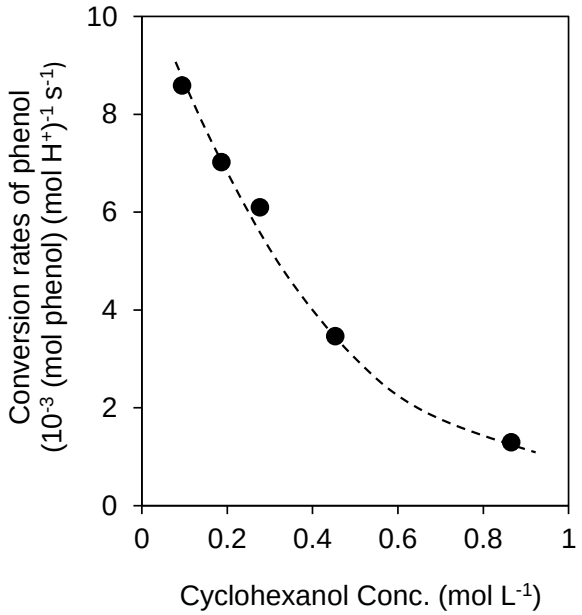

Figure 4-6. Measured turnover frequencies (TOFs) for the conversion of phenol as a function of cyclohexanol concentration in decalin (0.09−0.9 M, based on decalin density at r.t.) over HBEA-150 at 160 °C. Reaction conditions: phenol (5.0 g), cyclohexanol (1.0, 2.0, 3.0, 5.0 and 10.0 g), HBEA-150 (0.1 g), decalin (100 mL), T= 160 °C, 5 MPa H_2 (ambient temperature), stirred at 700 rpm. The initial consumption rates of phenol were determined under the conversion of cyclohexanol lower than 30%. The corresponding conversion and yield plots are shown in Figure S18.

4.3.4 Alkylation of phenol with cyclohexene on HBEA150: spectroscopic and kinetic assessment

The gas-phase IR spectra of adsorbed cyclohexene over siliceous BEA (BAS: 0; LAS: 0.03 mmol g^{-1}) and HBEA-150 (BAS: 0.19 mmol g^{-1}; LAS: 0.04 mmol g^{-1}) at 40 °C are shown in **Fig. 4A-19**. Cyclohexene was molecularly adsorbed on siliceous BEA, while alkenyl carbenium ions were observed when cyclohexene was adsorbed on HBEA-150 (see discussion in **Section A5**, **Appendix**). On acidic zeolites, surface alkenyl carbenium ion originating from the adsorption of olefin has been evidenced by IR or NMR spectroscopies.[47,48] The alkenyl carbenium ions can form either via hydride transfer between olefin and the alkyl carbenium ion, or through hydride abstraction from olefin by LAS.[49] Siliceous BEA and HBEA-150 contained similar amounts of LAS but only the latter showed bands of alkenyl carbocation. Thus, LAS-catalyzed hydride abstraction of cyclohexene, forming alkenyl carbenium ions, is unlikely on both samples.

This, in turn, points to the other formation pathway for the alkenyl carbenium ion on HBEA-150, that is, hydride transfer between cyclohexene and the cyclohexyl carbocation (**Fig. 4-7**).[47,49] To summarize, by proving the presence of cyclohexenyl carbocation on HBEA-150, we indirectly established the formation of the unstable cyclohexyl carbocation upon cyclohexene adsorption on HBEA in the gas phase.

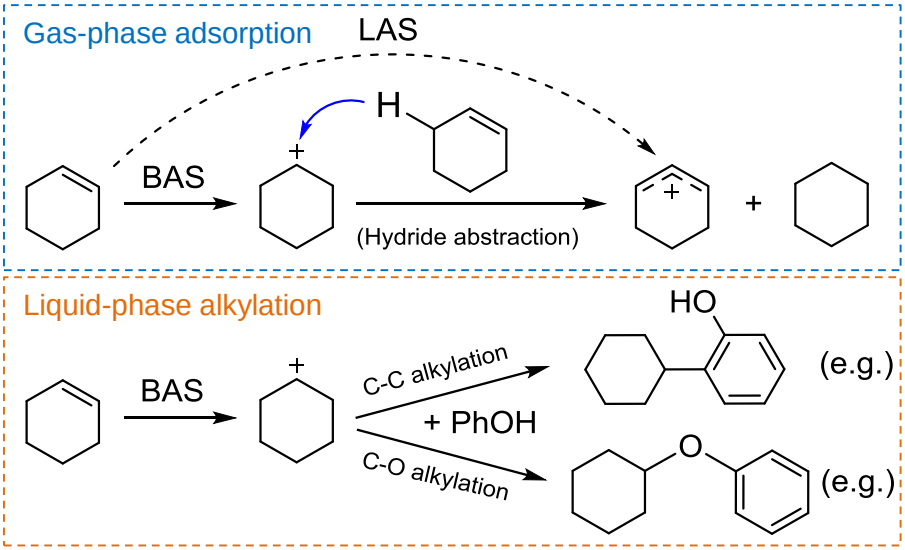

Figure 4-7. Proposed intermediates of cyclohexene in gas-phase adsorption and liquid-phase alkylation on HBEA-150. Gas-phase adsorption was measured on an infrared spectrometer at 40 °C and the liquid-phase alkylation reactions were carried out at 120-160°C.

However, there was no evidence for the formation of cyclohexenyl cation during liquid phase reactions of phenol and cyclohexene, as inferred from the absence of observable cyclohexane in the products (cyclohexane would have been formed if hydride transfer between cyclohexene and cyclohexyl carbenium ion took place, as depicted in **Fig. 4-7**) and the absence of skeletal rearrangement (cyclohexenyl cation to 1-methycyclopentyl cation[48]). The absence of hydride transfer between cyclohexene and cyclohexyl cation is expected, as the cyclohexyl carbenium ion is the direct electrophile which rapidly attacks phenol in phenol-cyclohexene alkylation (**Fig. 4-7**). The proposed mechanism and corresponding elementary steps are shown in **Scheme 4A-2.**

It was difficult to study the kinetics of phenol-cyclohexanol alkylation, not only because significant catalyst deactivation had occurred before alkylation started, but also because a number of species (phenol, cyclohexanol, cyclohexene and water) were already present at the initial stage of alkylation. As discussed above, cyclohexene/carbenium ion is the direct alkylating agent for the BAS-catalyzed alkylation of phenol with cyclohexanol. Thus, the kinetic study of alkylation was performed using equimolar amounts of phenol and cyclohexene over HBEA-150 in decalin at 120-150 °C (**Fig. 4A-21**). Two-ring products including 2-CHP, 4-CHP, 1-CC and CHPE were primary products, among which the selectivity to CHPE (O-alkylation) decreased with increasing temperature. C-alkylation at the ortho-position (2-CHP) was always faster than that at the para-position (4-CHP). The rate of C-alkylation was 3-5 times higher than the dimerization of cyclohexene.

For both C- and O-alkylation products, the reaction orders with respect to phenol and cyclohexene concentrations were determined to be ~ 1.0 and ~ 0.4 (**Fig. 4A-22)**, respectively, at 120 °C where deactivation was least pronounced. The first order in phenol, along with its appreciable adsorption at the BAS as discussed in the previous section, indicates that phenol alkylation on HBEA occurs via an E-R type mechanism in decalin. The reaction order in phenol would be fractional if the kinetic mechanism were of L-H type. The fractional order in cyclohexene is also consistent with the above consideration and proves that cyclohexene reacts in an adsorbed state.

The initial formation rates of different phenol-cyclohexene alkylation products at 120–150 °C are compiled in **Table 4-3**. The Arrhenius plots are shown in **Fig. 4A-23**. The apparent activation energies were comparable at 46–49 kJ mol^{-1} for C-C bond coupling products, while being lower for the O-alkylation, only ~ 26 kJ mol^{-1} (**Table 4-3**). For alkylation of phenol with cyclohexene in 1,2-dichloroethane (solvent) catalyzed by a variety of sulfonic resins, intrinsic activation barriers of 68, 74 and 20 kJ mol^{-1} for 2-CHP, 4-CHP and CHPE, respectively, were obtained from fitting experimental results with an E-R model.[50] In another report,[31] an intrinsic activation energy of 70 kJ mol^{-1} was obtained for liquid phase alkylation of benzene with octenes over HY zeolite also based on an E-R model. Considering that the apparent activation energy contains an negative enthalpy term related to olefin protonation ($E_{a,app} = E_{a,int} + \Delta H_{olefin,prot}$), the $E_{a,app}$

of 46–49 kJ mol^{-1} measured in this work for phenol alkylation appears comparable to those reported earlier for alkylation of benzene. Note that these activation energies for the formation of alkylation products were much lower than that for cyclohexanol dehydration, ~140 kJ mol^{-1}. Alkylation, however, did not proceed at a rate commensurate with this low activation barrier because of unfavorable entropy factors, *i.e.*, bimolecular reactions lead to significant losses of entropy at the TS.

Table 4-3. Turnover frequencies and apparent activation energies for frequencies for the initial products of HBEA150-catalyzed alkylation of phenol with cyclohexene in decalin.[a]

Products	Rate[b]	Temperature (°C)				E_a[c] (kJ mol^{-1})
		120	130	140	150	
1-cyclohexylcyclohexene	$TOF_{1\text{-}CC}$ (s^{-1})	0.023	0.032	0.046	0.063	48
Cyclohexyl phenyl ether	TOF_{CPE} (s^{-1})	0.22	0.28	0.33	0.39	26
2-cyclohexylphenol	$TOF_{2\text{-}CHP}$ (s^{-1})	0.12	0.18	0.24	0.34	46
4-cyclohexylphenol	$TOF_{4\text{-}CHP}$ (s^{-1})	0.085	0.11	0.16	0.22	49

[a] Typical conditions: cyclohexene (0.05 mol), phenol (0.05 mol), HBEA-150 (100 mg), decalin (100 mL), 5 MPa H_2 (ambient temperature), stirred at 700 rpm; [b] TOF is determined as products formation rates (mol g^{-1} s^{-1}) normalized to the concentration of total BAS (HBEA150). [c] Apparent activation barriers are determined from the Arrhenius plots for TOFs (a directly measured property).

4.3.5 Comparison of alkylation of phenol with cyclohexanol in decalin and in water

In decalin, the TOF of phenol-cyclohexene alkylation was > 1 s^{-1} on HBEA at 160 °C. Since the activity was very low at the initial stage of phenol-cyclohexanol alkylation in decalin (~3.5×10^{-3} s^{-1} at 0.45 M alcohol concentration, 160 °C; see **Fig. 4-1** and **4-6**), adsorbed cyclohexanol species (*i.e.*, dimer) can be excluded as the direct alkylating agent. Considering that carbenium ion is a far more potent electrophile than an alkoxonium ion, the absence of phenol alkylation with cyclohexanol, at least before 70% of cyclohexanol was converted, could be explained in two ways: 1) no carbenium ion would be directly formed if dehydration of cyclohexanol (dimer) occurred via an E2 mechanism; 2) even if

E1-type elimination reactions of the alcohol-derived species could lead to carbenium ion, the activation barrier for producing such a cationic intermediate was found to be high (140 kJ mol^{-1} for elimination from a protonated alcohol dimer), a value inconsistent with the low activation energies measured for alkylation of phenol with cyclohexene. Thus, the carbenium ion that alkylates phenol should be formed via adsorption and protonation of olefin at the BAS, rather than from alcohol. This means that in decalin, alkylation of phenol with cyclohexanol is essentially equivalent in mechanism to alkylation of phenol with cyclohexene. However, cyclohexene is not able to adsorb at the BAS in the presence of cyclohexanol. Only after the coverage of cyclohexanol gets significantly reduced, leading to less strongly adsorbed monomer species, cyclohexene re-adsorbs, forming first a π-complex with the BAS and then transforming into a protonated state. The elucidation of the nature of the protonated olefin, *i.e.*, whether it is carbenium ion or surface alkoxide, is beyond the scope of this work. While some surface alkoxide could be more stable in zeolites, the electrophilicity of carbenium ion must be higher than surface alkoxy species. Note that results in **Fig. 4-6**, as discussed earlier, point to another source of carbenium ion from the elimination of alcohol monomer, a pathway available only at low alcohol concentrations. The contribution of this alcohol monomer elimination-alkylation pathway to the alkylation rate, however, is still much less than the olefin protonation-alkylation pathway.

The phenol-cyclohexanol reaction was also performed on HBEA-150 in aqueous phase at 170 °C (**Figs. 4-9** and **4A-24**). In a previous study, we reported aqueous phase alkylation of phenol with cyclohexanol on the same catalyst at 200 °C.[8,32] Like in decalin, alkylation of phenol with cyclohexanol in aqueous phase was also very slow at the beginning, and became an order of magnitude faster only after 40 min when 70% of cyclohexanol was converted (**Fig. 4-9**). These observations indicate that alkoxonium ion is also not an effective alkylating agent in aqueous phase and that the more potent electrophile, carbenium ion, was very low in its concentration during the first 40 min. Moreover, it appears that the re-adsorption of cyclohexene became significant at a much reduced cyclohexanol concentration, *i.e.*, after 70% of cyclohexanol was converted, and produced carbenium ions at a higher rate. Alkylation dramatically slowed down after 120 min due to deactivation.

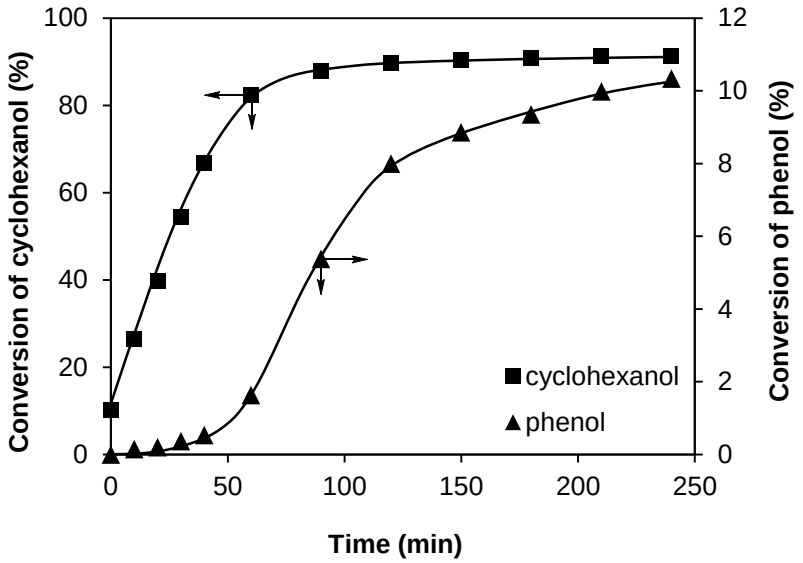

Figure 4-9. Conversion of phenol and cyclohexanol as a function of time in the aqueous-phase phenol-cyclohexanol alkylation reaction on HBEA-150. Reaction conditions: 5.0 g phenol, 5.0 g cyclohexanol, 1.0 g HBEA-150, 100 mL water, 5 MPa H_2 (ambient temperature), stirred at 700 rpm, 170 °C. The corresponding concentration-time profiles are shown in Figure S23.

There are two major differences when comparing the observations made in decalin and in water. First, the rate of cyclohexanol dehydration was the same (~0.06 s^{-1} at 170 °C) in the absence (**Chapter 2**) or presence of phenol (**Fig. 4A-24**), in contrast to the case in decalin (*i.e.*, TOF of cyclohexanol dehydration being 0.37 and 0.23 s^{-1} at 160 °C with and without phenol, respectively; see discussion in Section 2.3). The rate of dehydration in aqueous phase was also independent of cyclohexanol concentration (**Chapter 2**), in contrast to the inverse dependence of dehydration rate on concentration (**Fig. 4-5**). These results strongly suggest that cyclohexanol does not form the low-reactivity dimer species in the HBEA pores saturated with water during aqueous phase reactions (**Chapter 2**). Hence, aqueous-phase phenol alkylation accelerated after a majority of cyclohexanol was converted (**Fig. 4-9**) not because of a shift in the monomer-dimer equilibrium in favor of the more reactive monomer route producing carbenium ion.

Second, the initial alkylation rate (6×10^{-4} s^{-1} in the first 40 min at 170 °C; **Fig. 4-9**) in aqueous phase was much lower than that in decalin (3.5×10^{-3} s^{-1} at 160 °C; **Fig. 4-6**) for almost identical reactant concentrations. The initial alkylation rate in aqueous phase did

not vary with the alcohol concentration (**Fig. 4A-25**), in contrast to the observation in decalin (**Fig. 4-6**). Again, this is in line with the absence of dimer species in HBEA pore in aqueous phase. After 40 min (**Fig. 4-9**), *i.e.*, phenol-cyclohexene alkylation regime, the alkylation rate in water (at 170 °C, ~5.8×10^{-3} s^{-1} within 60-90 min; **Fig. 4-9**) was still much lower than that in decalin (at 160 °C, 0.22 s^{-1} within 40-60 min; **Fig. 4-1 (a)**). The saturation uptake of phenol was determined to be ~ 1.40 and ~ 1.22 mmol g_{HBEA}^{-1} in water and decalin, respectively (**Fig. 4A-26**). Similarly, the saturation uptake of cyclohexanol was determined to be 1.57 and 1.23 mmol g_{HBEA}^{-1} in water and decalin, respectively. Thus, it is not the different concentrations of the two reactants in the pore that caused the strikingly different dehydration and alkylation kinetics in decalin and in water.

We have already shown that when the reaction is performed in aqueous phase, high concentrations of water in the pore (at least 10 water per BAS in HBEA under reaction conditions; results not shown) lead to complete proton transfer from the framework hydroxyl to the cluster of water inside the pore (**Chapter 2**), forming hydrated hydronium ions confined in the pore as the actual active site for dehydration and alkylation. The energetics for alcohol and phenol to associate with the hydronium ion and for olefin and carbenium ion to interact with the hydronium ion are anticipated to be very different from the corresponding interactions between the reactants and intermediates with the "dry" framework proton (see discussion in the **Section A10** in **Appendix**).

To further understand the drastic solvent effect, the kinetics of aqueous phase cyclohexene-phenol alkylation was also explored in detail (Section S9, SI). At 150 °C, the total alkylation rate was ~9.5×10^{-4} s^{-1} in aqueous phase (**Table 4A-5**), three orders of magnitude lower than in decalin, ~1.0 s^{-1} (**Table 4-3**). In aqueous phase, hydration of cyclohexene was the dominant reaction (**Fig. 4A-29**). The apparent activation energy for cyclohexene hydration was determined at ~103 kJ mol^{-1} (**Fig. 4A-31**), while the $E_{a,app}$ was ~ 130 kJ mol^{-1} for both C- and O-alkylation in aqueous phase (**Fig. 4A-32**). In aqueous phase, hydration of olefin and alkylation shared the same step, *i.e.*, the protonation of cyclohexene to cyclohexyl carbenium ion. This protonation of cyclohexene by hydronium ions is endergonic according to DFT calculations (**Fig. 4A-33**, $\Delta G°$= + 58 kJ mol^{-1}). Thus, the cyclohexyl carbenium ion is expected to be a minority species in

aqueous environments. The measured activation energy for cyclohexene hydration is consistent with the DFT-calculated value (92 kJ mol^{-1}) for olefin protonation by the hydronium ion, suggesting that protonation of olefin is rate-determining for olefin hydration in water. Aqueous-phase alkylation reactions showed higher apparent activation barriers (~130 kJ mol^{-1}) than olefin hydration, probably because the TS for alkylation following cyclohexene protonation is also kinetically relevant and lies at a higher energy level than the TS for protonation.

To sum up, phenol-cyclohexanol/cyclohexene alkylations catalyzed by framework-bound proton (*i.e.*, BAS in decalin) and hydronium ions (*i.e.*, BAS in water) show distinct energetics of the elementary steps. Phenol-cyclohexanol alkylation is not as effective in aqueous phase as in decalin, because the generation of cyclohexyl cation from cyclohexanol is even more costly in aqueous phase (~160 kJ mol^{-1}) (**Chapter 2**) than in decalin (140 kJ mol^{-1}, **Table 4A-3**). Cyclohexene protonation at the hydronium ion (a weaker acid than a bridging hydroxyl) has a significantly higher barrier than olefin protonation at the framework-bound proton, leading to the higher activation barriers for alkylation in aqueous phase than in decalin. Liquid-phase alkylation will be assessed in the future by DFT calculations.

4.4 Conclusions

In decalin, phenol alkylation with cyclohexanol and cyclohexene is catalyzed primarily by Brønsted acid sites on solid surfaces. Among the investigated solid acids, large-pore zeolites, *i.e.*, HBEA and HY explored in this work, are the most effective catalysts for phenol-cyclohexanol alkylation. For phenol alkylation with either cyclohexanol or cyclohexene, C-alkylation occurs preferentially at *ortho*/*para* positions in a virtually irreversible manner, while O-alkylation is kinetically favored and reversible. Alcohol dimer, which is the dominant surface species in HBEA pores, does not generate carbenium ion to alkylate phenol. The surface coverage of the adsorbed alcohol monomer, which more readily produces the carbenium ion than does the dimer, increases with decreasing solution concentration of cyclohexanol, leading to exponential increase in alkylation rates at reduced alcohol concentrations. Phenol alkylation

accelerates after a majority of cyclohexanol is converted to cyclohexene, because re-adsorption and protonation of the olefin at the framework-bound proton provides a low-activation-energy route for generating the carbenium ion. Phenol alkylation with cyclohexene occurs via an E-R type mechanism on HBEA in decalin solvent. The rate of alkylation is much lower in water than in decalin, because the generation of the cyclohexyl cation from cyclohexanol is very costly in aqueous phase (~160 kJ mol^{-1} in water) and olefin protonation by the hydronium ion has a significantly higher barrier than protonation by a framework-bound proton.

4.5 Appendix

A1. Physicochemical properties of the catalytic materials

Table 4A-1. BET surface area and pore volume of the studied catalytic materials. The BET surface areas and pore volumes of γ-Al_2O_3[1] and SAC-13 are taken from previous reports[2,3].

Samples	BET surface area ($m^2\ g^{-1}$)			Pore volume ($cm^3\ g^{-1}$)		
	Micro	Meso	Total	Micro	Meso	Total
HBEA-150	502	122	624	0.20	0.17	0.37
HBEA-38	492	139	631	0.22	0.15	0.37
HY-80	746	99	845	0.32	0.18	0.50
HY-30	793	65	858	0.33	0.13	0.46
HZSM-5-90	302	86	388	0.14	0.26	0.40
γ-Al_2O_3	-	-	248	-	-	0.67
SAC-13	-	-	200	-	-	0.60

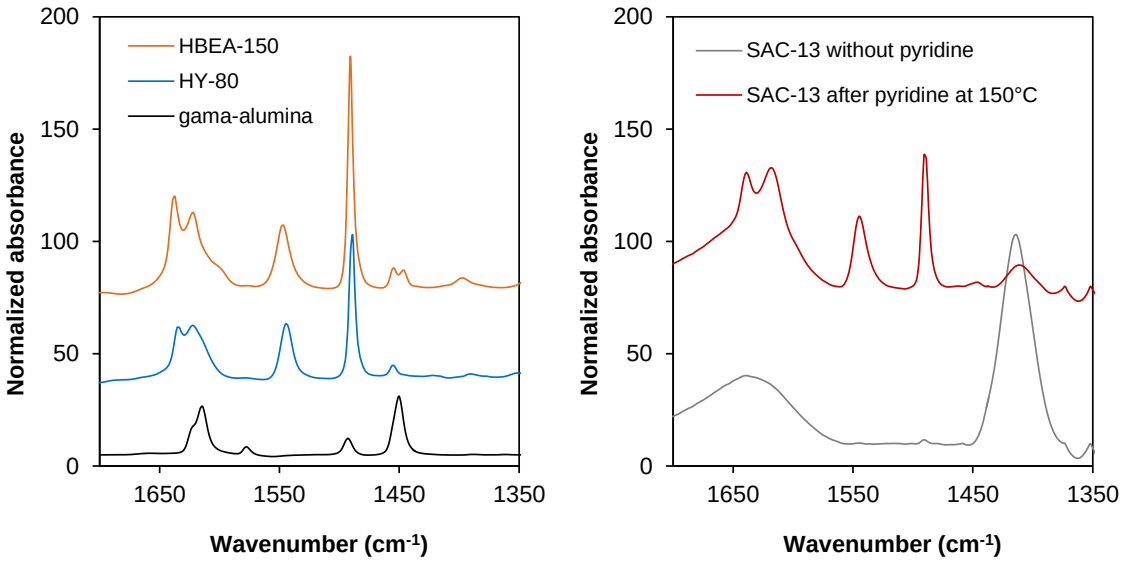

Figure 4A-1. IR spectra of adsorbed pyridine on different catalysts at 0.1 mbar of equilibrium pressure and 150 °C

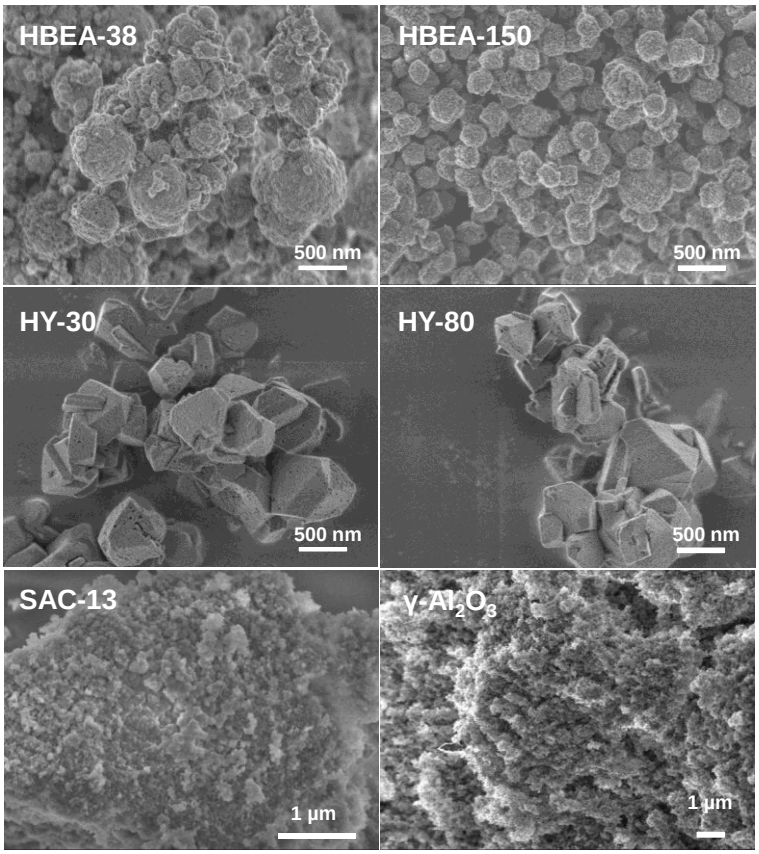

Figure 4A-2. Morphology and particle size characterization of different catalysts by SEM.

The infrared (IR) spectra of adsorbed pyridine on selected catalysts are shown in **Fig. 4A-1**. The characteristic peaks of BAS and LAS adsorbed pyridine appear at 1540 cm^{-1} and 1450 cm^{-1}, respectively. HBEA-150 and HY-80 exhibit both Brønsted and Lewis acidity, while γ-Al_2O_3 only contains Lewis acidity and SAC-13 only contains Brønsted acidity.

Typical scanning electron microscopy (SEM) images of different catalysts are shown in **Fig. 4A-2**. HBEA-38 and HBEA150 exhibit almost identical particle morphology with average diameters of ~0.2−0.3 μm. Both HY samples have similar morphology and particle size around 0.6–1.0 μm. The X-ray diffraction (XRD) patterns are shown in **Figure 4A-3**.

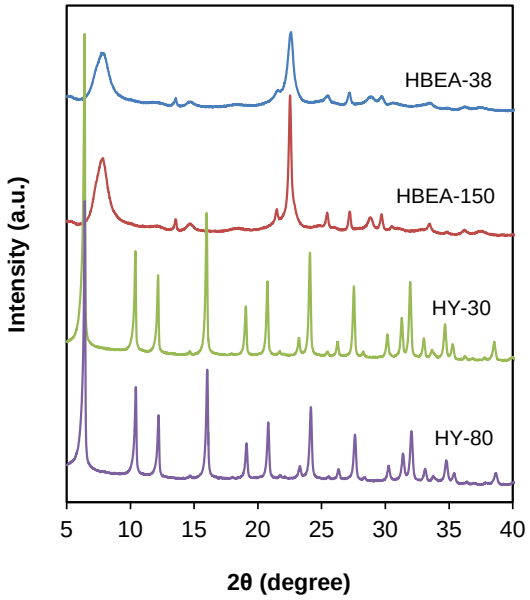

Figure 4A-3. XRD patterns of zeolite catalysts

A2. Alkylation of phenol with cyclohexanol/cyclohexene in decalin

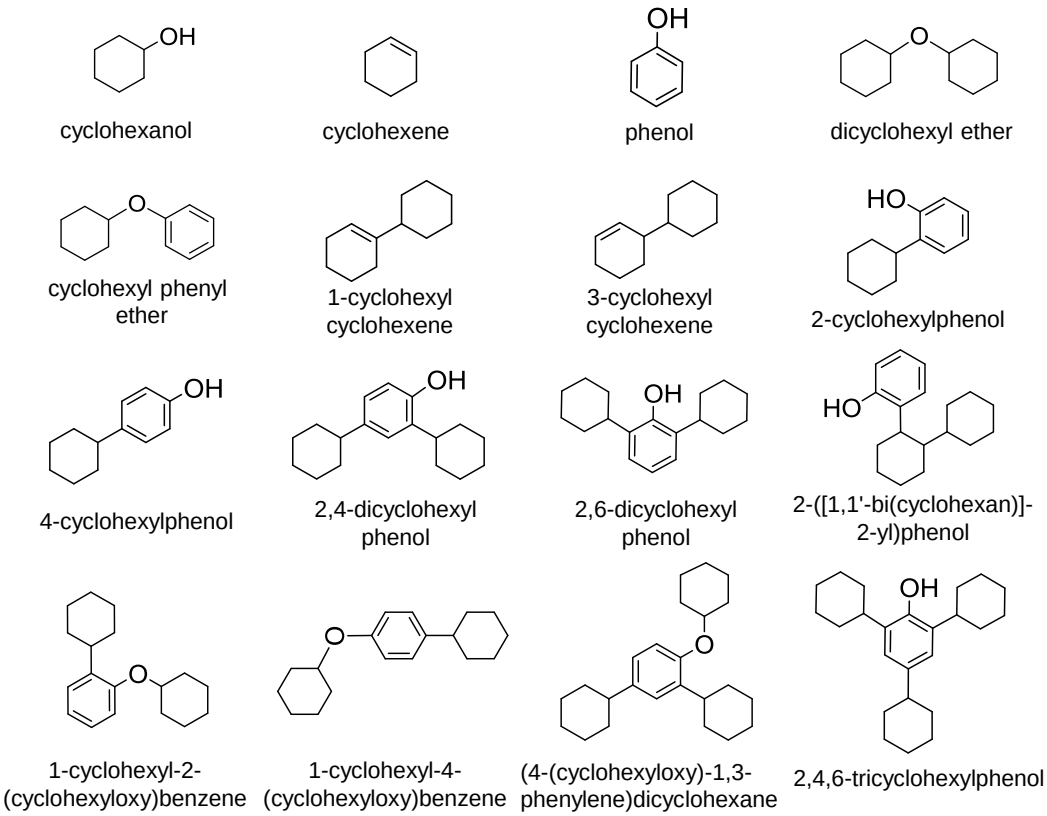

Figure 4A-4. A compilation of main compounds involved in acid-catalyzed alkylation of phenol with cyclohexanol and cyclohexene in decalin at 120-160 °C.

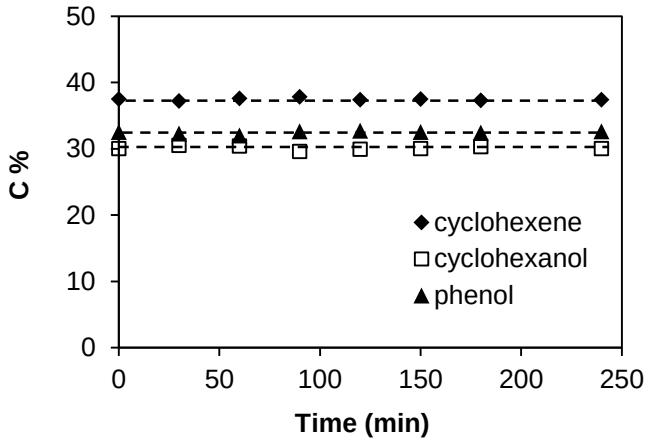

Figure 4A-5. A mixture of cyclohexanol, cyclohexene and phenol in decalin over α-Al_2O_3 at 160 °C. Reaction conditions: 5.0 g cyclohexanol, 5.0 g cyclohexene, 5.0 g phenol, 1.0 g α-Al_2O_3, 100 mL decalin, 5 MPa H_2 (ambient temperature), stirred at 700 rpm.

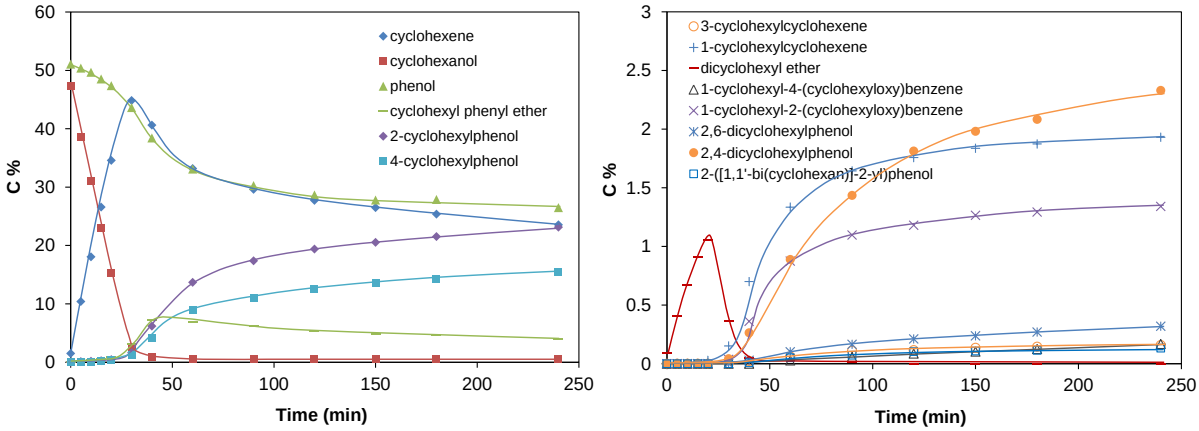

Figure 4A-6. Alkylation of phenol with cyclohexanol as a function of time on HBEA-38 in decalin at 160 °C. Reaction conditions: 5.0 g phenol, 5.0 g cyclohexanol, 0.1 g HBEA-38, 100 mL decalin, 5 MPa H_2 (ambient temperature), stirred at 700 rpm

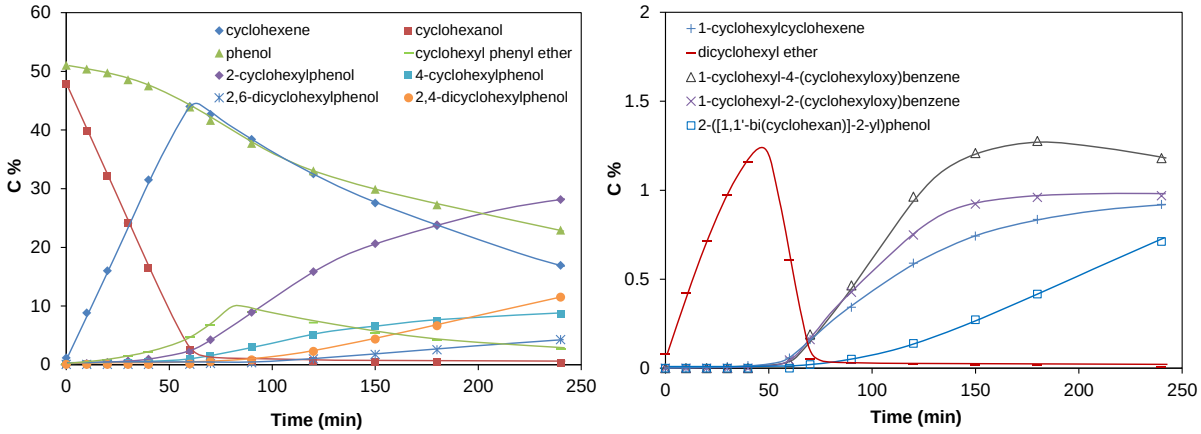

Figure 4A-7. Alkylation of phenol with cyclohexanol as a function of time on HY-80 in decalin at 160 °C. Reaction conditions: 5.0 g phenol, 5.0 g cyclohexanol, 0.2 g HY-80, 100 mL decalin, 5 MPa H_2 (ambient temperature), stirred at 700 rpm

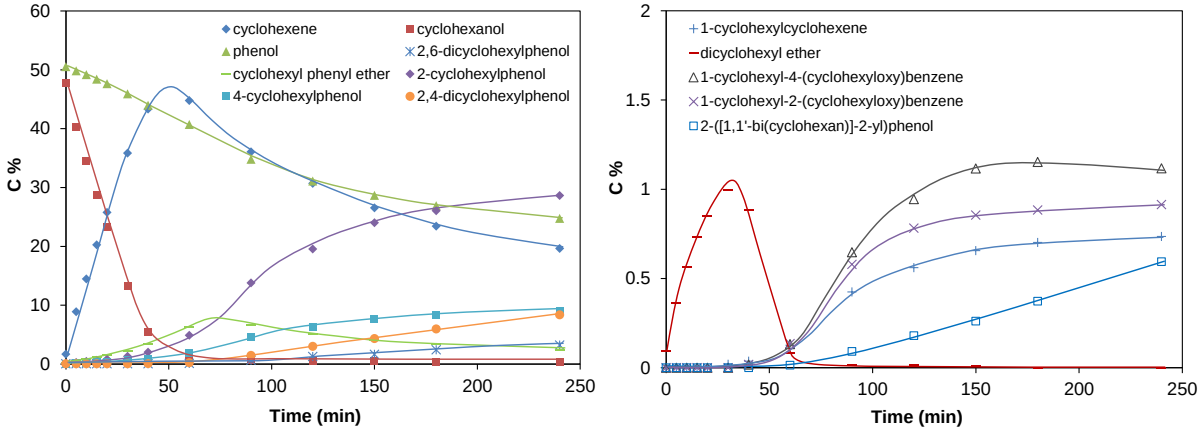

Figure 4A-8. Alkylation of phenol with cyclohexanol as a function of time on HY-30 in decalin at 160 °C. Reaction conditions: 5.0 g phenol, 5.0 g cyclohexanol, 0.1 g HY-30, 100 mL decalin, 5 MPa H_2 (ambient temperature), stirred at 700 rpm

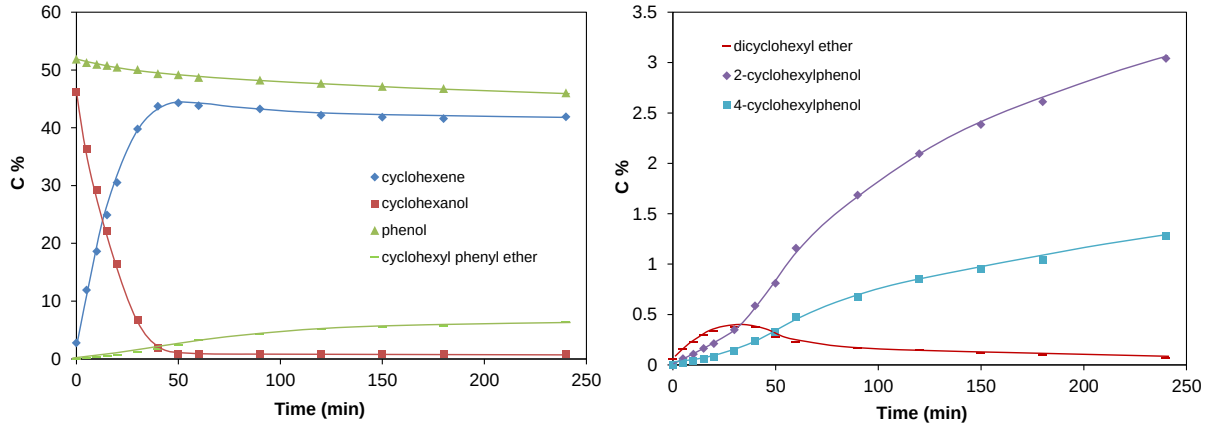

Figure 4A-9. Alkylation of phenol with cyclohexanol as a function of time on SAC-13 in decalin at 160 °C. Reaction conditions: 5.0 g phenol, 5.0 g cyclohexanol, 0.1 g SAC-13, 100 mL decalin, 5 MPa H_2 (ambient temperature), stirred at 700 rpm

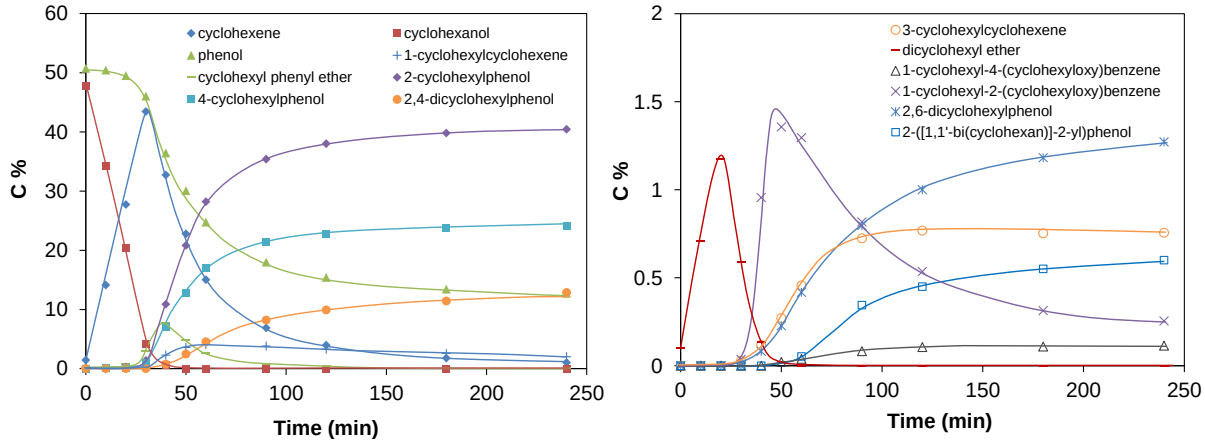

Figure 4A-10. Alkylation of phenol with cyclohexanol as a function of time on HBEA-150 in decalin at 160 °C. Reaction conditions: 5.0 g phenol, 5.0 g cyclohexanol, 0.4 g HBEA-150, 100 mL decalin, 5 MPa H_2 (ambient temperature), stirred at 700 rpm

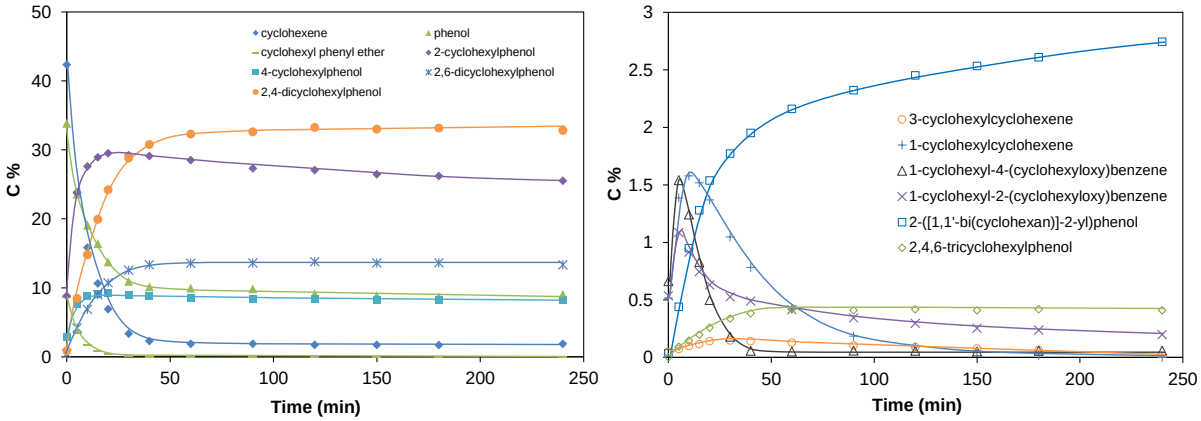

Figure 4A-11. Alkylation of phenol with cyclohexene as a function of time on HY-80 in decalin at 160 °C. Reaction conditions: 5.0 g phenol, 5.0 g cyclohexene, 1.0 g HY-80, 100 mL decalin, 5 MPa H_2 (ambient temperature), stirred at 700 rpm

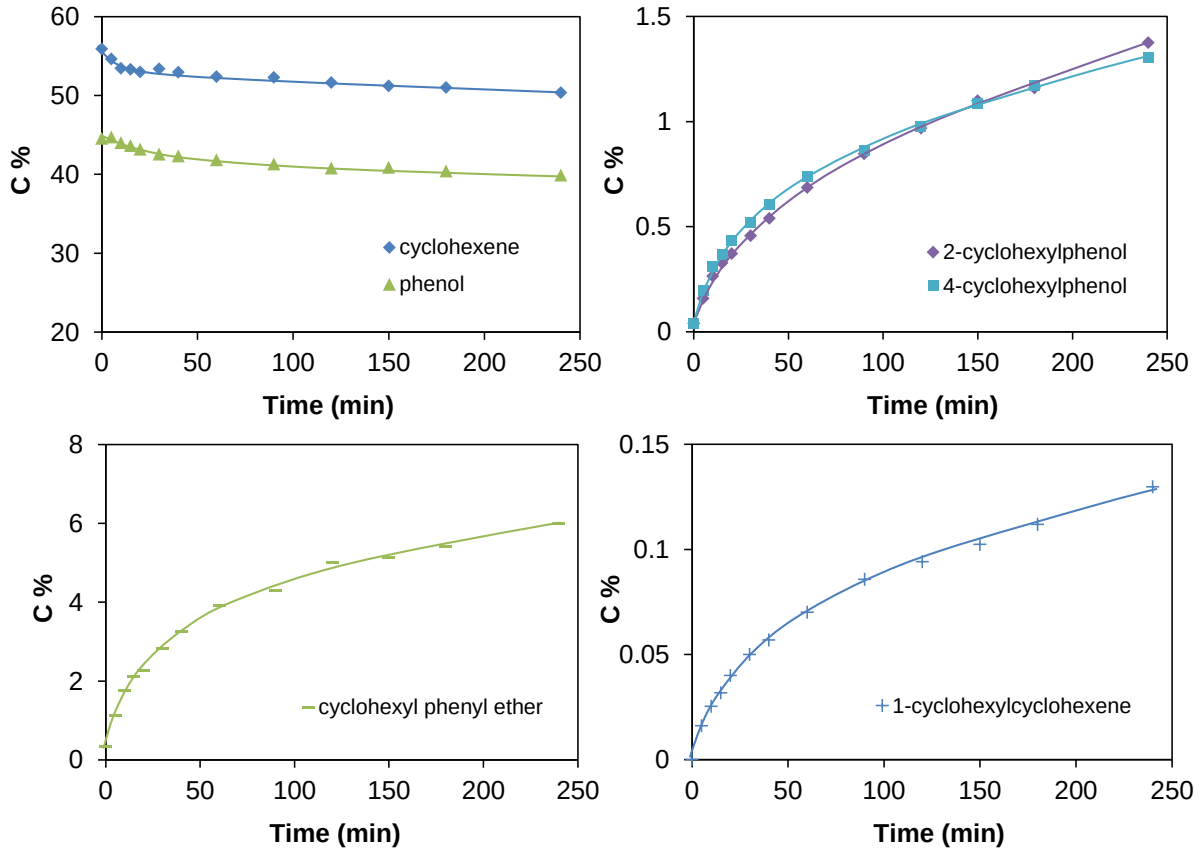

Figure 4A-12. Alkylation of phenol with cyclohexene as a function of time on HZSM-5-90 in decalin at 160 °C. Reaction conditions: 5.0 g phenol, 5.0 g cyclohexene, 1.0 g HZSM-5-90, 100 mL decalin, 5 MPa H_2 (ambient temperature), stirred at 700 rpm

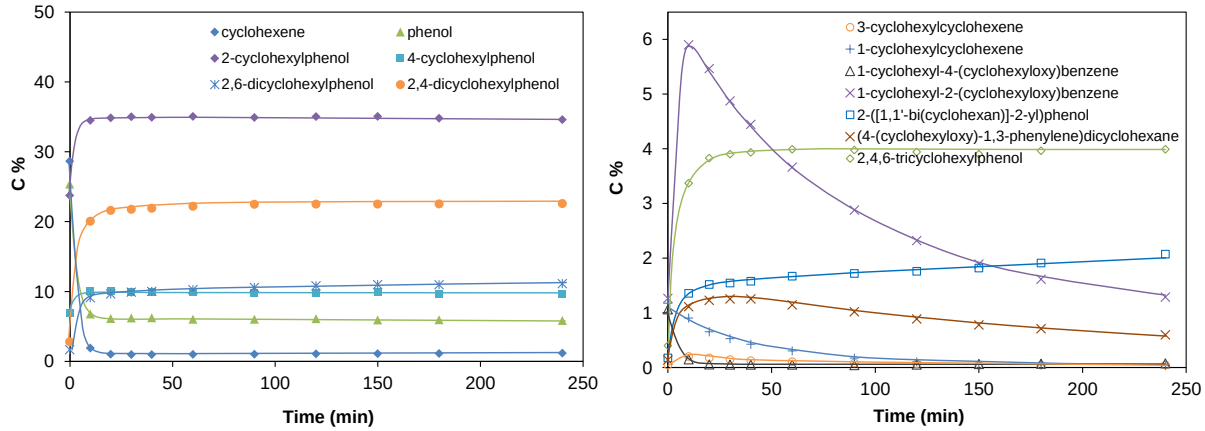

Figure 4A-13. Alkylation of phenol with cyclohexene as a function of time on SAC-13 in decalin at 160 °C. Reaction conditions: 5.0 g phenol, 5.0 g cyclohexanol, 0.60 g SAC-13, 100 mL decalin, 5 MPa H_2 (ambient temperature), stirred at 700 rpm

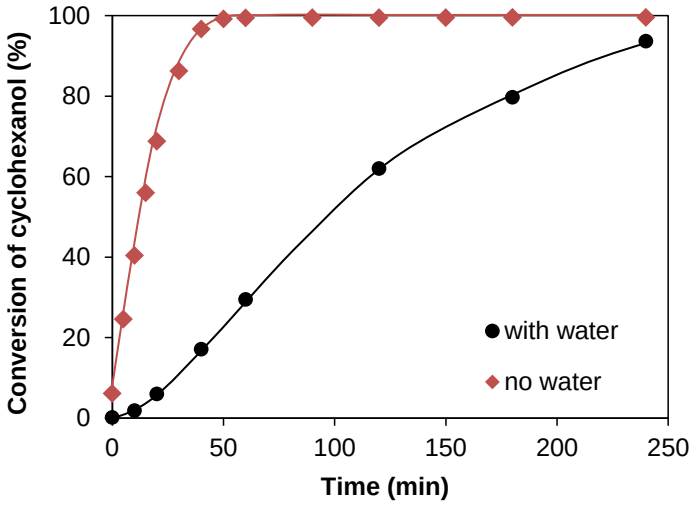

Figure 4A-14. Dehydration of cyclohexanol over SAC-13 in decalin in the presence/absence of initially added water at 160 °C. Reaction conditions: 5.0 g cyclohexanol, 0.1 g SAC-13, 0 or 1.0 g water, 100 mL decalin, 5 MPa H_2 (ambient temperature), stirred at 700 rpm

Table 4A-2. The impact of initially added water on the phenol-cyclohexene alkylation over SAC-13 in decalin at 160 °C.

Reaction conditions	Water	Conversion (%)	Yield of products (C%)					
			2-CHP	4-CHP	2,4-DCHP	2,6-DCHP	1-CC	CHPE
5.0 g Phenol, 5.0 g cyclohexene, 0.1 g SAC-13, 160°C, 700 rpm, 240min	0 g	Phenol: 96.6, Olefin: 82.3	37.6	10.1	18.9	9.9	0.9	0.04
	1.0 g	Phenol: 7, Olefin: 8	1.8	0.9	0	0	0.06	4.6

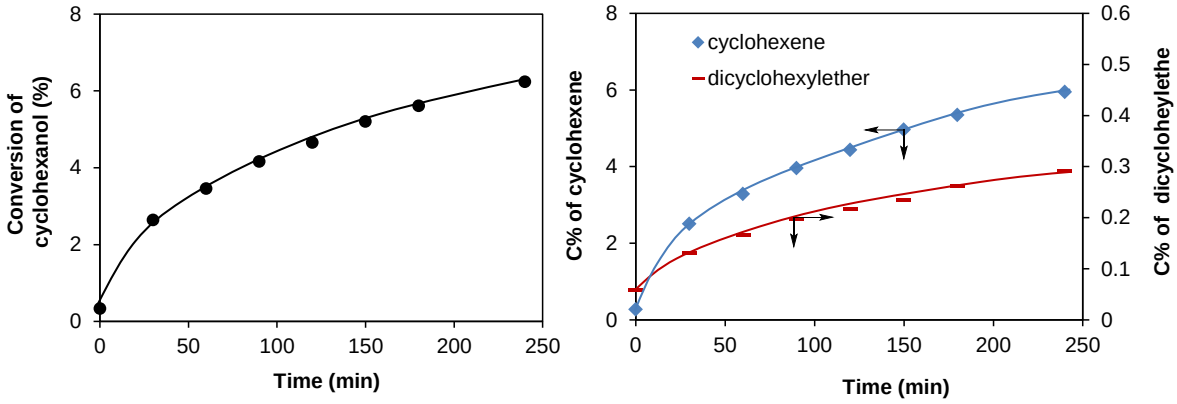

Figure 4A-15. γ-Al_2O_3 catalyzed dehydration of cyclohexanol in decalin at 200 °C. Reaction conditions: 5.0 g cyclohexanol, 1.0 g γ-Al_2O_3, 100 mL decalin, 5 MPa H_2 (ambient temperature), stirred at 700 rpm

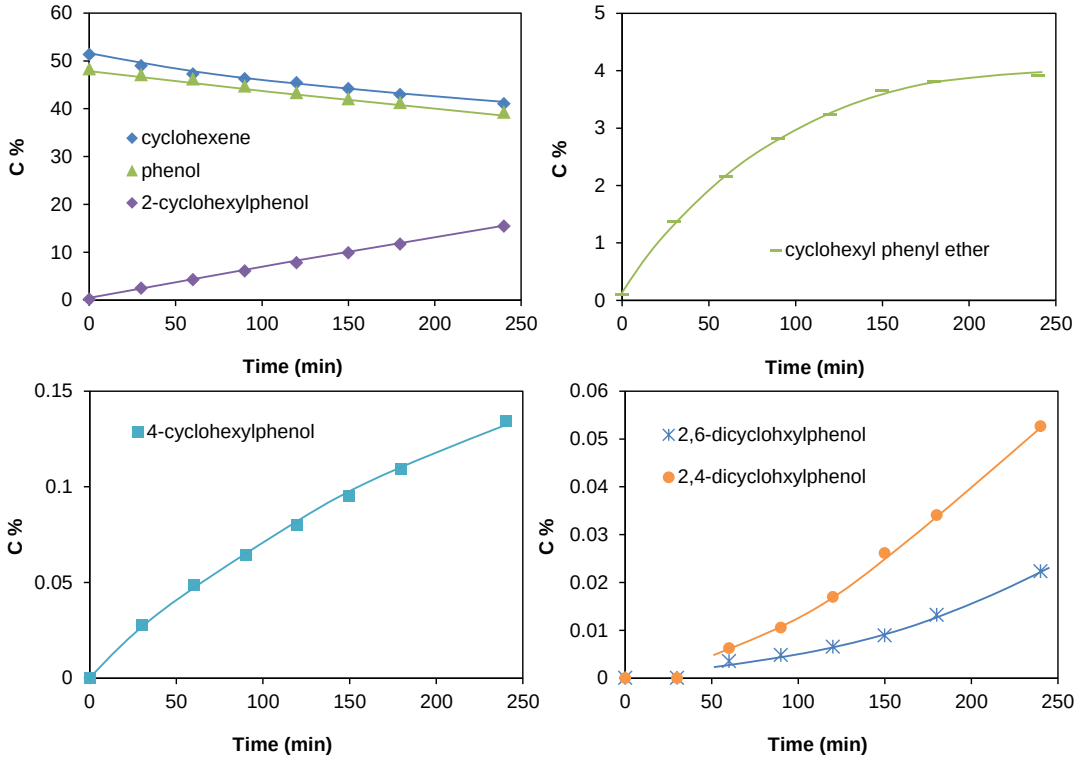

Figure 4A-16. Alkylation of phenol with cyclohexene as a function of time on γ-Al_2O_3 in decalin at 200 °C. Reaction conditions: 5.0 g phenol, 5.0 g cyclohexene, 1.0 g γ-Al_2O_3, 100 mL decalin, 5 MPa H_2 (ambient temperature), stirred at 700 rpm

A3. Additional data and discussion about cyclohexanol dehydration in decalin with and without phenol

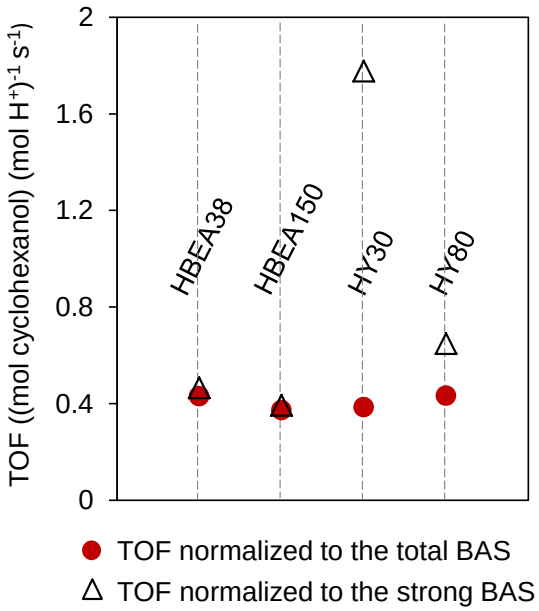

Figure 4A-17. Dehydration of cyclohexanol to cyclohexene over different solid acids in decalin in the presence of phenol at 160 °C. Reaction conditions: 5.0 g cyclohexanol, 5.0 g phenol, 0.2 g HBEA-150 or HY-80, 0.1 g HBEA-38 or HY-30, 100 mL decalin, 5 MPa H_2 (ambient temperature), stirred at 700 rpm

Table 4A-3. Reaction rates, turnover frequencies and apparent activation energies for HBEA-150-catalyzed dehydration of cyclohexanol to cyclohexene.[a]

Products	Rate[b]	Temperature (°C)				$E_{a,app}$[c]
		130	140	150	160	(kJ/mol)
Cyclohexene	r_C (mol·g^{-1}·s^{-1})	2.03 x 10^{-6}	5.60 x 10^{-6}	1.59 x 10^{-5}	4.38 x 10^{-5}	140
	TOF_C (s^{-1})	0.011	0.029	0.083	0.228	

[a] Typical conditions: cyclohexanol (5.0 g), HBEA-150 (100 mg), decalin (100 mL), 5 MPa H_2 (ambient temperature), stirred at 700 rpm; [b] TOF is determined as cyclohexene formation rate (mol g^{-1} s^{-1}) normalized to the concentration of total BAS (HBEA-150); [C] Activation barriers are determined from the Arrhenius plots for TOFs (a directly measured property).

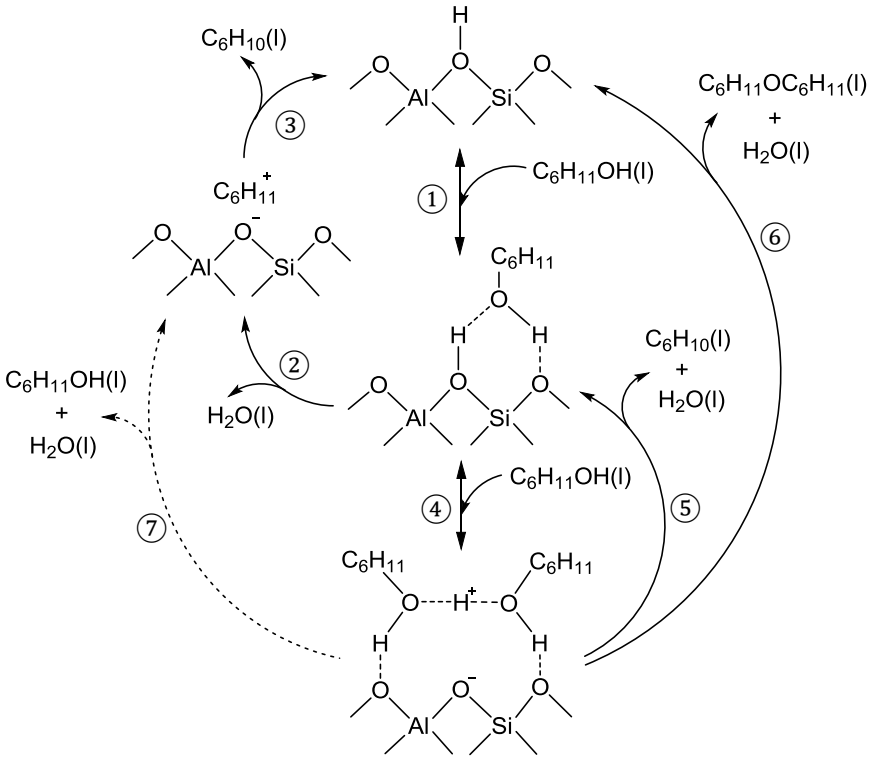

Scheme 4A-1. Proposed elementary steps for cyclohexanol dehydration over HBEA150 in decalin.

The E1-type mechanism has been suggested for the dehydration of cyclohexanol in liquid phase.[4](**Chapter 2**) The dehydration of cyclohexanol to cyclohexene over HBEA-150 zeolite is proposed to occur via monomer- and dimer-mediated pathways illustrated in **Scheme S1**, analogous to those reported for gas phase alcohol dehydration reactions.[5,6] The catalytic cycle starts with the adsorption of cyclohexanol at the BAS to form cyclohexanol monomer (alkoxonium ion) (step 1). Subsequent decomposition of the monomer leads to the formation of a surface-bound carbenium ion-like intermediate and water via C-O bond cleavage (step 2). Deprotonation of the carbenium ion intermediate produces cyclohexene as the product, which then desorbs and regenerates the BAS site (step 3). The cyclohexanol monomer can also interact with another cyclohexanol to form a protonated dimer (step 4). The dimer-mediated route is proposed to directly dissociate a cyclohexene and water along with forming an alkoxonium ion (step 5). Alternatively, the dimer species can decompose to form diethyl ether (DCE) and water (step 6). Note that the direct dissociation of a cyclohexanol dimer to a cyclohexanol and carbenium ion (step 7) is not supported by a recent DFT study[7] and our experimental observations. A separate

contribution will address the detailed kinetics and mechanism of the dehydration of cyclohexanol on HBEA-150 in decalin.

Based on this mechanism, we derived the following rate expression for olefin formation via monomer- and dimer-mediated dehydration routes:

$$r_{\text{olefin}} = [\text{H}^+]_0 \frac{k_M + k_D K_D [\text{C}_6\text{H}_{11}\text{OH}]}{1 + K_D [\text{C}_6\text{H}_{11}\text{OH}]} \qquad \text{(S-1)}$$

where k_M and k_D are the intrinsic rate constants of water elimination from the monomer and dimer pathways discussed in the previous section, respectively; K_D is the equilibrium constant for alcohol dimer formation from an alcohol monomer interacting with a liquid-phase alcohol; $[\text{H}^+]_0$ represents the total concentration of BAS. This equation and the derivation has been already reported previously for 1-propanol dehydration,[5] so the details for derivation are not repeated here.

A4. Dependence of initial alkylation rate of phenol on cyclohexanol concentration

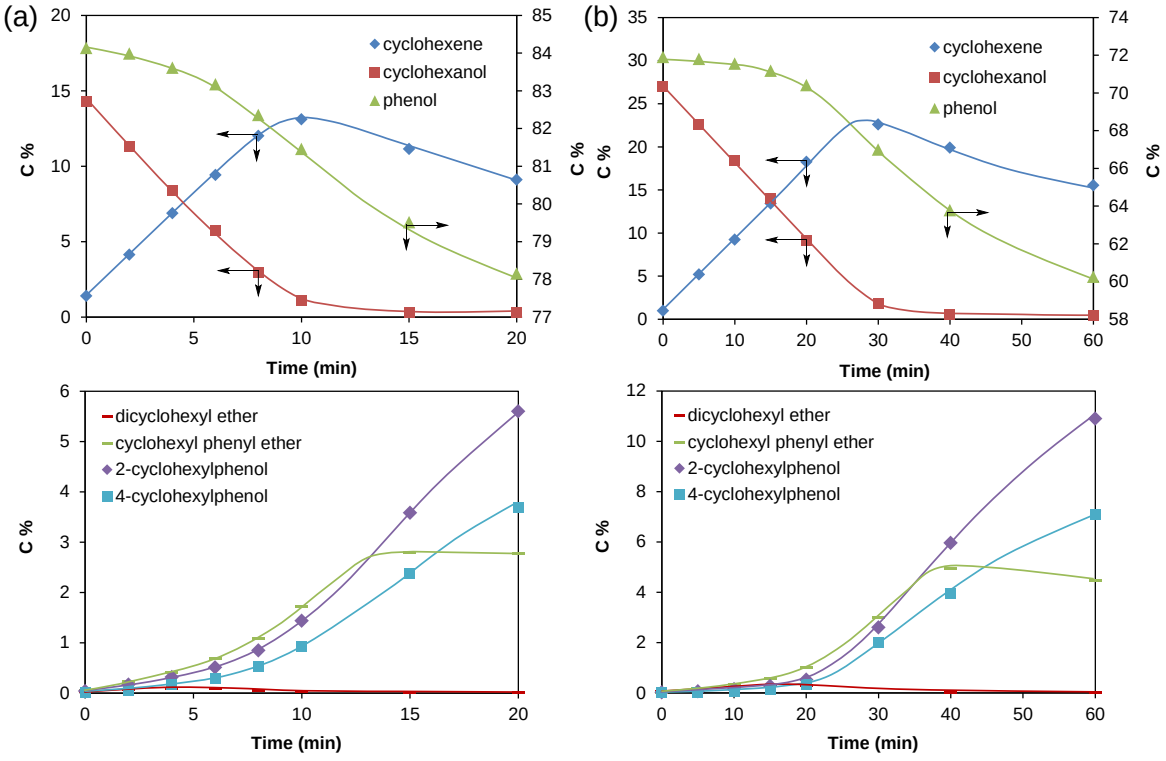

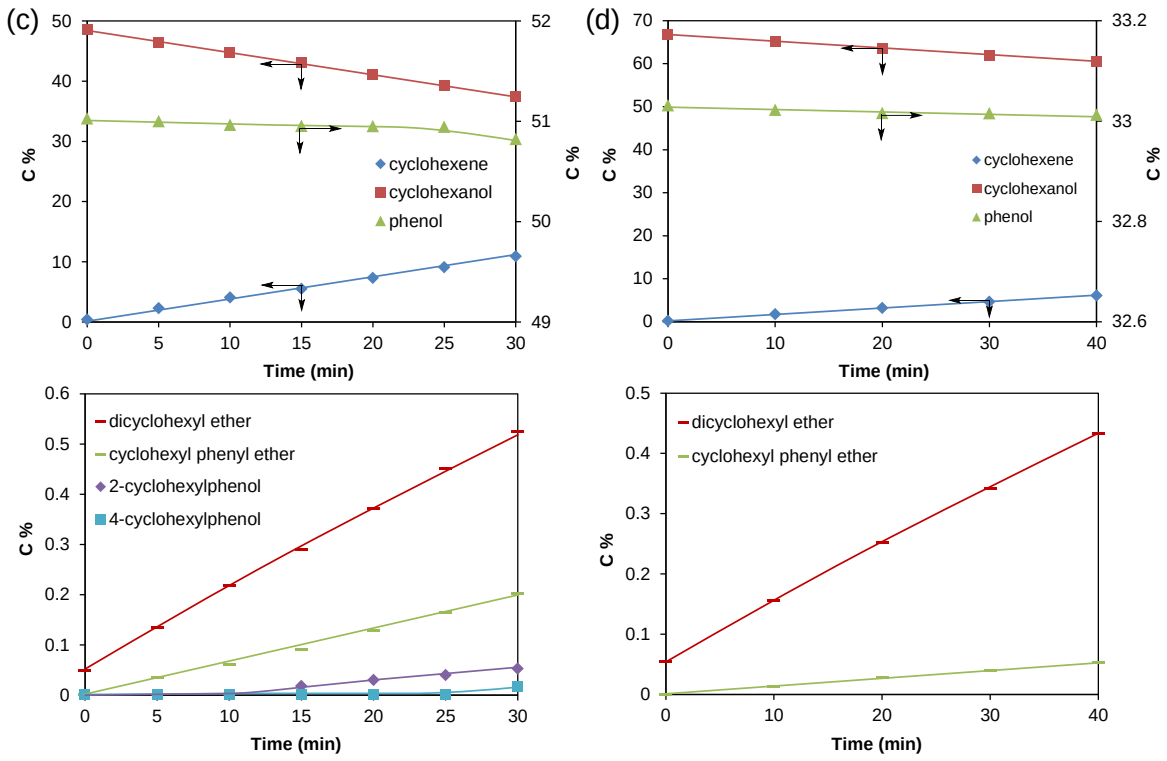

Figure 4A-18. Concentration-time profiles of phenol-cyclohexanol alkylation with 5.0 g phenol and 1.0, 2.0, 5.0 and 10.0 g cyclohexanol (a, b, c and d, respectively) on HBEA-150 in decalin at 160 °C. Reaction conditions: 0.1 g HBEA-150, 100 mL decalin, 5 MPa H_2 (ambient temperature), stirred at 700 rpm.

A5. IR spectra of adsorbed cyclohexene on siliceous BEA and HBEA-150

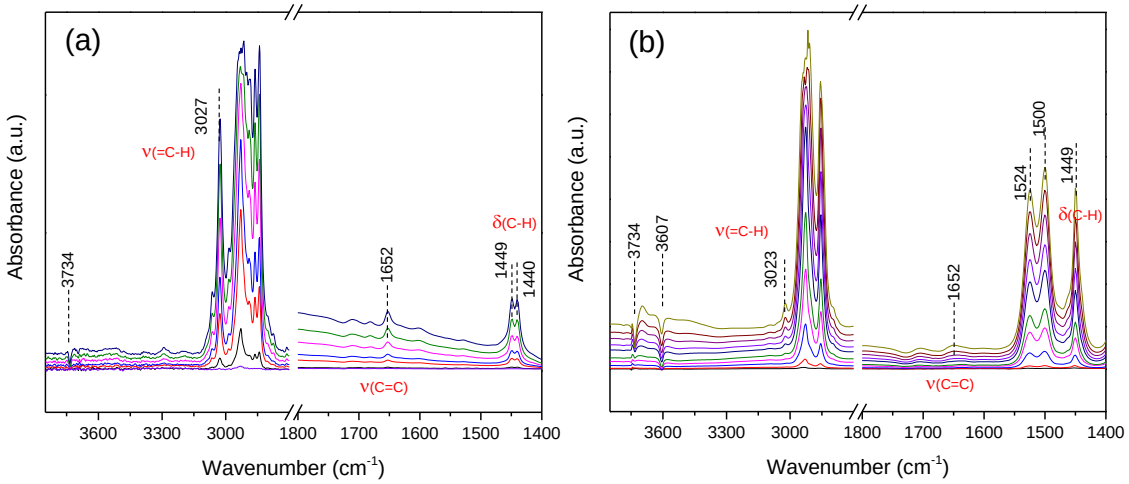

Figure 4A-19. Gas-phase IR spectra of adsorbed cyclohexene on siliceous BEA (a) and HBEA150 (b) at 40 °C.

The gas-phase IR spectroscopy of adsorbed cyclohexene over siliceous BEA and HBEA-150 measured at 40 °C are shown in **Figure S19 (a)** and **(b)**, respectively. The decreasing intensity at 3734 and 3607 cm^{-1} with cyclohexene adsorption is attributed to the interaction of cyclohexene with the non-acidic terminal and internal SiOH groups, and with the Brønsted-acidic bridging hydroxyl groups, respectively. Cyclohexene was molecularly adsorbed (hydrogen-bonded) on siliceous BEA (**Figure S19 (a)**). The $\nu_{=C-H}$ and $\nu_{C=C}$ bands of cyclohexene appeared at 3027 and 1652 cm^{-1}, respectively. The bands at 2800-3000 and 1440-1449 cm^{-1} are ascribed to the ν_{C-H} and δ_{C-H} of adsorbed cyclohexene, respectively, similar to that of gaseous cyclohexene.[8,9] When cyclohexene was adsorbed on acidic HBEA-150 at high pressure, similar bands at 3023, 1652 and 1449 cm^{-1} appeared (**Figure S19 (b)**). Alkenyl or the oligomeric alkenyl carbenium ions have been characterized by IR and NMR as the surface intermediates formed from olefin on acids zeolites, and the bands at 1490-1530 cm^{-1} in IR spectra have been assigned to alkenyl carbenium ions[9] (**Figure S19(a)**).

A6. Additional discussion on phenol-cyclohexene alkylation mechanism

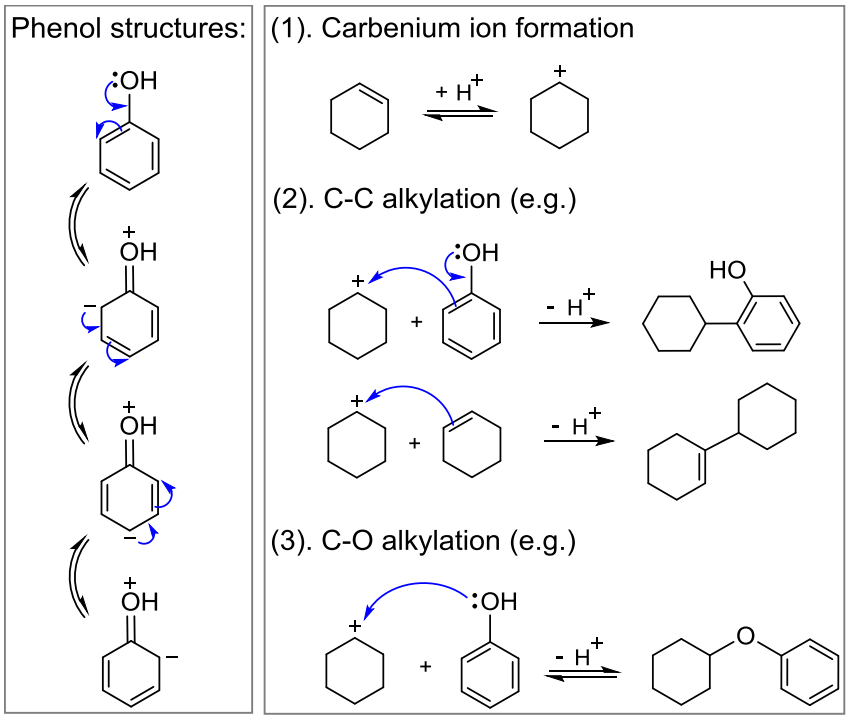

Scheme 4A-2. Proposed reaction mechanism for the alkylation of phenol with cyclohexene over BAS.

Acid catalyzed alkylation of phenol with cyclohexanol in nonpolar liquid-phase is proposed to occur via a pathway in which the cyclohexyl carbenium ion generated by cyclohexene adsorption and protonation at BAS attacks phenol (**Scheme S2**). The olefin adsorbs on the BAS in quasi-equilibrium leading to the formation of surface alkyl carbenium ion which is the reactive intermediate for the rate-limiting C-C and C-O bond formation. As is well known, the charge distribution at the aromatic ring is greatest at sites ortho and para to the OH substituent, as a result of resonance (**Scheme S2**). The dimerization of cyclohexene also occurs. Protons transferring back accompanied by the C-C and C-O bond coupling regenerate the active sites.

Next, we propose the elementary steps and derive the rate expressions for phenol alkylation with cyclohexene (Scheme 3).

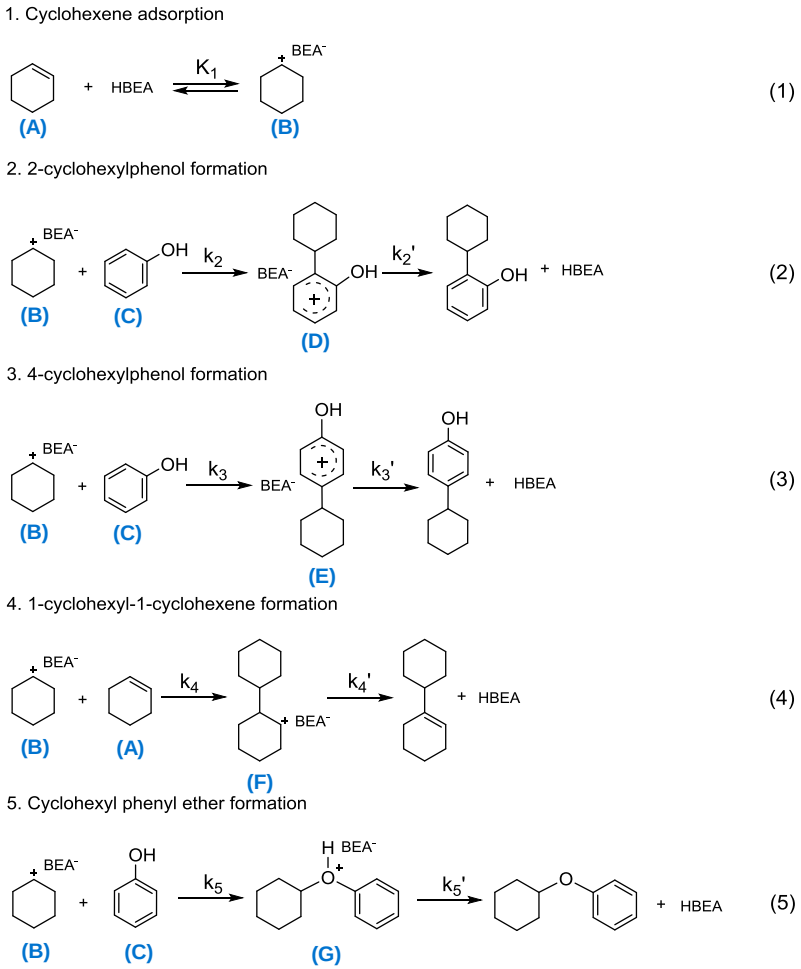

Scheme 4A-3. Proposed elementary steps in the alkylation of phenol with cyclohexene over HBEA-150 based on the mechanism analysis (E-R model) in main text.

This is an Eley-Rideal (E-R) type kinetic model based on the following assumptions: a) all the reactions are catalyzed by BAS and all the sites are energetically equivalent at any grade of coverage; b) step (1) is quasi-equilibrated with an equilibrium constant of K_1 for cyclohexene adsorption; c) steps (2), (3), (4) and (5) are rate-determining steps (RDS) for the formation of *ortho*/*para* alkylation products, olefin oligomerization and ether, respectively; d) Quasi-steady state assumption is applied to each of the surface intermediates involved in steps (2), (3), (4) and (5). Accordingly, the following equations should hold:

$$[\mathrm{B}] = K_1[\mathrm{A}][\mathrm{H}^+] \quad \text{(S-2)}$$

$$r_{2-CHP} = r_D = k_2[\mathrm{B}][\mathrm{C}] \quad \text{(S-3)}$$

$$r_{4-CHP} = r_E = k_3[\mathrm{B}][\mathrm{C}] \quad \text{(S-4)}$$

$$r_{1-CC} = r_F = k_4[\mathrm{B}][\mathrm{A}] \quad \text{(S-5)}$$

$$r_{CPE} = r_G = k_5[\mathrm{B}][\mathrm{C}] \quad \text{(S-6)}$$

$$[\mathrm{B}] + [\mathrm{H}^+] = [\mathrm{H}^+]_0 \quad \text{(S-7)}$$

Eqs. (S-2) to (S-6) are based on **Scheme S3**. Eq. (S-7) is the site balance equation, with $[\mathrm{H}^+]_0$ representing the total surface concentration of BAS. Using these equations, the rate expressions for all the primary alkylation products can be derived as follows:

$$TOF_{2-CHP} = \frac{r_D}{[\mathrm{H}^+]_0} = \frac{k_2K_1[\mathrm{A}][\mathrm{C}]}{1 + K_1[\mathrm{A}]} \quad \text{(S-8)}$$

$$TOF_{4-CHP} = \frac{r_E}{[\mathrm{H}^+]_0} = \frac{k_3K_1[\mathrm{A}][\mathrm{C}]}{1 + K_1[\mathrm{A}]} \quad \text{(S-9)}$$

$$TOF_{1-CC} = \frac{r_F}{[\mathrm{H}^+]_0} = \frac{k_4K_1[\mathrm{A}]^2}{1 + K_1[\mathrm{A}]} \quad \text{(S-10)}$$

$$TOF_{CPE} = \frac{r_G}{[\mathrm{H}^+]_0} = \frac{k_5K_1[\mathrm{A}][\mathrm{C}]}{1 + K_1[\mathrm{A}]} \quad \text{(S-11)}$$

A7. Detailed kinetic data for alkylation of phenol with cyclohexene on HBEA-150 in decalin

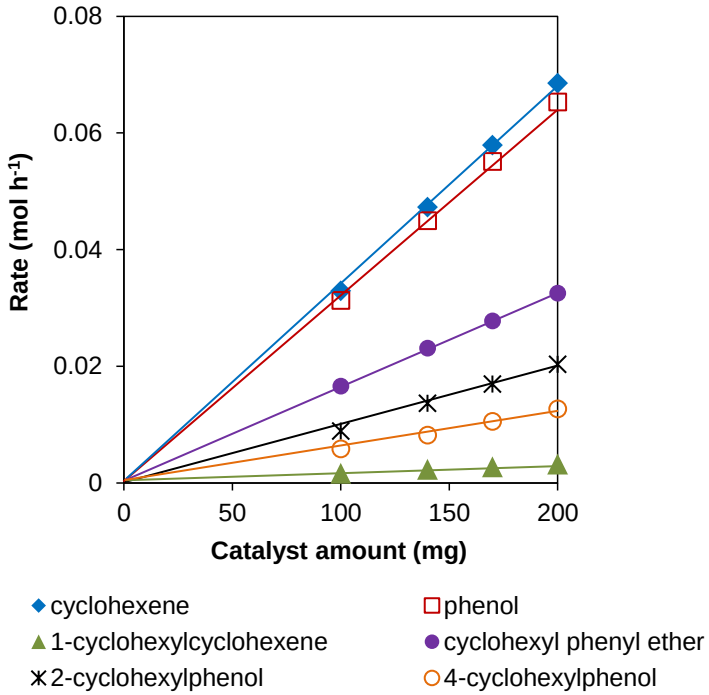

Figure 4A-20. Effect of catalyst amount on the alkylation reaction of phenol with cyclohexene. Reaction conditions: cyclohexene (0.05 mol), phenol (0.05 mol), HBEA-150 (100 mg, 140 mg, 170 mg, 200 mg), decalin (100 mL), T= 120 °C, 5 MPa H_2 (ambient temperature), stirred at 700 rpm.

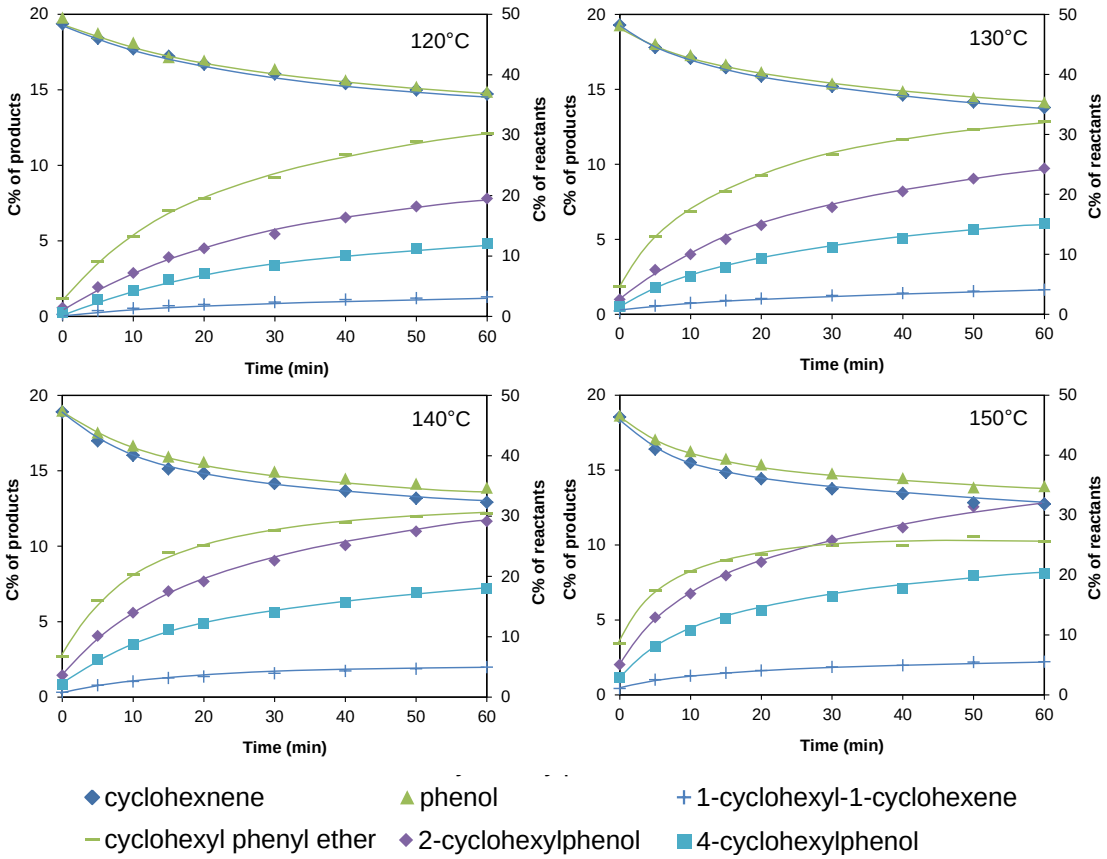

Figure 4A-21. The plots of the carbon-based concentrations of reactants and products in alkylation of phenol with cyclohexene at 120−150 °C. Reaction conditions: cyclohexene (0.05 mol), phenol (0.05 mol), HBEA-150 (0.1 g), decalin (100 mL), 5 MPa H_2 (ambient temperature), stirred at 700 rpm

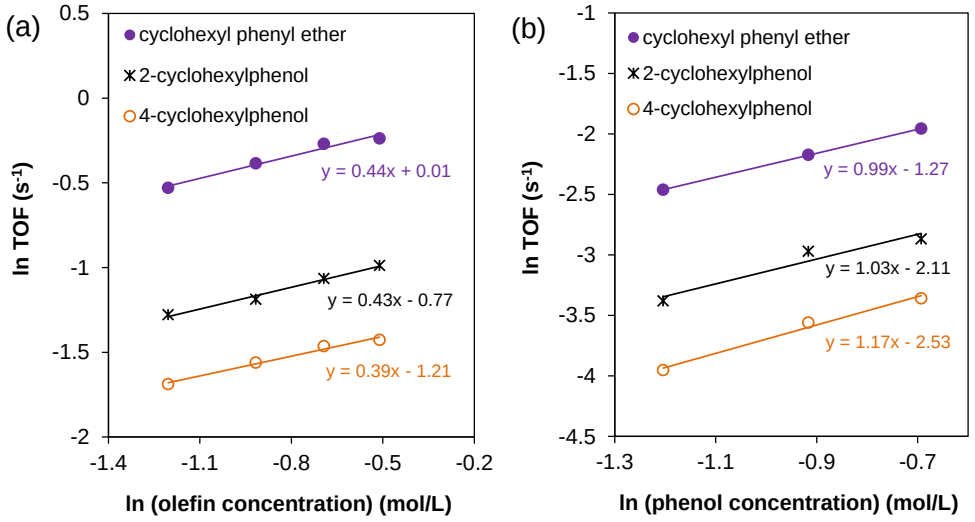

Figure 4A-22. The dependence of the alkylation rates on the concentration of cyclohexene (a) and phenol (b) on HBEA-150. Reaction conditions: (a) phenol (0.50 mol), cyclohexene (0.03, 0.04, 0.05 and 0.06 mol), HBEA-150 (0.1 g), decalin (50 mL), T= 120 °C, 5 MPa H_2 (ambient temperature), stirred at 700 rpm;

(b) cyclohexene (0.50 mol), phenol (0.03, 0.04 and 0.05 mol), HBEA-150 (0.1 g), decalin (50 mL), T= 120 °C, 5 MPa H_2 (ambient temperature), stirred at 700 rpm.

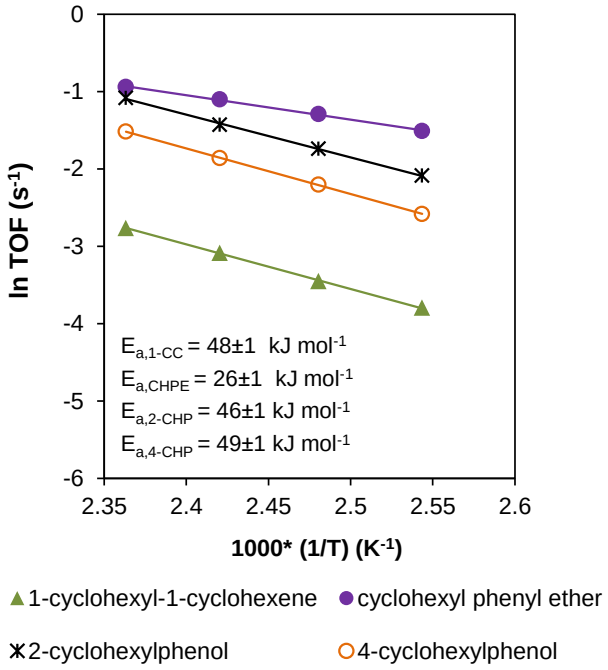

Figure 4A-23. Arrhenius plots of the formation rates of major alkylation products during phenol alkylation with cyclohexene at 120−150 °C. Reaction conditions: cyclohexene (0.05 mol), phenol (0.05 mol), HBEA-150 (0.1 g), decalin (100 mL), 5 MPa H_2 (ambient temperature), stirred at 700 rpm

A8. Alkylation of phenol with cyclohexanol in water

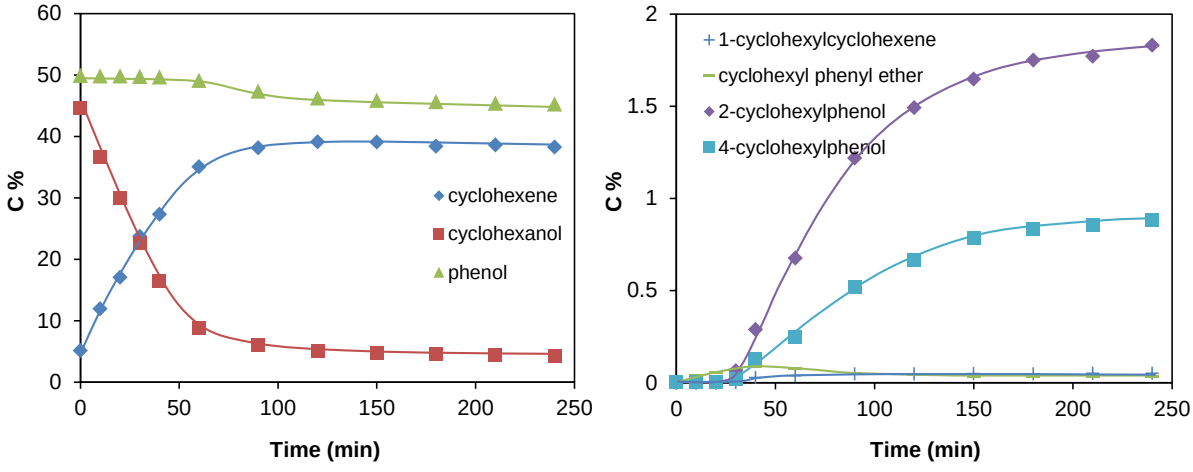

Figure 4A-24. Carbon-based concentration-time profiles of aqueous phase phenol-cyclohexanol alkylation. Reaction conditions: 5.0 g phenol, 5.0 g cyclohexanol, 1.0 g HBEA-150, 100 mL water, 5 MPa H_2 (ambient temperature), stirred at 700 rpm, 170 °C.

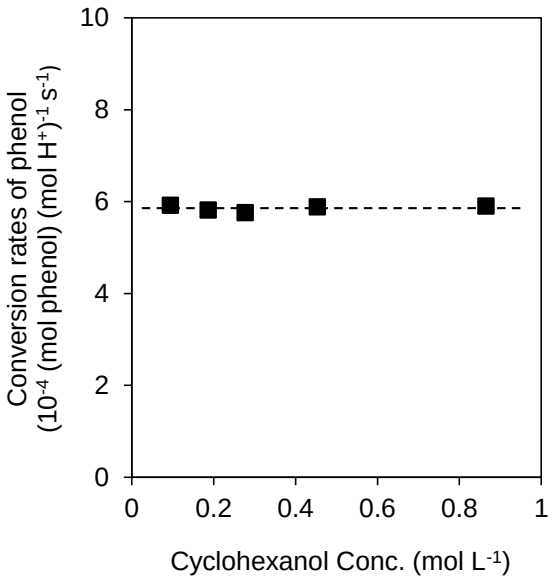

Figure 4A-25. Measured turnover frequencies (TOFs) for the conversion of phenol as a function of cyclohexanol concentration in water (concentrations based on water density at r.t.) over HBEA-150 at 170 °C. Reaction conditions: phenol (5.0 g), cyclohexanol (1.0, 2.0, 3.0, 5.0 and 10.0 g), HBEA-150 (1.0 g), water (100 mL), T = 170 °C, 5 MPa H_2 (ambient temperature), stirred at 700 rpm.

S9. Adsorption of phenol and cyclohexanol on HBEA-150 from water and decalin

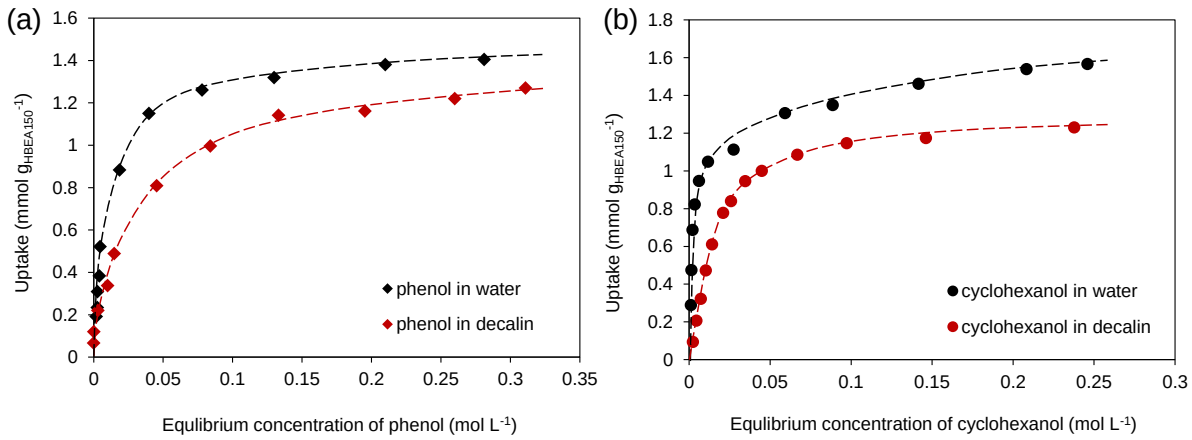

Figure 4A-26. Liquid-phase adsorption of phenol and cyclohexanol on HBEA150 at 25 °C: (a) phenol; (b) cyclohexanol. Adsorption constants were obtained by fitting the experimental points using a Langmuir-type isotherm.

Table 4A-4. Saturation uptake and equilibrium constants for phenol and cyclohexanol adsorption from aqueous phase and decalin onto HBEA150. Adsorption constants were derived from fitting the experimental points by Langmuir isotherm.

	Aqueous phase		Decalin	
Adsorbate	Phenol	Cyclohexanol	Phenol	Cyclohexanol
Saturation uptake (mmol g_{HBEA}^{-1})	1.40	1.57	1.22	1.23
K_{ads}	100	250	44	73

$$q = \frac{q_{sat}\, K_{ads} C_0}{1 + K_{ads} C_0}$$

where q and q_{sat} (mmol g_{HBEA}^{-1}) represent the uptake at a certain concentration and saturation (maximum) uptake, K_{ads} is adsorption constant, and C_0 is the equilibrium concentration of phenol and cyclohexanol in aqueous phase and decalin (mol L^{-1}).

A10. Evidence for the active site in HBEA being a "dry" proton during dehydration and alkylation reactions in decalin

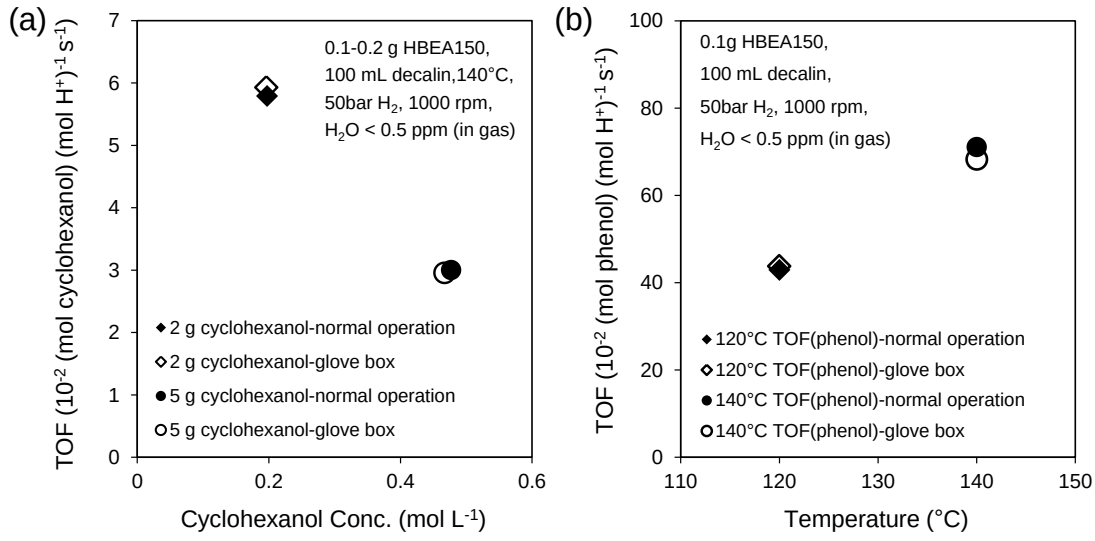

Figure 4A-27. Comparison of rates of HBEA-catalyzed cyclohexanol dehydration (a) and phenol-cyclohexene alkylation (b) in decalin operated under normal conditions (closed symbols) and in a glove box (open symbols). Normal operation: the reactants, solvent and catalyst were handled in atmospheric

environment not specifically protected from moisture. Glove-box: the reactants, solvent and catalyst were dried and charged into the reactor in glove box; see the detailed procedure in the main text.

Figure S27 shows that the level of water concentration during normal operation, in the air, reactants and zeolite HBEA, did not affect the catalytic rates of both dehydration and alkylation reactions in decalin. In the dehydration of cyclohexanol, all initial rates (TOFs) were obtained at conversions < 10%. Taking ~ 0.47 mol L^{-1} concentration (5 g cyclohexanol, **Figure S27(a)**) for example, the TOF was calculated at <6% conversion of cyclohexanol. The amount of water produced from cyclohexanol was ~0.054 g at 6% conversion, which would equal to a maximum partial pressure of ~36 kPa at 160 °C. As shown in **Figure S28**, no water uptake was observed at water pressure of 100 kPa at 400-450 K on fully siliceous BEA zeolite. By the same token, we attribute the unchanged rates in the presence of the produced water over the highly siliceous HBEA (Si/Al=75) (**Figure S27(a)**) also to negligible water adsorption in the pore at 160 °C in decalin. In other words, in decalin, the BAS still remain as dry protons, not as hydronium ions. At least, it is safe to conclude that the amount of water in the pore, if any, is not enough to induce considerable extents of proton transfer from the framework hydroxyl. Similarly, phenol-cyclohexene alkylation on HBEA, a reaction that does not produce water, yielded the same results under normal conditions and in glove box, further supporting our conclusions about the state of the BAS being "dry". Therefore, the alkylation and dehydration kinetics over HBEA in decalin reflects the catalytic behavior of acidic protons on the framework, in contrast to the aqueous phase catalysis which reflects the behavior of hydronium ions.

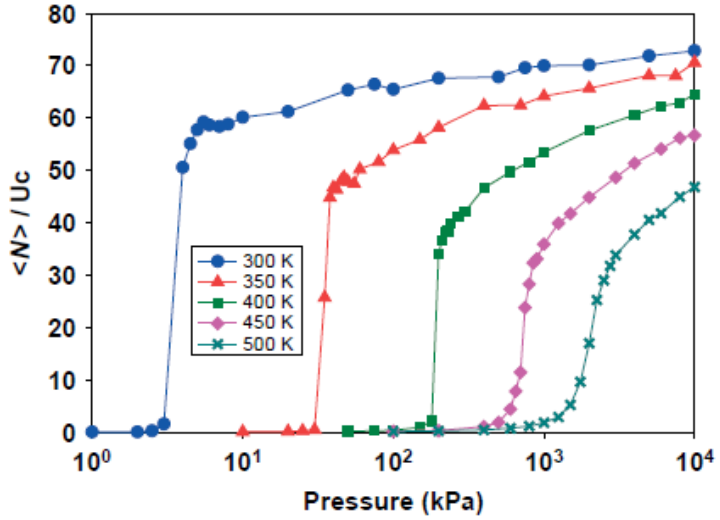

Figure 4A-28. Simulated adsorption isotherms of water over fully siliceous BEA zeolite at different temperatures as a function of water uptake [10].

A11. Detailed kinetic data for alkylation of phenol with cyclohexene on HBEA-150 in aqueous phase

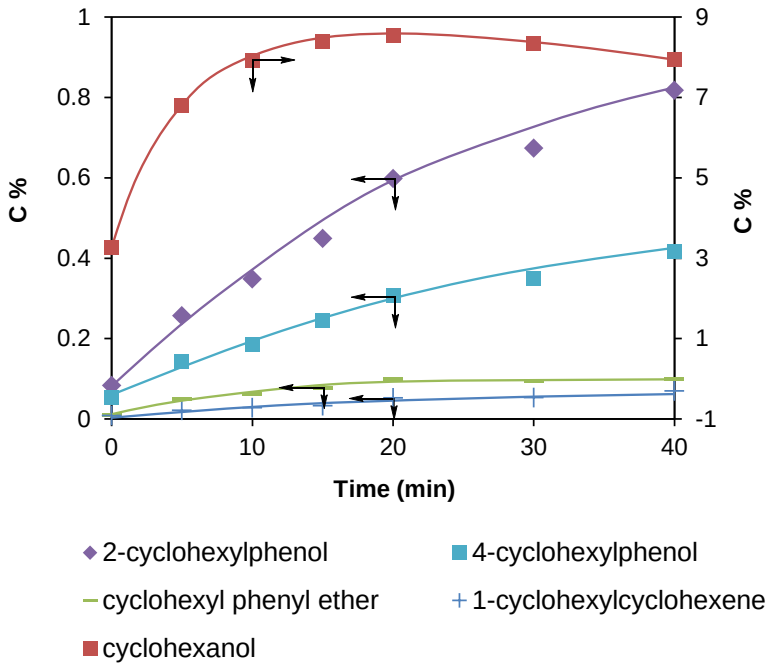

Figure 4A-29. A typical plot of the carbon-based concentrations of products in alkylation of phenol with cyclohexene in aqueous phase at 170 °C. Reaction conditions: cyclohexene (0.05 mol), phenol (0.05 mol), HBEA-150 (0.4 g), water (100 mL), 5 MPa H_2 (ambient temperature), stirred at 700 rpm

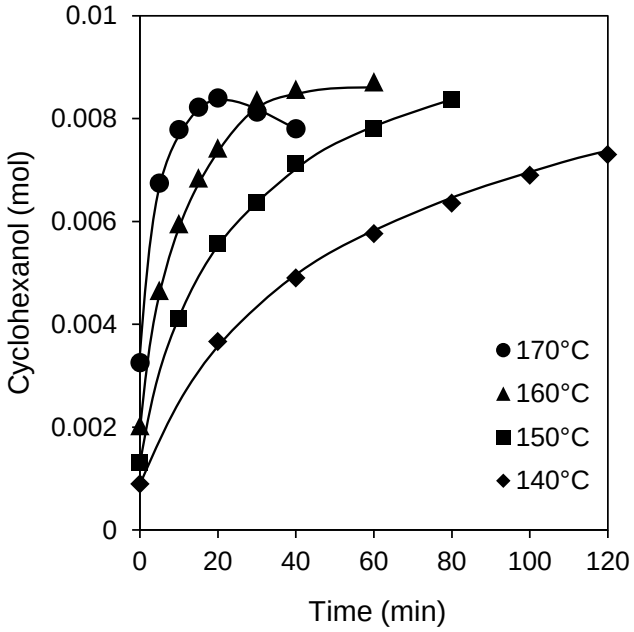

Figure 4A-30. Mole of cyclohexanol formed as a function of reaction time during the alkylation of phenol with cyclohexene at 140−170 °C in aqueous phase. Reaction conditions: cyclohexene (0.05 mol), phenol (0.05 mol), HBEA-150 (0.4 g), water (100 mL), 5 MPa H_2 (ambient temperature), stirred at 700 rpm

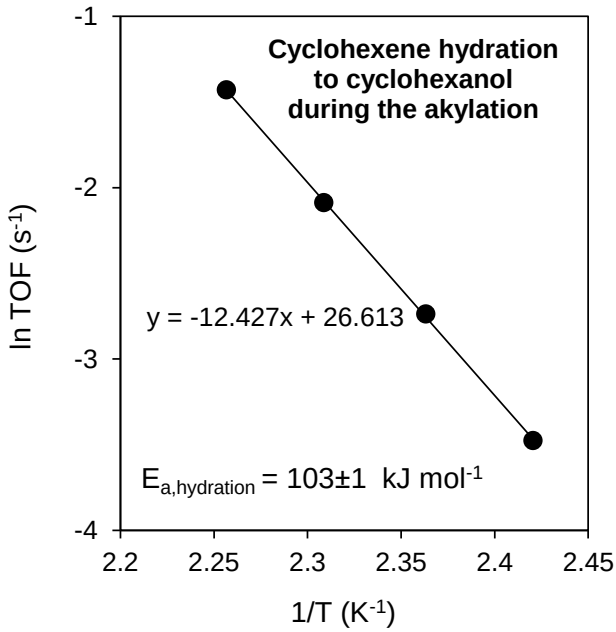

Figure 4A-31. Arrhenius plot of the cyclohexene hydration to cyclohexanol during phenol alkylation with cyclohexene at 140−170 °C in aqueous phase. Reaction conditions: cyclohexene (0.05 mol), phenol (0.05 mol), HBEA-150 (0.4 g), water (100 mL), 5 MPa H_2 (ambient temperature), stirred at 700 rpm

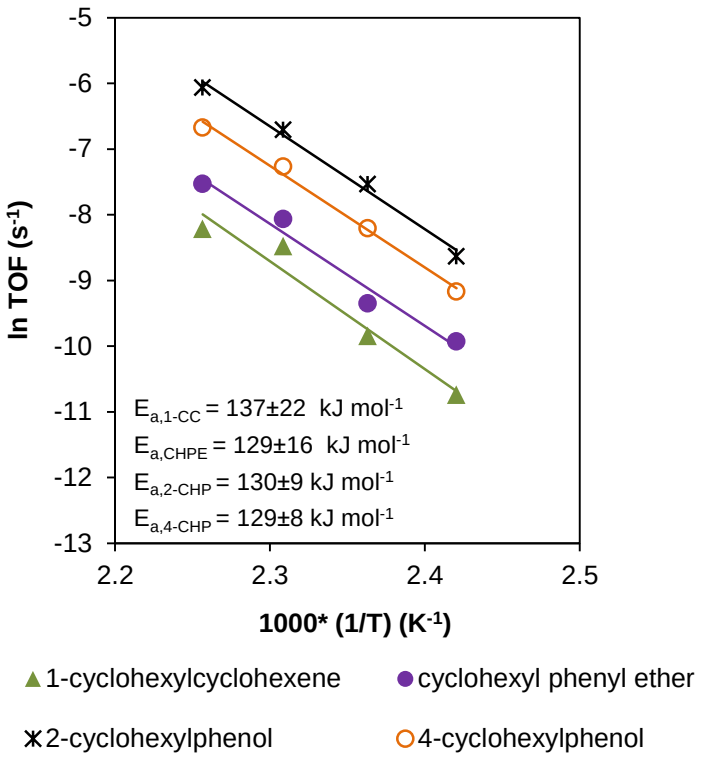

Figure 4A-32. Arrhenius plots of the formation rates of major alkylation products during phenol alkylation with cyclohexene at 140−170 °C in aqueous phase. Reaction conditions: cyclohexene (0.05 mol), phenol (0.05 mol), HBEA-150 (0.4 g), water (100 mL), 5 MPa H_2 (ambient temperature), stirred at 700 rpm.

Table 4A-5. Turnover frequencies and apparent activation energies for initial products of HBEA150-catalyzed alkylation of phenol with cyclohexene in aqueous phase.[a]

Products	Rate[b]	Temperature (°C)				E_a (kJ mol^{-1})
		140	150	160	170	
cyclohexanol	$TOF_{cyclohexanol}$ (s^{-1})	0.031	0.065	0.124	0.24	103
1-cyclohexylcyclohexene	$TOF_{1\text{-}CC}$ (s^{-1})	2.16×10^{-5}	5.29×10^{-5}	2.08×10^{-4}	2.71×10^{-4}	137
Cyclohexyl phenyl ether	TOF_{CHPE} (s^{-1})	4.89×10^{-5}	8.72×10^{-5}	3.15×10^{-4}	5.37×10^{-4}	129
2-cyclohexylphenol	$TOF_{2\text{-}CHP}$ (s^{-1})	1.78×10^{-4}	5.34×10^{-4}	1.22×10^{-3}	2.33×10^{-3}	130
4-cyclohexylphenol	$TOF_{4\text{-}CHP}$ (s^{-1})	1.04×10^{-4}	2.73×10^{-4}	7.00×10^{-4}	1.27×10^{-3}	129

[a] Typical conditions: cyclohexene (0.05 mol), phenol (0.05 mol), HBEA-150 (0.4 g), water(100 mL), 5 MPa H_2 (ambient temperature), stirred at 700 rpm; [b] TOF is determined as reactants consumption and products formation rates (mol g^{-1} s^{-1}) normalized to the concentration of total BAS (HBEA-150).

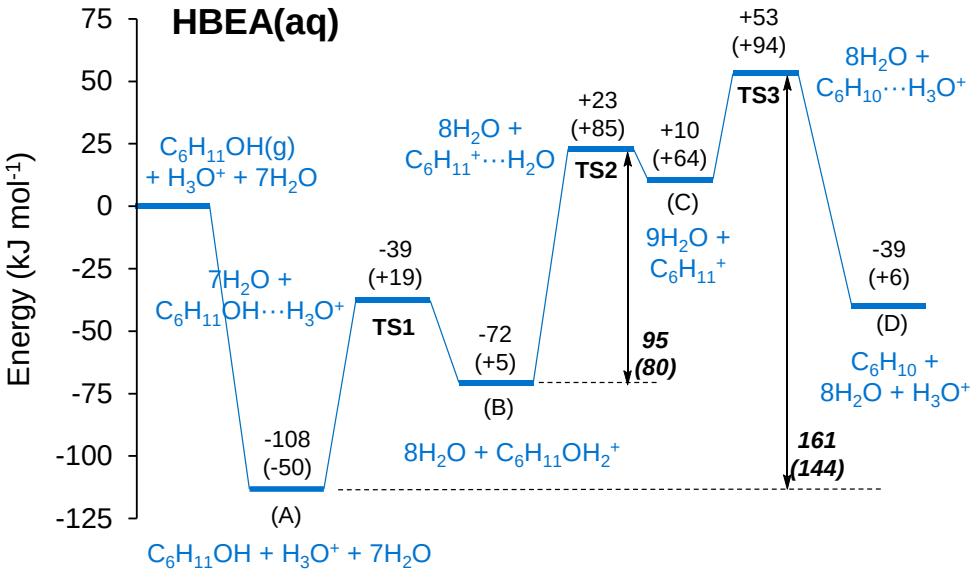

Figure 4A-33. The energy diagram of HBEA-catalyzed cyclohexanol dehydration in aqueous phase based on DFT calculations (**Chapter 2**).

A12. References for Appendix

1. Schachtl, E.; Zhong, L.; Kondratieva, E.; Hein, J.; Gutiérrez, O. Y.; Jentys, A.; Lercher, J. A. *ChemCatChem* **2015**, *7*, 4118.

2. Siril, P. F.; Davison, A. D.; Randhawa, J. K.; Brown, D. R. *J. Mol. Catal. A* **2007**, *267*, 72.

3. Ngaosuwan, K.; Lotero, E.; Suwannakarn, K.; Goodwin, J. G.; Praserthdam, P. *Ind. Eng. Chem. Res.* **2009**, *48*, 4757.

4. Vjunov, A.; Hu, M. Y.; Feng, J.; Camaioni, D. M.; Mei, D.; Hu, J. Z.; Zhao, C.; Lercher, J. A. *Angew. Chem. Int. Ed.* **2013**, *53*, 479.

5. Zhi, Y.; Shi, H.; Mu, L.; Liu, Y.; Mei, D.; Camaioni, D. M.; Lercher, J. A. *J. Am. Chem. Soc.* **2015**, *137*, 15781.

6. Knaeble, W.; Iglesia, E. *J. Phys. Chem. C* **2016**, *120*, 3371.

7. John, M.; Alexopoulos, K.; Reyniers, M.-F.; Marin, G. B. *J.Catal.* **2015**, *330*, 28.

8. Shi, Y.; Zhang, W.; Zhang, H.; Tian, F.; Jia, C.; Chen, Y. *FUEL PROCESS TECHNOL.* **2013**, *110*, 24.

9. Yang, S.; Kondo, J. N.; Domen, K. *Catal. Today* **2002**, *73*, 113.

10. Nguyen, V. T.; Nguyen, P. T. M.; Dang, L. X.; Mei, D.; Wick, C. D.; Do, D. D. *Mol.Simul.* **2014**, *40*, 1113.

4.6 References

[1] K. Weissermel, H.-J. A. *In Industrial Organic Chemistry*; 3rd ed. ed.; VCH Weinheim, 1997.

[2] Yadav, G. D.; Pathre, G. S. *Ind. Eng. Chem. Res.* **2007**, *46*, 3119.

[3] Roberts, V. M.; Stein, V.; Reiner, T.; Lemonidou , A.; Li, X.; Lercher, J. A. *Chem. Eur. J.* **2011**, *17*, 5939.

[4] Huber, G. W.; Corma, A. *Angew. Chem. Int. Ed.* **2007**, 46, 7184.

[5] Zhao, C.; Lercher, J. A. *Angew. Chem. Int. Ed.* **2012**, 51, 5935.

[6] Zhao, C.; He, J.; Lemonidou, A. A.; Li, X.; Lercher, J. A. *J. Catal.* **2011**, *280*, 8.

[7] González-Borja, M. Á.; Resasco, D. E. *AIChE J.* **2014**, *61*, 598.

[8] Zhao, C.; Camaioni, D. M.; Lercher, J. A. *J. Catal.* **2012**, *288*, 92.

[9] Ma, Q.; Chakraborty, D.; Faglioni, F.; Muller, R. P.; Goddard, W. A.; Harris, T.; Campbell, C.; Tang, Y. *J. Phys. Chem. A* **2006**, *110*, 2246.

[10] Sarish, S.; Devassy, B.; Bohringer, W.; Fletcher, J.; Halligudi, S. *J. Mol. Catal. A* **2005**.

[11] Anand, R.; Gore, K. U.; Rao, B. S. *Catal. Lett.* **2002**, 81, 33.

[12] de Klerk, A.; Nel, R. J. J. *Ind. Eng. Chem. Res.* **2007**, 46, 7066.

[13] Sad, M. E.; Padró, C. L.; Apesteguía, C. R. *Catal. Today* **2008**, *133-135*, 720.

[14] Gagea, B. C.; Parvulescu, A. N.; Parvulescu, V. I.; Auroux, A.; Grange, P.; Poncelet, G. *Catal. Lett.* **2003**, *91*, 141.

[15] Karthik, M.; Vinu, A.; Tripathi, A. K.; Gupta, N. M.; Palanichamy, M.; Murugesan, V. *Micropor. Mesopor. Mater.* **2004**, *70*, 15.

[16] Samolada, M. *J. Catal.* **1995**, *152*, 52.

[17] Tanabe, K. In *Studies in Surface Science and Catalysis*; B. Imelik, C. N. G. C. Y. B. T., Vedrine, J. C., Eds.; Elsevier: 1985; Vol. Volume 20, p 1.

[18] Modrogan, E.; Valkenberg, M.; Hoelderich, W. *J. Catal.* **2009**, *261*, 177.

[19] Pierantozzi, R.; Nordquist, A. F. *Appl. Catal.* **1986**, *21*, 263.

[20] Yadav, G. D.; Kumar, P. *Appl. Catal. A* **2005**, *286*, 61.

[21] Chaudhuri, B.; Sharma, M. M. *Ind. Eng. Chem. Res.* **1991**, 30, 227.

[22] Bregolato, M.; Bolis, V.; Busco, C.; Ugliengo, P.; Bordiga, S.; Cavani, F.; Ballarini, N.; Maselli, L.; Passeri, S.; Rossetti, I.; Forni, L. *J. Catal.* **2007**, 245, 285.

[23] Schmerling, L. *J. Am. Chem. Soc.* **1945**, *67*, 1778.

[24] Feller, A.; Guzman, A.; Zuazo, I.; Lercher, J. A. *J. Catal.* **2004**, 224, 80.

[25] Corma, A. *Chem. Res.* **1995**, *95*, 559.

[26] Olah, G. A.; White, A. M.; O'Brien, D. H. *Chem. Res.* **1970**, *70*, 561.

[27] Anand, R.; Daniel, T.; Lahoti, R. J.; Srinivasan, K. V.; Rao, B. S. *Catal. Lett*. **2002**, *81*, 241.

[28] Velu, S.; Sivasanker, S. *Res. Chem. Intermed.* **1998**, 24, 657.

[29] Smirniotis, P. G.; Ruckenstein, E. *Ind. Eng. Chem. Res.* **1995**, 34, 1517.

[30] Corma, A.; Martínez-Soria, V.; Schnoeveld, E. *J. Catal.* **2000**, *192*, 163.

[31] Craciun, I.; Reyniers, M.-F.; Marin, G. B. *J.Catal.* **2012**, *294*, 136.

[32] Zhao, C.; Song, W.; Lercher, J. A. *ACS Catal*. **2012**, *2*, 2714.

[33] Olah, G. A.; Kaspi, J.; Bukala, J. *J. Org. Chem.* **1977**, *42*, 4187.

[34] Harmer, M. A.; Farneth, W. E.; Sun, Q. *J. Am. Chem. Soc.* **1996**, *118*, 7708.

[35] Ngaosuwan, K.; Lotero, E.; Suwannakarn, K.; Goodwin, J. G.; Praserthdam, P. *Ind. Eng. Chem. Res.* **2009**, 48, 4757.

[36] Climent, M. J.; Corma, A.; Iborra, S.; Martínez-Silvestre, S.; Velty, A. *ChemSusChem* **2013**, *6*, 1224.

[37] González-Borja, M. Á.; Resasco, D. E. *AIChE J.* **2015**, *61*, 598.

[38] Taylor, D. R.; Ludlum, K. H. *J. Phys. Chem.* **1972**, *76*, 2882.

[39] Ronchin, L.; Vavasori, A.; Toniolo, L. *J. Mol. Catal. A* **2012**, *355*, 134.

[40] Chiang, H.; Bhan, A. *J.Catal.* **2010**, *271*, 251.

[41] Zhi, Y.; Shi, H.; Mu, L.; Liu, Y.; Mei, D.; Camaioni, D. M.; Lercher, J. A. *J. Am. Chem. Soc.* **2015**, *137*, 15781.

[42] Knaeble, W.; Iglesia, E. *J. Phys. Chem. C* **2016**, *120*, 3371.

[43] Lee, K. Y.; Arai, T.; Nakata, S.; Asaoka, S.; Okuhara, T.; Misono, M. *J. Am. Chem. Soc.* **1992**, *114*, 2836.

[44] Macht, J.; Janik, M. J.; Neurock, M.; Iglesia, E. *J. Am. Chem. Soc.* **2008**, *130*, 10369.

[45] Macht, J.; Janik, M. J.; Neurock, M.; Iglesia, E. *Angew. Chem. Int. Ed.* **2007**, *46*, 7864.

[46] John, M.; Alexopoulos, K.; Reyniers, M.-F.; Marin, G. B. *J. Catal*. **2015**, *330*, 28.

[47] Yang, S.; Kondo, J. N.; Domen, K. *Catal. Today* **2002**, *73*, 113.

[48] Xu, T.; Haw, J. F. *J. Am. Chem. Soc.* **1994**, *116*, 7753.

[49] Kiricsi, I.; Förster, H.; Tasi, G.; Nagy, J. B. *Chem.Rev.* **1999**, *99*, 2085.

[50] Ronchin, L.; Quartarone, G.; Vavasori, A. *J. Mol. Catal. A* **2012**, *353-354*, 192.

Chapter 5

Summary and Conclusions

The aim of this thesis is to investigate the fundamental chemistry involved in the catalytic upgrading of lignin-derived bio-oils, based on the reliable kinetic evaluation, in conjunction with the detailed characterizations and theoretical calculations. Cyclohexanol and phenol are selected as the platform molecules for the relevant dehydration and alkylation reactions over acid catalysts in liquid phase under the mild conditions. The research in this thesis may supply some hints or guidance for catalyst design and processing optimization for the two important objectives in biomass conversion, *i.e.*, O-removal and C-C bond coupling.

In aqueous phase, adsorbed water leads at Brønsted acid sites (BAS) in the zeolite to the formation of hydronium ions. The kinetics of the acid-catalyzed dehydration of cyclohexanol is investigated using a mineral acid, H_3PO_4, and HBEA zeolite, aiming to understand the enhancement of the rates of the liquid-phase dehydration on solid acids by the presence of steric constraints. Isotopic experiments reveal that the aqueous-phase dehydration of cyclohexanol, whether catalyzed by hydronium ion in HBEA or aqueous H_3PO_4, occurs predominantly via an E1-type mechanism with the cleavage of C_β–H being the kinetically relevant elementary step. The dehydration rates at confined hydronium ions are higher by more than an order of magnitude compared to the hydronium ions in unconstrained water. The higher activity of hydronium ions in constrains is caused by an increased association between hydronium ions and alcohol, as well as a greater entropy of activation. Hydronium ions within sterically constrained zeolite pores bear a strong resemblance to enzyme catalyst, and this contribution allows us to understand and predict the similar processes in confined spaces, as well as to design the acid catalysts.

The kinetics of the acid-catalyzed dehydration of cyclohexanol is investigated using two HBEA zeolites (Si/Al = 71 and 75) with different Al T-site distributions. The distribution of BAS among different crystallographic of the BEA framework is inconsequential to cyclohexanol dehydration in liquid phase, both in water and in neat cyclohexanol. Aqueous phase adsorption measurements, in combination with density functional theory (DFT) calculations, demonstrate that cyclohexanol molecules are primarily hydrogen-bonded to the hydronium ions in zeolites at reaction temperatures of 160−200 °C. Proton transfer from the hydronium ion cluster to cyclohexanol is

thermodynamically unfavorable for HBEA in aqueous medium, rendering protonated alcohol as the minority species. The number of intraporous water molecules in aqueous phase or solvent-free conditions significantly changes the solvation environments of the BAS and alters its acid strength. In consequence, proton transfer from the $H_3O^+(H_2O)_n$ cluster to cyclohexanol becomes favorable as fewer water molecules are associated with the proton. This change in the nature of the active site results in a significantly lower activation barrier and less entropy gain for dehydration of neat-alcohol than in aqueous medium. DFT calculations show that, in the absence of water, the protonated cyclohexanol dimers (also confirmed by the IR adsorption of cyclohexanol on HBEA) are the dominant surface species which undergo C–O bond cleavage via a concerted pericyclic pathway.

The alkylation of phenol with cyclohexanol/cyclohexene in liquid hydrocarbon, decalin, is investigated over a range of solid acids under mild conditions (≤ 160 °C). The reactions are primarily catalyzed by Brønsted acid sites (BAS) on solid surfaces. Among the investigated solid acids, large-pore zeolites such as HBEA and HY are the most effective catalysts for phenol-cyclohexanol alkylation. O-alkylation is kinetically favored and reversible, while C-alkylation occurs preferentially at *ortho*/*para* positions in an irreversible manner. For reactions carried out in decalin, carbenium ion is the direct electrophile for phenol alkylation with either cyclohexanol or cyclohexene. A dominant fraction of cyclohexanol in HBEA pores takes on a protonated dimer form. Carbenium ion can be produced from the alcohol monomer H-bonded to the BAS, but not from the protonated dimer. Adsorption and protonation of olefin at the BAS also produces carbenium ion, and exhibits a relatively low apparent activation barrier (< 50 kJ mol^{-1}). Olefin re-adsorption, however, is hindered by the presence of alcohol dimer, leading to low alkylation rates at the initial stage (i.e., before cyclohexanol is largely converted) of phenol-cyclohexanol alkylation on HBEA zeolites. Reducing the concentration of cyclohexanol leads to exponential increases in initial dehydration and alkylation rates, because the coverage of the alcohol monomer, which more readily generates the carbenium ion, increases with decreasing cyclohexanol concentration. Collectively, adsorption and kinetic measurements show that phenol alkylation with cyclohexene occurs via an Eley-Rideal type mechanism on HBEA in decalin. The rate of alkylation is

much lower in water than in decalin, because the generation of the cyclohexyl cation from cyclohexanol is very costly in aqueous phase and olefin protonation by the hydronium ion has a significantly higher barrier than protonation by a framework-bound proton.

Finally, according to the research we have shown in this thesis, we may provide some ideas on the rational design or screening for acid catalysts used in the transformation of biomass. For instance, in aqueous phase, the enthalpy-entropy compensation induced by the pore constraints of zeolites results in a smaller Gibbs free energy barrier, causing a higher rate constant for hydronium-ions-catalyzed dehydration of cyclohexanol. As such, the catalytic performance would be enhanced by altering the microenvironment of acid sites. Building or stabilizing the active centers, *e.g.*, acid or metal sites, in confined structures would be a possible strategy to achieve the conversion steps such as O-removal and hydrogenation in high efficiencies. In addition, we demonstrate in alkylation chapter that the moderately strong BAS and spacious microporous environment are important criteria for effective phenol-cyclohexanol alkylation (C_6-C_6) to producing C_{12}-C_{18} compounds. That is, the zeolites screening should take into account the dimensions of reactants, products, and the probable TS, as well as the activity of these molecules or intermediates, in particular when bio-oils which contain the components with a wide range of carbon numbers and a variety of functional groups are used as feedstocks. Moreover, in organic solvents (neat cyclohexanol or decalin), the monomer-dimer distribution depends mainly on the concentration of alcohol in zeolite pores, which further impacts the rates of dehydration to olefin. Similarly, by using a lower concentration of cyclohexanol, the initial rate of alkylation is also remarkably enhanced. Therefore, the dehydration and alkylation routes can be kinetically tailored by adjusting the concentration of cyclohexanol, which supplies us an effective approach to enhancing the reaction rates in practice, *e.g.*, using a CSTR to maintain a low concentration of the alcohol reactant during the relevant reactions. Furthermore, in aqueous phase, here we may also predict that at high concentrations of cyclohexanol in bulk solution, the intraporous water molecules would be ultimately replaced by the alcohol molecules and the reaction would bear a resemblance to that in organic phase. These details are worthy to be further investigated in the future.

List of Publications

Journals

Yuanshuai Liu, Aleksei Vjunov, Hui Shi, Sebastian Eckstein, Donald M. Camaioni, Donghai Mei, Eszter Barath, Johannes A. Lercher*, *"Enhancing the catalytic activity of hydronium ions through constrained environments"*, *Nat. Commun.* 8, 14113 doi: 10.1038/ncomms14113, **2017**.

Yuanshuai Liu, Eszter Barath, Hui Shi*, Jianzhi Hu, Donald M. Camaioni, Johannes A. Lercher*, *"Kinetic and mechanistic roles of co-reactant and solvent in liquid-phase alkylation of phenol on zeolite HBEA"*, to be submitted to *ACS Catal.*, **2017**.

Yuanshuai Liu, Eszter Barath, Hui Shi*, Donald M. Camaioni, Johannes A. Lercher*, *"Solid acid catalyzed alkylation of phenol with cyclohexanol and cyclohexene in liquid phase"*, in preparation, **2017**.

Yuanshuai Liu, Hui Shi, Aleksei Vjunov, Donald M. Camaioni, Donghai Mei, Eszter Barath, Johannes A. Lercher*, *"The impact of water on the liquid-phase dehydration of cyclohexanol"*, in preparation, **2017**.

Yuanshuai Liu, Yue Liu, Hui Shi, Donald M. Camaioni, Johannes A. Lercher*, *"Detailed kinetic assessment of cyclohexanol dehydration over solid acids in apolar liquid media"*, in preparation, **2017**.

Zhenchao Zhao, Hui Shi, Chuan Wan, Mary Y. Hu, Yuanshuai Liu, Donghai Mei, Donald M. Camaioni, Jian Zhi Hu,* Johannes A. Lercher*, *"In situ 13C MAS NMR investigation of phenol alkylation in decalin over zeolite HBEA"*, submitted to *JACS*, **2017**.

Yuchun Zhi, Hui Shi, Yuanshuai Liu, Johannes A. Lercher*, *"Similarities and contrasts between gas phase and liquid phase dehydration of 1-propanol on H-ZSM-5"*, in preparation, **2017**.

Wenji Song[§], Yuanshuai Liu[§], Eszter Barath, Lucy Wang, Chen Zhao, Donghai Mei*, and Johannes A. Lercher*, *"Dehydration of 1−octadecanol over H-BEA: A combined experimental and computational study"*, *ACS Catal.* **2016**, 6, 878-889. ([§]:co-first authorship)

K. Alexopoulos, M.-S. Lee, Y. Liu, Y. Zhi, Y. Liu, M.-F. Reyniers*, G. B. Marin, V.-A. Glezakou, R. Rousseau*, J. A. Lercher*, *"Anharmonicity and Confinement in Zeolites: Structure, Spectroscopy, and Adsorption Free Energy of Ethanol in H-ZSM-5"*, *J. Phys. Chem. C* **2016**, 120, 7172-7182.

Wenji Song, Yuanshuai Liu, Eszter Barath, Chen Zhao*, and Johannes A. Lercher* *"Synergistic effects of Ni and acid sites for hydrogenation and C−O bond cleavage of substituted phenols"*, *Green Chem.* **2015**, *17*, 1204-1218.

Giovanni Maria Piccini, Maristella Alessio, Joachim Sauer*, Yuchun Zhi, Yuanshuai Liu, Robin Kolvenbach, Andreas Jentys, and Johannes A. Lercher* *"Accurate Adsorption Thermodynamics of Small Alkanes in Zeolites. Ab initio Theory and Experiment for H-Chabazite"*, *J. Phys. Chem. C* **2015**, 119, 6128−6137.

Si Hu, Jie Shan, Qing Zhang, Yan Wang, Yuanshuai Liu, LanLan Zhang, Yanjun Gong* Zhijie Wu and Tao Dou. *"Methanol to propylene over high-silica nanosheets of MFI zeolite"*, *Appl. Catal. A* **2012**, 215, 445-446.

Poster Presentations

Yuanshuai Liu, Eszter Barath, Johannes. A. Lercher* *"Zeolite-catalyzed cyclohexanol reactions in liquid phase: alkylation and dehydration",* 50. Jahrestreffen Deutscher Katalytiker, Weimar (Germany), 03/2017.

Hui Shi, Yuanshuai Liu, Jianzhi Hu, Donald M. Camaioni, Johannes. A. Lercher* *"Solid-acid-catalyzed alkylation of phenol in aqueous and hydrocarbon solvents",* 25th North American Catalysis Society Meeting (NAM), Denver (USA), 06/2017.

Wenji Song, Yuanshuai Liu, Chenz Zhao, Johannes. A. Lercher* *"Understanding the relation between metal and acid sites for C-O bonds cleavage of phenol and its derivatives",* 46. Jahrestreffen Deutscher Katalytiker, Weimar (Germany), 03/2013.

Patents

Yanjun Gong, Tao Dou, Si Hu, Qing Zhang, Lanlan Zhang, Yuanshuai Liu, Feiying Yang, Jing Sun. *"Modification of HZSM-5 for the highly selective conversion of methanol/dimethyl ether to propylene"*. CN103418420 A.